



Compendium solar spectrum formation

Robert J. Rutten^{1,2,3}

¹ Lingezicht Astrophysics, Deil, The Netherlands

² Institute of Theoretical Astrophysics, University in Oslo, Oslo, Norway

³ Rosseland Centre for Solar Physics, University in Oslo, Oslo, Norway

*Myself when young did eagerly frequent
doctor and saint, and heard great argument
about it and about; but evermore
came out by the same door as in I went.*

Omar Khayyam (1048–1131)

Abstract. The solar spectrum conveys most of our diagnostics to find out how our star works. They must be understood for utilization but solar spectrum formation is complex because the interaction of matter and radiation within the solar atmosphere suffers non-local control in space, wavelength, and time. These complexities are summarized and illustrated with classic literature. They combine in chromospheric spectrum formation.

arXiv:2103.02369v7 [astro-ph.SR] 9 Apr 2022

Contents

1	Preamble: on-line format and on-line material	2
2	Introduction	3
3	RT basics	5
	Intensity	5
	Matter–radiation interactions	6
	Bound-bound, bound-free, free-free interactions	6
	Pair combinations	6
	Equilibria	7
	Bound-bound redistribution	8
	Bound-free redistribution	8
	Free-free redistribution	8
	Thomson and Rayleigh scattering	8
	Extinction and emissivity	8
	Source function	9
	Line source function	10
	Transfer equation along the beam	10
	Transfer equation in optical depth	10
4	LTE: Holweger models	11
5	NLS: Auer & Mihalas models	12
6	NLS+NLW: Avrett models	12
7	NLS+NLW+NLT: Oslo simulations	14
	1D HD RADYN simulation	14
	2D MHD Stagger simulation	15
	3D MHD Bifrost simulations	15
8	NLS+NLW+NLT chromosphere spectrum	16
	Quiet chromosphere	16
	Active chromosphere	16
	Chromospheric and coronal heating	17
9	Conclusion	17
	Acknowledgments	18
	Detailing notes	18
	References	50
	Version history and status	56

12	equivalent temperatures
13	intensity calibration
70	Schuster-Schwarzschild approximation
48	Milne-Eddington approximation
37	contribution, response, sensitivity
23	extinction diagrams, H-minus
27	deepest wavelengths
22	white-light corona
16	dielectronic ionization and recombination
24	emission measure, DEM
25	multi-DEM analysis
34	coronal clouds
35	sophisticated clouds
28	$\sqrt{\epsilon}$ law
29	$\sqrt{\epsilon}$ validity
31	epsilon is small: ALI, acceleration, net radiative bracket
40	no Thomas photoelectric control
30	beware of Menzel departure coefficients
32	photon pumping, lasering, Wien transcription
33	photon loss, no nanoflame heating, photon suction
49	spectral interlocking
50	line haze modeling
19	detour and cross redistribution
51	Fe I 6302 Å polarimetry doublet
51	Mg I 4571 Å
18	Ba II 4554 Å
18	Mn I lines as activity monitor
36	Na I D, Mg I b, Ca II 8542 Å heights
41	H α photosphere and chromosphere visibilities
17	Ca II H & K core reversals
63	Ca II K _{2V} and CN spectroheliograms
45	Mg I 12 micron emission lines
49	optical Fe I lines with $S \approx B$
49	weak Ce II and Fe II emission lines
70	He I D ₃ off-limb
96	optical He I lines
72	Rydberg HI lines
99	Rydberg HI candidate for ALMA
55	RE upper photosphere

Yellow-page detailing notes, roughly grouped

- 2 other texts
- 7 ADS page opening, silly publishers
- 9 quanta, bosons, photons
- 8 spectral bandwidth and vision

- 44 classic abundance determination
- 47 NLTE masking
- 56 Fe ionization in VALIIC
- 57 ALC7 line formation plots
- 71 Ha–Ha scattering
- 71 ALC7 H α – Ca II 8542 Å comparison
- 64 Carlsson–Stein shocks
- 65 Carlsson four-panel breakdown
- 66 internetwork clapotisphere
- 74 internetwork shocks in Ca II H and H α
- 68 internetwork acoustics with ALMA
- 42 MCs, network, plage, faculae
- 69 bright-point shifts 1600–1700 Å
- 79 internetwork fields
- 70 Lockyer chromosphere, He I D₃, flash color
- 80 spicules-II
- 81 RBE–RRE–fibril ionization-recombination
- 60 quiet-Sun H α scenes
- 82 quiet-Sun SDO images
- 77 photosphere, chromosphere, corona: hydrogen ionization
- 78 no transition region
- 84 transition radiation, sheath ionization, coronal contact cooling
- 86 SoLO campfires
- 85 CBP foot visibility
- 93 IBIS–SDO active-region blinker
- 20 dark EUV features
- 73 dynamic fibrils
- 92 active-region moss
- 91 EBs and FAFs
- 94 around and upward heating
- 95 FIP effect
- 97 Ly α dream
- 98 Ly α features
- 100 filament blobs
- 21 ALMA as thermometer
- 68 internetwork acoustics with ALMA
- 87 quiet chromosphere with ALMA
- 99 Rydberg H I candidate for ALMA
- 88 ALMA – H α – SDO alignment
- 89 ALMA – GONG – SDO alignment
- 90 ALMA – SOLIS – SDO alignment
- 14 optical spectrum atlases and line lists
- 46 plane-parallel atmosphere files
- 44 Kieler program for 1D LTE spectrum synthesis
- 54 Pandora program for 1D NLTE spectrum synthesis
- 38 MULTI program for 1D NLTE spectrum synthesis
- 39 MULTI3D program for 3D NLTE spectrum synthesis
- 59 RH program for 1D-2D-3D NLTE–PRD spectrum synthesis
- 75 Bifrost program for 3D radiative MHD simulation
- 76 public Bifrost star
- 26 CHIANTI package for CE analysis
- 58 my IDL programs
- 83 SDO – STX alignment programs
- 10 solar telescopes
- 11 solar image restoration
- 15 solar neutrinos
- 61 seismology success story
- 62 no gravity-modes success story
- 67 no coronal heating by acoustic or gravity waves
- 17 Wilson–Bappu effect
- 79 basal flux
- 53 LTE diehard
- 52 illustrious quartet
- 1 personal background
- 3 posting course notes
- 4 projection technology
- 5 mainframe computing
- 6 personal computing
- 43 Bilderberg study week on the quiet photosphere

1. Preamble: on-line format and on-line material

This is a compact graduate-level course on solar spectrum formation.¹ It is display-oriented adding many figures to basic equations but for brevity and to avoid repetition this text contains only few figures and equations, instead linking to [webposted teaching material](#) and [public publications](#).² I therefore recommend on-screen ereading with web access.³

The links make this compendium Wikipedia-style multi-layer: you may delve deeper by opening linked graphs, equations, references that suit your interest. In addition this is a two-tier text with a relatively straightforward presentation in the main text (p. 5-17, contents above) but detailing specific topics in yellow-page elaborations⁴ (p. 18-49, list above).⁵ There is no subject or name index because your pdf viewer offers search. Items easily found in Wikipedia are not detailed here.

The links and two-tier format invite study at different levels:

- read only the six pages on radiative transfer basics (*Sect. 3*) and go through the corresponding [SSF](#) equation displays for a theory overview (as I did in my zoom lecturing). Readers only interested in optically thin spectrum formation may stop already at the separation point (p. 9); for thicker readers the graphs of line formation in the didactic ALC7 star (*Sect. 6*) starting at [[SSX \(pdf 79\)](#)] are suited exercise material, with exam in [[SSF \(pdf 113\)](#)];
- also read the main text of *Sects. 4–7* with [SSX](#) example inspections for an overview of classic developments;
- also study detailing endnotes and their sources on topics of interest to you;
- brainwash your brain by draining mine in reading everything and opening each linked page and studying all references for a full-fledged full-semester comprehensive course on many

¹ Except high-energy spectra, radio spectra, polarization spectra, particle spectra. For high-energy radiation start with [Rybicki and Lightman \(1986\)](#). For radio diagnostics start with [Gary and Hurford 2004](#); they were treated by P.K. Manoharan in this school. For polarization and spectropolarimetry (treated by Rohan Eugene Louis and Debi Prasad Choudhary) [del Toro Iniesta \(2007\)](#) is a clear introduction, [Landi Degl’Innocenti and Landolfi \(2004\)](#) the comprehensive bible, C.U. Keller’s lectures at the [2009 Dwingeloo school](#) a summary. For high-energy particles see [Reames \(2021\)](#). Neutrinos are largely done (*endnote 15*).

² Weblinks are blue, internal crosslinks are maroon. Weblinks open the desired page, not a roundabout path as for “on-line material” or a silly-publisher maze (*endnote 7*). Acrobat may need web access in Preferences > Trust Manager. The suggestion is to open blue links (best in a browser parallel to your pdf viewer) till you are blue in the face – meaning lack of sub-skin scattering (‘tis [all scattering](#) here) by blood drained [too far from your brain](#).

³ An off-line or slow-connection alternative is to download my files first, open them in parallel, and use the pdf page number specified in every link. This may especially suit [SSX](#) which is the largest – but this recipe is no good for the many other page and abstract openers.

⁴ Navigation: yellow endnotes are linked in the main text with maroon bold-italics topic definers. Each ends with a return link [Main call] to avoid getting marooned there and a link [Back] that also returns there or back to another link that you used – working in Firefox, Ubuntu acroread and xpdf, macOS Preview but not in Ubuntu evince, chrome, macOS Safari (try the back button instead). Footnotes are just that (plenty, my trademark I’m told). Their number jumps back to their call.

⁵ Naturally a personal selection favoring topics that I have been involved in and references and figures I knew best and came first to mind in this writeup for the [Calicut school](#). Plus reminiscences from my half century in solar physics.

intricacies of solar spectrum formation and some underlying solar physics, with this text serving as convenient pointer and page and reference opener;

- when no longer a student but a researcher (doctor?) and/or teacher (saint?) this text may serve as page- and reference-opening resource in taking your pick in Khayyam-wise refreshing arguments you heard before.

My [online teaching material](#) used here amounts to nine files listed and linked at the top of [Table 1](#) [[1 personal background](#)].

The first three are lecture notes. ISSF was a bachelor-level introduction to [Sac Peak](#) summer students in 1993. IART was my Utrecht course for second-year bachelors students, written in Dutch in the 1980s, translated by R.C. Peterson in 1992 and revived by L.H.M. Rouppe van der Voort in 2015. It follows [Rybicki and Lightman \(1986\)](#) with most emphasis on explaining their first chapter summarizing basic RT up to NLS treatment. RTSA was initially written in 1995 for my Utrecht masters course, intended as an easier-to-read rehash of [Mihalas \(1970\)](#) [[2 other texts](#)] with emphasis on solar NLS $\sqrt{\epsilon}$ scattering and adding NLW in particular for solar bound-free continua. I immediately made it web-available [[3 posting course notes](#)]. The 2003 update (still incomplete) is linked at [ADS](#) and therefore most frequently used but at Oslo and elsewhere IART is preferred as broader course material. None of these courses includes NLT nor multi-level detours while these are now appreciated as key ingredients of chromospheric spectrum formation. I included them in more recent summary tutorials ([Rutten 2017a](#), [Rutten 2019](#)) and do so here: this text represents an update.

The next three files in [Table 1](#) are sets of projection displays that I use in teaching since the passing of the viewgraph era⁶ [[4 projection technology](#)]. [Figure 2](#) shows an example. SSI is bachelors level, SSF and SSX are masters–graduate level. These also contain newer aspects. I showed a selection in my workshop lectures.

The final three linked files in [Table 1](#) are practicals. They date back to the 1990s⁷ and therefore use IDL but are easily coded in Python [[5 mainframe computing](#)] [[6 personal computing](#)]. I recommend SSA and SSB, designed to accompany IART, for fresh RT students to gain hands-on insights. The third is a practical for RTSA developed by former graduate students that still awaits conversion into proper SSC format.

Here I refer and link to these nine files for equations and graphs that otherwise would swamp this text. In oral 3D bodily-on-the-spot teaching I would project and discuss these; here you should open and scrutinize them yourself.

Navigation: links to these nine files (square-bracketed blue) should open the particular page in your browser. Similarly, blue links to ADS-accessible literature should open the cited page⁸ [[7 ADS page opening, silly publishers](#)]. The citations themselves should open the ADS abstract page.⁹

⁶ The [RTSA equation compendium](#) still supplies 90 viewgraph pages copying all RTSA's 545 labeled equations. The first few are empty. I used to overhead-project ([endnote 4](#)) them next to the blackboard.

⁷ Secondary teaching goals were to start students on IDL ([beginner instruction](#)), [image and Fourier processing](#), [time-sequence analysis](#), article-like [report writing](#) using latex and bibtex, giving [presentations with viewgraphs](#).

⁸ With most pdf viewers, but some may instead shunt you to the first page. This may also happen for pay-walled publications even with a license ([endnote 7](#)). For such I add the pdf page number for manually going to the cited page.

⁹ Using the `\citeads` commands in [these recipes](#). They make a classic reference list superfluous except for the few non-ADS non-WWW pub-

Table 1. Acronyms and abbreviations, roughly grouped.

ISSF = introduction to solar spectrum formation
IART = introduction to astrophysical radiative transfer
RTSA = radiative transfer in stellar atmospheres
SSI = introduction to solar spectrum formation
SSF = solar spectrum formation theory
SSX = solar spectrum formation examples
SSA = stellar spectra A (Cannon – Payne – Minnaert)
SSB = stellar spectra B (Avrett – Chandrasekhar – Unsöld)
SSC = stellar spectra C [Mihalas – Judge – Feautrier]
LAR-1 = <i>Lingezicht Astrophysics Report 1</i> (Rutten 2020)
RT = radiative transfer ~ summed fermion-boson changes of I_ν
TE = thermodynamic equilibrium ~ detailed balance in all
SB = Saha-Boltzmann population equilibrium ($\rightarrow S_\nu = B_\nu$)
SE = statistical equilibrium \equiv sum net population rates zero
LTE = local thermodynamic equilibrium \equiv SB populations
NLTE = no LTE = non-LTE ~ no SB but still SE
NSE = no SE = non-E = NEQ ~ populations with memory
RE = radiative equilibrium $\sim \int \alpha_\nu [S_\nu - J_\nu] d\nu = 0$
CE = coronal equilibrium ~ SE + thin collisional creation
DEM = differential emission measure = CE density part j_ν
EM = emission measure $\equiv \int DEM(T) dT$
FIP = first ionization potential = neutral-atom ionization energy
NLS = non-local in space ~ J_ν important
NLW = non-local in wavelength ~ other J_ν important
NLT = non-local in time ~ NSE with some memory
CS = coherent scattering ~ monofrequent, monochromatic
CRD = complete redistribution ~ resample extinction profile
PRD = partial redistribution ~ mix CS and CRD
HD = hydrodynamics ~ no magnetism
MHD = magnetohydrodynamics ~ single-fluid HD + B
UV = ultraviolet e.g., AIA 1600 & 1700 Å
EUV = extreme ultraviolet ~ shorter AIA wavelengths
DOT = Dutch Open Telescope @ La Palma, 0.45 m
SST = Swedish 1-m Solar Telescope @ La Palma, 1 m
DKIST = Daniel K. Inouye Solar Telescope @ Maui, 4 m
SDO = Solar Dynamics Observatory @ space
AIA = Atmospheric Imaging Assembly @ SDO
HMI = Helioseismic & Magnetic Imager @ SDO
IRIS = Interface Region Imaging Spectrograph @ space
ALMA = Atacama Large Millimeter Array @ Chajnantor
MC = small kilogauss magnetic concentration (“fluxtube”)
RBE = rapid blue-shifted excursion in blue wing $H\alpha$
RRE = rapid red-shifted excursion in red wing $H\alpha$
CBP = coronal bright point ~ small hot quiet-Sun loop group
EB = Ellerman bomb (or burst, heed footnote 144)
FAF = flaring active-region fibril e.g., in AIA 1600 Å

2. Introduction

Understanding solar spectrum formation is necessary to understand our star. The state of its matter is relatively simple: just gas, no fluids nor solids, even close to ideal. However, complexity is brought at wide-ranging spatiotemporal scales by dynamics and electrodynamics with ionization and charging varying from none to full. The resulting structures and features may vary from fully transparent to extremely opaque between different spec-

fications. I do add one (p. 50-56) but with titles, bibcodes for copy-paste into your `\citeads` calls and links as in my [solar physicist publication lists](#), which with my more useful [solar abstract collection](#) are a byproduct of my [wholesome bibtexing](#) with my entire [bibfile collection](#).

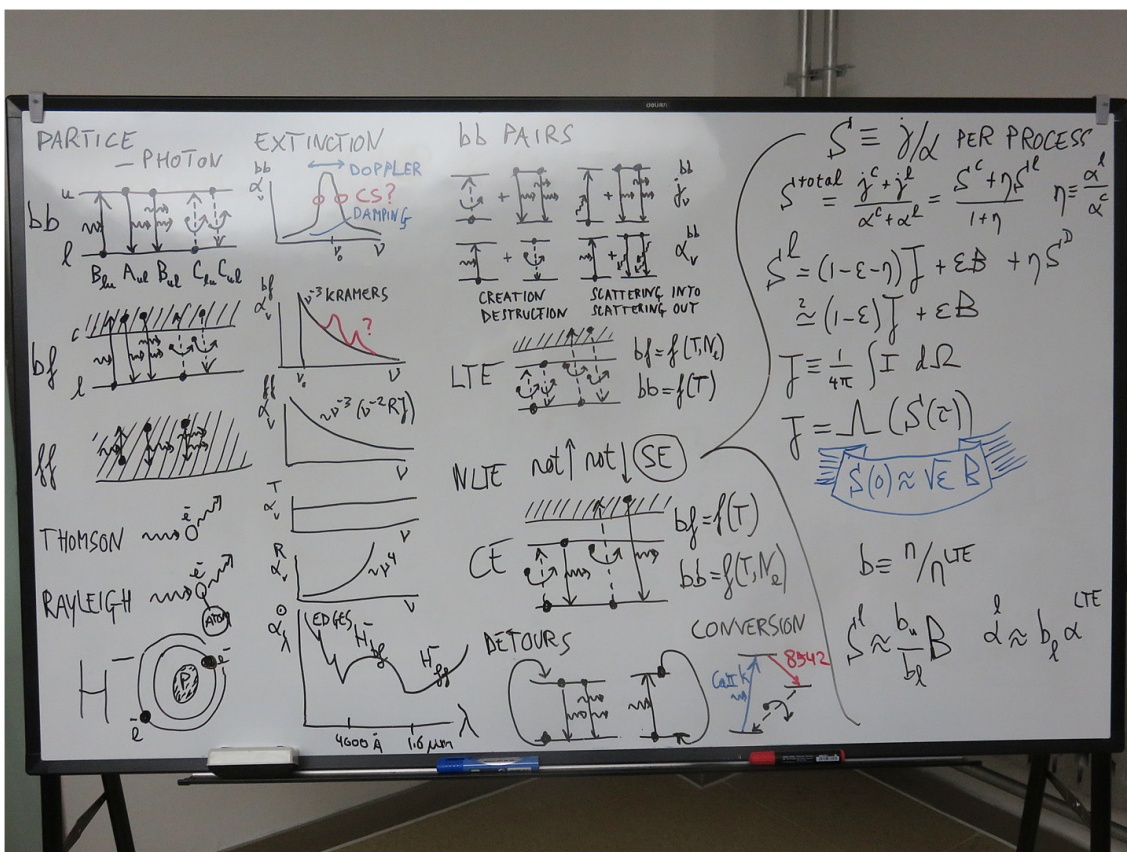


Fig. 1. Snapshot course summary, October 2018, Shandong University, Weihai. First column: particle–photon processes. Second column: corresponding extinction profiles. Third column: process pairs. Last column: key equations. The first word is already wrong but nevertheless I publicly signed this painting.

BASIC QUANTITIES

Monochromatic emissivity
 $dE_\nu \equiv j_\nu dV dt d\nu d\Omega$ $dI_\nu(s) = j_\nu(s) ds$
 units j_ν : $\text{erg cm}^{-3} \text{s}^{-1} \text{Hz}^{-1} \text{ster}^{-1}$ I_ν : $\text{erg cm}^{-2} \text{s}^{-1} \text{Hz}^{-1} \text{ster}^{-1}$

Monochromatic extinction coefficient
 $dI_\nu \equiv -\sigma_\nu n I_\nu ds$ $dI_\nu \equiv -\alpha_\nu I_\nu ds$ $dI_\nu \equiv -\kappa_\nu \rho I_\nu ds$
 units: cm^2 per particle (physics) cm^2 per $\text{cm}^3 =$ per cm (RTSA) cm^2 per gram (astronomy)

Monochromatic source function
 $S_\nu \equiv j_\nu / \alpha_\nu = j_\nu / \kappa_\nu \rho$ $S_\nu^{\text{tot}} = \frac{\sum j_\nu}{\sum \alpha_\nu}$ $S_\nu^{\text{tot}} = \frac{j_\nu^c + j_\nu^l}{\alpha_\nu^c + \alpha_\nu^l} = \frac{S_\nu^c + \eta_\nu S_\nu^l}{1 + \eta_\nu}$ $\eta_\nu \equiv \alpha_\nu^l / \alpha_\nu^c$
 thick: (α_ν, S_ν) more independent than (α_ν, j_ν) stimulated emission negatively into α_ν, κ_ν

Transport equation with τ_ν as optical thickness along the beam
 $\frac{dI_\nu}{ds} = j_\nu - \alpha_\nu I_\nu$ $\frac{dI_\nu}{\alpha_\nu ds} = S_\nu - I_\nu$ $d\tau_\nu \equiv \alpha_\nu ds$ $\tau_\nu(D) = \int_0^D \alpha_\nu ds$ $\frac{dI_\nu}{d\tau_\nu} = S_\nu - I_\nu$

Plane-parallel transport equation with τ_ν as radial optical depth and μ as viewing angle
 $d\tau_\nu \equiv -\alpha_\nu dz$ $\tau_\nu(z_0) = -\int_\infty^{z_0} \alpha_\nu dz$ $\mu \equiv \cos \theta$ $\mu \frac{dI_\nu}{d\tau_\nu} = I_\nu - S_\nu$

[start](#) [index](#)

Fig. 2. Screenshot of [SSF (pdf 23)]. SSF offers 119 similarly-styled theory displays (with a negative evaluation in [SSF (pdf 120)]). SSX offers 185 example displays. SSI offers only 16 introductory displays – you might start with these. The light-blue button *start* at bottom left should open the contents overview, *index* at bottom right a thumbnail index. The display title may return to the previously shown one. For me most figures open full-page when I click on them and many blue linkers open figures, images, blinkers and movies elsewhere in my laptop – hence not for you.

tral samples. Using the emergent spectrum as diagnostic to solar structures and solar happenings requires full elucidation of radiative interactions within the solar atmosphere. Observation, theory and simulation constitute the three-fold way to enlightenment. Shortcuts as 1D, 2D, LTE, CE, SE may be misleading into dead ends.

Brief history: the solar spectrum caused the dawn of astrophysics in the nineteenth century in the hands of Fraunhofer, Herschel, Bunsen and Kirchhoff [SSF (pdf 3)] and others. Followed by stellar spectrum classification [SSF (pdf 6)] at Harvard by many ladies [SSF (pdf 5)] but foremost Cannon [SSF (pdf 7)] – I invite you to now do practical SSA 1.1 (pdf 5) before reading further.¹⁰ In the twentieth century stellar spectrum interpretation evolved from basic concepts to understanding with Schwarzschild, Russell, Milne, Eddington, Minnaert, Chandrasekhar and others. Major breakthroughs were Payne’s demonstration with the Saha law that Cannon’s classification represents temperature ordering [SSF (pdf 57)], the Pannekoek–Wildt–Chandrasekhar identification of H^- as major continuous opacity provider (endnote 23), and Grotrian’s establishing the outrageous high temperature of the corona (endnote 22). Solar spectrum interpretation went from LTE (Unsöld, endnote 53) to NLTE with Menzel, Thomas, Athay, Hummer, Jefferies, Mihas, Avrett and others. Then started (M)HD simulation modeling by Nordlund, Schüssler, Stein, Carlsson, Steiner and others with spectral synthesis programs by Carlsson, Uitenbroek, Heinzel, Leenaarts, Pereira and others, presently emphasizing the new frontier of NLT interpretation. ADS serves nearly all their works.

This text gives an overview dividing radiative transfer (RT) complexities between nonlocal in space (NLS), nonlocal in wavelength (NLW), nonlocal in time (NLT). Solar physicists generally appreciate NLS better than NLW and NLT least.

NLS means that radiation received from the location we are studying is influenced by local radiation there that came from elsewhere. It is daily familiar to us since our daytime outdoors is NLS illuminated. Whether sunshine or overcast, all photons we see were made in the Sun and made it into our eyes by scattering, mostly multiple. As NLS as it can get! Very much out of LTE since the radiation temperature is about 6000 K, higher than our local 300 K [8 *spectral bandwidth and vision*].

NLW means that radiation received from the location we are studying is influenced by radiation at other wavelengths at that location. We do not suffer NLW because sunshine scattering around us is monochromatic (monofrequent): every detected photon still has the energy (frequency, color) with which it left the Sun. All solar Fraunhofer lines also reach our retinas unmolested (but disk-averaged and unnoticed¹¹). We see the sky blue and the setting Sun red not because of underway color change but because Rayleigh scattering off molecules has higher probability at shorter wavelength. The green flash¹² combines that with larger refraction in the blue.

NLT means that radiation received from the location we are studying is influenced by what happened there or thereabouts beforehand. We suffer outdoors NLT because our sunshine is eight minutes retarded – but the same for all photons so we don’t care.

¹⁰ Cut and order [these spectral ribbons](#) (pdf 7). Young kids often do this illuminating rediscovery exercise from Zwaan better than [solar colleagues](#) by sorting spectra without prejudice. Cannon’s “early – late” suggests counting lines as wrinkles or by element number. [*Spoiler: answer.*] In actual teaching I then present [SSF (pdf 2)]–16. The eye-opening Payne part is treated in practical SSA2 (pdf 9).

¹¹ Even when you look at your beloveds although they get so richly adorned: 27500 colorful lines (not wrinkles) visible on their face!

¹² My most beautiful was from the Neemach Mata temple in Udaipur.

Solar NLS defines outward decline of line source functions¹³ that is well exemplified by the Na I D lines and most exemplified by $Ly\alpha$, but it also brightens ultraviolet continua in and from the solar atmosphere [SSF (pdf 109)]. More below.

Solar NLW is exemplified by most atomic lines having opacity deficiencies up to an order of magnitude from sensing the scattering ultraviolet continua in ionization. This is less commonly appreciated, for example not in profile-fitting “inversion” codes nor in spectral irradiance modeling. More below.

Solar NLT is exemplified by solar $H\alpha$ which is a NLS $\sqrt{\epsilon}$ scattering line but it is also NLW because $Ly\alpha$ defines its extinction (opacity) and a loop ionizing per scattering Balmer continuum from $n=2$ with cascade recombination back to $n=2$ including $H\alpha$ photon losses contributes to its source function. It is also NLT because this loop is controlled by the n_2 population which lags badly in gas that was first heated and then cools, as happens continuously in the dynamic structures constituting the solar chromosphere and even in long-lived filaments/prominences (endnote 100). Solar NLT can reach many orders of magnitude but is ignored in almost all modeling by invoking statistical equilibrium (SE). More below.

I summarize the theory in Sect. 3, followed by classic developments in order of complexity in Sects. 4–7. The extremes of solar spectrum formation are easiest: LTE in the deep photosphere, CE in the corona. In between is the hardest nut to crack: the NLS+NLW+NLT spectrum of the chromosphere discussed in Sect. 8.

3. RT basics

The figures on the preceding page show didactic overviews of this section. Table 1 specifies acronyms I bombard you with¹⁴. A summary of main RT quantities and equations is in the [RTSA RT Rap (pdf 275)] and [SSF (pdf 107)].

Intensity. The basic RT quantity is specific intensity I_ν , describing energy in a beam of photons at a given location at a given time at a given frequency in a given direction, measured per units of area, time, frequency bandwidth and beam spreading [ISSF Sect. 3.1 (pdf 9)] [IART Sect. 2.1 (pdf 22)] [RTSA Eq. 2.1 (pdf 29)]. The last is hardest, [ISSF Fig. 2 (pdf 8)] may help. It ensures that intensity does not vary with travel distance [SSF (pdf 25)], the macroscopic way to express that photons do not decay and may travel through the whole universe, not hindering one another being bosons [9 *quanta, bosons, photons*], to most informatively convey the whole universe to us for inspection with splendid spectral encoding to measure distance of and conditions in the source wherever it is.¹⁵

¹³ I call this $\sqrt{\epsilon}$ scattering after the blue-bannered equation in Fig. 1 which results for isothermal constant- ϵ atmospheres from the 2-level simplifications of Eq. 3 and Eq. 4 below. More in endnote 28.

¹⁴ It would be good to hover your cursor over an acronym to Wikipedia-style pop up its meaning. I have tried latex command pdftooltip in pdfcomment.sty for such popups but they worked too different between pdf viewers.

¹⁵ History: the stupendous insight that spectroscopy permits measurement of local atomic properties in faraway objects independent of distance came to R. Bunsen on his evening stroll with G. Kirchhoff along the Philosopher’s Path in Heidelberg after they had pointed their spectroscope from their laboratory window at a fire in nearby Mannheim and detected barium and strontium in it, inspiring the idea that all Fraunhofer lines that do not darken at sunset from being terrestrial describe the same elements within the Sun as those giving bright lines at their specific refrangibilities (wavelengths) when sprinkled in their Bunsen-

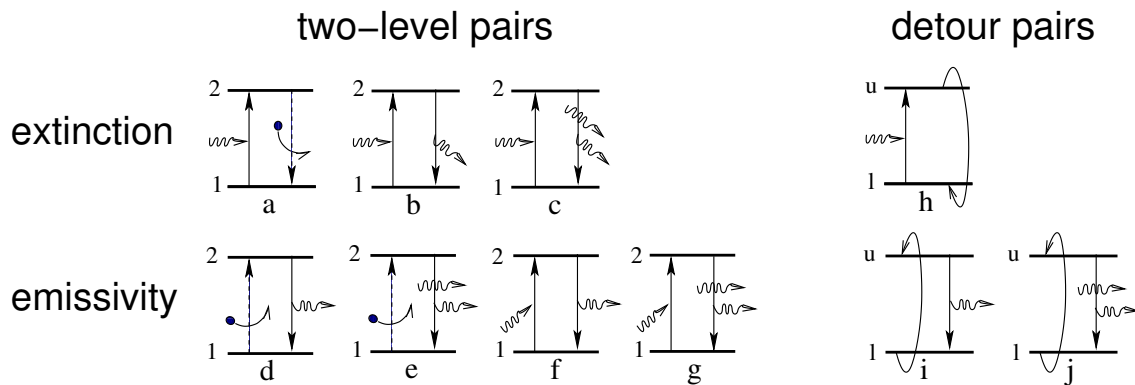


Fig. 3. Atomic transitions governing line formation arranged in photon-involving pairs. The intensity in the beam of interest travels from left to right. All photons drawn here are at the line frequency = jump energy. The pairing categorizes what may happen to an atom after excitation (at left in each pair). It won't stay excited long, for a 2-level atom only between $1/A_{ul} \approx 10^{-8}$ s (resonance) and $1/A_{ul} \approx 10^{-2}$ s (forbidden) until **b**, **d** or **f** occurs spontaneously, yet shorter if the atom while excited meets a deexciting collider **a** or an inviting akin photon to join on its way (**c**, **e**, **g**). Multi-level detour paths (righthand cartoons) combine other-wavelength transitions involving other levels and may include analogous bound-free transitions. There may be radiative or collisional deexcitation to another lower level or radiative or collisional excitation to a higher level including ionization and recombination. Other transitions eventually return the atom to the start-off level l . There may be endless up-down scattering in between so the detour possibilities are infinite. The upper row shows pair combinations contributing to line extinction: collisional photon destruction (**a**), scattering out of the beam (**b** and **c**), photon conversion out of the beam (**h**, into other-wavelength photons and/or kinetic energy). The lower row shows pairs contributing to line emissivity: collisional photon creation (**d** and **e**), scattering into the beam (**f** and **g**), detour photon production into the beam (**i** and **j**). Pairs **c** and **g** have equal probability by requiring one photon in the beam and one with arbitrary direction.

Common sense suggests that the Sun is brighter than a distant star, but that is irradiance which is flux [SSF (pdf 24)] [RTSA Eq. 2.4 (pdf 30)] not measured per unit of beam spreading (solid angle [RTSA Fig. 2.1 (pdf 30)]). If the distant star is solar-type it shows the same intensity, also when your time-travel starship parks you just above its surface.¹⁶ If your giant ground-based telescope resolves it the stellar intensity in the focus is the same as the solar intensity in the focus of photon-starved DKIST [10 solar telescopes] [11 solar image restoration].

At far-infrared, mm and radio wavelengths the Planck function simplifies to the Rayleigh-Jeans limit [SSI (pdf 3)] so that the intensity of an optically thick object with an LTE source function equals its temperature – if calibrated into absolute units. In the optical and shorter-wavelength domains the Wien non-linearity implies that intensity contrast comparisons between different wavelengths in terms of temperature need conversion into brightness temperature [12 equivalent temperatures] which requires absolute units [13 intensity calibration] as in the optical spectrum atlas of Neckel (1999) [14 optical spectrum atlases and line lists] and the ultraviolet spectrum atlas of Curdt et al. (2001).

Matter–radiation interactions. Photons live forever¹⁷ after their creation unless they meet fermions and interact. Also their creation is fermion business. For atoms, ions and molecules the photon-involving processes are bound-bound transitions producing spectral lines and bound-free and free-free transitions producing continua. In addition there are Thomson scattering of existing photons by free electrons and Rayleigh scattering of

burner flame (W. Gratzer, Eureka and Euphorias p. 138). Kirchhoff later honorably quoted Herschel (1827): “colours communicated by the different bases to a flame afford, in many cases, a ready and neat way of detecting extremely minute quantities of them” but with his laws [SSF (pdf 3)] founded astrophysics elaborated here.

¹⁶ If our universe were infinite, eternal and filled with stars our night sky would be boringly solar-bright everywhere, also in neutrinos.

¹⁷ Heeck (2013) concludes (pdf 4) that they live at least 3 years – in their rest frame, meaning 10^{18} years for us.

existing photons by bound electrons. These processes can provide local emissivity or extinction changing the intensity in a given beam, in particular the intensity along the “line-of-sight” towards our telescope. Other photon-producing or photon-affecting processes may be ignored for the solar atmosphere unless you are a radio astronomer (cyclotron, synchrotron, plasma radiation) or high-energy astronomer (pair annihilation).

Photons being bosons means that they like to sit in the same place and therefore that any interaction producing or scattering a photon has a stimulated addition in which the new or scattered photon coherently accompanies similar passing radiation that enhances the interaction probability. This contribution scales with $\exp(-h\nu/kT)$, negligible in the Wien limit [SSI (pdf 3)]. For scattering it has the same probability between extinction and emissivity (pairs **c** and **g** in Fig. 3).

Bound-bound, bound-free, free-free interactions. The five bound-bound interactions are spontaneous photo-deexcitation, photo-excitation, induced photo-deexcitation, collisional excitation and collisional deexcitation measured with the Einstein coefficients A_{ul} , B_{lu} , B_{ul} , C_{lu} , C_{ul} . The radiative first three are transition properties that do not depend on circumstances (by keeping the local photon supply outside the B definitions). Einstein therefore derived their ratios assuming strict detailed balance (valid only in ideal TE) and declared these valid anywhere so that A_{ul} (or the classical oscillator strength f) is the single radiative probability parameter [SSF (pdf 70)], [ISSF Sect. 5.1 (pdf 23)], [IART Chapt. 5 (pdf 60)], [RTSA Sect. 2.3.1 (pdf 39)].

The same five hold for bound-free ionization and recombination with appropriate nomenclature, and the same five hold for free-free interactions (but collisional three-body up or down transitions have no radiative interest).

Pair combinations. Combining the above interactions in successive pairs is so important that I do not refer to Fig. 1 (pdf 3) of Rutten (2019) but copy it here in Fig. 3. It came from [SSF (pdf 105)] and is an extension of [RTSA Fig. 3.3 (pdf 85)] with

multi-level detours. Ca II and H α detour examples are shown in Fig. 2 (pdf 4) of Rutten (2019). With these added this is a complete inventory of how line photons can be locally created and modified in bound-bound manner.¹⁸ Below I refer to these pairs by their alphabetic labels. Similar pair diagrams can be drawn for bound-free transitions (some in Fig. 1).

Equilibria. [SSF (pdf 69)] summarizes bound-bound equilibria with the 2-level simplification at left in Fig. 3. It assumes that any excitation is followed by de-excitation in the same transition, ignoring multi-level NLW and so restricting RT to a single wavelength (CS) or the narrow spectral band covering a single transition (CRD).

TE = “*thermodynamic equilibrium*” describes a homogeneous isothermal fully-enclosed gas where nothing ever happens and where every type of excitation occurs just as frequently as its de-exciting counterpart (“detailed balance”): as many collisions down as up, as many radiative transitions down as up, with all rates defined by the temperature. Maybe this boring paradise occurs approximately at the center of a black hole (bar slow Hawking losses), but not within the Sun since its non-enclosedness implies net outward energy leak from the hot core to the cold universe with the accompanying outward temperature decline through the entire Sun pushing the fusion-produced energy surplus to eventually escape [15 solar neutrinos].

SE = “*statistical equilibrium*” foregoes detailed balancing but requires overall balancing. All level populations are instantaneously balanced at the current ambient temperature, density and radiation without memory of earlier circumstances. For each level the total rate equation [SSF (pdf 75)] [RTSA Eq. 2.100 (pdf 52)] summing changes to its population ends up zero: every moment as much coming in as going out, with excesses between coming in or going out some particular way compensated by other excesses going out or coming in. The SE assumption underlies all following equilibria except NSE.

LTE = “*local thermodynamic equilibrium*” assumes TE at the local temperature while permitting temperature and density gradients and small leaks, clearly a cheap cheat. Its definition is that Saha-Boltzmann (SB) partitioning applies to all populations, as for element Schadeenium¹⁹ in my recommended SSA 2 Cecilia Payne exercise (pdf 9). It is often thought that LTE is defined as equality of the source function S_ν to the Planck function B_ν , but this is a corollary [RTSA Sect. 2.3.2 (pdf 43)] [RTSA Eq. 2.7.3 (pdf 45)]. Colleagues that think this usually ignore or are not aware of NLTE departures in opacities (e.g., for ALMA, *endnote 21*).

LTE holds closely within the Sun and to some extent for many lines and continua in the low photosphere. The condition is that collisions both up and down heavily outweigh photons up and down in Fig. 3 and its bound-free counterparts. Photon destruction **a** and photon creation **d** + **e** must dominate over spontaneous and stimulated scattering, also for all steps in the photon conversion sequences at right. Thus, the photons must behave as “honorary gas particles” (Castor), likewise boxed in to local circumstances; what we observe must be only a small

leak. In SB partitioning the level population ratios sense only the temperature [RTSA Eq. 2.86 (pdf 49)] because the dominating up and down collisions both require one collider so that their density cancels. The ionization stage ratios sense temperature more complicatedly by folding the Boltzmann factor with the Maxwell distribution for the caught electron into the Saha distribution [RTSA Eq. 2.88 (pdf 50)]; they scale inversely with the electron density from the need to catch one.

NLTE = “*no local thermodynamic equilibrium*” is a misnomer. Usually it means relaxing SB while assuming SE with accounting for NLS, less often NLW, much less often NLT. Often named and written non-LTE.

CE = “*coronal equilibrium*” assumes SE but low electron density and absence of local irradiation so that only **d** and its bound-free counterpart remain. All ups are collisional and all downs are spontaneously radiative from lack of impinging particles and photons. Every photon is locally created by a collision obeying the local kinetic temperature. They occur infrequently but in their ground state ions can wait endlessly for suited colliders. After eventual excitation no collider or stimulating photon arrives within the $1/A_{ul}$ decay probability for spontaneous deexcitation. The resulting photon escapes outward to space and may enter our telescope (fat chance), or it drowns inward in the Sun, or it gets bound-free scattered in other gas (more below). In this case the level ratios sense both temperature and collider density since there is only the required up collision without frequent down collision required for LTE. The stage ratios sense only temperature because each ionization is collisional and each recombination is radiative, both requiring a single electron catch. CE and SB are thin versus thick SE partitioning extremes. [SSX (pdf 174)] compares them for photospheric electron density; the SB peaks shift left by about -0.05 in $\log(T)$ per tenfold N_e reduction.

A complication and a boon is that dielectronic excitation must be included beyond the single-electron jump pairings in Fig. 3. The reason is that at coronal temperatures the mean Maxwellian energy is far above the desired standstill value for the free electron to be caught at ionization threshold in one-electron recombination (peak probability in hydrogenic Kramers $\alpha_v^{bf} \sim v^{-3}$ edge decay). The shift of the Maxwell peak to larger energy for higher temperature gives $1/T$ dependence to radiative recombination rates. With dielectronic excitation this too large thermal energy is cut down by using a large part for simultaneous bound-bound excitation of another electron, both in dielectronic ionization up and in dielectronic recombination down. They are multi-level additions behaving in CE as pair **d**: up only collisions, down only spontaneous photons [16 dielectronic ionization and recombination]. The temperature-only sensitivity of CE stage partitioning is therefore maintained; the rate ratio between direct and dielectronic depends only on temperature (Maxwell peak shift). The complication is that many possible bound-bound transitions to high levels must be included and evaluated with CHIANTI (*endnote 26*). The boon is that the dielectronic variants produce photons in many lines including the diagnostics in the AIA EUV passbands and help keep the corona cool through substantial radiative losses. Classical Fig. 1 (pdf 4) of Burgess (1964) shows the high-temperature importance for He I ionization. The radiative rate drops as $1/T$ but the dielectronic rate first peaks two-orders-of-magnitude higher before its $1/T$ decay sets in. Classical Fig. 3 (pdf 20) of Jordan (1969)²⁰

¹⁸ In 3D teaching I draw these cartoons on the whiteboard as in Fig. 1 and point to them all the time. In the blackboard era I drew them with chalk and threw pieces at inattentive students until hitting Minnaert (pdf 2).

¹⁹ Naming: which you can't pronounce. My Utrecht colleague Aert Schadee invented this didactic element. Tini Veltman called his revolutionary algebra solver for the CERN CDC 6600 “schoonschip” (shipshape) to annoy his CERN colleagues on pronunciation.

²⁰ Carole Jordan is the CE counterpart of SB Cecilia Payne, moving to Oxford from Culham rather than to Cambridge USA from Cambridge UK. My SSA exercises should become Annie Cannon – Cecilia Payne

shows its importance for coronal iron partitioning (the lower panel shows partitioning without it from House 1964). The “Jordan versus Payne” CE–SB comparisons on [SSX (pdf 174)] include it also. A nice summary following Burgess (1964) is given in Sect. 6.2.5 (pdf 144) of Jefferies (1968) [17 *Ca II H & K core reversals*].

NSE = “no statistical equilibrium”²¹ admits NLT temporal memory in populations, i.e., not all level population rate equations [RTSA Eq. 2.100 (pdf 52)] sum to zero. The term “non-equilibrium ionization” (often abbreviated to NEQ) usually concerns hydrogen where the actual NLT agent is slow collisional settling of Ly α in cooling gas whereas H ionization occurs in an SE Balmer loop (more below).

Bound-bound redistribution. On page 2 (pdf 2) Eddington (1929) asked “the crucial question whether light absorbed in one part of a line is re-emitted in precisely the same part of the line”: to what extent a resonance-scattered photon remembers the frequency it had in the preceding photo-excitation (pairs **b**, **c**, **f**, **g**). The one extreme is that it does precisely in “coherent” scattering (CS). In Eddington’s days this was thought to be the rule, but in his landmark thesis²² Houtgast (1942) showed that most solar lines in the visible obey the other extreme, suffering complete redistribution (CRD) meaning complete loss of memory and representing a new sample of the line extinction profile rather than δ -function frequency conservation. CRD is indeed valid for most lines except the strongest (large extinction) whose photons escape high in the atmosphere where collisions governing collisional redistribution (“damping”) are rare. These lines must be described by partial redistribution (PRD) which combines Doppler redistribution in the core (CS in the frame of the atom but an redistributing average over the observed individually-Doppler-shifted photon ensemble) with coherency in the inner wings and collisional redistribution in deeply-formed hence collision-rich outer wings [SSF (pdf 89)]. The principal example is Ly α . Other well-known PRD lines are Mg II h & k and Ca II H & K ([SSF (pdf 92)], [SSF (pdf 93)]). My personal example is Ba II 4554 Å [18 *Ba II 4554 Å and Mn I lines*]. Other strong lines suffer less or no PRD [19 *detour and cross redistribution*].

I must concede that PRD theory remains “not yet” in [RTSA Sect. 3.4.3 (pdf 92)]. Classic: Hummer (1962) [SSF (pdf 90)]. Clearest explanation so far: Chapter 5 (pdf 110) of Jefferies (1968) summarized in [SSF (pdf 91)]. The introduction to Sukhorukov and Leenaarts (2017) is a good literature overview. Recent developments are listed in [SSF (pdf 94)]. Next to frequency redistribution there is also angle redistribution to worry about for moving gas due to its Doppler anisotropy – what gas in the solar atmosphere doesn’t move? See Leenaarts et al. (2012b).

Bound-free redistribution. Bound-free transitions are similar to bound-bound transitions and may be described by the same rate equations [RTSA Sect. 3.2.3 (pdf 68)]. Resonance scattering (radiative up and down in the same transition, pairs **b**, **c**, **f**, **g**) is also the same except that the bound-free spectral extent is much wider and that recombination catches an electron as a fresh sam-

²¹ Naming: I used to write non-E, also in earlier versions of this compendium. Others use NEQ. I switched to NSE analogously to NLTE. If you write non-LTE you might write non-SE.

²² Scanned by A.V. Sukhorukov and put on ADS by me.

ple of the kinetic energy distribution without remembering the energy of the electron kicked out in preceding ionization, hence pairwise only memory of ionization to the threshold but not of the excess above it. Therefore there is always CRD over the ionization edge.

A particular case is bound-free scattering of EUV line photons imaged in narrow bands as by EIT, TRACE, AIA. They may be extinguished in bound-free photo-ionization of HI, He I or He II, most likely followed by spontaneous photo-recombination because the colliding-particle and suited-photon densities are too low for other bound-free equivalents than scattering pair **b**. Through CRD such a bound-free scattered photon not only gets a random redirection but also a new wavelength, most likely near the ionization threshold (probability for HI given by Kramers ν^{-3} decay [RTSA Eq. 2.74 (pdf 45)]), hence far from the line. Bound-free scattering so redirects radiation out of the line of sight and also out of the passband; it may locally darken the narrow-band image (often misnamed “absorption”) [20 *dark EUV features*].

Free-free redistribution. Every collider is a fresh sample of the kinetic energy distribution giving redistribution over the probability ν^{-3} decay [RTSA Eq. 2.76 (pdf 46)], a continuum without threshold. In addition there is no memory of a preceding transition so that pair combinations as in Fig. 3 make no sense. If the kinetic energy distribution is the Maxwell distribution defined by temperature then that fully defines both emissivity (Bremsstrahlung) and extinction so that their ratio (source function) is the Planck function. Thus, free-free transitions always have $S_\nu = B_\nu$, because they are intrinsically collisional.

A particular case is ALMA for which at longer wavelengths the main agent is hydrogen free-free (electrons meeting protons) [SSX (pdf 32)]. ALMA is therefore often appreciated as a thermometer, but it is as often not appreciated that the extinction is likely NLT controlled and may be orders of magnitude above the local SB value, just as for H α . ALMA is a thermometer but without easy knowledge where you stick it [21 *ALMA as thermometer*].

Thomson and Rayleigh scattering. In terms of Fig. 3 these scatterings are described by pairs **b**, **c** and **f**, **g**, none of the others. In the Thomson limit (short of Compton) they still suffer Doppler redistribution. Pairs **c** and **g** cancel in occurrence probability, averaged for Doppler redistribution.

A particular case is Thomson scattering by free electrons making the white-light corona so beautifully visible during eclipses and with LASCO [22 *white-light corona*].

Extinction and emissivity. The extinction coefficient²³ α_ν and the emissivity²⁴ j_ν are the macroscopic ways of quantifying the above processes locally along a given beam with given intensity [SSF (pdf 23)], [ISSF Sect. 3.2 (pdf 9)], [IART Chapter 3

²³ Naming: often called “absorption coefficient” but I follow Zwaan in using “extinction” because the photon is taken out of the particular beam (direction and frequency) but may still exist in another direction (scattering pairs **b** and **c**) or at another frequency (conversion pair **h**). Absorption is then only pair **a**, sometimes called “true absorption”.

²⁴ Naming: Zwaan, Jefferies, Mihalas and others called this “emission coefficient”. I followed them in IART and also while writing RTSA in 1995, but at an Oslo school that summer P.G. Judge used “emissivity” and I realized that that is a better name because it is not a coefficient, not a fraction of something but measuring new radiation.

(pdf 34)], [RTSA Sect. 2.1.2 (pdf 32)]. Extinction is measured as cross-section ($\text{cm}^{-1} = \text{cm}^2/\text{cm}^3$) so it adds up for different processes acting at one wavelength: (multiple overlapping) lines and continua. A photospheric overview is in [SSF (pdf 68)] [23 *extinction diagrams, H-minus*]. The ultraviolet bound-free edges of Si I, Mg I, Fe I and Al I contribute the electrons needed for H⁻ by pairing relatively large abundance with low ionization energy [SSF (pdf 56)], with their joint abundance giving $N_e \approx 10^{-4} N_H$ and keeping the gas near-neutral.²⁵

Line broadening and the Voigt function are summarized in [SSF (pdf 64)] and detailed in [RTSA Sect. 3.3 (pdf 72)].

The strongest disk-center optical lines are Ca II H & K and the Balmer lines (largest dips in the top-right panel of Fig. 10 (pdf 18) of Rutten 2019; extinction comparisons in [SSF (pdf 60)] and [SSF (pdf 62)]).

Optical thickness $\tau_\nu \equiv \int \alpha_\nu ds$ is summed extinction along the beam, with $\tau_\nu = 1$ the 1/e decay separator between optically thin and thick (transparent or intransparent). This is a property of the gas parcel (structure, cloud, layer, shell, object), not of a spectral feature. Effective thickness likewise measures transparency for monofrequently scattering radiation [IART Sect. 7.3.3 (pdf 103)] [RTSA Sect. 2.6.3 (pdf 58)].²⁶

A particular point is that photons contributed by stimulated emission are not counted positively as contribution to emissivity but negatively as contribution to extinction. It facilitates the description because extinction (**a** + **b** + **c** + **h**) and stimulated emission (**e** + **g** + **j**) both need beam photons and therefore similar quantification (Einstein *B* values [SSF (pdf 70)]). Moreover, with this subtraction the cancelation of stimulated scattering pairs **c** and **g** is effectuated. If this isn't done the extinction would be overestimated by including **c** and optical depth scales in the Rayleigh-Jeans domain would suggest larger opaqueness and further out escape than actually the case.

For coronal spectrum formation one usually assumes CE throughout which implies that all extinction is negligible and emissivities can be evaluated without RT. It then suffices to compute and sum all emissivities along the line of sight per wavelength [24 *emission measure, DEM*] [25 *multi-DEM analysis*]. This is done with the CHIANTI package [26 *CHIANTI*].

Thin–thick separation point. If your problem is so optically thin in all its aspects that assuming CE suffices you may stop reading here. Endnotes 16, 20, 22, 24, 25, 26, 33, 34 may cater to you (but beware of my scorn in *footnote 26*).

²⁵ Gaseous matter is mostly plasma throughout the universe but in cool-star photospheres almost all electrons and in our surroundings all electrons are tied to nuclei. We live in an extraordinary neutral environment energized by an extraordinary near-neutral environment.

²⁶ Naming: “optical thickness” is also used for non-optical EUV or radio wavelengths. It expresses the degree of blocking reached by extinction of whatever sort of particular radiation in counterpart to geometrical thickness. “Degree of intransparency” would have been better, with limits transparent versus intransparent = opaque, and with translucent for effectively thin (or the nice “foggy” of Schuster 1905). You should use “optical depth” only for integrated extinction along the line of sight into your feature or radially into your 1D, 2D or 3D model star – too often it is used wrongly for optical thickness. Colleagues that wrongly call a spectral line thick or thin I call “thinnies” derogatorily. How can a line be thin – define a width threshold in Å or Hz or cm^{-1} or km s^{-1} ? A physical structure can be thin or thick or effectively thin or thick in a spectral feature (maybe the Sun is thin in neutrino lines) but no line is ever thin or thick. Never say “*this line is thin*” or earn my scorn!

Source function. I wonder who gave this key non-thin quantity its well-suited name in describing weighted local addition of new photons to a given beam by dividing local emissivity and extinction:

$$S_\nu \equiv j_\nu/\alpha_\nu \quad S_\nu^{\text{tot}} = \frac{\sum j_\nu}{\sum \alpha_\nu}, \quad (1)$$

where the first is per spectral feature as the line in Fig. 2, the second the total for overlapping lines and continua. Their emissivities and extinctions add linearly but the combination ratio weights component source functions [SSF (pdf 23)] [ISSF Fig. 7 (pdf 16)] [RTSA Sect. 2.1.2 (pdf 32)].²⁷ It seems like dividing cows and horses since their dimensions are just [cm^{-1}] versus [$\text{erg cm}^{-3} \text{ s}^{-1} \text{ Hz}^{-1} \text{ sr}^{-1}$], but the resulting dimension is that of intensity [SSF (pdf 23)] which 'tis all about.

The source function is a key quantity for optically thick colleagues (mostly studying the photosphere and chromosphere) because it separates local physics and surround physics, or atomic perspective and environmental quality. Take a strong spectral line, meaning large line extinction coefficient. Its local addition of many bound-bound transitions to continuous transitions at its wavelength adds a high narrow spike in extinction versus wavelength. This is local physics: the required particles must be present in sufficient number set by elemental abundance, partitioning over ionization stages and over atomic levels within stages that is primarily set by temperature and density (closer to SB than to CE), and by the transition probability. In the emissivity there is a similar spike given by lookalike particles in the upper level. In the ratio, however, this spike may vanish completely – as for LTE with the featureless Planck function as ratio. Then the ratio is completely set by the temperature, an environmental rather than an atomic physics quantity. When LTE is not valid the local environment also senses nonlocalness, surely in space (NLS), likely also in wavelength (NLW), possibly also in time (NLT). Thus, optically thick colleagues evaluate local atomic properties to define the extinction which defines where their signal comes from, then evaluate the source function to see what environmental effects may make it depart from the local temperature. This split between asking “Where?” and “What?” is often described as “accounting for NLTE” but too often meaning only for the second.

However, such split interpretation gets mixed when environmental effects also affect the extinction. This happens when that is controlled by other transitions sensitive to source function nonlocalness. The extinction of optical atomic lines being defined by scattering bound-free ultraviolet continua is one example, the dominance of Ly α in controlling H α extinction and ALMA HI free-free extinction is another. In such cases, opacity NLTE gets more important than source function NLTE. Colleagues that see NLTE only as a source function issue may miss the crux of their problem.

Also, the source function is a composite because it is a process property. Multiple processes operating at a given wavelength each have their own source function and combine weighted via the sums in Eq. 1. In the solar photosphere optical lines often combine a scattering line source function with a near-LTE continuous source function because the latter is dominated by H⁻ bound-free interactions. These are not necessarily LTE as is the case for free-free interactions. Ultraviolet bound-free continua get far from LTE but in the optical and infrared the ambient thermal kinetic energy is similar to or exceeds the transition energy

²⁷ The frequency-independence for CRD across a line holds only for S_ν^l , not for S_ν^{tot} weighted with the continuum contribution [RTSA Eq. 2.23 (pdf 33)].

and at sufficiently deep formation collisions reign, making LTE a good approximation [27 *deepest wavelengths*]. The Na I D lines are the darkest lines in the optical spectrum (*endnote 36*) because they are photospheric $\sqrt{\varepsilon}$ scatterers (*endnote 36*). In hotter stars where hydrogen is ionized the reverse occurs: weak LTE lines appear in emission on the dark Thomson-scattering continuum (Fig. 1 (pdf 215) of Rybicki and Hummer 1992). The solar Ca II H & K wings also contain weak emission lines but these are from NLTE interlocked scattering (*endnote 49*) with Fe II 3969.4 Å close to H ϵ the weirdest: it responds deeper than its quasi-continuum near-LTE background (Fig. 8 (pdf 9) of Cram et al. 1980).

Line source function. Most classic treatments of NLTE scattering in the line source function assume a gas of 2-level atoms to keep the description monochromatic (CS) or limited to a single line (CRD). I did the same in RTSA, with a long derivation inventing “sharp-line atoms” enabling monofrequent use of the Einstein coefficients in [RTSA Sect. 3.4 (pdf 84)], an elegant derivation by Zwaan of the $\sqrt{\varepsilon}$ law in [RTSA Sect. 4.3.1 (pdf 112)], and the classic numerical CRD results for this law in an isothermal atmosphere of Avrett (1965) in [RTSA Fig. 4.12 (pdf 128)] [28 *square root epsilon law*]. Isothermal and 2-level seems far-fetched but the $\sqrt{\varepsilon}$ law is often applicable [29 *validity of $\sqrt{\varepsilon}$ law*] and yet more often instructive. An equation summary is shown in [SSF (pdf 79)] and as [RTSA concluding “RT rap” (pdf 275)].

Two-level scattering source function evaluation became a key part of numerical spectrum synthesis with many programs following the key concepts of opposite-direction averaging of Feautrier (1964) [RTSA Sect. 5.2 (pdf 137)] and of operator splitting of Cannon (1973), leading to approximate lambda iteration (ALI) and similar methods [RTSA Sect. 5.3.2 (pdf 145)]. Some of these programs are detailed below in *Sects. 4–6*.²⁸

The extension with multi-level detours is still lacking in my courses, so I add that here. The best descriptions so far are in Sect. 8.1 (pdf 199) of Jefferies (1968)²⁹ and in Sect. II (pdf 1) of Canfield (1971a), both using ratios rather than fractions as probability parameters. Split the line extinction coefficient into the destruction (a for absorption), scattering (s), and detour (d) contributions of Fig. 3:

$$\alpha'_\nu \equiv \alpha_\nu^a + \alpha_\nu^s + \alpha_\nu^d \quad \varepsilon_\nu \equiv \alpha_\nu^a / \alpha'_\nu \quad \eta_\nu \equiv \alpha_\nu^d / \alpha'_\nu \quad (2)$$

where ε is the collisional destruction probability of an extinguished photon and η is its detour conversion probability. With these, the general line source function becomes

$$S_\nu^l = (1 - \varepsilon_\nu - \eta_\nu) J_\nu + \varepsilon_\nu B_\nu(T) + \eta_\nu S_\nu^d \quad (3)$$

for CS and

$$S_{\nu_0}^l = (1 - \varepsilon_{\nu_0} - \eta_{\nu_0}) \overline{J_{\nu_0}} + \varepsilon_{\nu_0} B_{\nu_0}(T) + \eta_{\nu_0} S_{\nu_0}^d \quad (4)$$

for CRD with $\overline{J_{\nu_0}} \equiv (1/4\pi) \iint I_\nu \varphi(\nu - \nu_0) d\nu d\Omega$ the “mean mean” intensity averaged over all directions and the line profile, with ν_0 the line-center frequency and also used as line identifier.

Equations 3 and 4 describe physical contributions to local NLTE divergence between S^l and B . In each the first term represents the reservoir of photons that contribute new photons to the

beam by direct scattering (**f** and **g**), the second describes collisional beam-photon creation (**d** and **e**), the third the contribution of new beam photons via detours (**i** and **j**) which themselves may contain collisional, scattering and also such bound-free steps.

A convenient formal way to quantify $S^l \neq B$ inequality is to use NLTE population departure coefficients $b \equiv n/n_{\text{LTE}}$ for the lower (b_l) and upper (b_u) level [30 *Menzel departure coefficients*]. In the Wien approximation (negligible stimulated emission) these yield the simple relations [SSF (pdf 73)]:

$$\alpha^l \approx b_l \alpha_{\text{LTE}}^l \quad S_{\nu_0}^l \approx (b_u/b_l) B_{\nu_0}(T). \quad (5)$$

The formation graphs for many lines from ALC7 starting at [SSX (pdf 79)] employ these (*endnote 57*).

Equations 3 and 4 show that LTE $S = B$ equality holds when $\varepsilon = 1, \eta = 0$ and/or $J = S^d = B$, both closely correct below the standard $h = 0$ surface at $\tau_{5000}^c = 1$. Above it ε becomes small from lower electron density [31 *epsilon is small*] while η is usually smaller. Most chromospheric lines and bound-free continua are heavily scattering with $S \approx J$ (but free-free continua always have $S = B$ because each interaction is collisional). For such scatterers the two-level simplification $\eta = 0$ is a good approximation but weaker spectral features may suffer detour complications [32 *photon pumping, laser, Wien transcription*] [33 *photon loss, no nanoflame heating, photon suction*].

Transfer equation along the beam. The differential and integral forms are

$$\frac{dI_\nu}{ds} = j_\nu - \alpha_\nu I_\nu \quad I_\nu(\tau_\nu) = I_\nu(0) e^{-\tau_\nu} + \int_0^{\tau_\nu} S_\nu(t_\nu) e^{-(\tau_\nu - t_\nu)} dt_\nu \quad (6)$$

with geometrical thickness s and optical thickness τ_ν measured in the beam direction [ISSF Sect. 3.3 (pdf 12)]. [ISSF Fig. 5 (pdf 14)] treats a spectral line from a homogeneous isothermal cloud with LTE processes, say a galactic HI cloud showing the 21-cm line to a radio astronomer.³⁰ Appreciate how the line grows or sinks with increasing cloud opacity until it hits the $I_\nu = S_\nu = B_\nu$ optically thick limit (more formal graph in [IART Fig. 3.3 (pdf 42)] and [ISSF Fig. 4 (pdf 13)]). Thick isothermal LTE clouds show no lines (as “black holes have no hair”).

Such simple clouds [34 *coronal clouds*] became the basis for “cloud modeling” started by Beckers (1964)³¹ for H α motes on the disk and also much used for filaments. Assuming the cloud homogeneous with Gaussian (“microturbulent”) line broadening yields the classic cloud parameters [SSX (pdf 2)]: line-center optical thickness, line-of-sight velocity, source function, Doppler width, incident intensity profile from below/behind (review Tziotziou 2007) [35 *sophisticated clouds*].

Transfer equation in optical depth. For very optically thick objects as the Sun there is no interest in what impinges the other side since nothing comes through. We therefore flip τ to measure optical depth instead, either along the line of sight ($\tau_{\nu\mu}$) or more often radially into the Sun against height (τ_ν). With this flip the

³⁰ This is the most-shown of my didactic xfig diagrams, also with sloppy attribution to René Rutten, nowadays as Python animation.

³¹ J.M. Beckers (1934–2021) defended this thesis at Utrecht University with M.G.J. Minnaert as formal adviser but did the work in Sydney with R. Giovanelli as effective adviser. At his request I put it on ADS (Beckers 1964). It was printed by the US Airforce because he had already moved to Sunspot where I got to know him – then a solar physics paradise, now a ghost town (Rutten 2018).

²⁸ An online tool for hands-on experimentation with various methods is at <http://rttools.irap.omp.eu> and described by Lambert et al. (2016). It produces plots as [RTSA Fig. 5.2 (pdf 147)] on your screen.

²⁹ Erratum: remove minus in the equation below Eq. 8.8.

radiative transfer equation upsets its source to negative³²:

$$\frac{dI_{\nu\mu}}{d\tau_{\nu\mu}} = I_{\nu\mu} - S_{\nu} \quad \mu \frac{dI_{\nu}}{d\tau_{\nu}} = I_{\nu} - S_{\nu}, \quad (7)$$

the first along the line of sight, the second for viewing angle $\mu = \cos(\theta)$ into a plane-parallel atmosphere [SSF (pdf 23)] [RTSA Eqs. 4.10, 4.11 (pdf 97)], [RTSA Eqs. 4.28-4.31 (pdf 105)]. The corresponding integral “formal solutions” for the intensity $I_{\nu}^{+}(0, \mu)$ that emerges from a non-irradiated atmosphere are

$$\int_0^{\infty} S_{\nu}(\tau_{\nu\mu}) e^{-\tau_{\nu\mu}} d\tau_{\nu\mu} \quad (1/\mu) \int_0^{\infty} S_{\nu}(\tau_{\nu}) e^{-\tau_{\nu}/\mu} d\tau_{\nu}, \quad (8)$$

which are simple and easy to evaluate for LTE but complex and nonlinear when the NLTE scattering and detour terms in Eqs. 2–4 contribute to α_{ν} and S_{ν} involving radiation in other directions, at other frequencies, in other transitions, at other times. Since Eqs. 5 express NLTE deviations in populations an equation system results combining radiative transfer for multiple to many angles and frequencies and population variations for multiple to many species and levels [RTSA Sect. 2.6.1 (pdf 52)]. Solution is necessarily iterative [RTSA Chapt. 5 (pdf 133)], or nowadays through machine learning taught from validated iterative solutions.

The recipe for quick interpretation is to apply the Eddington-Barbier³³ approximation

$$I_{\nu}^{+}(\tau_{\nu}=0, \mu=1) \approx S_{\nu}(\tau_{\nu}=1) \quad (9)$$

with τ_{ν} and S_{ν} the totals [ISSF Eq. 35 (pdf 13)], [IART 321 (pdf 45)], [RTSA Eq. 2.44 (pdf 38)], [RTSA Eq. 4.32 (pdf 106)], [SSF (pdf 29)], [SSF (pdf 51)]. It simplifies the split between asking “Where?” and “What” to a single location.³⁴

The split is valid in LTE making this recipe easiest for LTE in which emergent line profiles map temperature variation with height through Planck-function sensitivity conversion and with extinction-coefficient profile weighting [SSI (pdf 16)]. Absorption lines map outward declining source functions, emission lines increasing source functions. Avrett sketched this sign change for VALIIC lines in [SSX (pdf 36)] with flips from sampling its temperature minimum near 1600 \AA ³⁵ and near $160 \mu\text{m}$. The latter is closer to LTE.

Absorption lines go together with limb darkening [SSF (pdf 51)] [RTSA Fig. 2.4 (pdf 39)], emission lines with limb brightening. Just beyond the limb the first flash-reverse into the latter [RTSA Fig. 7.2 (pdf 168)].³⁶

The “four-panel” diagrams in [SSF (pdf 31)] ff are a cartoon course on Eddington-Barbier spectrum formation with increasing complexity. You should blink the absorption–emission pairs by full-page flipping. Then do the exam on [SSF (pdf 40)], first

³² The source function can go negative in laser (endnote 32).

³³ Unjustly named (Paletou 2018) – as often with Eddington.

³⁴ When you see $I_{\nu} \approx S_{\nu}(\tau_{\nu} = 2/3)$ you read text from an unresolved nighttime colleague confusing flux and intensity [SSF (pdf 29)] [RTSA Eq. 2.7 (pdf 31)]. They also add a telltale π in their B_{ν} definition.

³⁵ The ultraviolet flip from absorption to emission was already described by de Jager (1963). It shows well in [SSX (pdf 34)] from Schefler and Elsaesser (1974). Also note the sign of the Lyman and He I bound-free edges. An LTE-level examination question was why the intensity drops to lower wavelength while the sampled temperature increases.

³⁶ Ca II H & K and the Balmer lines are also the strongest in the optical flash spectrum, but there out of the blue (yellow rather) joined by He I D₃ which is virtually absent on the disk (endnote 96).

for Na I D₂ (answer $h \approx 500 \text{ km}$) and then for the blend. If you decide $h \approx 150 \text{ km}$ for the blend by reading off where its center intensity equals the source function just as for Na I D₂ you are a million times wrong [36 Na I D, Mg Ib, Ca II 8542 Å heights]. Be aware that use of the Eddington-Barbier approximation is often a fallacy [37 contribution, response, sensitivity].

Be also aware that solar-atmosphere structures may be optically thick without being effectively thick so that radiation scatters through. Filaments or fibrils may appear intransparent in H α while illumination from behind is still important. This is even the case for H α in the “chromosphere” plateau of 1D standard models, as in [SSX (pdf 91)] which not only shows $S \approx J > B$ across the model temperature minimum from backscattering but also has photospheric photons scattering through the model chromosphere. This caveat was beautifully demonstrated in Fig. 7 (pdf 7) of Leenaarts et al. (2012a) by comparing 1D H α synthesis for a Bifrost (endnote 75) simulation with MULTI [38 MULTI program] and 3D H α synthesis with MULTI3D [39 MULTI3D program]. In the columnar 1D line synthesis the deep-photosphere granulation is better visible than lower-contrast chromospheric fibrils but in 3D synthesis the granular contrast is smoothed away by lateral scattering [40 no Thomas photoelectric control] [41 H α photosphere and chromosphere visibilities].

The most important equation of classical 1D 2-level scattering is the Schwarzschild equation [RTSA Eq. 4.14 (pdf 98)] defining the Λ operator [RTSA Eq. 4.20 (pdf 101)]; a synopsis is given after Eq. 10 (pdf 9) of Rutten (2019). Its cutoff at the surface produces outward $J_{\nu} < S_{\nu}$ divergence for small inward increase of $S_{\nu}(\tau_{\nu})$ but outward $J_{\nu} > S_{\nu}$ divergence for steep increase [RTSA Fig. 4.2 (pdf 100)], [RTSA Fig. 4.4 (pdf 103)], [RTSA Fig. 4.9 (pdf 121)]. Be aware that steep horizontal gradients are similarly important in 3D radiative transfer. Steep horizontal gradients occur for example already in the photosphere in and above granulation and in and around MCs constituting network and plage [42 MCs, network, plage, faculae]. Obviously they occur in and around the multitude of small dynamic structures constituting the higher atmosphere.

[SSF (pdf 108)] gives a summary of the key line formation equations.

4. LTE: Holweger models

The classic Holweger models (Holweger 1967 and HOLMUL of Holweger and Müller 1974) were a pinnacle of solar LTE interpretation [43 Bilderberg study week]. They replaced curve of growth³⁷ abundance determination by individual line-by-line fitting which became an abundance industry [44 classic abundance determination]. It employed critical ad-hoc adjustment parameters: fake line broadening for duplicating observed line broadening with “microturbulence” [RTSA Eq. 3.80 (pdf 82)] (adding height-dependence as in Fig. 11 (pdf 19) of Vernazza et al. 1981) and “macroturbulence” [RTSA Eq. 3.81 (pdf 83)] (with “radial-tangential” anisotropy added by Gray 1977), and fake wing extension with a collisional damping “enhancement factor”. The Holweger models ignored the existence of the solar chromosphere to avoid self-reversals in strong optical lines [45 Mg I 12-micron emission lines], but nevertheless HOLMUL became highly popular³⁸ with abundance determiners because it worked so well, giving them smaller spread for multiple lines

³⁷ Treated in practical SSA 3 (pdf 28). Fig. 4 (pdf 6) of Rutten and Zwaan (1983) may have been the last solar Fe I one.

³⁸ ADS shows 900+ citations but declining rate this century.

than other standard models of the time [46 *plane-parallel atmosphere files*]. No wonder because the model was made as best fit to photospheric lines, in particular of Fe I, so that fitting similar lines with the model was a self-fulfilling prophecy³⁹, debated Fe abundance itself (e.g., Kostik et al. 1996). Earlier Rutten and Kostik (1982) showed that such model fitting is also self-correcting [47 *NLTE masking*].

So-called “inversion” codes (I find “best-fit” better suited) are automated versions of Holweger’s trial-and-error model derivation procedure [48 *Milne-Eddington approximation*]. Copying Holweger’s fads also copies the fallacies including NLTE masking, an important failure because NLTE scattering in the ultraviolet bound-free edges controls the opacity of minority-species atomic lines throughout the spectrum. In the optical these often have source functions close to LTE through interlocking [49 *interlocking Fe I, Ce II, Fe II lines*] but their interlocked opacities have NLTE deficits up to an order of magnitude from ultraviolet overionization set by steep temperature gradients in deeper layers. This fallacy has been long ignored but was at last addressed by Smitha et al. (2020). Worse: in the actual 3D solar photosphere matter and radiation gradients also occur and act horizontally, requiring 3D line synthesis (see Smitha et al. 2021). Proper quantification of such ultraviolet extinction control is severely hampered by the dense ultraviolet line haze with its own NLTE properties [50 *line haze modeling*]. Stronger lines need NLTE modeling not only for their extinction but also for their source function set by their own scattering or by non-2-level de-tour transitions. When “inversion” codes are proudly advertised as NLTE usually only the modeled-line resonance scattering is meant, not the extinction-affecting scattering in the bound-free continua nor resonance scattering in the line haze affecting those and neglecting LTE forcing by stronger interlocked ultraviolet lines [51 *Fe I 6302 Å doublet, Mg I 4571 Å*].

Holweger’s assumptions of 1D modeling, LTE and no chromosphere were also revived in SATIRE irradiance modeling for network and plage (Unruh et al. 1999) which therefore suffers similarly from mistreating the opacity-affecting NLTE ultraviolet continua and their NLTE line haze. More explanation in Sect. 4 (pdf 11) of Rutten (2019).

The Asplund revolution (Asplund et al. 2009)⁴⁰ ended the HOLMUL popularity, primarily by including simulated granulation (Nordlund et al. 2009 with the foundation laid in Nordlund 1984a) [52 *illustrious quartet*]. Its main effect is that its temperature inhomogeneity upsets the notion that spatially-averaged intensity may be modeled as spatially-averaged temperature because at optical and shorter wavelengths this notion is undone by the Wien nonlinearity of the Planck function (Uitenbroek and Criscuolo 2011). The simulated granulation undid the need for turbulence fudging and better atomic physics (Barklem et al. 2000) undid the need for damping fudging.

Another Asplund ingredient was NLTE spectrum synthesis but yet without detailed spectral synthesis of ultraviolet overionization weakening atomic minority-species lines as reviewed for

³⁹ Not “garbage-in = garbage-out” but model-out \approx model-in propelling its assumptions and limitations. The modern equivalent is machine learning: teaching it with specific sets of models or simulations delivers answers propelling (if not advocating) their fallacies.

⁴⁰ At over 5000 citations one of the most cited publications of solar physics but still less than the 8000+ for its pre-revolution predecessor Anders and Grevesse (1989). If you desire citations you must cater to non-solar colleagues. My most-cited article (Carlsson et al. 1994) was non-solar: stellar lithium abundance determiners outnumber solar spectrum analysts. It was also the most boring, tabling minor NLTE corrections eagerly cited as negligible.

Fe I by Rutten (1988) and quantified from granular/intergranular 1D models by Shchukina and Trujillo Bueno (2001). Such synthesis should be 3D to include also the steep horizontal temperature gradients (Fig. 4 (pdf 6)) by which hotter granules irradiate cooler intergranular lanes in the ultraviolet where the Balmer continuum escapes. This irradiation also causes line weakening and therefore abundance underestimation when neglected; correction may give a shift back towards the classic “high” values (Grevesse and Sauval 1998, non-Springerwalled Grevesse et al. 1996) desired by helioseismologists (review in Sect. 6 (pdf 118) of arXived Christensen-Dalsgaard 2021).

5. NLS: Auer & Mihalas models

NLS is the realm of 2-level modeling treated extensively in [RTSA Chapt. 4 (pdf 95)], numerical developments around the Λ operator summarized in [RTSA Chapt. 5 (pdf 133)], and numerical PRD formalisms “not yet” in RTSA. [SSF (pdf 111)] shows a cartoon summary also shown as Fig. 4 (pdf 10) of Rutten (2019) and discussed in Sect. 4 (pdf 11) there. Non-local scattering makes J depart from B in setting S according to Eq. 3 and Eq. 4, for bound-free continua and for lines of increasing strength (or different parts of strong PRD lines). The ultraviolet continua gain $S \approx J$ excess over the photospheric B decline per Λ [SSF (pdf 86)]. Strong lines obtain low S per Λ from $\sqrt{\epsilon}$ scattering by seeing actual temperature gradients as near-isothermal from τ scale compression (endnote 29).

The classic warm-star HI analyses of Auer and Mihalas (1969a, 1969b) advertised here were an early pinnacle of 2-level modeling [53 *LTE diehard*]. Not purely 2-level since adding the HI continuum level and so including the Lyman and Balmer continua to Ly α in the first publication and to H α in the second. The key results were atmospheric temperature stratifications copied in Mihalas (1970) and in [RTSA Fig. 7.10 (pdf 187)]. A large didactic boon is that the effects of these transitions are well separated in height and therefore distinguishable. “Big whopper” [RTSA exercise 12 (pdf 254)] poses five pages of hard questions on their graphs that I challenge you to answer.⁴¹ The hardest is to understand: “Amazingly, the photon losses in the subordinate Balmer- α line, located in the low-energy red part of the spectrum, cause heating of the whole outer atmosphere of this hot star.” [RTSA (pdf 189)]. Because their graphs did not include J we did a multi-level re-do including Avrett-style S, B, J graphs (pdf 5) and radiative heating/cooling graphs (pdf 6) in Wiersma et al. (2003), giving as answer: “The photon losses in Ba α suck population from the proton reservoir through a collisionally-dominated Rydberg recombination flow and so boost the outward temperature rise” (pdf 7). All yours to understand.

6. NLS+NLW: Avrett models

The various solar-atmosphere models masterminded by E.H. Avrett (called “Pandora stars” below [54 *Pandora program*]) are all classic pinnacles of plane-parallel (1D) NLTE modeling: VALIIM of Vernazza et al. (1976), the VALIII models, in particular quiet VALIIIC, of Vernazza et al. (1981), MACKKL of Maltby et al. (1986), the FAL models, in particular quiet FALC, of Fontenla et al. (1993) and quiet ALC7 of Avrett and Loeser (2008) with an update in Avrett et al. 2015.⁴²

⁴¹ [Spoiler: my answers to most RTSA problems including this one.]

⁴² VALIIIC now has 2100+ citations at increasing rate. Practical SSB 1 (pdf 5) dissects the FALC stratifications with comparison to our own atmosphere which is transparent to sunlight by missing H $^-$ treated in the

Their strength is comprehensive inclusion of many ultraviolet transitions. A weakness is ignoring Wien nonlinearity in assigning observed intensities to averaged temperatures of inhomogeneities, the same mistake as in HOLMUL abundance determination rectified in the hydrodynamic Asplund revolution.

NLW was still lacking in VALIIM which only accounted for scattering in the Si I continuum so that its Fig. 23 (pdf 38) multi-page analogon to multi-page VALIII Fig. 36 shows erroneous $S_\nu \approx B_\nu$ in the ultraviolet above the Si I threshold at 1682 Å where other electron-donor bound-free contributions dominate [SSX (pdf 68)]. This was remedied in VALIIIC but overestimating their effect because not enough line-haze blending lines were included, resulting in a too steep upper-photosphere temperature decline. Including more and more lines from the growing Kurucz tabulations (e.g., Kurucz 2009) then brought the upper-photosphere back up, announced in Avrett et al. (1984), shown in model C' in Avrett (1985), and tabulated in MACKKL; since then it has remained the same. It is remarkably similar to HOLMUL and even to Kurucz or Uppsala LTE-RE models [RTSA Fig. 7.3 (pdf 169)] [55 RE upper photosphere].

I love the Avrett models, in particular VALIIIC because of the many diagrams in Vernazza et al. (1981) and especially its many-page Fig. 36 continuum formation diagrams (some copied in [RTSA (pdf 204)] – [RTSA (pdf 206)] and in [SSX (pdf 61)] – [SSX (pdf 67)]). Since VALIIIC obeys all the standard RT equations, meaning all those in RTSA, these graphs describing spectral continua arising from the VALIIIC density and temperature stratifications provide valuable insights on spectrum formation and its intricacies. They are of enormous didactic value because *everything* in Avrett's output graphs is fully understandable from the input physics \approx RTSA physics [56 Fe ionization in VALIIIC]. The same holds for the newer Avrett models and his latest ALC7. Therefore I made many ALC7 demonstration figures: [SSX (pdf 72)] showing ALC7 stratifications, [SSX (pdf 75)] ultraviolet continua, [SSX (pdf 76)] hydrogen line formation, [SSX (pdf 77)] overview of strong-line formation, then [SSX (pdf 78)] ff explaining line-formation plot formats [57 ALC7 line formation plots] followed by such plots for thirteen ALC7 lines in [SSX (pdf 82)] ff. They were all made [58 my IDL programs] with the 1D version of github-public RH [59 RH program]. They represent a detailed view of how all these lines form in the ALC7 atmosphere. In addition [SSX (pdf 98)] ff show ALC7 formation comparisons between comparable pairs of lines and [SSX (pdf 102)] ff compare the formation of twelve lines between three Avrett models.⁴³ Any student of thick solar spectrum formation should be able to understand and appreciate all these curves in all their gory detail. I invite you to study and explain:

- N_e stratification;
- Eddington-Barbier validity in all lines;
- ε decline in scattering lines;
- PRD-split source functions of Ba II 4554, Ca II K, Mg II k, Ly α ;
- thermalization depth for all lines, in particular H α ;
- NLTE extinction dip of Mg I 4571, Fe I 6301.5, Mg I b₂ but not for Na I D₁, He I 10830;

continuum part of SSI and in practical SSB 2 (pdf 13). Practical SSB 3 (pdf 22) makes you synthesize the Na I D lines from FALC assuming LTE and hence misrepresenting their cores.

⁴³ ALC7–FALC in [SSX (pdf 102)] ff, FALC–FALP in [SSX (pdf 115)] ff, ALC7–FALP in [SSX (pdf 128)] ff, each with twelve line buttons at bottom. The display titles may return to the previously shown display. The *start* button at bottom-left should return to the SSX contents overview.

- LTE extinction of Mg II k, H α , H β , He I 584;
- slight rise in NLTE over-extinction for Ly α ;
- line formation differences between different Pandora stars.

However – the stern caveat is that I love the Avrett models only for representing educational solar-analog “Pandora stars” [SSX (pdf 58)]. These computationally existing stars extend infinitely plane-parallel (1D) without any inhomogeneities or any magnetism or any sort of waves or any type of reconnection – no granules, spicules, floccules, let be filaments, flares, CMEs, and whatever else that makes our kind Sun non-plane-parallel interesting. The Pandora stars are a marvelous boon to a RT teacher like me but they also had and have detrimental effects on far too many colleagues misled into accepting their stratifications as a valid average over small fluctuations around realistic means. The first figure of Vernazza et al. (1981) in [SSX (pdf 60)] is a double champion of solar physics: the most-shown figure but also the most misinterpreted. It misled many solar physicists into thinking it describes the Sun instead of an unrealistic plane-parallel-layer star. *The solar atmosphere is not stably layered but dynamically structured.*

Take H α as example. In his VALIIIC diagram [SSX (pdf 60)] Avrett, admirably careful, drew its core coming from the VALIIIC chromosphere, its wing from the low VALIIIC photosphere with an extended gap in between that is not present in his formation spans of Ca II K and Mg II k. He did so because at low temperature the Boltzmann excitation and therefore the extinction of H α are negligible. Correct – but the actual H α core in actual quiet Sun mostly samples opaque fibril canopies⁴⁴ reaching much higher [60 quiet-Sun H α scenes].

Worse, Pandora-star chromospheres do not represent average canopy-fibril temperatures but ultraviolet radiation temperatures reached in acoustic shocks in internetwork regions underneath the fibril canopies. The shocks result from upward propagating waves excited by the 3-min components of the photospheric p -mode interference pattern [61 seismology success story] [62 no gravity-modes success story].

The warning bell for shocks upsetting plane-parallel modeling were the already much-discussed double reversals in the cores of Ca II H & K (endnote 17). The Pandora stars give fairly good renderings of the mean disk-center H & K profiles but any plane-parallel model can do this (cf. Ha-Ha line formation in endnote 71 for H α), even the mean reversals with PRD (Fig. 18 (pdf 26) of Avrett 1985), but they cannot reproduce spectral-atlas mean-profile reversal asymmetries: the violet-side peaks in H & K are higher than the red-side peaks (the red Ca II H_{2K} peak is barely visible in the atlas profile in Fig. 11 (pdf 10) of Rutten et al. 2011). For decades spectroheliograms had suggested Ca II H_{2V} and K_{2V} “cell grains” as cause [63 Ca II K_{2V} and CN spectroheliograms]. These small bright grains occur intermittently but ubiquitously in internetwork cell interiors and are not magnetic (although some authors tenaciously claimed this). The wide confusing literature on this phenomenon upsetting plane-parallel modeling, not a minor deviation to be glossed over but a key phenomenon requiring understanding, was reviewed by Rutten and Uitenbroek (1991a) concluding here (pdf 51) that these grains are an acoustic interference phenomenon along the lines

⁴⁴ Naming: “canopies” spreading around magnetic features over field-free surroundings were introduced as magnetic ones from multi-line magnetometry including Ca II 8542 Å and H α by Giovanelli and Jones (1982). They warned that H α fibril contrasts likely mark opacity or source function variations rather than lateral field variations. A good rendering is in the simulation-assisted inversion map in Fig. 7 (pdf 9) of Jafarzadeh et al. (2017).

of Liu and Skumanich (1974). This was then brilliantly proven with observation-driven RADYN simulations by Carlsson and Stein (1997) [64 *Carlsson-Stein shocks*]. They showed that the upward-propagating three-minute waves pistoned by the p -mode pattern maxima convert non-linearly into shocks producing cell grains [65 *Carlsson four-panel breakdown*] and that the ultraviolet radiation temperatures are Wien-weighted to the shock maxima and not linear temperature averages. This was shown in Fig. 4 (pdf 8) of Carlsson and Stein (1994) where the upgoing waves are still wave-like in the AII edge and fully shocking in the Lyman continuum. Their model-building experiment in Fig. 5 (pdf 11) (summary in [SSX (pdf 157)]) demonstrated that the nonlinear Wien weighting skews the apparent average over internetwork shocks into an Avrett-style apparent “chromosphere” which is not the chromosphere but mimics the underlying internetwork-shock domain [66 *clapotisphere*].

In AIA 1700 and 1600 Å movies these acoustic internetwork waves appear as fast-moving fast-evolving wisps of emissivity amid stable network evident as bright grains representing kilogauss “fluxtube” MCs. The 1600 Å images sample these wisps slightly higher because the summed photo-ionization extinction of electron donors Mg I, Fe I, Si I, and Al I increases for shorter wavelength (compare emergence heights and main contributors on the successive pages of VALIII Fig. 36 from page 670 (pdf 37)). This height difference produces the Fourier phase differences in the upper panel of Fig. 18 (pdf 18) of Krijger et al. (2001) reproduced per RADYN simulation by Fossum and Carlsson (2005b) [67 *acoustic and gravity wave heating*].

ALMA samples these internetwork wave patterns also and may measure their actual temperatures linearly, but only in the very quietest areas [68 *internetwork acoustics with ALMA*].

The MCs outlining network appear with brighter contrast at 1600 Å than at 1700 Å. Plane-parallel colleagues attribute this enhancement also to increased donor-ionization opacity and standard “network” and “plage” models therefore have less steep upper-photosphere temperature decay than their “quiet” companions for internetwork. However, the actual fluxtube brightness is photospheric hole-in-the-surface radiation, with deeper holes at shorter wavelength. This is also known for decades as reviewed in the caption of Fig. 73 (pdf 91) in LAR-1 [69 *MC shifts 1600–1700 Å*]. Actual MCs are close to RE throughout the photosphere without evidence of kinetic heating as expected for structures that inhibit convection (Fig. 7 (pdf 7) of Sheminova et al. 2005).

Thus, Pandora-star “chromospheres” that are primarily based on ultraviolet continua actually represent, non-linearly, complex interference patterns of clapotispheric shocks plus misinterpreted network surface holes. Nothing to do with the solar on-disk chromosphere in H α that carries the name originally given by Lockyer (1868) for the colorful off-limb appearance of the Balmer lines and He I D₃ [70 *Lockyer chromosphere, He I D₃, flash color*]

Yet worse, actual H α canopies in quiet areas are mostly made by spicules-II (endnote 80) that reach heights around 7000 km (Pereira et al. 2014) far beyond any Pandora-star atmosphere. On the disk they are observed as outer H α -wing RBEs and RREs (endnote 80) – so much for ascribing outer-wing intensities to deep-photosphere sampling and so much for assigning brightness to heating since they heat to EUV visibility (Henriques et al. 2016) but are dark. Their subsequent cooling recombining return flows produce most of the dark H α line-core fibrils (“coarse motes”) around network (Rutten et al. 2019). Both types of ubiquitous dynamic H α structure are transparent in the ultraviolet

continua used for constructing Pandora stars. [71 *Ha–Ha scattering*].

Yet worse, there even exist publications (not to be named) that used the VALIIC diagram in [SSX (pdf 60)] to define “height differences” as the 400 km there between Ca II K₃ and the core of H α to identify and measure wave propagation and explain coronal heating. Maybe there exist plane-parallel stars in a parallel plain universe where this is a viable tactic (but do those have coronae?).

7. NLS+NLW+NLT: Oslo simulations

NLT is the current frontier in solar spectrum interpretation, not just in underlying MHD phenomena as the Carlsson-Stein shocks (endnote 65) but also by not assuming SE in spectrum synthesis. Anything you see may not be so much how it appears now but rather what happened before.⁴⁵

The key publications I summarize here are the 1D(t) HD RADYN analysis of acoustic shocks by Carlsson and Stein (2002) and the 2D(t) MHD Stagger simulation of network and internetwork shocks by Leenaarts et al. (2007). The first showcases the physics, the second demonstrates the effects. Neither includes spectrum synthesis but the hydrogen rate analyses of the first and the hydrogen population results of the second make these classics of solar spectrum formation.

1D HD RADYN simulation. Carlsson and Stein (2002) studied hydrogen partitioning in acoustic shocks as those of Carlsson and Stein (1997) in an exemplary analysis. Key results are summarized in [SSX (pdf 165)]. The main agent is Ly α . They found that detailed radiative balance is generally a close approximation for Ly α at chromospheric heights (the discussion on VALIII p. 662 (pdf 29) concerns larger heights): about as many photons go up as down, many more than collisions up or down. Most photons are created per pair **d** but then resonance scatter many times without coming far because their mean free path is small (1 cm in the center panel of [SSX (pdf 32)]) with scattering thermalization length about 10 km due to the immense $n_1 \approx N_H$ density while the probabilities of destruction **a** and Balmer detour **h** are small [SSX (pdf 90)]. This approximation was imposed as input by Leenaarts et al. (2007) to avoid quantifying large numbers that effectively cancel.

Fig. 3 (pdf 4) of Carlsson and Stein (2002), reproduced in the [SSX (pdf 165)] summary, illustrates this Ly α photon balancing as negligible net 1-2 rate. The fat transitions there (large net photon rate) are photo-ionization in the Balmer continuum and recombination with $\Delta n = 1$ steps [72 *Rydberg H I lines*] ending with fat H α . For given n_2 population (highly NSE in post-shock cooling) this loop obeys SE but it is far out of LTE because the impinging Balmer continuum originates in the deep photosphere, with radiation temperature about 5300 K [SSX (pdf 76)]. Where this value exceeds the local temperature photon pumping enhances ionization. There are also contributing photon losses in heavily scattering H α [SSX (pdf 91)] which operates within the low-energy 3.6 eV hydrogen top (footnote 89) representing a minority-species photon-suction loop as in the neutral alkalis (endnote 33).⁴⁶

⁴⁵ Outdoors example: airliner contrails signify that aircraft engines passed before. If you don’t know that aircraft exist you may have to invoke flying saucers to explain long white fibrils on our sky.

⁴⁶ In the VALIIC “chromosphere” Balmer continuum pumping and H α photon losses represent large but balancing terms in the radiative energy budget [SSX (pdf 69)], so that losses in Ca II H & K, the Ca II in-

The key hydrogen balance for NLT is the Ly α collision balance. The collisional up and down rates differ much in temperature sensitivity due to the Boltzmann ratio in their Einstein relation [SSX (pdf 166)] [RTSA p. 23 (pdf 43)] [RTSA Sect. 3.2.5 (pdf 70)]. The exponential C_{lu} sensitivity determines the settling time scale at which Ly α reaches Boltzmann equilibrium. A few cases are plotted in Fig. 6 (pdf 7) of Carlsson and Stein (2002), reproduced in [SSX (pdf 166)]. In hot shocks the frequent Ly α up- and down collisions make the balance reach Boltzmann equilibrium in seconds, but in subsequent post-shock cooling gas the settling time scale increases to multiple or many minutes. During this time the large n_2 overpopulation also governs large NSE overionization since the whole top of the hydrogen atom including the proton population is defined by this lower boundary condition. The Balmer-top SE loop just adds yet more overionization with respect to SB if the temperature drops below 5300 K.

2D MHD Stagger simulation. The next step in NSE simulation was Leenaarts et al. (2007), going from 1D to 2D and from HD to MHD. [SSX (pdf 167)] is a summary. The three panels at its top are cutouts showing three of the nine quantities in Fig. 1 (pdf 4) at a sample time step. They demonstrate that the simulation (evolved after starting from an LTE initializing simulation) portrays a quiet solar scene with two opposite-polarity MCs 8Mm apart that resemble network fluxtubes, with internetwork in between showing a canopy-like dome with cool to very cool gas and less steep upward density decay underneath. For me the 9-panel thumbnail in [SSX (pdf 167)] is a button that opens a movie running the whole simulation. Please [download it here](#) and play it. It vividly shows how shocks (thin blue filaments in temperature) travel up along the MCs and more erratic between them, the latter kicking up the apparent canopy. The first represent field-guided dynamic fibrils [73 *dynamic fibrils*] as evident from their characteristic time-slice parabolas in the lefthand column of Fig. 3 (pdf 6). The internetwork shocks are acoustic Carlsson-Stein shocks (*endnote 64*).

The last panel of the three in [SSX (pdf 167)] and of the nine in Fig. 1 (pdf 4) and its movie version show the NLTE departure coefficient b_2 of HI level $n = 2$, upper level of Ly α and lower level of H α . Its variations are enormous, reaching values up to $b_2 = 10^{12}$ in cooling post-shock blobs⁴⁷. This is not NLTE at the 0.1-1 dex level traditionally regarded as significant in solar and stellar abundance studies – this is 12 dex of retarded overpopulation! The next to last panel of Fig. 1 (pdf 4) and its movie version shows the departure for the HI continuum level ($n = 6$ in the atom model) and illustrates that Balmer continuum pumping adds up to another 3 dex for the coolest clouds (instantaneously).

Fig. 2 (pdf 5) of Leenaarts et al. (2007) is also best studied in its [movie version](#). Its panels show behavior of the y -axis quantity along the dashed vertical lines in the fourth panel of Fig. 1 (pdf 4), at left sampling the lefthand MC and at center sampling internetwork. In the lower three rows of the Fig. 2 *movie* the thick curves are the simulation results, the thin curves the values obtained by assuming LTE instead so that the curve separations correspond to the departure coefficients in Fig. 1 and its movie version. Playing this movie shows shocks running up

framed lines and Mg II h & k dominate [SSX (pdf 70)]. The total curve in [SSX (pdf 70)] defines the unspecified local heating needed to maintain the VALIIC atmosphere (*endnote 33*), much more for its chromosphere than for its 10 \times thinner transition region.

⁴⁷ This panel also shows high-up green arches. I think that these are artifacts stemming from the input tractability assumption that Ly α obeys detailed radiative balance everywhere (it does lower down).

with time in the temperature curves in the lefthand top panel. The actual shocks in the Fig. 1 *movie* tend to go slanted in the internetwork, so that the righthand Fig. 2 *movie* column samplings are not along-the-shock path histories [74 *internetwork shocks in CaII H and H α*] but sample different shocks at different times while the lefthand *movie* column samples dynamic fibril shocks better along their near-vertical paths. The *movie* strikingly demonstrates that the ionization fraction, proton density and n_2 population density in the lower rows reach LTE values in shocks but thereafter do not drop steeply along with the temperature. Instead they hang roughly at the value they got in the shock. There should be eventual settling to the LTE value, but long before that the next shock arrives: shocks repeat faster than the settling time scale. The persistently-high n_2 population results in the dark appearance of dynamic fibrils (seen well in the SST/SOUP H α *movie of endnote 73*) throughout the downstroke phase of their timeslice parabolas whereas they would fade fast with the lowering temperature if SE LTE were valid.

The second row shows that hydrogen generally does not ionize fully in the shocks but only a few percent. However, this already means two orders of magnitude increase of the electron density which in neutral-hydrogen gas sits at the 10^{-4} abundance fraction of the electron donor metals (VALIII Fig. 47 (pdf 67) [SSX (pdf 72)]). This increase in collision frequency appears sufficient to obtain LTE Boltzmann equilibrium in Ly α within the shocks, giving LTE Balmer extinction (bottom panels of the Fig. 2 *movie*). Another condition for this equilibrating is that a feature should be thick enough to contain Ly α , optically thicker than the thermalization length from its surface. At partial ionization hydrogen retains sufficient n_1 opacity to keep these shocks effectively thick in Ly α .

The upshot for the HI top up from $n = 2$, in particular H α , is that it combines all three types of nonlocalness: NLS in H α from its Ha–Ha resonance scattering (*endnote 71*), NLW from Ly α -controlled SB extinction in heated gas, NLT from the slow supra-SB Ly α settling in cooling gas. The combination makes the dynamically refurbished quiet-Sun chromosphere observed in H α and likewise with ALMA a NLS+NLW+NLT phenomenon (*Sect. 8*).

3D MHD Bifrost simulations. Since these classic simulations the Oslo simulators went to 3D(t) MHD Bifrost [75 *Bifrost program*] of Gudiksen et al. (2011) [SSX (pdf 159)]. The cubic Bifrost stars are far more solar-like than the plane-parallel Pandora stars by being 3D(t) harboring dynamism and magnetism. Unlike the Pandora stars they contain realistic granulation, overshooting granulation and gravity waves, acoustic waves (with box modes as p -mode surrogate) and shocks, MCs arranged in network patterns, dynamic fibrils, bipolar-network-connecting chromospheric fibrils, and reconnective Ellerman bombs (EB). However, they still lack other solar features and their cube sizes are yet too small for supergranulation, active regions, and larger-scale coronal fine structure [76 *public Bifrost star*].

Bifrost spectral synthesis has mostly concentrated on the IRIS diagnostics. Obviously it beats Pandora-star spectral synthesis in NLS, although most analyses rely for tractability on columnar modeling with the RH 1.5D program of Pereira and Uitenbroek (2015). The Pandora stars handle NLW better with respect to ultraviolet ionization and the problematic ultraviolet line haze (*endnote 50*). Various Bifrost runs included NLT for hydrogen (as in the classics above), but not in subsequent spectral synthesis except the NLT analysis of EUV helium lines by Golding et al. (2017).

8. NLS+NLW+NLT chromosphere spectrum

SE is usually a sound assumption for thick spectral modeling of photospheric structures (SE NLTE) and for thin spectral modeling of coronal structures (SE CE). Chromospheric structures in between are the hardest to model. In these hydrogen varies between neutral and ionized and NLT reigns next to NLS and NLW in cycling them through thick and thin [77 *photosphere, chromosphere, corona: hydrogen ionization*] [78 *no transition region*]. For a review see Carlsson et al. (2019).

Quiet chromosphere. Away from active regions the chromosphere consists of clusters of MCs making up plage and network, the latter partially outlining clapotospheric internetwork “cell interiors” with occasional MCs on their way to cell boundaries [79 *internetwork fields and basal flux*].

In the optical the quiet chromosphere is seen only in Balmer lines, Ca II lines and He I lines. The Lockyer definition implies it is made up by the fibrils seen around network in the H α core and with lesser extent in Ca II 8542 Å (*endnote 81*),⁴⁸ H α fibrils around network are largely made by spicules-II [80 *spicules-II*] [81 *RBE-RRE-fibril ionization-recombination*].

In AIA UV images the quiet chromosphere is transparent. They sample clapotosphere underneath and yet deeper in MC holes in the photospheric surface. These are cooler than their surroundings but appear brighter (Fig. 75 (pdf 91) of LAR-1).

In AIA 304 Å images quiet areas show two major chromosphere constituents: ubiquitous extended heating patches (“floculi” would be a good descriptor) and sparser brighter feet of coronal bright points (CBP). For a quick overview inspect the 10 “triple” image sets in Figs. 17 (pdf 35)–46 (pdf 64) of LAR-1 [82 *quiet-Sun SDO images*]. The first of each triple is a large-field 193 Å image showing coronal activity, coronal holes, and CBPs. The second is a clipped “fire detector” multiplication of precisely co-aligned 304 Å and 131 Å images in which grey patches show heated quiet chromosphere and cyan-colored pixels mark CBP feet. The third is the corresponding HMI magnetogram showing what underlies and probably causes the CBPs. The 10 triple sets sample low and high activity and low and high latitude and permit inspecting multiple coronal holes.

The heated chromosphere patches in the detector images appear everywhere around network but fewer in coronal holes. Their surface patterns are cospatial with the fibrillar H α canopies around network (Appendix B (pdf 11) of LAR-1) and serve in my SDO pipeline [83 *SDO-STX alignment*] to cross-align AIA 304 Å images directly to HMI magnetograms. I attribute this component to spicules-II ejected from network. These also occur in coronal holes. The lack of corresponding fire-detector network there may be traditionally ascribed to lack of EUV irradiation from above but may also be due to lack of coronal contact cooling due to lower coronal surround density [84 *transition radiation, sheath ionization, coronal contact cooling*].

⁴⁸ Ca II H & K are richer in sampling chromospheric canopies than H α , as in Fig. 2 (pdf 5) of Jafarzadeh et al. (2017) and in Fig. 3 (pdf 4) of Bose et al. (2019), partly thanks to PRD source function splitting but also because H & K do not skip the clapotosphere in their inner wings and have six times less wide thermal broadening.

CBPs⁴⁹ are sparser but not rare in quiet areas. They are best seen in 193 Å images as small ensembles of EUV-bright loops located at and connecting bipolar network (silly-walled LRSP by Madjarska 2019). They appear as mini active regions, are likely due to ongoing flux emergence and flux assembly into network, and are probably heated by reconnection near their loop tops with subsequent heating of their chromospheric feet [85 *CBP foot visibility*] (Madjarska et al. 2021), likely by particle beams (Frogner et al. 2020, cf. LAR-1). These features can live fairly long, the smallest [86 *Solo campfires*] the shortest, but AIA 193 Å movies show frequent change suggesting continuous renewal. The representative AIA 193 Å images in the triple blinkers suggest that CBPs are the main agent in quiet-Sun coronal heating and cause the diffuse AIA 193 Å brightness spread widely around them, together and with contributions from prior CBPs. Such diffuse brightness is absent in coronal holes where heating does not spread to surrounding surface areas along closed loops but instead follows open-field up and out, likely as coronal plumes (Wang et al. 1997).

To reproduce such dynamic nature numerically, even for just “quiet” chromosphere, poses enormous challenges because the MHD simulations must produce spicules-II as copiously as actual solar network does and must then be combined with 3D(t) NLS–NLW–NLT (“NSE”) spectral synthesis including PRD at least for Ly α to recover the observed H α chromosphere and in addition must produce small-scale bipolar activity causing and governing CBPs as observed.

ALMA has the potentiality to sample and measure the quiet chromosphere sharper and faster than its imaging by DKIST [87 *quiet chromosphere with ALMA*] [88 *ALMA-H α -SDO alignment*] [89 *ALMA-GONG-SDO alignment*] [90 *ALMA-SOLIS-SDO alignment*].

Active chromosphere. For chromospheric activity phenomena I refer to Jongchul Chae’s contribution in this school because I have not worked on these except EBs and FAFs [91 *Ellerman bombs and flaring active-region fibrils*]. Hence no discussion of spot chromospheres, flares, filaments, etc. here. I restrict this section to two exemplary active region scenes in different diagnostics.

The first scene is the DST/IBIS – SDO multi-wavelength image mosaic of Cauzzi and Reardon (2012) and Reardon and Cauzzi (2012a, 2012b) showing AR 1092 near disk center on 2010-08-03 in the early days of SDO⁵⁰. I received these concurrent co-aligned images in 2011 from K.P. Reardon and combined them into [this pdf blinker](#)⁵¹. The IBIS selection samples Ca II 8542 Å, H α (also H α core width and core-minimum

⁴⁹ Naming: solar physicists have a habit of calling small unresolved features “points” needing a better name when they get resolved. Ca II H_{2V} and K_{2V} cell points became grains, facular points (or filigree or magnetic bright points or G-band bright points) became flowers and then MCs. We need a better term for CBPs (also named X-ray bright points, XRBPs, XBPs) – heated small bipolar network-connecting loop groups? Quiet-Sun EUV patches?

⁵⁰ The deterioration of AIA sensitivities, worst for chromosphere and prominence telltale 304 Å, during the immensely productive – bread and butter for very many colleagues – first SDO decade makes me long for AIA-v2 – with yet more pixels, yet more wavelengths, yet faster?

⁵¹ In a sequence suited to pairwise page blinking. Most pdf viewers furnish blinking by flipping pages in-place with the cursor arrow or page up-down keys. Full-page, fit-to-page, presentation-mode viewing may help. Multiple-page jumping may be possible with a back key. Myself I instead use my showex browser (*footnote 125*).

Dopplershift as defined in [Cauzzi et al. 2009](#)), and the (small) equivalent width of He I D₃. The SDO selection adds comparable HMI and AIA diagnostics.

This IBIS–SDO blinker represents an active-region counterpart to the final showex inspection of the quiet-Sun SST and SDO sequences in my [alignment practical](#). These two solar displays are utterly different. The SST set is a time sequence of a small quiet coronal-hole field with only some network. The IBIS set is only a single snapshot, not permitting time-delay cause-and-effect sequence inspection, but shows a larger active-region field containing dense unipolar plage, mossy plage [[92 moss](#)], a large regular spot, active-region filaments, and even a small flare originating in the spot which behaves as a CBP with loop brightening and feet heating. Blinking these images represents a vivid course in active-region phenomenology and also exhibits aspects discussed above [[93 IBIS–SDO active-region blinker](#)].

One striking difference between quiet and active scenes is that quiet closed-field areas permit H α and He II 304 Å co-alignment by reversing H α intensity ([endnote 84](#), [Appendix B \(pdf 11\)](#) of [LAR-1](#)) whereas active areas permit co-alignment using normal H α intensity ([blinker p6–p10](#)). I attribute this difference to different ratios between roundabout (“around”) chromosphere heating that dominates in quiet closed-field areas and upward chromosphere heating that dominates in the hearts of active network and plage from more numerous and denser MC clustering [[94 around and upward heating](#)]. I also wonder whether or how upward chromosphere heating in the hearts of active network and plage contributes to the slow-wind FIP composition bias [[95 FIP effect](#)].

The enigmatic appearance of the chromosphere in optical He I lines may also have mostly to do with upward heating [[96 optical He I lines](#)].

The second display I link to is an appetizer for things hopefully to come: comparable active regions in H α and Ly α in [Fig. 2 \(pdf 6\)](#) of [Rutten \(2017b\)](#) [[97 Ly \$\alpha\$ dream](#)]. These scenes both sample hydrogen atoms but differ strikingly in appearance. The lines have discordant formation in the ALC7 atmosphere [[SSX \(pdf 28\)](#)] but nevertheless should sample common ionization features, I think with bright Ly α grains showing dynamic heating and dark H α fibrils showing NLT cooling [[98 Ly \$\alpha\$ features](#)]. ALMA samples hydrogen ions and may be able to measure both types of feature at fast enough cadence to establish and correlate cause–effect delays. ALMA may also sample hydrogen lines permitting super-sensitive chromospheric magnetometry [[99 Rydberg HI candidate for ALMA](#)].

Finally, there are dark filaments in these active-region scenes suggesting “chromospheric” neutral hydrogen gas in the corona. Filaments generally appear long-lived but may nevertheless be made dynamically [[100 filament blobs](#)]. At high resolution and fast cadence ALMA may also diagnose their formation including frequent refurbishment and accompanying retarded-opacity visibility.

Chromospheric and coronal heating. An opinionated text as this should address “one of the longest standing unsolved mysteries in all of astrophysics”⁵², certainly a text harping on the chromosphere since generally the blame for coronal heating is sought there – while heating the chromosphere to observed temperatures is less glamorous but requires more energy for its larger mass.

⁵² J.T. Schmelz, ISSI talk July 2021 for a covid-zoom audience.

The literature on outer-atmosphere heating is bewilderingly varied. The traditional emphasis for the coronal part is on loop modeling following [Rosner et al. \(1978\)](#) debating AC (Alfvénic wave) versus DC (reconnection) mechanisms, both dictated by dynamical fluxtube topography in the photosphere. Chromospheric heating is attributed to a yet wider variety of agents. However, regarding the chromosphere as a layer (not dynamically structured and pervaded) and coronal loops as homogeneous structures (not dynamically multistrand and multithermal) both seem as misleading as regarding the photosphere a plane-parallel layer without convection, waves, magnetism.

My theme here is spectral evidence. Blinking the SDO triples ([endnote 82](#)) and the IBIS–SDO images ([endnote 93](#)) suggests that a more important split than “corona versus chromosphere” is “quiet versus active”. I summarize my impressions from these representative blinkers.

The SDO triples suggest that quiet chromosphere⁵³ heating is AC-type with spicules-II fired from vorticity-rich network and producing return-flow fibrillar H α and He II 304 Å canopies, the latter mapped well in the AIA fire detector images. The major telltale is the good pattern matching of the bright canopies seen in AIA 304 Å and the dark fibril canopies seen in H α around the magnetic network seen in HMI magnetograms, and their ubiquity. This is “around” heating ([endnote 94](#)) and does not heat the corona but may cool it ([endnote 84](#)). ALMA may become its best diagnostic ([endnote 87](#)).

The SDO triples also suggest that quiet corona heating arises chiefly from CBPs, especially the larger ones, with DC loop-top reconnection resulting in diffuser coronal connectivity to nearby CBP areas. Their beam-heated feet are also well-mapped in the AIA fire detector product.

These two quiet-Sun heating agents appear remarkably unrelated, even though both stem from MC dynamics in network and plage outside active regions. Both are ubiquitous because network is ubiquitous.⁵⁴ Spicule-II quiet-chromosphere heating does not need MC bipolarity, CBP quiet-corona heating does. Both act also but less effectively in coronal holes where coronal plumes seem an open-field CBP alternative. The SDO database offers tremendous material for further study.⁵⁵

The IBIS–SDO images suggest that active regions add unidentified “upward” heating ([endnote 94](#)) feeding long-loop connectivity to distant other active regions, likely with FIP abundance offsets ([endnote 95](#)).

9. Conclusion

Understanding the solar spectrum has come a long way but isn’t there yet. The basic physics was well understood by the 1970s – no dark matter nor dark energy in the solar atmosphere.⁵⁶ Numerical modeling started about then with the advent of electronic computing which was welcome because analytic theory had reached its limit in [Kourganoff \(1952\)](#). Numerical study provided great insights even though initially mostly within the

⁵³ Once again *ad nauseam*: not the “chromosphere” of Pandora stars mimicking the Wien-skewed ultraviolet of clapotospheric shocks ([endnote 66](#)) and MC holeshine ([endnote 42](#)), but quiet-Sun internetwork canopies observed in H α , HI Ly α , He II Ly α and also in Ca II H & K, Mg II h & k and with ALMA.

⁵⁴ But neither occurs for the simulated network in the public Bifrost star ([endnote 76](#)) hampering teaching machine learning with it.

⁵⁵ If I still had graduate students I would suggest the first five [research projects \(pdf 9\)](#) listed in the [LAR-1](#) conclusion.

⁵⁶ For a conflicting speculation search ADS with *abs:"axion quark" and "solar orbiter"* (not to be cited).

misleading straitjacket of plane-parallel atmospheres. Nowadays the major challenge is to obtain realistic spectrum synthesis from realistic solar-atmosphere simulations to provide guidance to interpret high-quality observations conveying solar truth – with the proviso that “*simulations are great tools but still toys*” (Martínez-Sykora). Full 3D(t) synthesis of all spectral features for every voxel at all times of a RADYN-style 3D(t) MHD-etc simulation is a bridge too far, so that the simulation synthesis frontier lies in clever shortcuts (reviews by [Pereira 2019](#) and [Leenaarts 2020](#); NSE simplification on p. 20 (pdf 20) of [Rutten 2019](#)).

Shortcuts as adopting 1.5D columnar synthesis ignoring non-radial matter and radiation gradients, Holweger-style “inversion” suffering NLTE masking, neglect of ultraviolet NLS scattering and NLW interlocking, ignoring NLT memory by assuming SE may be as misleading as believing plane-parallel models – but just as those they may be educational steps along the way.

The tantalizing trophy is spectral understanding of the chromosphere which I now define as the hectic domain separating dense near-LTE near-neutral photospheric gas and tenuous near-CE ionized coronal gas, where hydrogen intermittently ionizes and recombines cycling between neutral and plasma state with full NLS+NLW+NLT and HD ↔ MHD ↔ plasma complexity: *the chromosphere ain't stacked in layers but is dynamically structured and unstuck in time (endnote 81)*.

Key property: frequent dynamic refurbishment.

Prime diagnostics: HI Balmer lines, Lyman lines, mm continua, helium lines – all enriched by retarded opacity enhancement in cooling gas.

Lowest-hanging fruit: spicule-II heating of quiet chromosphere and CBP heating of quiet corona. In activity: moss, the FIP effect a ripening plum, the Wilson-Bappu relation overdue.

High-hanging fruit: 150+ years since [Lockyer \(1868\)](#) [[SSX \(pdf 12\)](#)] coined “chromosphere” in the dawn of astrophysics [[SSF \(pdf 2\)](#)] ff) we Khayyam-wise have no explanation for his bright yellow “helios” line. Cracking this nut likely helps to understand prominence visibilities.

Every aspect treated here must be considered: the Sun is a most beautiful complex being. We are fortunate that our kind star offers such great inspiring complexity to keep us on our toes.

Acknowledgements

I thank Ram Ajor Maurya and M.K. Ravi Varma for inviting me to teach this subject at their [Calicut school](#). I enjoyed my teaching sessions but suspect that the (unseen) students came out by the same door as in they went [[SSF \(pdf 120\)](#)]. I also thank the organizers for requesting this writeup and endorsing hyperlinks.

Earlier invitations to teach, in Bandung, Mitaka, Palo Alto, Seoul, La Laguna, Freiburg, Newcastle and Weihai (usually a [full week](#) for this material) led to displays SSF and SSX; I hope more will come in a post-covid future.

F. Paletou, J. Leenaarts, T.M.D. Pereira, P.R. Young and C.J. Schrijver contributed improvements.

As always I relied much on ADS. ADS also taught me [pdf page opening](#) and keeps its robust classic linkers active since its 2019 revamp. ArXiv provides a splendid open-access ADS-linked long-lasting publication platform.

Stackexchangers solved latex problems. M.J. Rutten started hosting [robrutten.nl](#) for link speed and persistence.

Detailing notes

Welcome to the yellow pages! These endnotes are take-or-leave elaborations adding literature, comments, opinions, history.

Topic selection: personal, favoring topics that I have been involved in and references and figures I knew best and came first to mind in this writeup for the [Calicut school](#). With preference for my own displays when these open faster than ADS.⁵⁷

I also sprinkle work-habit reminiscences through these notes because during my half century in solar physics the way we work changed drastically by revolutionary advances which may appear old-hat granted to you: photomultipliers, image intensifiers and electronic computing (1960s), solid-state image detection, electronic writing and internet communication (1980s), WWW and ADS (1990s), lately Wikipedia (2000s).

Navigation: each note ends with a link [Main call] returning to its calling location in the main text and a link [Back] that also returns there when you came from there or back to another link that you used – working in Firefox, Ubuntu acroread and xpdf, macOS Preview but not in Ubuntu evince, chrome, macOS Safari (try the viewer back button instead; for Acrobat check the [shortcut table](#)). Footnote numbers jump back to their call.

1. Personal background

I developed this material in decades of teaching at Utrecht University and abroad. In the 1960s I learned solar spectrum formation at Utrecht from C. (Kees) de Jager⁵⁸. Our bible was Unsöld’s book ([endnote 53](#)) but NLTE theory had started and was loudly advocated to us by A.B. Underhill, then also professor at Utrecht. The guru was R.N. Thomas but I found his writings incomprehensible and Kees much clearer⁵⁹. Jefferies’ (1968) book⁶⁰ was a welcome improvement on Thomas-speak⁶¹, with the [preface](#)

⁵⁷ Example: compare the opening speeds of [[SSX \(pdf 60\)](#)] and [Fig. 1 \(pdf 3\)](#) for the most-shown figure of solar physics. Both load relatively slow, in 1–3s and 5–10s at my Lingezicht 600 Mbps. Because these speeds and their ratio depend on connection and location I welcome [email with your values](#) for these two with your download speed; as thank-you I will notify you at future arXiv updates. When they are slow you may meanwhile be comforted by [footnote 76](#).

⁵⁸ [Cornelis \(Kees\) de Jager](#) (1921–2021) achieved fast expansion of Utrecht astronomy after M.G.J. Minnaert (including my job), started Flemish astrophysics at Brussels, started Dutch space research, was instrumental in starting ESRO and its transition to ESA, founded *Space Science Reviews* and co-founded *Solar Physics*, was IAU General Secretary, twice president of COSPAR, president of ICSU, and much more – including running marathons and giving public lectures up to record age. I honored his 80th birthday with a review of solar atmosphere modeling ([Rutten 2002](#)) and his 100th birthday with an SDO triptych album in LAR-3 ([Rutten 2021](#)). He passed away four weeks later. I then put his thesis on solar hydrogen lines ([de Jager 1952](#)) on ADS with help from Oslo and co-authored an “In Memoriam” for *Solar Physics* ([Rutten et al. 2022](#)), a mishandled affair (cdejsp_log.txt in the tarred [arXiv source](#)).

⁵⁹ Just as R.M. Bonnet who wrote “*As seen through the writings of Thomas, radiative transfer for me would have remained an unintelligible theoretical exercise forever*” and found De Jager much clearer, acknowledging “*the clarity of Kees’ views*” ([page 2 \(pdf 2\)](#) of [Bonnet 1996](#)). More Kees versus Thomas in [footnote 146](#).

⁶⁰ [Jefferies \(1968\)](#) was scanned by A.V. Sukhorukov and put on ADS by me with Jefferies’ consent, enabling page openers here.

⁶¹ Telltale specimen: NASA “orange book” *Stellar Atmospheric Structural Patterns* ([Thomas 1983](#)). I called it [Nebraskan Franglais \(pdf 2\)](#) ([Rutten 1985](#)); [Jordan \(1996\)](#) called it “hard-to-read vintage Thomas”; L.E. Cram suggested to read it a dozen times to get its meaning. ADS lists 26 citations versus 250 for [Jefferies \(1968\)](#), 408 for [Mihalas \(1970\)](#), 2097 for [Mihalas \(1978\)](#). However, Thomas (1921–1996) was truly a game-changer in stellar-atmosphere RT. JILA (which he co-founded) celebrated his centennial while I wrote this which made me reread my

(pdf 6) stating that the then literature “can well be criticized as being overly esoteric”.

I had started on solar radio diagnostics (Fokker and Rutten 1967) but switched to optical spectrum formation thanks to De Jager’s lecturing and then concentrated on the chromosphere thanks to J. Houtgast who took me as junior help to both 1966 eclipses to record the flash spectrum. Half a century later the chromospheric spectrum still fascinates me, as evident in *Sect. 8* which is more status report than course.

C. (Kees) Zwaan⁶² took over the Utrecht radiative transfer courses in the 1970s, modernized RTSA and set up IART. I copied much of his (neatly hand-written Dutch) material when I took over IART in 1985, RTSA in 1994 with English-version webposting in 1995 (*endnote 3*). I then also started [teaching abroad](#), appreciating getting to know an appreciable fraction of later colleagues worldwide.⁶³

I quit teaching at Utrecht at my mandatory retirement in 2007. In 2011 Utrecht University [abruptly quit its astronomy](#) (even its A&A and ApJ subscriptions) and effectively killed [Dutch solar physics](#). The DOT is mothballed since. I still [teach abroad](#) when invited but without Utrecht affiliation. [[Back](#)] [[Main call](#)]

2. Other texts

An inventory of relevant textbooks is in the [[RTSA bibliography](#) (pdf 17)]. I found [Mihalas \(1970\)](#) easier to read than [Mihalas \(1978\)](#). Newer books are Oslo-school-triggered [Castor \(2007\)](#) and comprehensive [Hubený and Mihalas \(2014\)](#), both more advanced than this course. The textbook on heliophysics of [Schrijver et al. \(2019\)](#) is complementary: no radiative transfer, barely photosphere and chromosphere but much about what the Sun gives us beyond spectrum-formation puzzles. The lectures on solar magnetism at the [2009 Dwingeloo school](#) are also complementary. [[Back](#)] [[Main call](#)]

3. Posting course notes

At my RTSA completion in the spring of 1995 Mats Carlsson suggested to ftp the postscript files to Oslo for printing as hand-out in his first Oslo RT school. I did and realized I might spread them likewise for printing by anybody, asked our software engineer how to make a website (“You? In latex because that’s all you know”) and started [my website](#) (still latex). This was my start in self-publishing; RTSA should have been LAR-1.⁶⁴ Initially I offered it in 10-page chunks for piecemeal ftp and printing and announced it by email to colleagues, then put an ad in SolarNews in 1997 and finally asked ADS to link to it as single pdf file in 2003 ([Rutten 2003](#)). It still says “Not yet” in enough places to forego publisher offers to print it. This compendium

[1997 Thomas memorial](#) and realize that in publishing this link-strewn compendium I finally fulfill my “[On publishing](#)” (pdf 9) promise there.

⁶² [Cornelis \(Kees\) Zwaan \(1928–1999\)](#) was my thesis adviser and a close friend. He was a phenomenal educator with main interest in solar and stellar magnetism wrapped up in [Schrijver and Zwaan \(2000, 2008\)](#). I not only took over his teaching but also his DOT stewardship. The revolutionary “open principle” of the DOT (no vacuum but rely on wind flushing to avoid convective turbulence from heating in the convergent beam to focus) was his idea and proposal to [R.H. Hammerschlag](#). DKIST is sort of open.

⁶³ I much missed face-to-face contact with the students in this zoom school. Just talking to your own screen is no good. I also missed what-where student presentations and joint meal and pub sessions.

⁶⁴ Except that part was written away from [Lingezicht](#) when a quarter-million Dutch evacuated central Holland in fear of the Rhine.

(also self-published but arXived and hence on ADS) represents an overdue update.

This RTSA experience taught me that the effort of formal publishing isn’t needed to spread course notes beyond the course; later I also posted [ISSF](#) and [IART](#) (yet to be ADSed). However, at the time I didn’t yet think of reading on-screen whereas now I work paper-free⁶⁵ (except when browsing classic monographs from the [Lingezicht](#) library) and expect active links in what I read⁶⁶. With the take-or-leave link-rich format of this text I Wikistyle my course offerings.⁶⁷ [[Back](#)] [[Main call](#)]

4. Projection technology

When I was a student boxes of slides were brought by teachers to class, by speakers to meetings. A “slide” was a black-and-white or color transparency made from a negative (emulsion on a glass plate, later 35-mm film) exposed in a camera and chemically reversed (“developed”) into positive and mounted in a frame holder to slide it into the focal plane of the enlarging projector lens.⁶⁸ Hence the funny name.⁶⁹

In the late 1970s Fresnel-lens overhead projectors for page-size⁷⁰ transparencies (viewgraphs, viewfoils) took over. They were better than both fixed-order antique slide and modern viewscreen projection⁷¹ in easy shuffling, skipping, overlap showing, and the bodily obviousness of the speaker passing to the next one.⁷²

The menu openers of [SSI](#), [SSF](#), [SSX](#) restore selection flexibility. Their selection and pointing per on-screen cursor made me forego using a bamboo stick or laser pen before covid-19 zoom practice.

Perhaps the covid-19 transition from 3D reality to 2D video and also the hyperjump from 3D printed-text reading to 2D page linking exploited here will in future transform to 3D augmented-virtuality attending and many-D avatar observation and simulation exploring. [[Back](#)] [[Main call](#)]

5. Mainframe computing

Utrecht University first had Dutch-made Electrológica X1 and X8 mainframes, then modernized to a CDC 6600 from lobbying by later Nobelist Tini Veltman who knew it from CERN. It was

⁶⁵ If you still say “paper” for a publication or even for a presentation or if you read this text on non-linking paper after printing it you are likely older than me, maybe in spirit.

⁶⁶ Publishers reselling printed works anew as electronic files should earn their predator/vulture profit by activating crossreferences and hyperlinking citations and likewise retroactively update all files that they sell. Textbooks that aim at on-line study should add pdf page openers wherever they refer to earlier results. Research publications discussing other’s results should also do this.

⁶⁷ It has been suggested that `html5`, `reveal.js` and `SVG` suit better than slow pdf opening but while ADS and arXiv serve pdfs that’s my way – comforted by *footnote 76*.

⁶⁸ Kodak carousel projectors didn’t slide but dropped the transparency from a circular “tray” permitting repeating sequence showing.

⁶⁹ Dutch “lantaarnplaatje”, later “diapositief” or “dia” was better. If you say “next slide” for your next presentation display you are a worse mastodon than me.

⁷⁰ Europeans using A4 had to take care not to exceed letter-size projecting in the US.

⁷¹ Dutch called viewgraphs “sheets” and call a computer projector “beamer” but in the US that is a BMW motorcycle or car.

⁷² Some speakers had the obnoxious habit of covering the not yet discussed part of the viewgraph (called “strip-teasing” by [P. van der Kruit](#)), unfortunately sometimes aped by modern powerpointers. Some boring teachers put their whole course on a continuous polyester roll without page-selection liveliness in repeating the same course every year.

the first supercomputer but far less powerful than the one in your smartphone.

One delivered programs punched into papertape rolls in brown bags, later punched into Hollerith cards in boxes, at the job-submission desk at the computer center, a large climate-controlled building with whitecoated staff tending the single (but many-cabinet) holy-cow machine. The output from the chain printer (per line slamming a chain of upfront-spinned characters on fanfold paper at 1000 lines/minute) was then collected from the computer center; towering stacks of printout⁷³ adorned many offices.

Multilevel NLTE runs as my 15-level Fe II for Cram et al. (1980) took a full week or more from getting low priority in queued time sharing by booking an overestimate of the required processor time – the job was killed at request overrun. Two-minute jobs had guaranteed return within the day, eight-minute jobs overnight, mine waited on those (mostly black-box runs of SPSS by sociology students) and primarily got done in weekends.⁷⁴ My inch-thick NLTE printout had graphs printplotted at the printer line and character resolution to be traced on overlay transparent paper for the observatory draftsman to draw figures as Fig. 5 (pdf 6). All labeling is also handdrawn! I wrote the manuscript in pencil, editing snail-mail coauthor iterations per eraser, and finally read it aloud into a dictaphone audio cassette tape for an observatory typist.

The CDC 6600 was succeeded by various CDC CYBER models. We then started jobs from monitors at Sonnenborgh Observatory that were modem-connected via permanent phone lines (“terminals”) – a fisticuffs-fought-over dozen. Finally we used a self-written CDC UT-200 emulator with cardreader input and lineprinter output on our HP 2114A prior to the 1987 astronomy relocation to the campus outside Utrecht. The CDC machine was replaced by a cheaper Data General Eclipse computer (scoring a Pulitzer with Tracy Kidder’s *The soul of a new machine*) and we got our own MicroVax, then switched to distributed workstations serving X-terminals (Sun, Silicon Graphics, DEC). [Back] [Main call]

6. Personal computing

Utrecht’s Observatory first single-user computer was a 1970 HP 2114A “mini-computer”. For the price of a luxury car a large heavy box with 4K core memory (actual magnetic cores) running ALGOL with a papertape operating system, a papertape-typing Teletype console and a fancy handheld electric papertape winder. After papertape (first 5-hole telex tape, then 8-hole bytes) came 80-character IBM Hollerith cards for FORTRAN “records” (still quaintly defining fits file header format), magnetic tape on reels and in cassettes, bendable magnetic diskettes, optical video platters permitting random image access, non-bendable floppy disks up to a full megabyte. My Atari ST “home computer”, the first with megabyte memory, needed a multi-hour multi-disk sequence for its floppy-disk operating system to latex my lecture notes but my later “subnotebook” ST-Book clone had a 40 MB hard disk. Result inspection needed laserprinting the postscript

⁷³ With only uppercase letters so not suited for manuscript printing. Slower daisywheel printers enabled that later and made me switch wavelengths from Ångström to nm until latex and laserprinters arrived.

⁷⁴ I then controlled my jobs from home with an expensive Digi-Log gadget combining an acoustic phone receptacle for 110 baud (then equal to bps) modulated whistling feeding a modem, a keyboard for input and 40 character/line video output to our analog TV as monitor. During weekends I so occupied both our telephone and television.

output. Then came zip disks of 100 MB and even 250 MB, read-write CDs and DVDs – all museum stuff now.

I transitioned from Ultrix on DECstations at work, the Atari at home (ten years!) and the ST-Book for travel (five years) via a heavy Dell and a dysfunctional Mac to Ubuntu on Toshiba laptops. Help went from thick vendor manuals in large binders to ICT personnel to graduate students to Stackexchange. FORTRAN still exists but IDL (my start on it was for teaching SSA and SSB) presently museum-ripens in the Python take-over. Me too. So it goes. [Back] [Main call]

7. ADS page opening, silly publishers

I describe linking citations to the ADS abstract page and opening particular pages in ADS-accessible pdf files on this webpage. The latex macros and usage examples are given in my report recipe for astronomy students. ADS pdf opening does not work for publications at what I call “silly publishers” who do not furnish direct pdf access on the ADS abstract page; I avoid citing these altogether. More detail in my recipes for publications.

Until 2022 ApJ and A&A furnished ADS pdf openers after one year⁷⁵ while permitting arXiving immediately; now they are open-access immediately. Thus, the immense top-quality astrophysics literature in ApJ and A&A from their start to the present is directly accessible: any particular page with a figure or equation or paragraph worth showing is only a single click/tap away in the very sentence where it is cited.⁷⁶ This text has many such openers. You should use them too (footnote 66).

In contrast, Springer promises “documents⁷⁷ at your fingertips” but requires many clicks/taps that may impose hefty payment and do not bring you to the right page. *Solar Physics*⁷⁸ has

⁷⁵ For license-limited articles ADS links to the publisher html access. Lean Library then silently uses your remote-institute license to pass directly to the pdf but presently opens the first page, making proper-page arXiv pdf opening preferable.

⁷⁶ Unfortunately many browsers reload the full pdf for every page, taking a while (footnote 57). But during these long seconds you might comfortably contemplate the much slower pre-internet/ADS chore: go to your institute library or some dark storage for older publications, locate the journal shelf, find a ladder, climb it, get the volume, descend, find the paper (literally), find the page, find a table and make notes or get to the nearest Xerox, write the full reference neatly on an index card (for alphabetic reshuffle by the manuscript typist), return the volume to its place, return the ladder, get back to your office. More modern on-line procedure: click/tap the citation in the text to jump to the reference at the end (or find it), open the ADS abstract page or DOI-linked publisher page (or find it), find a download button and load the pdf, find the desired page. Still too many actions and prone to silly-publisher mazes; you also may have trouble to get back to where you were reading. Much better to open the desired page per single click/tap parallel to your reading! What you miss from old-style library browsing is serendipitous finding adjacent articles or volumes of unexpected interest to you, but this is well-compensated by ADS listing which publications cited the one you are looking up.

⁷⁷ Springerese for publications, not passports. “Reviewer” means referee, “ticket” means into a black hole unless “escalated”.

⁷⁸ History: unfortunately C. de Jager and Z. Švestka started *Solar Physics* in 1967 as proprietary for-profit business of a commercial publisher (Reidel > Kluwer > Springer), similar to De Jager’s start of *Space Science Reviews* in 1962 also at Reidel. Actually A. Reidel pushed De Jager into starting *Solar Physics* because he liked the commercial success of the earlier journal and wanted more. A year later J.H. Oort got upset about the commercial nature of Z. Kopal’s new journal *Astrophysics and Space Science*, also at Reidel, and urged S.R. Pottasch and J.-L. Steinberg to found A&A as a non-profit astronomy organization (Pottasch 2011) that contracts production to a hired publisher (Springer > EDP), similarly to the non-profit AAS contracting ApJ production

no ADS pdf openers⁷⁹ since Springer bought it in 1996 whereas ADS still page-opens scans from the preceding Reidel-Kluwer era.⁸⁰ *Living Reviews in Solar Physics* is open access but also has no ADS pdf openers since Springer bought it.⁸¹ [Back] [Main call]

8. Spectral bandwidth and vision

Only our eyesight is adapted to solar radiation temperature but not simply to the Planck function for the solar effective temperature. Stating that needs specification whether our retinas measure per wavelength, frequency, wavenumber or count photons – see [SSF (pdf 50)] and remember $d\nu = -(c/\lambda^2) d\lambda$.

The third panel shows why J.W. Brault said in 1978 that the intensity at Ca II H & K was too low for his Kitt Peak Fourier Transform Spectrometer: a photon-counting wavenumber device (but we got the only center-limb H & K scans in the FTS archive). The last panel shows why high-energy astrophysicists plot λB_λ or νB_ν .

History; the spectral sensitivity of our eyesight was optimized in our aquatic past for the penetration of sunlight in sea water, as for giant squids whose giant eyes have similar but better design (Feynman I Fig. 36-10) and might suit nighttime astronomers better. As early mammals ashore we became dichromats being nocturnal to hide from predating dinosaurs. After these were blasted into oblivion⁸² early hominids restored red-detecting cones to spot low-hanging fruit, giving us color-triangle vision (Feynman I Sect. 35) to appreciate Kodachrome Basin. [Back] [Main call]

9. Quanta, bosons, photons

Since high-energy, polarization and radio spectra are not treated

out (Univ. Chicago > IoP). More recently some editorial boards of well-established Elsevier journals have quit the over-profitable publisher and started a fresh non-profit remake – a repair the *Solar Physics* editors might consider.

⁷⁹ Springer also forbids arXiving accepted manuscripts forever unless open access is paid. Springer permits arXiving only for the initially submitted version, not the peer-reviewed iteration – an affront to referees whose voluntary unpaid community effort in improving the manuscript is blatantly discarded.

⁸⁰ The hospitable and well-browsable library of the SST which was my classroom in a dozen intensive two-week solar-physics courses (my best teaching experience) conveniently offers all older *Solar Physics* printed volumes including their often noteworthy frontispieces, the pick of solar imaging at their time and worth inspection. Some would be great page openers here (spectroheliograms as the Gillespie ones revived in *endnote 63*) but Springer offers only a few, without index, costly, non-openable whereas images in the pre-1996 ADS scans have too low scan quality.

⁸¹ Example: opening some of the 62 informative figures in authoritative LRSP Nordlund et al. (2009) (*endnote 52*) would suit well in this display-oriented course. The ADS abstract page shows a pdf-promising green-dotted pdf button but it serves the hassle of navigating the Springer maze. Among solar physics publications the LRSP reviews are top candidate to page-link but notwithstanding their open access such showcasing is sillily inhibited by Springer – unless they are arXived: then ADS directly page-opens that pdf instead. This one wasn't arXived hence silly-walled. The LRSP editors should push authors to arXive, retroactively.

⁸² The Chicxulub impact (66 Myr ago) was likely so devastating because the soft sulfur-rich and feldspar-rich Yucatan limestone went pulverized up into the stratosphere causing global acid rain, global re-entry firestorms and long global winter (cf. Pankhurst et al. 2021). So it goes. The equal-size but kayakable Manicouagan impact (215 Myr) without known mass extinction was into hard Precambrian Grenville gabbro rock with energy dissipation in fluidizing shock waves.

in this compendium (*footnote 1*) I ignore the wave/particle duality of electromagnetic radiation by simply taking photons as bullets of non-relativistic energy $h\nu$ without impulse or wave properties beyond frequency: the “quanta” introduced by Planck. On p. 134 of “Inward Bound” Pais (1986) calls his quantum explanation (Planck 1900b) for the brilliant -1 that he put a few weeks before in his empirical radiation law (Planck 1900a) the most revolutionary physics discovery of the nineteenth century and adds that Einstein was likely the first to recognize this “as if the ground was pulled from under him”. Without the -1 the Wien simplification resembled the Boltzmann distribution understood from probability theory but the -1 required energy quantization. Much later (1916) Einstein added that also for impulse and in 1924 attributed light particles to Bose-Einstein statistics. See Pais (1982) “Subtle is the Lord” Chaps. 19 and 21 for more. On p. 405 Pais attributes the name “photon” to paywalled Lewis (1926).

Here the simplistic bosonic lightspeed bullet of energy suffices, as does the Bohr model for fermionic atoms and ions. The bullets get created by excitable fermions and may be absorbed or scattered by other fermions – that's all! Radiative transfer has a bad name of intransparency (literally correct) but remains simple physics. As is solar physics: no dark matter or energy while the solar neutrino problem went away (*endnote 15*). Inside just gaseous loose bosons and fermions humming harmoniously in boxed-in resonances with tiny leaks enabling our lives and also filling our careers with magnetic complexities from the Navier-Stokes and Maxwell equations and non-fluid properties converging outwardly into tenuous extrasolar plasma outside – that's all! Solar physics is not reductionist inward-bound discovery of laws for everything but Spinozist outward-bound discovery of what nature most inventively makes from them. [Back] [Main call]

10. Solar telescopes

These are intensity telescopes and therefore photon-starved, worse when larger (nighttime colleagues won't believe this). Reason: for pixels that resolve the diffraction limit the flux of photons per pixel does not vary with aperture size while smaller pixels sample smaller solar surface area (that's the game) for which the solar change time (say crossing at solar sound speed) is faster.

DKIST therefore needs four times faster data-taking cadences than the SST unless it is used as (expensive) light bucket. DKIST thus has four times less time for multi-frame collection for numerical post-detection restoration (*endnote 11*), e.g., at H α only 1 s for all desired wavelengths. A frequent design or set-up mistake is to overdo spectral resolution and coverage at the cost of angular and temporal resolution.

It is easier to sacrifice angular resolution so that larger aperture light-buckets more photons, the nighttime ELT approach. On the other hand, fortunately our resolvable daytime star kindly offers wavefront-encoding granulation everywhere on her surface so that we do not need a Na I D laser star for every isoplanatic patch (as ELT should have but won't). Thanks to adaptive optics and numerical reconstruction, both enabled by this granular encoding, groundbased optical telescopes pointed within the solar disk may reach their diffraction limit over their full field of view when the seeing is good: modern telescopes that do not reach double-digit percentage granular rms contrast (*endnote 52*)

are not doing their job (Scharmer et al. 2019).⁸³ [Back] [Main call]

11. Solar image restoration

Speckle and MOMFBD restoration exploit the lucky circumstance that the terrestrial seeing-freezing time is only about 10 ms, e.g., giving DKIST time to collect a hundred independently disturbed frames to obtain seeing statistics at $H\alpha$ within its solar change time (endnote 10). But for say five-wavelength $H\alpha$ sampling 20 frames per wavelength is not enough for good speckle reconstruction which needs 50-100 frames, whereas MOMFBD (van Noort et al. 2005) needs only 5-10 frames, an important advantage. However, the latter technique is less robust and needs better seeing, optics quality and adaptive optics – so far performing best at the SST.

At the DOT we used two-channel speckle reconstruction (Keller and von der Lühe 1992, Keller 1994; demonstration) to reduce speckle burst sizes per wavelength to 20 in five-wavelength $H\alpha$ sampling by adding simultaneous many-frame wide-band registration as is also done for SST MOMFBD. Comparisons (the two telescopes share their seeing) showed that SST MOMFBD yields much better quality than DOT two-channel speckle but needs a higher seeing-quality Fried value to work, typically $r_0 \approx 10 - 12$ cm for the SST while only $r_0 \approx 5 - 7$ cm for the DOT.⁸⁴

MOMFBD and two-channel speckle reconstruction both bring the important advantage of perfect co-registration of the different wavelengths with the wide-band sequence, which independent speckle reconstruction per wavelength does not give. Since optical wide-band registration shows granulation it is then easy to cross-align that sequence to SDO/HMI continuum and on to all other SDO diagnostics with my co-alignment pipeline (endnote 83). [Back] [Main call]

12. Equivalent temperatures

These serve for deWiening Planck function temperature sensitivity in intensity-related and population-related quantities. They are formal by being defined as the temperature value that entered into the pertinent TE expression equals the quantity: brightness temperature T_b for I_ν into the Planck function, radiation temperature T_{rad} for J_ν into the Planck function, excitation temperature T_{exc} for actual level population ratio into the Boltzmann ratio making $S'_\nu = B_\nu(T_{\text{exc}})$, ionization temperature T_{ion} for actual level/continuum population ratio into the SB expression making $S^c_\nu = B_\nu(T_{\text{ion}})$ [SSF (pdf 72)] [RTSA Eqs.2.128 – 2/132 (pdf 57)] after Wijbenga and Zwaan (1972). Thus, the difference $T_{\text{exc}} - T_e$ is a deWiened alternative to the $S'_\nu - B_\nu$ measure of NLTE affect-

⁸³ To stop the hype in calling optical observations “high resolution” I propose as qualifying “Scharmer threshold” criterion that the continuum rms granulation contrast exceeds 80% of the sky-limited SST value in Fig. 6 (pdf 8), even though that remains significantly below simulation estimates reaching 20% at 5000 Å (Wedemeyer-Böhm and Rouppe van der Voort 2009, cf. G-band comparison of Uitenbroek et al. 2007).

⁸⁴ This property and the DOT’s easy mosaicing from its parallactic configuration and superstable pointing (Hammerschlag tower and telescope mount, no adaptive optics) make the DOT highly suited for science programs with large-field five-wavelength $H\alpha$ mosaicing by the DOT as context imager for other telescopes. After the DOT lost Utrecht funding I proposed such in 2012 for co-pointing with IRIS (same resolution, field, cadence) but did not succeed in getting money – it did not help that I was officially retired for years already and that all Utrecht astronomy was then brutally closed down. I now suggest that moving the DOT to near ALMA is a good idea (endnote 88).

ing a source function. Scattering lines with small ϵ likely have $T_{\text{exc}} \approx T_{\text{rad}}$.

The required $[B]^{-1}$ operator (Eq. 1 (pdf 1) of Samain 1979) is straightforward but needs attention to units. My IDL [bright-temp.pro](#) handles it for B_ν and B_λ and different bandwidth units.

These conversions should always be applied when comparing intensity-related quantities at different wavelengths. Examples: Fig. 4 (pdf 5) of Rutten et al. (2011) comparing brightness scenes in Na I D₁, Mg I b₂ and Ca II 8542 Å, their atlas profile comparisons in Figs. 10 – 12 (pdf 10) there, and the intercomparable S, B, J panels for many lines from the ALC7 star in the displays starting at [SSX (pdf 82)]. [Back] [Main call]

13. Intensity calibration

For the optical spectrum Neckel (2003, 2005) provides limb-darkening expressions based on Brault’s FTS observations used by Neckel and Labs (1984) that Neckel (1999) converted into a calibrated atlas (endnote 14).

In the ultraviolet the SUMER atlas of Curdt et al. (2001) provides calibrated disk-center spectra for the 668–1611 Å range, with center-to-limb observations available in the SUMER archive. Earlier 1400–2100 Å absolute-intensity and center-to-limb estimates are in Samain (1979). Calibrated 1100–1900 Å flare spectra are shown and provided by Simões et al. (2019) in their inventory of spectral contributions to flare intensities in the AIA UV passbands. [Back] [Main call]

14. Optical spectrum atlases and line lists

Solar spectrum atlases started with the beautiful engravings of Fraunhofer and Kirchhoff, Rowland’s photographs, and then the graphical Utrecht Atlas of Minnaert et al. (1940)⁸⁵, all four sampled in [RTSA Fig. 3.1 (pdf 26)]. All lines in the Utrecht Atlas were laboriously measured⁸⁶ to produce the MMH solar line table of Moore et al. (1966). I have it as ascii file courtesy J.W. Harvey (in the magnetic-tape era) and consult this regularly although I also have the book.

While writing this note I realized that I might supply this file and similar leftovers from the past and started a [solar file archive](#) supplying them. They include the legendary Revised Multiplet Table of Moore (1959) (RMT, footnote 108) used as input to MMH, the more precise wavelength list of Pierce and Breckenridge (1974), the yet more precise wavelength list of Allende Prieto and García López (1998), the measurements for 750 clean optical lines in the Jungfrauoch disk-center atlas (Delbouille et al. 1973) starting at Table IV (pdf 11) of Rutten and van der Zalm (1984b), the corresponding measurements for 602 clean optical lines in the Sacramento Peak irradiance atlas of Beckers et al. (1976) starting at Table I (pdf 4) of Rutten and van der Zalm (1984a), and the flash-spectrum line intensities starting at Table 3

⁸⁵ History: made by scanning photographic spectrum plates taken at Mt. Wilson with an ingenious microdensitometer using analog tandem-galvanometer nonlinear “calibration curve” conversion of emulsion opacities into solar intensities, illustrated in Minnaert’s prefaces (English and Esperanto).

⁸⁶ History: manually by counting mm² area for each line dip to get its equivalent width, for which the atlas was printed on mm-grid paper. While I was a student De Jager purchased a planimeter as [this one](#) for faster measurement. Later I co-developed electronic tracing readers until replacing the Honeywell-Brown chart recorders of Houtgast’s microdensitometer and the Utrecht solar spectrograph with a self-built analog-to-digital converter and an 8-bit papertape puncher (Rutten and van Amerongen 1975). Regrettably the impressively noisy tape-spewing (120 bytes/s!) puncher got lost so that these gadgets are not on display in the De Jager-started Museum Sterrenwacht Sonnenborgh.

(pdf 51) of [Dunn et al. \(1968\)](#) that I got laboriously punched on Hollerith cards in the 1980s.

The next printed atlases were the Jungfrauoch photoelectric scans of [Delbouille et al. \(1973\)](#) and the Sacramento Peak flux scans of [Beckers et al. \(1976\)](#). The first was unwieldy from too large page size, the second had practical letter page size and also MMH line identifications in the margin. I toted my dog-eared copy to all my spectroscopic observing ever since, annotating every line of special interest. Both atlases also became available on magnetic tape (storing unprecedented millions of bytes) but the digital market was taken over by J.W. Brault's Fourier Transform Spectrometer at the Kitt Peak McMath telescope delivering precise atlases still available on the [NSO website](#) (if you master the non-trivial art of navigating that).

The FTS atlas that I use habitually, not available at NSO, is the "Neckel" disk-center intensity atlas named after [Neckel \(1999\)](#) announcing its availability. Its advantage is that Neckel converted Brault's FTS intensities into absolute units following [Neckel and Labs \(1984\)](#), enabling conversion into brightness temperature for comparing differing spectral regions (*end-note 12*). I also supply this atlas digitally in my [solar file archive](#)⁸⁷. [[Back](#)] [[Main call](#)]

15. Solar neutrinos

Fortunately the fusion-released gamma rays escape by slow outward diffusion converting them into more agreeable sunlight [[RTSA Shu quote \(pdf 110\)](#)] plus enthralling dynamo action causing magnetic flux escape and harmonious humming enabling internal sounding (see never-cited grand/t overview in [Athay et al. 2008](#)). In contrast, the neutrinos that are also released in hydrogen fusion are virtually unstoppable and escape directly from the solar core. For them we do not need RT theory, nor worry about the 10^{11} passing every second through our thumbnails. They posed a [big problem](#) last century when too few were detected. It was not a fault of the measurement nor of stellar structure theory but the blame was on particle physics: part of the solar neutrinos "oscillate" into another flavor on their way here. Photons, once they escape, fulfill their task of information carrying and information-transferring detectability much better.⁸⁸ [[Back](#)] [[Main call](#)]

16. Dielectronic ionization and recombination

Unstable levels: both processes excite one electron in a normal bound-bound transition and put a second electron into a level above the nominal ionization limit of the lower-stage ground state. This is possible because the orbitals are boosted by the first excitation; they may also be non-hydrogenic affected. Such a state is unstable because *autoionization* may occur, freeing the electron from there into escape. This usually leaves the fresh ion in its ground state and then the freed electron carries off the energy excess of the unstable state above that, but if the fresh ion is excited it decays, in CE always per line photon.

The other path out of the unstable level is decay of one (or both) of the excited electrons, in CE also always per line photon, into a configuration with the second electron in a regular bound level below the nominal ionization limit ("*radiative stabilization*").

⁸⁷ It is still available at [ftp.hs.uni-hamburg.de](ftp://hs.uni-hamburg.de) per cd pub/outgoing/FTS-Atlas, accessible per lftp since Firefox and Chrome don't open ftp links anymore. Earlier I retyped the announcement in [Neckel \(1999\)](#) into ADS but it is now Springerwalled.

⁸⁸ Solar neutrinos may convey information on scotogenic dark matter beyond my and your solar physics interest ([de Boer et al. 2021](#)).

Autoionization often has higher probability than spontaneous stabilization.

Dielectronic ionization: an energetic collider, usually hitting the lower ion in its ground state, kicks up two electrons with the first one taking a good part of its kinetic energy. With the remainder the second may ionize bound-free but is more likely put into a high level. If this is still below the ground-state limit both electrons decay radiatively, the second likely in a cascade, together a two-electron multi-level version of pair **d** converting kinetic energy into line radiation without ionization. However, if the second electron reaches an unstable level above the nominal limit then it may be freed by autoionization before its radiative decay, a sequence called "excitation-autoionization" by [Dere \(2007\)](#). The other still bound excited electron decays to the ground state of the new ion, also producing one or more line photons. In this double-excitation manner the energetic collider yields higher ionization probability than for one-electron collisional ionization by losing energy that escapes as line photons.

Dielectronic recombination: in the reverse sequence the energetic colliding free electron kicks a bound electron up to a high level and is itself captured into an unstable state which stabilizes already before re-auto-ionization through spontaneous radiative decay of one of the two excited electrons, often the lower one, to a stable level of the lower stage. If that is still excited it decays radiatively to the ground state; the other electron also, usually per multi-level cascade. Depending on the branching ratios some decays may temporarily end up in a metastable level comparable to Ca II 8542 Å in the Ca II detour example in [Fig. 2 \(pdf 4\)](#) of [Rutten \(2019\)](#) but then not go down from there collisionally as there but CE-wise radiatively in a forbidden transition such as the optical coronal emission lines [[SSX \(pdf 8\)](#)].

Radiative result: no continuum but line photons galore. [[Back](#)] [[Main call](#)]

17. Ca II H & K core reversals

On [page 128 \(pdf 146\)](#) [Jefferies](#) cited the suggestion of [Goldberg \(1964\)](#) that the double emission peaks of the Ca II H & K core reversals may be due to dielectronic recombination and also the demonstration by [Noyes \(1965\)](#) that this does not work for CRD in H & K. Noyes used Avrett's brandnew CRD scattering code producing the canonical $\sqrt{\epsilon}$ graphs of [[SSF \(pdf 80\)](#)] in the belief that CRD is a better approximation than CS which he had initially assumed in [Goldberg and Noyes \(1964\)](#), but actually H & K are PRD lines. Goldberg's mechanism seems to be collisional dielectronic ionization of Ca I leaving Ca II ions excited in the upper levels of H & K – but I note that Ca I is a minority species and think the idea was a red herring.

It does illustrate how during decades the Ca II H & K reversals were the most enigmatic features in the optical spectrum by being the only Fraunhofer-line departures from regular bell shape. This extended literature (e.g., early [Eberhard and Schwarzschild 1913](#)) was outstandingly reviewed by [Linsky and Avrett \(1970\)](#) (but not mentioning the Goldberg–Noyes dielectronic angle). [Athay and Skumanich \(1967\)](#) had suggested that the H₂ and K₂ dips map a temperature minimum as in NLTE cartoon [[SSF \(pdf 37\)](#)], but then [Shine et al. \(1975\)](#) showed that PRD upsets this notion as in cartoon [[SSF \(pdf 89\)](#)] with their [Fig. 9 \(pdf 7\)](#) copied in [[SSF \(pdf 92\)](#)]. In addition, such plane-parallel modeling cannot explain the observed asymmetry between the violet and red peaks (*Sect. 6*).

The Ca II H & K core reversals also govern the famous cool-star relation in [Fig. 1 \(pdf 9\)](#) of [Wilson and Vainu Bappu \(1957\)](#) which to my knowledge remains unexplained. Doing so will

make you famous! Since the main contribution to the peaks in solar irradiance is from activity-measuring calcium network and plage on classic spectroheliograms I suggest an approach along the lines of Scharmer (1976) and Ayres (1979) but applied to fluxtube atmospheres with attention to the slow network waves in the center panels of Fig. 3 (pdf 4) of Lites et al. (1993) and fluxtube shocks as in Kato et al. (2011) while subtracting or including the basal flux contribution (endnote 79). [Back] [Main call]

18. Ba II 4554 Å and Mn I lines

Ba II 4554 Å showed PRD signature near the limb in my eclipse observation in Fig. 9 (pdf 17) of Rutten (1978). It was confirmed in Figs. 1–3 (pdf 4) of Rutten and Milkey (1979) and Fig. 6 (pdf 5) and Fig. 11 (pdf 7) of Uitenbroek and Bruls (1992). The line is a valuable spectropolarimetry diagnostic (e.g., C.U. Keller course (pdf 4), Belluzzi et al. 2007) and also a good Doppler diagnostic of the upper photosphere (Shchukina et al. 2009, Kostik et al. 2009) because it combines large atomic mass, hence small thermal broadening, with considerable core broadening by isotope splitting and hyperfine structure making it suited for filter instruments and so yielding the astounding Dopplergram in Fig. 5 (pdf 4) of Sütterlin et al. (2001).

Other lines with large hyperfine broadening are the Mn I ones recommended by G. Elste to W.C. Livingston as candidates for long-term spectral irradiance monitoring because they are insensitive to infamous microturbulence. Livingston found larger cycle-dependent variation in Mn I 5394.7 Å than for other atomic lines (Fig. 16 (pdf 9) of Livingston et al. 2007). This enhanced sensitivity was attributed by Doyle et al. (2001) to pumping of Mn I 5394.7 Å by Mg II k but erroneously assuming CRD for Mg II k in the spectral synthesis of their demonstration. Vitas et al. (2009) showed that the actual reason is that hyperfine-broadened lines indeed lack the “microturbulent” thermal and granular Doppler smearing through which all narrower photospheric lines lose such sensitivity (MURaM demonstration in their Fig. 6 (pdf 8) and Fig. 7 (pdf 9)).

In a review of this issue in Rutten (2011) Fig. 1 (pdf 2) summarizes Livingston’s results and Fig. 2 (pdf 3) shows that in plage the Mn I blend (at -0.7 Å from Mg II k center) is not pumped at all because the blend is at the wavelength where the PRD source function departs most from the CRD one and sits in the dip outside the Mg II peak even in strong plage. The apparent Mn I over Fe I brightening of plage in Fig. 1 (pdf 2) in scans from Malanushenko et al. (2004) results from mean-field brightness normalization. The surrounding granulation is actually darker in the Mn I line than in the turbulence-sensitive Fe I line while these lines show the same actual plage brightness because the fluxtube “holes” schematized in Fig. 4 (pdf 5) reach as deep because both Fe I and Mn I ionize away. [Back] [Main call]

19. Detour and cross redistribution

Ca II H & K are the strongest lines in the visible and of the dominant ionization stage so that the two-level pairs in Fig. 3 suffice. In the ALC7 star they have $\varepsilon \approx 10^{-4}$ [SSX (pdf 88)], as do Mg II h & k [SSX (pdf 89)] while Ly α reaches $\varepsilon \approx 10^{-6}$ [SSX (pdf 90)]. The other strong lines in the visible are the Balmer lines, the Ca II infrared triplet, the Mg I b triplet, and the Na I D and KI resonance doublets. These are all scattering lines with $\varepsilon \leq 10^{-2}$ but from minority stages⁸⁹ with sizable contributions

⁸⁹ For Balmer lines regard only the hydrogen top with $n=2$ as “ground level” because its population is fully controlled by Ly α doing its own thing (Sect. 7), making this top a low-abundance severe-minority stage

by the detour pairs in Fig. 3, for H α ionization-recombination loops as at right in Fig. 2 (pdf 4) of Rutten (2019) contributing up to 10% [SSX (pdf 96)]. These detour contributions have no coherency. In addition, the Balmer lines have wide Doppler redistribution from the small hydrogen mass and their outer wings are formed deeply where collisional Stark redistribution is large (endnote 60). For Na I D₂ Uitenbroek and Bruls (1992) found PRD signatures only near the limb, none for KI 7699 Å. The much stronger Mg I 2852 Å resonance line has significant PRD effects (Canfield and Cram 1977).

Cross redistribution occurs for the Ca II triplet lines. In the detour sketch at left in Fig. 2 (pdf 4) of Rutten (2019) this concerns the consecutive loop 3933 up, 8542 down and back up, 3933 down. It was analyzed by Uitenbroek (1989) who showed in Fig. 2 (pdf 7) that PRD frequency dependence of the Ca II K source function affects the Ca II 8542 Å source function strongly through the Wien-reversing sensitivity transcription (endnote 32). However, since H & K are much stronger these large PRD effects do not affect emergent Ca II 8542 Å profiles from plane-parallel atmospheres as modeled there because in these the infrared lines are formed well below the heights of PRD source function splitting for H & K. This is likely not the case when both H & K and the triplet lines form together in chromospheric features without such height separation (e.g., spicules-II and return fibrils, endnote 80). [Back] [Main call]

20. Dark EUV features

When you see the same black features on bright backgrounds (on the disk but outside no-emissivity coronal holes) in multiple EUV wavelengths then out-of-the-passband scattering is the most probable mechanism. Cartoon in [SSX (pdf 10)] (where “volume blocking” is a bad misnomer); I drew it as Fig. 10 (pdf 12) of Rutten (1999) to answer a TRACE question by C.J. Schrijver. It shows that when black features are also present in He I 584 Å images (not in AIA alas) the agent is photoionization in the HI Lyman continuum. For shorter wavelengths the agent can also be He I or He II ionization (cf. Carlyle et al. 2014).

This may occur in filaments seen in EUV lines as in the IBIS – SDO active-region blinker of endnote 93. Other such features are “condensation” (meaning recombination) clouds, e.g., in coronal rain (Antolin and Rouppe van der Voort 2012, Antolin et al. 2015) visible in H α via NSE recombination cascade giving large opacity on the disk and large emissivity off-limb as in the temporal cycling of Froment et al. (2020) (Fig. 7 (pdf 10)). More in endnote 100. [Back] [Main call]

21. ALMA as thermometer

The extinction graphs on [SSX (pdf 32)] are a selection of the tableau in Fig. 1 (pdf 4) of Rutten (2017b). They specify SB extinction for the hydrogen mm continua in comparison with Ly α , H α and Ca II 8542 Å. The HI bf and ff continua and H α share an initial steep Boltzmann rise, less steep for Ca II 8542 Å and H⁻ ff, followed by slower decay or leveling out where hydrogen is fully ionized (lower panels). For non-SB NLTE this steep rise desteeptens somewhat, pivoting around the Balmer continuum brightness temperature of 5300 K because that defines radiative overionization from level $n=2$ at cooler and underionization at hotter temperatures; these NLTE corrections can reach 2-3 dex slope modi-

since $n_2/n_H < 10^{-7}$ [SSX (pdf 91)] while the proton fraction $n_p/n_H > 10^{-4}$ where the H α core forms. In this fixed-bottom minority-stage top H α is a resonance line comparable to the alkali resonance lines (endnote 33) but scattering higher while absent in the upper photosphere (endnote 40).

fication of the 10-dex rise (*Sect. 7*). The free-free curves increase with the passband wavelength by the Rayleigh-Jeans factor λ^2 in $\alpha_\lambda^{\text{ff}} \sim N_e N_p T^{-3/2} \lambda^2$ [RTSA Eq. 2.79 (pdf 47)]. The upshot is that hot features that reach optical thickness in H α are likely thicker to much thicker in the ALMA passbands. In the last column of Fig. 1 (pdf 4) hot features become even thicker than in Ly α , still optically thick at only 100-km geometrical thickness at hydrogen density only 10^{11} cm^{-3} .

The assumption of SB LTE in these curves holds for hot conditions giving fast collisional equilibrating, for the hydrogen diagnostics because their equilibrium is regulated by Ly α (*Sect. 7*) which defines the very large Boltzmann increase with NLTE ionization as minor slope correction. However, in post-heating cooling gas the actual extinction hangs per NSE retardance for minutes at the high values reached previously because Ly α settles slower (*Sect. 7*). This explains the large opaqueness of cooling H α return fibrils constituting chromospheric H α network canopies (*Sect. 8*) and their telltale differences with Ca II 8542 Å fibrils (*endnote 81*). For fibrils in H α and Ca II 8542 Å the intensity senses $\sqrt{\epsilon}$ scattering with fibril contrast variations that are defined primarily by individual Doppler modulation for Ca II 8542 Å with its $\sqrt{m_{\text{Ca}}/m_{\text{H}}} = 6.3$ less thermal broadening and by individual retardance history for H α , whereas for ALMA fibril contrasts instead represent actual instantaneous temperatures (*endnote 87*). Hence, the scenes appear different although sampling the same features, with H α core-width the closest to ALMA. However, apparent fibril widths are controlled by lateral scattering in Ly α for both H α and ALMA, so similar.

My prediction in Rutten (2017b) with a tutorial in Rutten (2017a) was therefore that ALMA shows chromospheric canopies wherever these are present in H α (*endnote 87*). The good pattern match between ALMA intensity and H α core width in Fig. 4 (pdf 6) of Molnar et al. (2019) confirmed it.⁹⁰ Earlier predictions based on plane-parallel modeling and various simulations suggested instead that ALMA samples lower “layers” and shocks but these efforts erred in assuming SE hydrogen ionization (*Sect. 7*).

Thus, while ALMA is a thermometer thanks to free-free source function LTE, due to NLT extinction NLTE it more likely samples H α canopies than internetwork acoustics (*endnote 68*) in the claptosphere underneath (*endnote 66*) – a blessing because we understand the latter for decades but do not understand the chromosphere. ALMA furnishes transition-radiation diagnostics that sample chromospheric canopies also seen in H α and in He II 304 Å (*endnote 87*). [Back] [Main call]

22. White-light corona

The reason why we must travel far to see the corona⁹¹ is evident

⁹⁰ In prediction 2 (pdf 9) of Rutten (2017b) I wrongly claimed dark-dark correspondence between ALMA and H α images. It should instead have been bright-bright correspondence between ALMA intensity and H α core width as indicator of kinetic temperature, evident in the bottom rows of Fig. 6 (pdf 7) of Cauzzi et al. (2009) which I plotted myself and should have remembered. The next-best indicator there is Ca II 8542 Å Doppler-shifted minimum intensity but there is no correlation for H α minimum intensity which is history-modulated rather than thermally sensitive. Indeed my ALMA to GONG H α pattern alignment in *endnote 89* uses dark-bright instead of dark-dark correspondence in quiet areas, similarly to my GONG H α pattern alignment to AIA 304 Å there. Active regions instead show bright-bright correspondences between these pairs, as evident for H α core intensity and He II 304 Å in the IBIS – SDO blinker of *endnote 93*.

⁹¹ Personal history: after starting my career with spectroscopy at three eclipses my wife and I became positively corona-infected eclipse

from the visibility diagram in [SSX (pdf 5)] after Fig. 6 (pdf 51) in the classic review by van de Hulst (1953).

The pearly white color and linear polarization of the K corona and its apparent radiation temperature (Mitchell and Mulders 1938) suggest photospheric light that is bent towards the viewer without wavelength selectivity (unlike blue-favoring Rayleigh scattering, hence Thomson scattering, Mie scattering, or reflection without refraction). The absence of photospheric Fraunhofer lines in the coronal spectrum, unlike their presence in the spectrum scattered by your nose, was a large disappointment for the first observers bringing spectroscopes to totality, played a role in the debate whether the corona is real or an illusion, and remained enigmatic during many decades.⁹² Thomson and Mie scattering are coherent so retain frequencies and hence should retain Fraunhofer lines. Then Grotrian (1931) noticed that Ca II H & K leave a washed-out dip and proposed here (pdf 22) that their 100 Å smearing corresponds to 7500 km s⁻¹ Doppler redistribution [SSX (pdf 6)]. However, he excluded thermal broadening with a reminder that the solar-atmosphere temperature is at most 6000 K while this deep-photosphere value gives only 550 km s⁻¹. He did not specify the corresponding broadening temperature $6000 \times (7500/550)^2 = 1.1 \cdot 10^6 \text{ K}$ – too outrageous since everybody knew that heat flows necessarily from hot to cool so further out from the deep may only be cooler – but hinted (with his footnote 3 (pdf 22)) that some sort of nonthermal ionization might play a role.

His second-law-challenging attribution to million-K thermal electron motion came after Edlén’s high-ionization term inventory enabling his identification of the enigmatic bright “coronium” lines [SSX (pdf 8)] also requiring such high temperature for ionization (cf. Russell 2018). Detection of synchrotron radio emission was the clincher for the greatest solar physics discovery so far. Explaining million-K coronal temperatures beyond incantation “nanoflare heating” citing Parker’s (1972) small-scale reconnection of twined, braided, knotted fields remains a challenge while dielectronic line emission helps keeping the corona cool (*endnote 16*).

For smooth-disk illumination the scattered brightness is locally proportional to N_e , but as pointed out by Minnaert (1930) limb darkening (and perhaps spots) must be accounted for in the local scattering source function $S_\nu = J_\nu$, and also the integration along the entire line of sight with problematic confusion between different structures, as evident in the marvelous Druckmüller eclipse images.

The outer-corona F component in [SSX (pdf 5)] is from Mie scattering by dust particles that move slower, maintaining Fraunhofer-line signatures. [Back] [Main call]

23. Extinction diagrams, H-minus

Diagrams of bound-free and free-free He and H α extinction for different stellar atmospheres assuming SB are shown in the four Figs. 8.5⁹³ of Gray (2005) and in [SSF (pdf 53)]. Three earlier versions in Gray (1992) are copied into [RTSA Fig. 8.14 (pdf 211)]. In both sets the first panel is for the Sun and shows the broad hump of H α bound-free extinction around 1 μm , unlike Kramers-law λ^3 decay below the 1.6 μm threshold because

tourists. Our traveling in 2020 to my 15th, completing three Saros 142 periods, was covid-canceled.

⁹² Nowadays appreciate when admiring the eclipse corona that you are illuminated by your cleanest sunshine ever: pearly white, no dark lines, beautiful polarization (Fig. 2 (pdf 3) of Snik et al. 2020), the most straightforward solar density diagnostic – and still the greatest enigma.

⁹³ Erratum: Fig. 8.5a has (in Gray’s words) a small error of 10^{-26} .

H^- is not a one-electron but a two-electron system, and the regular $\sim \lambda^3$ increase for H^- free-free extinction which dominates beyond the threshold. For hotter stars (other panels) the atomic $H I$ bound-free edges take over.

The telltale H^- pattern was first shown observationally in later forgotten Fig. 4 (pdf 19) of Lundblad (1923) and then in Fig. 4 (pdf 14) of Mulders (1936), see also (if you read French) Chalonge and Kourganoff (1946).⁹⁴ On p. 166 (pdf 28) Pannekoek (1930) already proposed H^- free-free as main stellar-atmosphere opacity agent but also this was forgotten until Wildt (1939) resuggested it, eventually proven by the landmark lengthy computation⁹⁵ by Chandrasekhar and Breen (1946) producing their Fig. 3 (pdf 10). It is treated in practical SSB 2 (pdf 13).

The classic comprehensive extinction “confusograms” in Figs. I–XV (pdf 17) of Vitense (1951) were redrawn in English in Novotny (1973), with the solar one shown in [SSF (pdf 54)] and reprinted in [RTSA Fig. 8.5 (pdf 199)] and four stellar ones in [RTSA Figs. 8.15–8.18 (pdf 212)]. Their not-so-trivial interpretation⁹⁶ is treated in [RTSA Problem 10 (pdf 252)].

I have emulation programs and comparable resulting diagrams for both Gray’s and Vitense’s graphs in my IDL [edulib](#). An overview of total extinction including lines in the FALC atmosphere is shown in Fig. 6 (pdf 13) of Rutten (2019). The minima are treated in [endnote 27](#). [[Back](#)] [[Main call](#)]

24. Emission measure, DEM

Colleagues studying the coronal EUV spectrum usually do not worry about photons after their creation when not ending in their telescope.⁹⁷ Unhindered travel to the telescope, no extinction, only emissivity counts in their production per pair \mathbf{d} . This must be evaluated for all lines within the passband⁹⁸ at every location

⁹⁴ History: while writing this I was pointed by Minnaert in footnote 1 (pdf 1) in Chalonge and Kourganoff (1946) to Lundblad (1923), a formidable read. “Scattering or real absorption?” is the key question here too; I admire his “collustrivity function” for J_ν , and wonder whether his Eq. 15 (pdf 7) is an early Eddington-Barbier – but yet after its succinct statement in Eqs. 36–37 (pdf 9) of Milne (1921), his first but yet more formidable publication (see Paletou 2018).

⁹⁵ History: at the bottom of p. 431 (pdf 2) Chandrasekhar and Breen (1946) wrote “In any case, to improve on the Hartree approximation would require an amount of numerical work which will be several fold; and the task is immense even as it is” with footnote: “the present work has required the numerical integration of 63 radial functions and the evaluation of 523 infinite integrals, not to mention the computation of numerous auxiliary functions and tables. (All this work was done with a Marchant.)” where a Marchant was a desktop mechanical calculator containing hundreds of gears which could add, multiply, and even divide by repeatedly cranking a handle. Chandrasekhar spent months of computer time on H^- , literally cranking. I still used a Marchant for being more precise than my three-digit Darmstadt slide rule in computing 1966 eclipse parameters from Besselian elements before learning ALGOL 60 for the 1970 eclipse and was happily surprised when in 1972 the HP-35 pocket calculator changed our world (nowadays called a phone because your advanced pocket computer does that too).

⁹⁶ When E. Vitense wrote her textbook Böhm-Vitense (1989) she didn’t copy her thesis graphs but simplified them in Fig. 7.8 = [SSI (pdf 7)].

⁹⁷ Solar physicists used to be either thin or thick. Thin ones excelled in atomic and later in plasma physics, thick ones in 2-level scattering and later in MHD. They now grow together. The Sun doesn’t care and magnanimously sends photons to both types adhering to her kind “Principle of Solar Communicativity” (pdf 9) formulated at the only solar IAU symposium ever in the USSR (Rutten 1990).

⁹⁸ For spectral-passband imagers as AIA usually a complex multi-temperature combination from registering multiple lines. Spectrometers as Hinode’s EIS register spectrally dispersed bands but do not inform precisely where from – slitjaw imaging as by IRIS is highly desirable

along the line of sight and integrated with confusion an issue. Locally the emissivity scales with the product $n_l N_e$ of lower-level population density and electron density, the latter representing the required collider for excitation per \mathbf{d} which is most likely an electron. Regard a resonance line from an ion ground state. Its population enters as $(n_l/N_E) A_E N_H$ with element E abundance $A_E = N_E/N_H$, hence local emissivity $\sim gf A_E G_{ij}(T) N_e N_H$ where G_{ij} is a conglomerate function of temperature describing the element partitioning defining n_l/N_E for this line ij and needing all sophistication of CHIANTI ([endnote 26](#)) for evaluation within the CE assumption. For a review see Del Zanna and Mason (2018). If the line is from an excited state function G_{ij} depends also on electron density. Integration over the volume of an unresolved emitting structure (say a loop) yields emission $\sim gf A_E \int G_{ij}(T) N_e N_H dV$ where N_H is often replaced by N_e taking $N_H = N_p \approx N_e (1 - 2B)$ with B the helium/hydrogen abundance ratio (Sect. 5 (pdf 20) of Pottasch 1964). The density dependencies $N_e N_H$ may be removed using the differential emission measure $DEM(T) \equiv N_e N_H (ds/dT)$ in $\text{cm}^{-5} \text{K}^{-1}$, a combined local gradient measure that defines the emission measure integrated over s along the line of sight as $EM \equiv \int N_e N_H ds = \int DEM(T) dT$ in cm^{-5} (Sect. 7 (pdf 113) of Del Zanna and Mason 2018). With this density removal the emission in the line from a feature becomes $\sim f A_E \int DEM(T) g G_{ij}(T) dT$ where the Gaunt factor g is under the integral because it depends on temperature (Eq. 2 (pdf 3) of Withbroe 1978). [[Back](#)] [[Main call](#)]

25. Multi-DEM analysis

The different AIA passbands are often characterized as each sampling a specific temperature with larger brightness implying more gas of that temperature. Of course this is a simplification because each passband is wide and contains multiple lines. Recognizing this it is tempting to exploit multiple AIA EUV passbands⁹⁹ with their different temperature sensitivities for constraining the temperature of a feature or just a pixel in “DEM analysis” as in Cheung et al. (2015) where the validations against “ground truth” simulation inputs in Figs. 6–9 (pdf 8) are impressive. However, on smaller scales than large AR-like features as modeled there multi-temperature confusion along the line of sight poses problems. In addition, for rapidly evolving or short lived features the assumption of SE within CHIANTI’s CE assumption is likely invalid because equilibrating is slow at low electron densities, a similar warning as treated extensively for hydrogen diagnostics including ALMA of denser cooling cooler gas in the remainder of this compendium after the thin–thick separation point (p. 9). [[Back](#)] [[Main call](#)]

26. CHIANTI

CHIANTI website. (Name suggestion: *Coronal Holism In Appreciating Non-Thick Ionization.*) Community effort by [these colleagues](#). It handles coronal spectroscopy with a large transition inventory for evaluating CE ionization equilibria, radiative losses, DEMs and more. The need to include numerous lines

– or miss the more interesting happening just off the slit. It is a pity that Fabry-Pérot imaging spectroscopy is not feasible at short wavelengths; SST/CHROMIS is the shortest (Scharmer et al. 2019). My paradise dream is slitless 2D imaging spectrometry resolving wavelength across $Ly\alpha$ (continued in [endnote 97](#)).

⁹⁹ Usually excluding 304 Å for “being too optically thick” for CE-based CHIANTI ([endnote 26](#)) – oops ([footnote 26](#)).

contributed by dielectronic processes (*endnote 16*) makes it ever-growing.¹⁰⁰ [*Back*] [*Main call*]

27. Deepest wavelengths

The FALC extinction spectra in Fig. 6 (pdf 13) of Rutten (2019) show the canonical minimum at the $1.6\mu\text{m}$ threshold of H⁻ bound-free extinction where one sees deepest into the Sun (e.g., Lamy et al. 1979). A nicer display is Avrett's holistic sketch in [SSX (pdf 36)] from Avrett (1990) plotting brightness temperature (*endnote 12*) through the entire VALIIC spectrum.¹⁰¹ Both left and right of the double-hump maximum at $1\mu\text{m}$ the extinction and formation height increase, sampling the photospheric temperature decrease until the VALIIC minimum above which lines and edges reverse into emission, with line crowding in the blue and UV sketched schematically. The shallow dip between the humps (continuum enlarged in [SSI (pdf 5)] and [SSF (pdf 55)]) spans the visible. The second hump is the opacity minimum at 4000Å . At shorter wavelengths metal ionization edges steeply increase the summed continuous extinction [SSI (pdf 7)].

The 4000Å extinction minimum provides nominally less deep sampling than the $1.6\mu\text{m}$ dip [SSF (pdf 55)], but effectively better because contribution functions steepen and intensity contrasts increase with the Wien response to temperature variations (Ayres 1989). In addition, the diffraction limit is also four times sharper (but needs yet better seeing since the Fried aperture $r_0 \sim \lambda^{6/5}$). Hence, SST/CHROMIS 4000Å imaging is currently the best in observing deepest granulation (Scharmer et al. 2019). For deep imaging of intergranular MCs the SST 3950Å wide-band filter is yet better because it samples the overlapping outer wings of Ca II H & K between these lines where reduction of collisional damping by lower density produces wing opacity reduction, hence hole deepening in MCs brightening them into increased contrast. See the SST sample in Fig. 2 (pdf 4) of Rutten (2020).¹⁰² [*Back*] [*Main call*]

28. Square root epsilon law

This T-shirt-qualifying law says $S_\nu(0) = \sqrt{\epsilon_\nu} B_\nu(T)$ at the top of an isothermal constant- ϵ 2-level-atom plane-parallel non-irradiated atmosphere [RTSA Eq. 4.81 (pdf 117)], as shown in Avrett's [RTSA Fig. 4.21 (pdf 128)]. The emergent intensity [RTSA Eq. 4.84 (pdf 117)] is similarly low: scattering lines get dark.

It seems a straightforward result from simple linear-looking Eq. 3 and Eq. 4 for such a simple atmosphere – but Hubený (1987b, 1987a)¹⁰³ to renamed it the Rybicki equation and analyzed why and how it works (which I did not understand and therefore handed out as student presentation topic in my RTSA course). I added two pages explanation myself [RTSA discussion (pdf 117)] (which Zwaan said he did not understand).

I also taught the definition of ϵ wrongly in IART (now correct in [IART Eq. 7.10 (pdf 101)]) until I finally grasped that

the cancellation of \mathbf{c} and \mathbf{g} even applies to Thomson scattering. [*Back*] [*Main call*]

29. Validity of $\sqrt{\epsilon}$ law

The ALC7 “chromosphere” is near-isothermal [SSX (pdf 72)] with near-constant ϵ in lines as Na I D₁ [SSX (pdf 80)] from increasing hydrogen ionization and hence near-constant (relatively increasing) electron density defining the collision frequency handling destruction pair \mathbf{a} . The gas density drops exponentially outward [SSX (pdf 72)] but electrons dominate the collision frequency by moving much faster than atoms. Avrett's canonical isothermal + constant $\sqrt{\epsilon}$ demonstrations [SSF (pdf 80)] therefore apply well to strong lines from ALC7.

In addition, strong lines experience an atmosphere as more isothermal than the continuum because their total τ scales are compressed in height with respect to the continuum τ scale due to their steeper buildup [SSF (pdf 38)], flattening their $B(\tau)$ gradient [SSF (pdf 85)]. Where the temperature decays obeying RE as in the upper photosphere (*endnote 55*), lines see yet shallower B_ν gradients.

Hence line core darkening by $\sqrt{\epsilon}$ scattering applies to many strong lines. [*Back*] [*Main call*]

30. Menzel departure coefficients

Be aware that Avrett and Fontenla used the Menzel definition of population departure coefficients that applies the next-ion population as normalization and is described carefully in VALIII Eqs. 13–18 (pdf 29). I use the more intuitive Zwaan definition [RTSA Eq. 2.104 (pdf 53)] [SSF (pdf 73)] using the total element population as normalization.¹⁰⁴ Colleagues may think to use the latter while using the former not realizing that between the two the values reverse for majority species as HI – which led Fontenla et al. (2009) to misinterpret their own results (Rutten and Uitenbroek 2012). Various other authors (not to be named) reversed the meaning of VALIII Fig. 30 (pdf 30) into its b_1 curve implying chromospheric hydrogen ground-state population ten times the total gas density – ignoring equation (18) above the figure. [*Back*] [*Main call*]

31. Epsilon is small

Another T-shirt slogan for this course. Its value sinks from unity in the deep photosphere to $\epsilon \approx 10^{-2} - 10^{-6}$ for Na I [SSX (pdf 80)], Ca II K [SSX (pdf 88)], Mg II k [SSX (pdf 89)], Ly α [SSX (pdf 90)] making the line source function mostly J hence NLS. For estimating emergent intensity with the Eddington-Barbier approximation you then need to know the local intensity in all directions defined by source function values elsewhere. If the $\eta_{\nu_0} S_{\nu_0}^d$ contribution is significant you also need to know the intensity in all directions in other transitions with other wavelengths. Worse, the same may hold for evaluating the $\tau_\nu(h)$ scale needed in your Eddington-Barbier interpretation or your line synthesis results or in your “inversion” code. RT is easy only when LTE holds everywhere at all participating wavelengths for all S and α processes or when there is no RT as in CE.

The smallness of ϵ is also numerically challenging. The source term ϵB may seem neglectable but it isn't because without it there are no photons to scatter. In the early days of electronic computing it was tempting to stop Λ iteration [SSF (pdf 101)] when the convergence reached tiny steps at the machine precision – but they were not negligible because still far from the answer needing many more [SSF (pdf 103)]. This was

¹⁰⁰ Example from P.R. Young for He-like O VII: currently CHIANTI specifies 577 levels, 127 below the ionization threshold and autoionization rates specified from 128 up. Since CHIANTI v9 the 25 levels of O VIII are added also.

¹⁰¹ I used it as RTSA exam by white-pasting labels and then ask explanation of every curve (my teaching is always graphic). Try yourself?

¹⁰² The sharpness difference between the SST and HMI magnetograms in Fig. 2 (pdf 4) is dramatic. However, also the SST lacks magnetic sensitivity; only the Hinode SP reaches non-kilogauss internetwork fields thanks to long integration in seeing-free space (*endnote 79*).

¹⁰³ History: written without library or computer access. The year may hint why.

¹⁰⁴ I used to write these as β_l and β_u following Wijnnga and Zwaan (1972) but stopped because colleagues use b wrongly anyhow.

remedied by operator splitting in approximate Λ iteration (ALI) [SSF (pdf 102)] [RTSA Sect. 5.3.2 (pdf 145)] and convergence acceleration [RTSA (pdf 150)] [SSF (pdf 103)].

Also, at small ε the up and down radiative rates may be large but nearly cancel; then using their “net radiative bracket” normalized difference can be numerically better and useful (Thomas 1960, Eq. 6.75 ff (pdf 151) of Jefferies 1968, Eq. 10 (pdf 6) of Carlsson and Stein 2002). [Back] [Main call]

32. Photon pumping, laser, Wien transcription

Photon pumping is multi-level NLW interaction where one transition may feed another photons and Wien sensitivity. Classic nighttime cases are planetary-nebulae and nebular lines ([SSX (pdf 142)] ff). The two detour loops in Fig. 2 (pdf 4) of Rutten (2019) are good solar examples.

At right the Balmer continuum overionizes hydrogen from level $n = 2$ in the upper photosphere because it escapes much deeper and at short wavelengths where the large Wien sensitivity produces $J_\nu > B_\nu$ as in [SSX (pdf 76)] for the ALC7 star. Hence the ALC7 proton density is “pumped up” with respect to the local SB value (the $n=2$ level has $b_2 \approx 1$ because Ly α is thermalized (lefthand plot [SSX (pdf 76)]). This photon excess contributes together with Brackett, Paschen and Balmer-line photon losses (suction, *endnote 33*) into downward overpopulation flow through the HI Rydberg levels (Fig. 3 (pdf 6) with explanation in Rutten and Carlsson 1994). Hotter features in the deep photosphere cause larger hydrogen overionization higher up and also sideways in cooler surroundings.

The $S^l/B \approx b_u/b_l$ ratio may so be controlled in the Wien domain and transcribe to the Rayleigh-Jeans domain where given departure ratio from unity has larger effect as plotted in [SSF (pdf 74)] from [RTSA Fig. 2.8 (pdf 54)]. Blow-up and then negative laser is reached at right (line extinction and source function both become negative for sufficient b_u/b_l [SSF (pdf 74)] [RTSA Eq. 2.116 (pdf 55)] but emissivity remains positive). Such blow-up (but not yet laser) is reached in the Mg I 12 micron lines (*endnote 45*).

For Fe II lines long-wavelength S^l/B blow-up from pumping in the ultraviolet with transcription of the exponential Wien sensitivity holding there to linear Rayleigh-Jeans sensitivity is illustrated in Fig. 5 (pdf 6) of Cram et al. (1980) and in Fig. 3 (pdf 10) of Rutten (1988). In the latter the high peak of the excitation temperature for Fe II lines at 7000 Å arises because it must accommodate the imposed b_u/b_l ratio, here b_u overpopulation excess because $b_l \approx 1$ for dominant-stage ground states. The b_u overpopulation results from radiative $J_\nu > B_\nu$ feeding in the ultraviolet (Fig. 1 (pdf 5)). At smaller temperature sensitivity larger T_{exc} excess is needed for the imposed b_u/b_l ratio.

The lefthand detour loop in Fig. 2 (pdf 4) of Rutten (2019) is for Ca II. Similar transcription of the Wien sensitivity of the PRD-split source function of Ca II K to Ca II 8542 Å is evident for the wing source functions (label g) of Ca II K in panel c and of Ca II 8542 Å in panel g of Fig. 2 (pdf 7) of Uitenbroek (1989). [Back] [Main call]

33. Photon loss, no nanoflare heating, photon suction

“Photon loss” means losing the energy content of a photon altogether from the object (star, atmosphere, feature), as “neutrino losses” means energy losses from a stellar core. In both the LTE and CE extremes the energy loss is direct because the emergent photon was locally created collisionally (bound-bound pair **d** or in LTE **e**, their bound-free equivalents, free-free). Where

the Maxwell distribution holds this is direct loss of local thermal energy.

For LTE it should be a negligible leak (otherwise LTE is not valid); an example is forbidden Mg I 4571 Å from ALC7 with $S^l \approx B$ out to $\log(\tau) \approx -4$ in [SSX (pdf 82)] (but not its opacity which is heavily depleted by ultraviolet overionization).

For CE summing all emergent photons from an EUV-bright feature quantifies radiative losses that measure required heating for a stable structure obeying SE (otherwise CE is not valid). Hence CHIANTI-computed radiative loss curves following classic Fig. 2 (pdf 6) of Cook et al. (1989) specify required steady coronal heating for stable emission. However, it is a mistake to count summed brightness of short-lived bright features as contribution to local heating: to the contrary, this energy heats the telescope detector while the many more photons missing that either illuminate the universe unremarkably or drown unnoticed in the photosphere. Only the non-radiation-lost remainder of the feature heating may count. What you see is what <you> get, not the gas; what you see does not tell you what that gets. Observing small flaring flames spoils their nanoflare heating candidacy unless their emission is demonstrably a small fraction.

For a two-level scattering line (initial **d** or **e** followed by many **b** or **c** steps with small chance of collisional destruction) the actual photon losses occur near the mathematical $\tau = 0$ surface, in the last scattering around depth $\tau = 1$, but the losses start being felt already near the thermalization depth. There the radiation is nearly isotropic (fully in the isothermal simplification) and becomes more and more anisotropic further out, ending up purely outward directed at the surface. The scattering decline towards the $\sqrt{\varepsilon}$ value there may be seen as inward-diffusing photon losses. The same holds within effectively thick features rather than a plane-parallel atmosphere.

For two-level atoms the losses deplete the upper level with larger fractional b_u decrease than the corresponding fractional b_l increase of the lower level due to the Boltzmann ratio between them: in two-level atoms the lower level is the main population reservoir with $n_1 \gg n_2$ and therefore close to LTE because there is nowhere else to go so that nearly the whole abundance sits in $n = 1$. The b curves in the first plot of [SSX (pdf 89)] for Mg II k in ALC7 are the textbook example. These ions are not two-level atoms but close to it because Mg is predominantly once-ionized throughout the ALC7 photosphere and chromosphere, as shown by the fractional lower-level population curve in the same plot. Hence Mg II h & k suffer NLS two-level scattering only, no NLW interlocking to other wavelengths nor NLT memories in time.

“Photon suction” is a NLW multi-level detour phenomenon, done by strong lines when the population reservoir is in the next stage, as for most neutral metals in the photosphere. It is the reverse of photon pumping in which incoming photons overexcite higher levels from a lower population reservoir (*endnote 32*); in photon suction outgoing photons draw population from a higher reservoir down into lower levels. The alkali resonance lines are the prime example.

Figure 6 (pdf 8) of Bruls et al. (1992) shows ground-level departure curves b_1 (still called β following Wijnbenga and Zwaan 1972) of K I and Na I increasing slightly until the height where ultraviolet underionization causes steep rises. This slight increase was surprising because neutral metals suffer ultraviolet overionization in the upper photosphere by sampling the hot Balmer continuum coming from below, evident in the ALC7 population panels for Mg I 4571 Å in [SSX (pdf 82)] and Fe I 6301.5 Å in [SSX (pdf 83)]. Such pumping may happen from excited levels, but the alkali ground-state ionization edges

at 2856 Å for KI and 2411 Å for NaI suffer it also. For them the overionization is fully compensated by population replenishment from the low-lying next-ion population reservoir, drawn from there in a net recombination flow along high levels that is driven by the photon losses in the resonance lines¹⁰⁵. If one starts a NLTE modeling iteration with LTE populations the ultraviolet $J_\nu > B_\nu$ excesses deplete the ground state but the NLTE scattering losses diffuse inward and draw recombination population until SE is reached with full suction compensation for the alkalis with their low ionization energies. A two-level-plus-continuum demonstration is shown in Fig. 2 (pdf 4) of Rutten and Carlsson (1994), with explanation. It was made by J.H.M.J. Bruls for the cover of Bruls (1992). [Back] [Main call]

34. Coronal clouds

The simplest clouds are fully transparent as CE assumes for coronal structures, e.g., loops. No RT whatsoever. In optically-thick RT terms: the homogeneous thin cloud solution [ISSF Eq. 27 (pdf 13)] has no impinging intensity from behind ($I_\nu(0) \approx 0$) in CE hence $I_\nu(D) \approx S_\nu \tau_\nu(D) = j_\nu D$ with D the geometrical cloud thickness along the line of sight. This holds for Thomson scattering producing the white-light off-limb corona (with $S_\nu \approx J_\nu$, *endnote 22*) and also for locally thermally created EUV radiation. In terms of Eq. 3 for the latter (applicable if we count escaping photons into α_ν^d with $\eta_\nu^d \approx 1$ for CE) both $J_\nu \approx 0$ and $S_\nu^d \approx 0$ so that $S_\nu^l \approx \varepsilon_\nu B_\nu(T)$ or $J_\nu^l \approx \alpha^a B_\nu(T)$ with exceedingly small α^a and ε_ν due to absence of collisional deexcitation.

Even though all line photons are thermally created the intensity stays far below saturation to the Planck function for lack of local enclosure. The corona is far hotter than the photosphere and its radiation is thermal and defined by its temperature just as for the optical continuum from the photosphere [SSI (pdf 4)] – but in contrast to the photosphere the corona radiates far below its thermal capacity because it lets all new photons depart instead of boxing them in. [Back] [Main call]

35. Sophisticated clouds

Cloud complexity was added by e.g.,

- Molowny-Horas et al. (1999): cloud model look-up tables for “inversion”;
- Heinzel et al. (1999) and Mein et al. (1996): source function variation along the line of sight. This was already done by Beckers (1968) in a famous spicule review by using NLTE population tables for hydrogen from Giovanelli (1967) – although warning against assuming SE below Eq. 10 (pdf 32), an early precursor of Carlsson and Stein (2002) dynamic H ionization indeed holding for spicules (*endnote 80*);
- Chae (2014): second cloud model for the incident profile;
- Heinzel et al. (2015): filament RT multi-thread RT with mutual irradiation.

For the incident profile often a field average or a nearby sub-field average is used but this is wrong in the case of backscattering as observed for H α filaments as sub-filament brightening towards the limb by Kostik and Orlova (1975), proposed for H α fibrils by Al et al. (2004), and occurring in 1D standard models (*endnote 40*). The near-equality of the dashed profiles in the lower panels of their Fig. 8 (pdf 7) made Rutten and Uitenbroek (2012) suggest as recipe (pdf 9) to use the outward intensity profile in a RE model at optical depth equal to the cloud’s thickness

as impinging background profile [SSX (pdf 3)]. This recipe improves the finding of Bostanci and Al Erdogan (2010) that a RE emergent-intensity estimate works best. [Back] [Main call]

36. Na I D, Mg I b, Ca II 8542 Å heights

[Spoiler: million difference in line identification [SSF (pdf 41)].] The same Fig. 4 (pdf 5) of Uitenbroek and Bruls (1992) is also the subject of less simple but recommended [RTSA Problem 7 (pdf 250)] on Na I D₂ line formation in the FALC star (*Sect. 6*) [Spoiler: my answers to most RTSA problems]. The Na I D lines are the deepest in the visible (Fig. 4 (pdf 17) of Rutten and van der Zalm 1984b, Fig. 10 (pdf 18) of Rutten 2019)¹⁰⁶. The Na I D lines are often called chromospheric. Your Eddington-Barbier estimate $h \approx 500$ km with [SSF (pdf 40)] puts the Na I D₂ formation just above the temperature minimum of the FALC star, but the line source function shows a $\sqrt{\varepsilon}$ scattering decline as if the FALC star has no non-RE heating whatsoever. The photons emerging there were made much deeper, near thermalization depth in the photosphere, and scattered out from there ignoring the temperature rise and then escape. Intensity variations of the core therefore correspond to photospheric temperature variations, not at the $\tau \approx 1$ Eddington-Barbier height. This scattering is quantified for Na I D₁ in the similar ALC7 star in [SSX (pdf 85)] where the S, B, J graph shows optical depth locations, destruction probability, thermalization length and decoupling height ([SSX (pdf 80)], *endnote 57*). The Na I D lines are the deepest because they are the strongest scattering lines of which the emergent intensity is fully controlled within the photosphere. However, in measuring Doppler or Zeeman modulation the Eddington-Barbier estimate for the inner wings may be appropriate because these signals are encoded at the last scattering.

Similar FALC results in Fig. 13 (pdf 11) of Rutten et al. (2011) compare Na I D₁ formation with Mg I b₂ and Ca II 8542 Å formation. Mg I b₂ forms similar to Na I D₁, decoupling slightly higher, but the source function of Ca II 8542 Å decouples above the FALC temperature minimum so that this line does convey FALC-chromosphere signature. The same is seen for the ALC7 star in [SSX (pdf 27)] and in comparing [SSX (pdf 85)] [SSX (pdf 84)] [SSX (pdf 87)].

Rutten et al. (2011) used high-quality SST observations to compare the three lines in intensity in Fig. 4 (pdf 5) in comparison with simulation results in Fig. 5 (pdf 6) and those smeared to observation-resolution in Fig. 6 (pdf 7), and then observed and simulated line-core Dopplergrams in Fig. 7 (pdf 8). These figures confirm non-chromospheric sampling by Na I D₁ and Mg I b₂ whereas Ca II 8542 Å does show chromospheric signatures (*endnote 81*). The main difference between the first two is that the Na I D lines have higher Doppler sensitivity than the Mg I b lines by having narrower cores with steeper flanks. This explains the remarkable difference between their wings in sampling upper-photosphere reversed granulation in Fig. 1 (pdf 2).

¹⁰⁶ History: the first was drawn with a Calcomp plotter, a mechanical device moving a pen with an ink cartridge transversely across a rotating drum with paper chart from a large roll, both motions computer-controlled in 0.01 inch steps. Each strip was a meter long and photographically reduced to photo-offset print size. Earlier the entire university computer (one for all, *endnote 5*) was required for such plotting. For job scheduling (per estimated duration) I had to count all steps in a two-minute job (*endnote 5*). The operators liked plotting these crowded spectral charts for giving them long steps-specified breaks. They also liked the endless runs of Veltman’s *schoonschip* (*footnote 19*) by G. ’t Hooft earning their joint electroweak renormalization Nobel by eventually producing only zeroes.

¹⁰⁵ The compensation was earlier noted in Fig. 1 (pdf 3) of Gomez et al. (1991) but there incomplete from lacking high levels in the model atom.

The steep Na I D flanks also make Na I D Dopplergrams a sharp proxy for localizing upper-photosphere shocks in MCs, as summarized in [SSX (pdf 54)].¹⁰⁷ [Back] [Main call]

37. Contribution, response, sensitivity

When using “the formation height” you may earn my scorn. Only thin clouds at specific height (as in *endnote 34*) share their height between different formation quantities. For thick objects a common characterizing escape height may be applicable when LTE holds for all contributing processes, but for scattering lines the intensity is set by temperature much deeper and more widely within the atmosphere or within an effectively thick structure than the Doppler and Zeeman response to line-of-sight velocities and magnetism (as in the Na I D example of *endnote 36*). Also, for weak lines the emergent intensity is dominated by background continuum processes rather than line processes (exemplified by their factor-million height ratio in [SSF (pdf 41)] with Schuster-Schwarzschild cloud modeling appropriate for the telluric blends).

In plane-parallel atmospheres the vertically emerging intensity is $I_\nu = \int S_\nu \exp(-\tau_\nu) d\tau_\nu$ with integrand or “contribution function” $S_\nu \exp(-\tau_\nu)$ sketched in [SSF (pdf 29)], an extended plume. The photons do not “escape from $\tau_\nu = 1$ ” but throughout this plume. Such contribution plumes are plotted against height, i.e., $dI/dh = j_\nu(h) \exp(-\tau_\nu(h))$, for many wavelengths in the VALIIC spectrum in fabulous many-page Fig. 36 Fig. 36 (pdf 33) of Vernazza et al. (1981) with excerpts in SSX. The first one in [SSX (pdf 61)] for the 500 nm continuum shows the expected contribution shape with initial $j_\nu(-h)$ rise set primarily by near-exponential inward density increase until stopped by the steep $\exp(-\tau)$ decrease and with $I(1, 0) \approx S(\log \tau = 0)$. The last one in [SSX (pdf 67)] for $\lambda = 40$ nm shows weird dI/dh shape without peak near $\log \tau = 0$ and two orders-of-magnitude deviation from the Eddington-Barbier value.

Earlier, sophistication beyond this simple integrand was based on weighting functions (e.g., Pecker 1951) and deriving such for line depression rather than emergent intensity (Gurtovenko et al. 1974). The most informative format became Carlsson’s integrand breakdown rewriting dI/dh into $[S_\nu] [\tau_\nu \exp(-\tau_\nu)] [d(\ln(\tau_\nu))/dz]$ in Eq. 6 (pdf 15) of Carlsson and Stein (1994) and grey-scale charting these three terms and their product as function of height and wavelength through the line of interest (Fig. 8 ff (pdf 16), *endnote 65*).

In the meantime “response functions” were formulated that estimate the effect of perturbations of a given quantity on an emergent line profile (classics Mein 1971, Beckers and Milkey 1975, Magain 1986) but nowadays this is done by numerical sensitivity analysis, for example the “multi-Multi” analysis in Fig. 12 (pdf 14) of Carlsson et al. (1992) varying many transitions in their Mg I model atom one by one (*endnote 45*), the successive step-function temperature perturbation to quantify UV intensity response of Fossum and Carlsson (2005b) and the NLTE-nonE versus LTE simulation-run comparison in Fig. 4 (pdf 7) of Leenaarts et al. (2007) (Sect. 7).

Scorn-avoiding moral: even if your nice simulation reproduces actual observations you still have to delve per sensitivity

analysis into your simulation to diagnose how and why, as difficult as diagnosing observations but with the advantages that you can check below $\tau = 1$ and know the inputs. Carlsson and Stein (1994) (more formally Carlsson and Stein 1997) remains the canonical example: intricate observed patterns, convincing reproduction with data-driven simulation (*endnote 64*), four-panel breakdowns (*endnote 65*). [Back] [Main call]

38. MULTI program

This NLTE spectral synthesis code of Carlsson (1986) is obviously named for going beyond the 2-level approximation. It initially used linearization following Scharmer and Carlsson (1985) with the brilliant Scharmer operator [RTSA Eq. 5.52 (pdf 148)] (yes, the same as the brilliant SST builder, *endnote 52*) to obtain I_ν rather than J_ν from S_ν with a local two-way along-the-beam Eddington-Barbier approximation. It was later extended with the faster combination of the diagonal OAB operator of Olson et al. (1986) and convergence acceleration of Ng (1974) [RTSA (pdf 150)]. Convergence comparison in [SSF (pdf 103)]. [Back] [Main call]

39. MULTI3D program

Extension of MULTI to 3D parallel computation by Leenaarts and Carlsson (2009). It uses short characteristics with further-away contributions corrected by iteration. [Back] [Main call]

40. No Thomas photoelectric control

$H\alpha$ is a special line from $n = 2$ at 10.2 eV sitting so high up in the HI Grotrian diagram (pdf 9)¹⁰⁸, close to the 13.6 eV HI ionization limit. It has a sizable ηS^d contribution from bound-free detours as the loop shown in Fig. 2 (pdf 4) of Rutten (2019). This was famously called “photoelectric control” by Thomas (1957) with a schematic source function diagram in Fig. 3 (pdf 5) of Jefferies and Thomas (1959) that was reprinted in Fig. 12-9 of Mihalas (1970) and Fig. 11-11 of Mihalas (1978). It looks similar to the $H\alpha$ source function in ALC7 with S^d_ν leveling out in the photosphere higher than B_ν in the temperature minimum, indeed similarly to the Balmer continuum as if it follows that [SSX (pdf 76)].

However, this “photoelectric control” designation was wrong because even $H\alpha$ is mostly scattering as shown in Fig. 12 (pdf 9) of Rutten and Uitenbroek (2012): while the detour photon contribution in the FCHHT-B chromosphere is much larger than the

¹⁰⁷ Repeating the corollary on page 15 (pdf 15)) of Rutten et al. (2011) that Fourier analysis of full-disk Doppler sampling with the proposed GOLF-NG space instrument (Turck-Chièze et al. 2012) update will not achieve chromospheric helioseismology as advertised, whereas hoped-for g -mode detection will be hampered by upper-photosphere reversed granulation, fluxtube shocks and “shutter” modulation by overlying features as in Figs 5 and 6 (pdf 6) of De Wijn et al. (2007).

¹⁰⁸ Naming: Grotrian diagrams are term diagrams including transitions (named after Grotrian 1928). The *Partial Grotrian diagrams of astrophysical interest* of Moore and Merrill (1968) is a reprint of Appendix A of Merrill (1956) prepared by C.E. Moore and is a venerable classic of astronomical spectroscopy. The Utrecht Sonnenborgh library had a dozen; I stole one and fifty years later still have it on my desk even though it is now ADS-available. In the scan the HI diagram (pdf 9) misses the horizontal $n = 2$ line (and the bottom of Pfund) present in the original; is there a conspiracy theory why this happened to the most important level of observational solar physics? More complete term and Grotrian diagrams are in the fat volumes of Bashkin and Stoner (1975, 1978, 1981, 1982). I also stole Moore’s famous RMT multiplet table (Moore 1959) but also got that per magnetic tape (and now supply it in my archive) although she forbade digitization because machine access would seduce lazy scientists to non-understanding automation – she wouldn’t have applauded machine learning. See her on this 1963 Minnaert farewell photo amid famous colleagues. This one shows R.N. Thomas between D.H. Menzel and J.T. Jefferies (with a box of slides, *endnote 4*) in front of E.H. Avrett. More photos by H. Nieuwenhuizen in his Minnaert farewell album and worse ones in his Utrecht farewell album.

collisional-creation contribution it is still much smaller than the scattering contribution. Even $H\alpha$ is foremost a two-level scattering line; the upper-photosphere $S \approx J > B$ excess is due to backscattering from the chromosphere. Such excess does not occur in the RE atmosphere at left in Fig. 7 (pdf 6) of Rutten and Uitenbroek (2012) whereas with “photoelectric control” by ηS^d it should since the ultraviolet continua in Fig. 5 (pdf 5) there have similar $S \approx J > B$ excess with or without a chromosphere.

Thomas’ “photoelectric control” was a red herring. There are some lines as the Mg II triplet around Mg II h&k for which source function enhancement in cooling recombining gas (possibly NSE) producing emission is likely, but the many Thomas-citing typecastings of $H\alpha$ as “photoelectric” were misled. [Back] [Main call]

41. $H\alpha$ photosphere and chromosphere visibilities

The large $Ly\alpha$ excitation energy of the $n = 2$ lower level of $H\alpha$ produces both extraordinary invisibility of photospheric fine structure and extraordinary visibility of chromospheric fine structure in this line. I summarize these here; more in Sect. 7 and Sect. 8. The resulting deep and wide small-Boltzmann-ratio opacity gap across the cool upper photosphere (endnote 60) not only permits deep back-scattering penetration (endnote 40) but also implies that most outward-directed $H\alpha$ photons created in the deep photosphere travel up in arbitrary direction until hitting opaque chromospheric fibrils at least 1000 km higher, and then most scatter through the fibrils with $\sqrt{\epsilon}$ darkening (the ALC7 “chromosphere” only reaches thickness $\log(\tau) \approx 1.3$ in $H\alpha$ with $\log(\epsilon) < -3$ and thermalization in the deep photosphere [SSX (pdf 91)]). The granulation pattern has larger contrast than fibrillar intensity modulation but is erased by this erratic-direction gap crossing over larger-than-granule distance. Columnar 1D spectral synthesis wrongly maintains it, hence the striking 1D–3D differences in Fig. 7 (pdf 7) of Leenaarts et al. (2012a). You see chromospheric $H\alpha$ fibrils in photons that were created in the granulation far underneath but forgot that on their way up.

The second $H\alpha$ specialty from being fed by $Ly\alpha$ (pdf 9) is extraordinary visibility in its outer wings of spicule-II chromospheric heating events (endnote 80) and in its core of cooling chromospheric return fibrils (endnote 81) by NSE opacity boosting (Sect. 7) that controls the location of its $\sqrt{\epsilon}$ source function decay and $\sqrt{\epsilon}$ darkness (endnote 71). The ALMA mm continua share in this boosting but sample temperature rather than scattering decline (endnote 21).

Optical He I lines sit at twice higher excitation energy (He I Grotrian diagram (pdf 11)) and even add coronal visibility (endnote 96). [Back] [Main call]

42. MCs, network, plage, faculae

For MCs (magnetic concentrations, small upright kilogauss “fluxtubes”) and their visibility as “bright point” I refer to the extensive caption of Fig. 73 (pdf 91) of LAR-1. They are bright from being holes in the surface and appear brighter from further hole deepening in the G band around 4308 Å due to CH lines and in the CN bandhead at 3883 Å (endnote 63) through molecule dissociation, in outer wings of strong lines (Leenaarts 2006b, 2006a) through less collisional damping. Sharp images from optical telescopes reaching the Scharmer threshold (footnote 83) show them on subarcsecond scales in intergranular lanes with irregular and fast-varying morphology (“flowers” in Berger et al. 2004). Any HMI magnetogram shows larger ones sprinkled as small black and white grains in irregular patterns all over the disk, denser in active regions but fewer towards the

limb where their upright Zeeman signature is not aligned with the line of sight. The corresponding bright grains in AIA 1700 and 1600 Å chart them better but unsigned and limbward shifted (endnote 69). Away from active regions the MC patterns constitute the somewhat cellular magnetic network¹⁰⁹.

Near the limb the small MCs are known as faculae, already visible towards the limb in white-light images that did not reach the high resolution of modern telescopes because they brighten limbward from slanted viewing and bunch up in projection. This fortunate visibility enabled N.R. Sheeley to use their numbers on historical Mount Wilson full-disk photographs as polar field proxy (Sheeley 2008 and earlier; Muñoz-Jaramillo et al. 2012). Larger patches of MC concentrations were traditionally recognized on Ca II H & K spectroheliograms and called flocculi (Hale and Ellerman) and plage (Deslandres). Their chromospheric appearance is coarser, hence more evident, than underlying photospheric MCs but corresponds closely to the MC surface grouping into network and plage. The ultraviolet MC grains are photospheric, as in Gillespie’s classic CN spectroheliogram of endnote 63. [Back] [Main call]

43. Bilderberg study week

History: the “International study week on the quiet photosphere” was organized by Kees de Jager (footnote 58) in 1967 at the Bilderberg hotel near Arnhem (famous from more famous Bilderberg conferences) in order to jointly derive the Bilderberg Continuum Atmosphere of Gingerich and de Jager (1968) which later got improved to the HSRA of Gingerich et al. (1971). The proceedings became the first issue of *Solar Physics* volume 3, reprinted separately as De Jager (1967). Kees had organized the well-attended Minnaert farewell symposium at Utrecht in 1963 (photos) and edited its proceedings starting Reidel’s Astrophysics and Space Science Library (De Jager 1965). He turned the Bilderberg successor into a true workshop, sharing out homework beforehand, setting up working groups on various topics, and inviting promising youngsters (Sect. 2 (pdf 2) of Bonnet 1996) and also his yet younger Utrecht students. The participants (fierce but friendly contestants) sat half-circling the speaker at the blackboard with me in the center to operate the slide projector (endnote 4). I also was the notulist, daily spreading progress notes per stencil mimeograph¹¹⁰. I later described this extraordinary expert meeting, the best I attended, in Rutten (2002) with a group photo (pdf 5) including Holweger (more Bilderberg photographs at the bottom of my astronomershots).

¹⁰⁹ Only partially outlining the downflow borders of supergranulation cells. The latter appear more regular towards the limb in HMI Dopplergrams since the cell borders are populated only incompletely with MCs. At Utrecht C.J. Schrijver once handed a large magnetogram to solar colleagues requesting to draw the magnetic network. The results varied so much (from sloppy by me to meticulous by Zwaan) that he concluded there is no objectively definable magnetic network. Nor is there a clear distinction between active network and small plage (“plagette”).

¹¹⁰ History: a stencil was a sheet of thin material that fitted a normal typewriter for typing without ink ribbon, making letter-shaped holes. Mistakes were filled in with lacquer for retyping. The mimeograph duplicated the stencil by forcing ink through the holes onto paper sheets, with the stencil mounted on a hand-cranked rotating inking drum rolling over fresh paper sheets pushed from an input bin to an output bin. All offices handled duplication this way (if not photographically) until Xerox plain-paper copiers became widespread. During the meeting O. Gingerich taught me how to add graphs showing the converging BCA model stratification by plotting results from his pre-computed stacks of hydrostatic equilibrium tables on graph paper and overlay the stencil for scratching the curves with a needle pencil into it, held together against a window as backlight.

E.A. Müller declared at its conclusion that she wouldn't use the new model with its chromosphere requiring complex NLTE to handle that but would instead stick to Holweger's model without chromosphere for its reliably well-working LTE. She then did so with HOLMUL (Holweger and Müller 1974). [Back] [Main call]

44. Classic abundance determination

Holweger used the ALGOL “Kieler program” of Baschek et al. (1966) for LTE spectral synthesis in a classical approach: impose a $T(h)$ “model” relation, evaluate density stratifications for the given element mix by assuming hydrostatic equilibrium [RTSA Sect. 7.2.3 (pdf 166)], compute continuum extinction from H⁻ and extinction of a given line per SB ($b_u = b_l = 1$ in [RTSA Eq. 9.6 (pdf 224)]), use the integral solution of the transport equation [RTSA Eq. 2.43 (pdf 38)] to obtain the emergent profile. He used line areas (“equivalent width” [RTSA Sect. 9.1.2 (pdf 224)]) as quality gauge, repeated this for many optical lines, and derived a best-fit temperature and corresponding density stratification by trial-and-error manual $T(h)$ adjustment.

His many followers in classic abundance determination then took these stratifications (“model atmosphere”) for granted and did similar line fitting for different lines of a given element to establish its abundance, with much debate about the reliability of oscillator strength (transition probability) gf values. [Back] [Main call]

45. Mg I 12-micron emission lines

Assuming LTE implies predicting self-reversing chromospheric cores in e.g., the Na I D lines treated in practical SSB 3 (pdf 22) but also in the strong Fe I lines that Holweger employed. Their absence was attributed correctly to NLTE scattering by others but Holweger insisted tenaciously that NLTE computer programs fatally overestimate NLTE departures by not including sufficient hydrogen-atom collisions [SSX (pdf 39)] and that the actual chromosphere starts higher. When he refereed Carlsson et al. (1992) explaining the enigmatic Mg I emission lines at 12 micron this was also his main complaint, but the Rydberg recombination modeled there was already collision-dominated.

The formation of these striking features is interesting. Naturally they were first attributed¹¹¹ to chromospheric formation (Brault and Noyes 1983) but they are photospheric, combining NLW photon pumping in photo-ionization (endnote 32), NLW photon suction (endnote 33) and a diffusive radiative-collisional Rydberg population departure flow. In the Rydberg top this is dominated by collisional decays, the opposite of coronal dielectronic radiative-down (endnote 16). See the cartoon explanations in Rutten and Carlsson (1994) including Mats' “Rydberg flows for kayakers” in Fig. 4 (pdf 7) (better quality). Carlsson et al. (1992) obtained excellent fits in Fig. 6 (pdf 10) with a 1D RE model atmosphere and likewise in Fig. 14 (pdf 15) with the non-RE MACKKL model. These fits are uncommonly good because

these lines form in the upper photosphere where RE reigns and 1D models apply best (endnote 55).

Actually, Lemke and Holweger (1987) had come close to model these emission lines properly but their Mg I model atom did not reach high enough up the collision-dominated Rydberg ladder. Their study was wildly and wrongly attacked by Zirin and Popp (1989), in turn severely rebutted by me in Carlsson et al. (1992). This impressed Zirin so much that he saw me as potential successor. I saw him as thin (footnote 26) because in the abstract he stated that these Mg I lines are thin. Wrong language (cf. footnote 129) and wrong altogether because these lines are the most beautiful $S(\tau)$ mappers in the solar spectrum (Fig. 5 (pdf 9)). [Back] [Main call]

46. Plane-parallel atmosphere files

I copied files with plane-parallel model atmospheres from the 1980s that I found I still have into my solar file archive started while writing endnote 14. These include HOLMUL, the HSRA model of Gingerich et al. (1971), the thesis model of Lites (1972), the VALIIM model of Vernazza et al. (1976), the radiative-equilibrium model of Bell et al. (1976), the models VAL3A–VAL3F of Vernazza et al. (1981) and the MACKKL model of Maltby et al. (1986). The FALC model of Fontenla et al. (1993) is supplied and analyzed in practical SSB1. All four FAL models of Fontenla et al. (1993) are available in RH (endnote 59) input format in the RH github Atmos directory, but my new solar file archive adds some more including VAL3C, MACKKL, models of Fontenla et al. (2009) and ALC7 of Avrett and Loeser (2008). [Back] [Main call]

47. NLTE masking

For a steep outward temperature decline the outward increasing ultraviolet $J > B$ excess from scattering and Λ results in NLW-type NLTE overionization of minority-species metals [SSF (pdf 111)]. Instead adopting Saha ionization then puts the height assigned to $\tau = 1$ too high so that the fitted temperature gradient gets too shallow and the same as for locations with less steep temperature decline. Different surface structures with different gradients (as granules and lanes) can so be fitted erroneously by a single shallow gradient.

Additionally, the neglect of source function NLTE for higher-up scattering in stronger lines results in undoing an actual chromospheric temperature rise, masking that also.

Fig. 8 (pdf 8) of Rutten and Kostik (1982) shows how a HOLMUL-like model so results from the steeper-gradient HSRA model of Gingerich et al. (1971), summary in [SSX (pdf 40)]. A cartoon is shown in Fig. 4 (pdf 14) of Rutten (1988). [Back] [Main call]

48. Milne-Eddington approximation

Inverters often apply the further simplification of assuming Milne-Eddington line formation, i.e., constancy of the line-to-continuum extinction ratio with height (Holweger instead evaluated continuum and line extinction in detail). This assumption was tested with a MURaM simulation and LTE line synthesis for comparable weak Fe I lines at different excitation energy in Fig. 8 (pdf 10) of Vitas et al. (2009); summary in [SSX (pdf 41)]. It is bad at low excitation, better at higher excitation as already evident in Fig. 3 (pdf 16) of Rutten and van der Zalm (1984b). [Back] [Main call]

49. Interlocking Fe I, Ce II, Fe II lines

Spectral species as e.g., Fe I and Fe II are rich in bound-bound

¹¹¹ History: they show high peaks in emission at the center of absorption troughs. Being unusual they were blamed on some instrumental defect and white-pasted by Goldman et al. (1980) in their infrared spectrum atlas. Brault and Testerman had already spotted these intriguing features (Fig. 1 (pdf 2) of Brault and Noyes 1983) at Kitt Peak; Brault therefore phoned them to ask why their atlas showed gaps precisely at these locations. Answer: “everybody knows that Fraunhofer lines are in absorption”. Murcray et al. (1981) (including two more Murcrays) then sensed their gaffe, dewhitened them and claimed discovery (without mentioning Brault) with fancy attribution to Si VIII and Mg VIII but not daring to exclude telluric origin. So it goes. They were identified as solar Mg I $n=7-6$ transitions by Chang and Noyes (1983).

transitions. Optical multiplets are mostly high up but connected by ultraviolet transitions to levels lower down (ground state or low-lying metastable levels), comparable to the Ca II triangle in Fig. 2 (pdf 4) of Rutten (2019) but in large number. With their small lower-level excitation energy these ultraviolet transitions tend to be strong, maintaining $S^l \approx B$ further out as in the right-hand cartoon of [SSF (pdf 111)] and forcing $b_u \approx b_l$ on their upper levels at the deeper heights where their weaker optical siblings reach $\tau \approx 1$. The low Fe I levels are all strongly collisionally coupled as evident in VALIII Fig. 34 (pdf 32). When the weaker higher-up lines so share strong-line b_l in their upper and lower levels they have LTE source functions – but their opacities scale with b_l and sense ultraviolet overionization in the upper photosphere as in the lefthand cartoon of [SSF (pdf 111)] and also evident in VALIII Fig. 34 (pdf 32). Summary: Fe lines suffer NLS and NLW. Their formation cannot be modeled by accounting only for NLS scattering in the line itself.

Other interlocking lines occur in lanthanide rare earths. They have multiplets with many members that overlap closely in energy. Ce II has most lines, peaking at 10 lines/Å around Ca II H & K. These are weak lines but scatter strongly with much crosstalk. They show up in emission inside the limb both outside and within the extended wings of Ca II H & K which was explained in the classic analysis of Canfield (1971b) following on Canfield (1971a) and his earlier thesis studies. They appear bland from wide multi-wavelength scattering producing their J , whereas similar Fe II blends in the wings of H & K (Rutten and Stencel 1980) show much spatial variation due to pumping by particular ultraviolet transitions (Cram et al. 1980) and so gaining ultraviolet Wien sensitivity (endnote 32). [Back] [Main call]

50. Line haze modeling

Photospheric species as Fe I and Fe II¹¹² are immensely rich in bound-bound transitions with dense line crowding into the “veiling line haze” of Labs and Neckel (1972) and Greve and Zwaan (1980), densest in the violet and ultraviolet (first extinction curve in Fig. 3 (pdf 13) of Rutten 2019). It is discussed as major obstacle in Sect. 6.1 (pdf 17) of Rutten (2019) together with various recipes to treat it in spectral synthesis, varying from the simple Zwaan-inspired Fig. 2 fudge (pdf 3) of Bruls et al. (1992) to brute-force solving all NLTE population equations for all transitions in Fontenla et al. (2015). Uitenbroek’s RH code (endnote 59) offers both these and also LTE and equivalent two-level scattering synthesis for all blend lines not treated in NLTE detail. The latter two are compared with observations in Fig. 10 (pdf 18) of Rutten (2019), showing that both fail. The Avrett-Loeser Pandora code uses an imposed gradual transition from $S_v^l = B_v$ to $S_v^l = J_v$ with SB opacities (endnote 54). At the end of the section (p. 19 (pdf 19)) I suggested a recipe solving for NLTE populations in a representative simple atom and applying the resulting departures to all blends. [Back] [Main call]

51. Fe I 6302 Å doublet, Mg I 4571 Å

A good example is the Fe I 6302 Å polarimetry doublet. The ALC7 star [SSX (pdf 83)] has a near-LTE source function from ultraviolet interlocking (endnote 49) and large opacity deficit from ultraviolet overionization. Their NLTE “inversion” fitting should use RH (endnote 59) with a large Fe model atom, sizable electron-donor atoms and a suited line-haze recipe or it will un-

derestimate their source functions from erroneous scattering and overestimate their opacities from erroneous ionization.

A similar example is Mg I 4571 Å which is an *intercombination transition* (pdf 20) with low *transition probability* (pdf 84) and therefore has $S = B$ up to large height. In the onset of the flash spectrum it shows its core in emission between absorption dips, similarly to the on-disk profiles of the Mg I 12 μm lines of endnote 45. This was indicated in Fig. 14 (pdf 21) of Rutten (1977) but later (visiting Tucson) I found it clearer on the *original limb spectrum plate* of Pierce (1968) showing unusual core-emission-plus-wing-dip pattern, with spatial variation along the tangential slit. The strong Fe II and Ti II lines on this telltale plate show emission wings and the weaker Fe II lines full emission, also with spatial variation, whereas the Ce II, La II and Sm II rare earth lines show Canfield-style blander emission as described in endnote 49. Similar limb emission differences occur for the blends in Ca II H & K in Rutten and Stencel (1980). Thus, Mg I 4571 Å is an LTE line in its source function. However, it suffers considerable NLTE extinction depletion even in 1D modeling [SSX (pdf 82)]. “Inversion” fitting will deliver temperatures but for proper opacity whereabouts estimation it requires a large Mg model atom plus the other electron donors and a line-haze recipe. [Back] [Main call]

52. Illustrious quartet

Å. Nordlund initially had a habit of publishing his revolutionary granulation simulations in non-page-limited proceedings (e.g., non-scanned Nordlund 1985a, 1985b). In scanned ADS-available Nordlund (1984b) he argued that the large difference in granulation contrast between his numerical simulation and observations was to be blamed on the latter, becoming the prototype of the numerical simulator habit to blame observations if these do not match the wonderful and necessarily correct computation¹¹³ – but actually Nordlund was right as eventually demonstrated by Scharmer et al. (2019).

Nordlund stems from B. Gustafsson at Uppsala who also suggested RT theory as venue to G.B. Scharmer at Stockholm who then became thesis adviser to Gustafsson’s student M. Carlsson (endnote 38). Nordlund and Carlsson each began fruitful collaborations with R.F. Stein at East Lansing who has Scandinavian roots. This illustrious Nordic quartet eventually co-authored Carlsson et al. (2004). M. Asplund is also a Gustafsson pupil.¹¹⁴ [Back] [Main call]

53. LTE diehard

I wonder what A. Unsöld, who at Kiel had told Holweger to produce a thesis proving that LTE suits the solar spectrum, made of the Auer – Mihalas results, representing extremes of the then rampant LTE-versus-NLTE debates. In 1967 he had written to Minnaert that Holweger had definitely proven the LTE veracity of the solar spectrum (in a recommendation for his attending the Bilderberg meeting of endnote 43) but the Auer–Mihalas results did upset his LTE bible “*Physik der Sternatmosphären*” (Unsöld 1955, 900+ citations) of which the Utrecht Sonnenborgh library

¹¹³ Generally it is better that simulations do not reproduce observations so that there is evidently something to learn without temptation to claim correctness from happenstance data reproduction (endnote 71).

¹¹⁴ Gustafsson’s astronomer production reminds me of C. Zwaan at Utrecht (PhD adviser for me, H.C. Spruit, A. Greve, A.A. van Balle-goijen, C.J. Schrijver, R.G.M. Rutten, K.L. Harvey-Angle, L.H. Strous, K.F. Tapping and others who left astronomy; PhD co-adviser for H. Uitenbroek, J.H.M.J. Bruls, N.M.H. Hoekzema). Utrecht University has a *great past* but *no present* in solar physics. So it goes.

¹¹² The classic Grotrian diagrams of Moore and Merrill (1968) (footnote 108) are only partial, with their Fe I (pdf 66) and Fe II (pdf 65) charts showing only major systems. Complete ones would be black all over.

had many copies for students (some stolen). The translation by H. Panofsky and A.K. Pierce was never printed; I believe that Unsöld insisted that any astrophysicist instead could and should learn German to read his book. I have it (honestly from eBay) and can read it but haven't opened it in years. So it goes. I know "diehard" is a word only in the Dutch language but it fits him well. He is at left in [this photo](#). [[Back](#)] [[Main call](#)]

54. Pandora program

NLTE spectral synthesis code of [Avrett and Loeser \(1992\)](#); more [here](#) and [here](#) and [here](#). Similarly to Holweger's method it applies hydrostatic plane-parallel equilibrium to a trial manually-fitted $T(h)$ temperature stratification but uses SE NLTE for radiation evaluation in a giant "equivalent two-level" iteration loop treating each bound-bound or bound-free transition that is explicitly taken into account (not added as background opacity) with two-level rate equations, letting iteration take care of multi-level crosstalk. The equation system is large enough to earn the ominous name.

Whereas Holweger concentrated on fitting observed optical lines, mostly from Fe I, Avrett concentrated on fitting observed disk-center continua, especially in the ultraviolet. For the line haze ([endnote 50](#)) Avrett added increasing numbers of lines from the ever-growing list of [Kurucz \(2009\)](#) and treated them with an imposed ad-hoc gradual source function transition from $S = B$ in the model photosphere to the continuum $S = J$ in the model chromosphere to avoid non-observed core reversals that otherwise show up above the temperature minimum in LTE sampling (p. 243 ff ([pdf 15](#)) of [Avrett and Loeser \(2008\)](#)). Seems reasonable, but using LTE opacities is wrong for over-ionized minority species. The brute force solution is to include all lines with full NLTE synthesis as attempted by [Fontenla et al. \(2015\)](#) in irradiance modeling.

I use the ALC7 Pandora star of [Avrett and Loeser \(2008\)](#) for my spectrum-formation demonstrations ([\[SSX \(pdf 72\)\] ff](#)). It isn't the Sun but it is well-suited to showcase its RTSA physics and it is self-consistent within this physics.¹¹⁵

Pandora is [web-available](#) but documented only in many pages of coding requests and specifications (including Fortran variable names) to R. Loeser that reside in Avrett's CfA office. P. Heinzel holds copies in Ondrejov. [[Back](#)] [[Main call](#)]

55. RE upper photosphere

The reason for the near-equality of the upper photosphere in all quiet-Sun 1D models since MACKKL to the older HOLMUL and RE models is that this is the most homogeneous domain of all. The granular convection has stopped. Acoustic waves do not yet shock. Magnetic fields are still mostly confined to slender fluxtubes at small density in the modeled "quiet" areas. Gravity waves do not yet couple into them ([endnote 67](#)).

In addition, the bulk of the escaping solar radiation is in the optical and forces radiative equilibrium (RE). In "grey"

RE [[RTSA Sect. 7.3.2 \(pdf 173\)](#)] the continuum gets gradient $S(\tau) \sim (1 + 1.5\tau)$ [[RTSA Eq. 7.43 \(pdf 176\)](#)] because for that gradient $\Lambda(S) \approx S$ [[SSF \(pdf 45\)](#)]. The continuum in the optical is dominated by H^- which has near-LTE $S_\nu \approx B_\nu$ in the bound-free range and strict LTE $S_\nu = B_\nu$ in the free-free range. Most lines in the optical also have $S_\nu \approx B_\nu$ ([endnote 49](#)). Hence the temperature gradient is set LTE-wise by the RE condition [[RTSA Eq. 7.33 \(pdf 174\)](#)].

Indeed, more modern Bifrost ([endnote 75](#)) simulations obtain about the same average temperature decay with relatively small spread at these heights [[SSX \(pdf 59\)](#)]. Profile fitting with 1D models is least suspect for lines formed there, as the Mg I 12 micron lines of [endnote 45](#). [[Back](#)] [[Main call](#)]

56. Fe ionization in VALIIC

RTSA teacher J. T. Wright (Penn State) has pointed out that in VALII [Fig. 22 \(pdf 37\)](#) the electron donor ranking is Mg–Si–Fe but VALIII [Fig. 47 \(pdf 67\)](#) has Fe on top – and reported that his students could not reproduce the latter. I checked with the RH code ([endnote 59](#)) and also got Mg on top, just as for MACKKL and newer Pandora stars.

What boosted Fe II in the VALIII publication? The steep VALIIC upper-photosphere temperature decline desteeptened in subsequent Pandora stars does not define donor ionizations directly because these follow scattering source functions given by [[RTSA Eq. 3.109 \(pdf 93\)](#)]. As in [[SSX \(pdf 42\)](#)] they are primarily controlled by the temperature at their deeper effective escape where all Pandora stars are about the same [[SSX \(pdf 58\)](#)]. The less steep upper-photosphere decline of the newer Pandora stars boosts these continua only indirectly with larger (but there minor) $\varepsilon\bar{B}$ contribution to \bar{S} and via Λ into slightly higher \bar{J} , giving somewhat larger ionization to all donors. The corresponding NLTE corrections are largest for VALIIC ([Fig. 34 \(pdf 32\)](#)), smaller for the newer Pandora stars because their B_ν stays closer to J_ν (compare Fe I 6301.5 Å formation between FALC and the warmer FALP in [[SSX \(pdf 117\)](#)]) – but all rank Mg on top in my RH modeling. I then suspected that this rogue non-RH-reproduced Fe II boosting in VALIIC came from details of line haze inclusion but trials putting the entire Kurucz line haze to absent, LTE or two-level scattering in RH (for comparisons see [Fig. 10 \(pdf 18\)](#) and its discussion in [Rutten 2019](#)) all gave Mg on top.

The actual Sun has Mg on top, showcased by the observed dominance of the Mg I lines around 12 μm ([endnote 45](#)). The companion Fe I Rydberg lines did not steal the similar Mg I 7.4 μm trough-and-peak show in [Fig. 1 \(pdf 5\)](#) of [Schoenfeld et al. \(1995\)](#) modeled so very well in [Fig. 6 \(pdf 9\)](#) of [Rutten and Carlsson \(1994\)](#) with a MACKKL-like RE photosphere ([Fig. 2 \(pdf 6\)](#) of [Carlsson et al. 1992](#)). Because these fits of upper-photospheric lines represent the best of all solar spectral-line syntheses with 1D standard models ([endnote 55](#)) I also tried RH on this chromosphere-free 1D star and again got Mg on top as champion electron donor reaching 35% from 200 km up to the atmosphere top. [[Back](#)] [[Main call](#)]

57. ALC7 line formation plots

These 17 triple-graph displays [[SSX \(pdf 78\)](#)] ff show populations, source functions, emergent profiles for 13 representative lines of the ALC7 star with common intercomparable graph formats.

The first graph [[SSX \(pdf 79\)](#)] shows lower and upper level population departure coefficients b_l and b_u [[SSF \(pdf 73\)](#)]. The other curves are NLTE and LTE fractional populations. Their di-

¹¹⁵ J. Fontenla diverged from Avrett after [Fontenla et al. \(1993\)](#), writing a Pandora alternative that is in principle equivalent but was used less self-consistently by enhancing the output similarity to the non-1D non-static non-SE spectra of the actual Sun with ad-hoc tricks. The first was to add best-fit pressure in the upper chromosphere beyond the turbulent pressure defined by [observed microturbulence \(pdf 19\)](#) in the Pandora stars by invoking the Farley-Buneman instability ([Fontenla 2005](#), [Fontenla et al. 2008](#), [Madsen et al. 2014](#), [Fletcher et al. 2018](#)) – but see [Gogoberidze et al. \(2009\)](#). The second ([Fontenla et al. 2007](#)) was to add best-fit non-gravitational acceleration to extend the model photosphere to reproduce dark CO lines that probably have 3D(t) NLT formation ([Uitenbroek 2000](#)) instead of obeying SE.

vergence follows the $\log(b_l)$ departure from zero ([SSF (pdf 73)], Eq. 5).

The second graph [SSX (pdf 80)] shows B , J and S^l (these must always be shown all three together). They are on equivalent temperature scales, deWiened to enable comparisons between different lines across the spectrum (endnote 12). On logarithmic intensity scales the S^l separations from B would equal the logarithmic separations of b_u from b_l in the first graph. The thick solid curve usually lies between the other two, identifying it as S^l obeying $S^l \approx (1 - \varepsilon)J + \varepsilon B$. For PRD lines it is split between monofrequent samplings. The $\log(\tau)$ marks are defined by the lower-level fractional population, abundance and density drop. The other two curves measure scattering governing $S^l - B$ split.

The third graph [SSX (pdf 81)] is the computed emergent profile on the same equivalent-temperature scale as the second graph to enable checking the Eddington-Barbier approximation. I did not add observed disk-center atlas profiles in view of the Ha–Ha Erlebnis in endnote 71: you might be tempted to overclaim a good fit as observation-proven model truth. [Back] [Main call]

58. My IDL programs

Under my Recipes for IDL with this inventory. RH plot programs in `rhlib`, LTE line formation programs in `ltelib`, SDO stuff in `sdolib`, SST data-handling programs in `sstlib`, image sequence browser `showex` in `imagelib`, etc. Installation is described in this SDO manual. I even offer a beginner IDL manual. For my SDO pipeline (endnote 83) do my alignment practical. [Back] [Main call]

59. RH program

The RH spectrum synthesis code of Uitenbroek (2001) is named after Rybicki and Hummer (1992) and follows their scheme of multi-level approximate lambda iteration [RTSA Sect. 5.3.2 (pdf 145)] not iterating Λ for J , but the Ψ operator for j_v . It permits overlapping lines, includes PRD and full-Stokes options, exists in 1D, 2D, 3D, spherical, and Cartesian versions, and also in parallel multi-column “1.5D” (Pereira and Uitenbroek 2015). It has various options to treat the worrisome ultraviolet line haze (endnote 50).

I supply some plane-parallel 1D “standard” model atmospheres in RH format beyond the github-supplied FAL models of Fontenla et al. (1993) in my solar file archive (endnote 46). My RH-output plotting programs are in my RH IDL lib.

For the ALC7 spectrum-formation graphs starting at [SSX (pdf 73)] I used RH 1D version-2 with H, He, Si, Al, Mg, Fe, Ca, Na, and Ba active, C, N, O, S, and Ni passive, and with 20 mÅ sampling of 343 000 lines between 1000 and 8000 Å in the atomic and molecular line list of Kurucz (2009). Fig. 6 (pdf 13) of Rutten (2019) gives an overview of their extinction in the FALC star. The line haze is prominent between $\log \lambda = 3$ and 4. [Back] [Main call]

60. Quiet-Sun $H\alpha$ scenes

Note the deep population chasm in the dashed curve in the first panel of [SSX (pdf 91)], first described by Schoolman (1972) and compared with Ca II H in [SSF (pdf 61)] from Leenaarts et al. (2006b). Observationally the gap is evident when you shift the SST/CRISP $H\alpha$ passband from line center to a wing for a quiet-Sun target. Up to about $\Delta\lambda = \pm 0.5$ Å the scene usually shows fibrils extending from network and then you suddenly drop into deep-photosphere granulation, skipping the middle and

upper photosphere. This opacity skip explains why the equivalent widths of the Balmer lines are so much smaller than for Ca II H & K with their wide-stretching outer wings and clapotispheric cell grain shock signatures (endnotes 63–66) in their inner wings. $H\alpha$ has $\sqrt{m_{Ca}/m_H} = 6.3$ wider thermal core broadening and wider Holtsmark-distribution damping-wing broadening but it lacks opacity underneath its fibrillar NLT canopies. These are more opaque in $H\alpha$ than in Ca II 8542 Å (endnote 81) but likely less than in the centers of Ca II H & K with the latter showing richer fine structure thanks to larger Dopplershift sensitivity from PRD source function splitting and less erasure of lower-down patterning by lateral scattering (endnote 40).

Only in rare utterly quiet areas you may see somewhat higher-up reversed granulation in $H\alpha$ near $\Delta\lambda = \pm 0.5$ Å. I offer two SST examples. The first is a very quiet target corner in the data of Rouppe van der Voort et al. (2007) in this Ca II H + $H\alpha$ blue-wing movie where reversed $H\alpha$ at $\Delta\lambda = -0.45$ Å shows reversed granulation as grey underlying pancakes.

The second is a similarly quiet SST target (in a disk-center coronal hole) that you may inspect yourself by doing my alignment practical (endnote 83). Its showex commands (footnote 125) for its SST data enable $H\alpha$ profile scanning to inspect scene changes, $H\alpha$ wing blinking against reversed granulation in the Ca II 8542 Å wings to identify it in $H\alpha$, and core comparisons to show the larger opacity and extent of the fibrillar canopies in $H\alpha$ than in Ca II 8542 Å (endnote 81). [Back] [Main call]

61. Seismology success story

I summarize this history here because the acoustic p -mode oscillations affect solar lines throughout the visible and ultraviolet everywhere while their identification and usage were the most exciting development in my half-century in solar physics (more in my decades-old 5-minute lecture (pdf 1)). In the daily HMI Dopplergram movies the 5-minute oscillation discovered by Leighton et al. (1962)¹¹⁶ appears everywhere as twinkling patches (clearest at disk center and smaller than supergranulation cells seen limbward) of apparently coherent oscillation somewhat larger than granules¹¹⁷. The patches are the surface interference pattern of many solar p -modes and contribute “radial macroturbulence” to the wash-out of narrower photospheric lines than Mn I ones (endnote 18). AIA 1700 Å movies show the 3-min components which are not evanescent but above the local cutoff frequency, propagate up and appear as fast-moving erratically-distributed coming and going brightness wisps in in-

¹¹⁶ Best-ever publication in observational solar physics (cf. Goldreich 1999): discovery of supergranulation, reversed granulation, 5-minute photospheric oscillation, $H\alpha$ return fibrils around network, and more. Not at all “preliminary” as the title claimed for this Part I, and all based on ingenious photographic spectroheliogram processing as analog precursor to IDL permitting Dopplergram subtraction, temporal differencing, space-time correlation and more with detector size well beyond the 4K×4K sensors of SDO. Fortuitously the resolution was just right for the p -mode interference blobs and the heliograph scan duration over the image of 4 min was just right for two-wing Doppler mode scanning (Fig. 1 (pdf 2)) with quick scan-direction reversal to produce time-delay correlation plates permitting the discovery of pattern reproduction after 5 minutes (Fig. 14 (pdf 22)) and also the everywhere dominance of this periodic motion field (Fig. 16 (pdf 25)). Part II followed with the discovery of the 3-minute chromospheric oscillation (Noyes and Leighton 1963, see Fig. 1 (pdf 7) of Noyes 1967). Part III identified the chromospheric network and the magnetic network as outlining supergranulation cell borders (Simon and Leighton 1964).

¹¹⁷ A DKIST show-off granulation movie will need (k, ω) filtering as in P. Sütterlin’s `conefit.pro` for the DOT.

ternetwork regions. They piston the higher-up Carlsson-Stein shocks (*endnote 64*),

Both the photospheric and claptospheric (*endnote 66*) oscillation patterns appear random and chaotic. White and Cha (1973) studied apparent phase patterns of the 5-minute oscillation and concluded that they are totally random: “any description of the observed motion in terms of simple deterministic functions will be inadequate”. Pure chaos – so much for future helioseismology! I was the referee, found it convincing, and gave a Utrecht colloquium reviewing 5-minute oscillations but only the discovery part (showing 35-mm slides (*endnote 4*) of the plates in Leighton et al. 1962) and the confusion part (speculating about gravity waves turning into Alfvénic waves after Lighthill 1967) itemized in [this later display \(pdf 1\)](#) but yet without the enlightenment part because I was not aware of the marvelous prediction of Ulrich (1970)¹¹⁸.

At the time the same held for F.-L. Deubner who was then contesting Frazier’s finding of substructure in the (k, ω) diagram (Deubner 1972)¹¹⁹. However, Deubner was asked to referee Wolff (1973) and so became aware of Ulrich (1970) and also Wolff (1972) stating that the Sun is spherical and that Ulrich’s modes must be spherical harmonics. Deubner then recognized the parabolic mode-location curves in Ulrich’s predictive (k, ω) diagram in [Fig. 2 \(pdf 6\)](#) as the fish to catch. He knew from [Fig. 6 \(pdf 17\)](#) of the authoritative (in beautiful French) (k, ω) description of Mein (1966)¹²⁰ that long duration and large extent were the way to (k, ω) resolution and fast cadence and fine sampling to (k, ω) extent. He found the ridges, best in his hand-drawn *note-in-press diagram* (pdf 4) in Deubner (1975) adding the detailed spherical-harmonic predictions of Ando and Osaki (1975). He showed it first at a conference in Nice, apologizing to Frazier (Deubner and Mc Intyre 1976)¹²¹, where it became the proceedings cover (Cayrel and Steinberg 1976) and made him famous.¹²² Upshot: the photospheric p -mode pattern pistonning chromospheric shocks appears random but is a **most regular and beautiful harmonic chord** (pdf 50).¹²³ [*Back*] [*Main call*]

62. No gravity-modes success story

The alkali resonance lines and some others are suited to build gas-filled resonance cell detectors in which atoms resonance-scatter optical sunlight, either irradiance for full-disk profile sampling following the initial application for Sr I 4607.3 Å of Blamont and Roddier (1961) or with imaging using magneto-

optical encoding following Öhman (1960, not on ADS) and Cimino et al. (1968) and mostly developed by A. Cacciani ([bibliography](#)). Using full-disk resonance-cell Na I and K I Doppler-shift detectors in around-the-world networks and in space (SOHO/GOLF) became a large industry in g -mode-searching low- l helioseismology but a romantic overpromise/overclaim saga rather than a success story as in *endnote 61*. For the latest claim/reject debate read [p. 85–86 \(pdf 85\)](#) of Christensen-Dalsgaard (2021) concluding “evidence for solar g modes remains uncertain”. [*Back*] [*Main call*]

63. Ca II K_{2V} and CN spectroheliograms

Ca II K_{2V} “cell grains” are ubiquitous in high-quality narrow-passband K_{2V} imaging as in the “Selected spectroheliograms” of Title (1966) (which I have on my desk but cannot find in ADS) and in this remarkable [Ca II \$K_{2V}\$ spectroheliogram](#) taken in 1975 by B. Gillespie with the East Auxiliary of the McMath telescope at Kitt Peak. It adorned the cover of Lites (1985) (negative) and was partly shown (positive) in [Fig. 3.9](#) (wrongly labeled K center) of Zirin (1988) and in [Fig. 1 \(pdf 2\)](#) of Rutten and Uitenbroek (1991b), [Fig. 2 \(pdf 4\)](#) of Rutten (2007) and elsewhere.¹²⁴ Later J.W. Harvey sent me a CD-ROM duplicate; while writing this I added this [original negative](#) in my [solar file archive](#).

The spectroheliograph had a dual-beam arrangement as at Mount Wilson (*footnote 116*); Gillespie took a synchronous companion spectroheliogram in the CN 3883 Å bandhead, also now in my file archive courtesy J.W. Harvey. I co-aligned the pair with [this IDL job](#) into [gillespie_ca.fits](#) and [gillespie_cn.fits](#) and advise zoom-in blinking.¹²⁵ The K_{2V} image shows bright cell grains (Rutten and Uitenbroek 1991a) so ubiquitous and numerous that it is hard to make out the calcium network except for diffuse fibril spreading around it (much more, covering most internetwork, if the spectroheliogram had selected K_3 center). Some of these bright grains mark migrating internetwork MCs as the “persistent flasher” of Brandt et al. (1994) (*endnote 79*) but the majority are Carlsson-Stein acoustic shock markers (*endnote 64*). The CN image shows yet more smaller bright grains but these are regular MC holes deepened by CN dissociation (*endnote 42*). Towards disk center (lower-right part of the image) they mostly coincide with calcium network grains appearing brighter and coarser; the few internetwork ones with bright K_{2V} counterparts are likely flashers. These are embedded in grey small-scale internetwork patterns partly marking reversed granulation and gravity waves (*endnote 67*) but mostly interference patterns of three-minute waves on their way up to shocking height (*endnote 66*). [*Back*] [*Main call*]

64. Carlsson-Stein shocks

In Carlsson and Stein (1994) they first described their marvelous numerical reproduction of observed internetwork shocks in [Fig. 2 \(pdf 4\)](#) of Lites et al. (1993) using a data-driven RADYN simulation. Summed over space and time these shocks contribute

¹¹⁸ The [acknowledgment \(pdf 10\)](#) thanks R.F. Christy (earlier his thesis adviser) for suggesting that the self-excited oscillations might be more than numerical instability of Christy’s stellar-structure code (the Nobel for starting helioseismology should go to that). E.N. Frazier is acknowledged for suggesting that the observed 5-minute oscillation might be the surface manifestation.

¹¹⁹ The telltale markings are by R.W. Noyes whose *Solar Physics* volumes were scanned by ADS.

¹²⁰ History: Deubner and Mein both completed conservatory schooling and hesitated between being musician or astronomer. They performed the Beethoven Op. 105.2 and Debussy cello-piano sonatas at the Zwaan retirement workshop (Rutten and Schrijver 1994) after rehearsing at *Lingezicht*.

¹²¹ McIntyre was not involved but wrote an ADS-misleading superfluous comment on terrestrial seismology. Bahcall (1999) did better but missed out on Christy and Frazier (*footnote 118*).

¹²² Scooping Ulrich and Rhodes who also had detected the ridges, while Ulrich (1970) may have scooped Leibacher and Stein (1971).

¹²³ Since my 1989 popular-astronomy hagiography “De zon zingt” I bring [my flute](#) to public lectures “The Singing Sun” to demonstrate overtone harmonics.

¹²⁴ When W.C. Livingston was asked for a chromosphere image he often sent a piece of this one.

¹²⁵ The [align job](#) is a good example of iterative Metcalf alignment of images with corresponding patterns but no close similarity in detail. My SDO – STX cross- and co-alignment pipeline (*endnote 83*) is built on this technique. Movie browser showex.pro in my IDL library (*endnote 58*) can load many concurrent movies and offers auto-blinking between selectable movie pairs at selectable speed and zoom-in magnification with scatter-diagram correlation and more. My SDO – SST [alignment practical](#) demonstrates its use. It can also load equal-size images and it can be run from the terminal command line (script in [my SDO manual](#)): showex gillespie_ca.fits gillespie_cn.fits.

(as “H_{2V} and K_{2V} cell grains”) to the asymmetry between the violet and red Ca II H & K core reversals (*endnote 17*). The characteristic intricate shock development pattern had been established in Fig. 4 (pdf 9) of Cram and Damé (1983) and was sketched in Fig. 2 (pdf 7) of Rutten and Uitenbroek (1991a). The resulting excellent match of the observed and simulated Ca II H_{2V} grain sequences in Fig. 14 (pdf 23) is highly convincing (and adorns the proceedings cover). These well-known results were then formally published in Carlsson and Stein (1995) and Carlsson and Stein (1997). More in *endnote 74*. [Back] [Main call]

65. Carlsson four-panel breakdown

Figs 8–12 (pdf 16) of Carlsson and Stein (1994) also introduced the informative Carlsson four-panel spectral-feature breakdown diagrams. For Ca II H one is shown in [SSX (pdf 156)], four in Figs. 4 (pdf 5)–7 (pdf 8) of Carlsson and Stein (1997), three for Na I D₁ and one for Ca II 8542 Å in Fig. 9 (pdf 8) of Leenaarts et al. (2010). I recommend studying these – by understanding them you join a select club!

In my courses they became examination material. An astute student noted that the second panel of [SSX (pdf 156)] exhibits the wrong assumption of CRD. Carlsson and Stein argued that their neglect of Ca II H PRD was compensated by not including Mg II h & k.

These diagrams clearly demonstrate the importance of NLT effects even though the spectral synthesis assumed SE. The observed bright Ca II H_{2V} grains (*endnote 17*) which the simulation reproduced so admirably exist only because previous shocks define the opacity distribution along the line of sight. The bright H_{2V} grain represents an upward traveling acoustic wave at too low height to show shock heating at its wavelength if the higher atmosphere were stationary; it gains its bright visibility from large higher-up downdraft after the earlier passage of a wave that shocked higher up. The downdraft pulls the line core redward and uncovers the grain. [Back] [Main call]

66. Clapotisphere

I called the above-the-photosphere under-the-chromosphere internetwork domain filled with Carlsson-Stein shocks “clapotisphere” in Fig. 12 (pdf 7) of Rutten (1995). “Clapotis” on sea charts marks locations with “wild” waves. In regular wind-driven ocean waves material motion is mostly vertical; the same holds for the 5-minute oscillation of the solar surface. Sea clapotis results from pattern interference by wave reflection off capes, harbor quays, or in meeting of different swell systems growing into “wild” nonlinearity. The chromospheric 3-min shocks are vertically NLT interfering in complex fashion, wild enough to need Carlsson breakdown diagrams (*endnote 65*). The photospheric *p*-mode oscillations that drive the shocks are also complex interference patterns but outstandingly regular, linear, and precisely predictable (*endnote 61*) [Back] [Main call]

67. Acoustic and gravity wave heating

Fossum and Carlsson (2005a) also laid the long-advocated attribution of coronal heating to acoustic waves (e.g., Ulmschneider and Kalkofen 2003) to rest (but see Yadav et al. 2021 for field-guided wave heating of the chromosphere). An earlier candidate for coronal heating were gravity waves proposed by Whitaker (1963)¹²⁶ who introduced the “diagnostic” *k*–*ω* diagram (pdf 22) in solar physics following geophysics Hines (1960) (*endnote 61*). The *k*–*ω* diagrams in Fig. 3 (pdf 3) of Rutten

and Krijger (2003) exhibit gravity-wave power and phase difference signatures. Gravity waves are copiously excited in granular overshoot. While I doubt that they heat the corona (but see Straus et al. 2008) they transform relatively easy into Alfvénic torsion waves (pages 19 ff (pdf 19) of Lighthill 1967)¹²⁷ and so may play a role in spicule-II heating of the quiet chromosphere (*endnote 80*). [Back] [Main call]

68. Internetwork acoustics with ALMA

Various SE-assuming simulations have predicted that ALMA samples acoustic internetwork waves on their way up to become shocks in the under-the-canopy clapotisphere (*endnote 66*) whereas I have predicted that these are obscured by fibrillar canopies wherever these are opaque in H α (*endnote 21*). Recently Eklund et al. (2021) modeled ALMA response using the Bifrost simulation of Carlsson et al. (2016) but since this lacks opaque internetwork H α canopies (*endnote 76*) this modeling applies only to very quiet non-shielded areas as the ones offered in *endnote 60* and described in *endnote 74* and likely sampled by datasets D6 and D9 of Jafarzadeh et al. (2021) showing enhanced 4–8 Mhz power in Fig. 11 (pdf 21).

AIA 304 Å images can assist in identifying such rare canopy-free locations. Even there traditional pixel-by pixel Fourier power, phase difference and coherency comparisons (as e.g., for internetwork acoustics in TRACE UV image sequences by Krijger et al. 2001) are misleading because the rapidly expanding thin shells seen in the two offered H α sequences imply the need for follow-the-motion along-the-feature tracking, as is the case for canopy fibril dynamics (*endnote 87*). [Back] [Main call]

69. MC shifts 1600–1700 Å

Away from disk-center magnetic bright points in AIA 1600 Å images shift limbward from their 1700 Å counterparts. These shifts do not result from higher formation but from increasing hole transparency giving larger hole depth in top-down viewing and further penetration into granules behind in slanted viewing. They are shown, quantified, undone and explained in Figs. 70–73 (pdf 88) of LAR-1. My SDO pipeline (*endnote 83*) has an option to unshift and subtract them to bring out flaring active-region fibrils (Vissers et al. 2015, Rutten 2016, *endnote 91*) that are brightened independently in 1600 Å images by emission in CIV lines. [Back] [Main call]

70. Lockyer chromosphere, He I D₃, flash color

I typed Lockyer (1868) into ADS, remain its main citer so far, and look forward to write “less refrangible” in publications ([SSX (pdf 12)] ff). Lockyer’s low total of ADS citations (but steepening reads) shows how citation ranking fails for the first professor in astrophysics and the founding editor (during 50 years!) of *Nature*. I recommend his delightful “The Spectroscope and Its Applications”.

Lockyer (1868) discovered He I D₃ (as did “Indian observer” Janssen shortly before him). It contributed its splendid yellow color (familiar to us from sodium street lights) to the chromatic beauty of the emission lines he knew as prominence lines but saw everywhere just outside the limb with his new (but “incomplete” and delayed beyond Janssen) spectroscope [SSX (pdf 12)], concluding that “prominences are merely local aggregations of a gaseous medium which entirely envelopes the sun”.

¹²⁷ A worthwhile read, followed by an outstanding discussion edited by R.N. Thomas, the best discussion record ever. See in particular pages 40 ff (pdf) on spicule vorticity.

¹²⁶ History: E.N. Parker’s first PhD student, plugging heating by gravity waves with Parker’s blessing (before nanoflares).

This was well before he saw himself the beautiful purple-pink of the flash chromosphere at eclipses, but he knew the visually-integrated color from prominences and chose the name to distinguish it from “*the white light-giving photosphere*” and the “*cool absorbing atmosphere*” – a reversing-layer Fraunhofer-line interpretation prior to Schuster-Schwarzschild modeling treated in the [SSA 3.3 \(pdf 31\)](#) practical, the opposite to Milne-Eddington modeling ([endnote 48](#)).

The chromospheric flash color at eclipses during a few seconds after second and before third contact (longer near the edge of the totality strip where Houtgast went on purpose) sums Lockyer’s lines dominated by $H\alpha$, plus white electron scattering (Sect. 7 on walled pdf page 8 of [Jejčić and Heinzel 2009](#)). The beautiful color represents HI, He I and freed H and He electrons: enjoy it yet more by appreciating it as the stuff the universe is made of. [[Back](#)] [[Main call](#)]

71. $H\alpha$ – $H\alpha$ scattering

Pandora stars yield $H\alpha$ disk-center profiles that correspond reasonably well to the observed disk-center atlas profile (VALIII [Fig 25–26 \(pdf 26\)](#)) Naively this may be seen as vindication of the model “chromosphere”. However, about the same profile is also produced in a NLTE RH computation of $H\alpha$ from an 1D RE atmosphere having no chromosphere whatsoever, only an RE photospheric temperature decline ([\[SSX \(pdf 3\)\], Figs 7–8 \(pdf 6\)](#) of [Rutten and Uitenbroek 2012](#)).

The reason is that $H\alpha$ makes its own $\sqrt{\varepsilon}$ scattering decline, more or less the same in $H\alpha$ optical depth scale irrespective of geometrical height scale and presence or absence of an upper-photosphere opacity gap. I call this “ $H\alpha$ – $H\alpha$ ” line formation. It similarly implies that actual $H\alpha$ from higher-located optically and effectively thick fibrils samples similar scattering declines. Where these appear darker they are not necessarily cooler, just more opaque.

Furthermore, in the ALC7 atmosphere Ca II 8542 Å has nearly the same $\sqrt{\varepsilon}$ decline with closely the same τ sampling (comparison in [\[SSX \(pdf 29\)\]](#)). The solar-atlas profiles of $H\alpha$ and Ca II 8542 Å in [Fig. 10 \(pdf 10\)](#) of [Rutten et al. \(2011\)](#) differ substantially but mostly from different thermal broadening and $H\alpha$ ’s abnormal opacity gap, both also known to ALC7 so that it reproduces both profiles reasonably well – but so does a Kurucz RE atmosphere without chromosphere and so do actual higher-up chromospheric fibrils (ha–ha).

In quiet-Sun resolving observations the actual nonthermal motions yield different scenes in the cores of these lines, except for their time-averaged core widths which sense mean temperature. In the wings both lines show spicules-II but $H\alpha$ more and longer. More in [endnote 81](#). [[Back](#)] [[Main call](#)]

72. Rydberg HI lines

The HI Rydberg ladder produces emission lines in the infrared by radiative-collisional recombination departure diffusion ([Carlsson and Rutten 1992](#)) similar to the Mg I 12-micron lines in [endnote 45](#). At that wavelength the HI and Mg I lines are still apart but they creep together for higher levels and longer wavelengths. The Rydberg levels producing lines near 12 micron have larger population for Mg I than for HI ([Fig. 1 \(pdf 2\)](#)) of [Rutten and Carlsson 1994](#)) but this likely reverses at ALMA wavelengths through NLT HI-top population boosting ([endnote 99](#)). [[Back](#)] [[Main call](#)]

73. Dynamic fibrils

Field-guided shocked waves in slanted active-region MCs that

(in my opinion) became the first success story in the century-old struggle to understand the rich zoo of solar $H\alpha$ features (e.g., [Hansteen et al. 2006](#), [De Pontieu et al. 2007](#), [Hegglund et al. 2007 \[SSX \(pdf 22\)\]](#)). Their slant contributes cut-off frequency lowering ([Eq. 4 \(pdf 6\)](#) of [Michalitsanos 1973](#); [Fig. 1 \(pdf 2\)](#) of [Bel and Leroy 1977](#)). Their signature is repetitive parabolic extension and (non-ballistic) retraction along their length in $x - t$ timeslices ([Fig. 7 \(pdf 7\)](#) of [De Pontieu et al. 2007](#)). Many are visible as dark up-and-down dancing stalks in phased rows in this magnificent 5-s cadence [SST/SOUP \$H\alpha\$ movie](#) (courtesy L.H.M. Rouppe van der Voort)¹²⁸. The rows map MC arrangements in active-region network and plage; the phasing along rows is set by the interference-pattern undulations of the combined p -modes ([endnote 61](#)). Their tops may heat to high temperature and show up as bright grains in the Si IV lines in IRIS 1400 Å slitjaw images ([Skogsrud et al. 2016](#)). Short ones are observed in sunspots ([Rouppe van der Voort and de la Cruz Rodríguez 2013](#)). [[Back](#)] [[Main call](#)]

74. Internetwork shocks in Ca II H and $H\alpha$

When Mats Carlsson hunted in the data of [Lites et al. \(1993\)](#) he found only few pixels with multi-cycle spectrum-versus-time behavior matching his RADYN output for the same pixel and selected the best for [Fig. 16 \(pdf 19\)](#) of [Carlsson and Stein \(1997\)](#), showing two less-well matching samplings in [Fig. 17 \(pdf 20\)](#). The first two are columns labeled 110 and 132 in the observed time slices in [Fig. 2 \(pdf 4\)](#) of [Rutten et al. \(2008\)](#), the latter two columns 149 and 30. The latter shocks may have been too slanted to produce vertical-column NLT signature as in the 1D simulation.

The quiet-target SST movie linked in [endnote 60](#) and [here again](#) shows fast-varying threads constituting $H\alpha$ “mushroom” shells following on and around Ca II H_{2V} grains, indeed not radial along the line of sight: internetwork shocks clearly are 3D(t) rather than 1D or 2D phenomena even if the p -mode wave piston is primarily radial. Per-pixel Fourier analysis to establish vertical phase relations is invalid for the resulting shocks and their mushroom aftermaths. The cadence of the movie is 7 seconds but faster is clearly desirable, confirming the need for 1 s spectral $H\alpha$ imaging with DKIST ([endnote 10](#)).

The showex SST displays in my [alignment practical](#) show $H\alpha$ mushroom threads well in the upper-left quiet corner of the SST field but at slower cadence. [[Back](#)] [[Main call](#)]

75. Bifrost program

This MHD simulation code of [Gudiksen et al. \(2011\)](#) is named after old-Norse Bifröst in the Icelandic Edda: *burning rainbow bridge between Earth and the realm of gods* (slightly more inviting than Pandora). Reference lists (until 2018 at the time of writing) are given in [\[SSX \(pdf 160\)\]](#) ff. ADS abstract search “*Bifrost*” and “*solar*” gives publication count and Hirsch $N=85$, $h = 19$, solid enough for a solid permanent position. “*MURaM*” and “*solar*” $N = 96$, $h = 20$ idem for the MHD simulation program of [Vögler et al. \(2005\)](#). Maybe you should simulate. [[Back](#)] [[Main call](#)]

76. Public Bifrost star

Many Bifrost studies employ the 10-min sequence of snapshots of the active-network simulation made public by [Carlsson et al. \(2016\)](#). At currently 115 ADS citations it has become a “stan-

¹²⁸ For Acrobat the 19MB size may exceed its limit, needing manual download from <https://robrutten.nl/rrweb/rjr-pubstuff/lar-2/halpha-soup-half.mpg>.

“dard model” successor to the Pandora stars, after 35 years a worthy 3D(t) MHD successor to the 1D static VALIIC presenting a more realistic rendering of active network than any plane-parallel model. It shares the didactic virtue of the Pandora stars in permitting experiments, tests, explanations. However, it remains a solar analog, not the Sun, and just as the Pandora stars which it presently replaces as canonical solar surrogate it may mislead those who think that the Sun adheres to the model and may similarly mislead use for teaching machine learning.

This particular Bifrost star has chromospheric fibrils connecting two opposite-polarity plage patches, analyzed by Leenaarts et al. (2012a, 2015) as $H\alpha$ fibril emulations. However, their short-loop bipolar-rooted configuration resembles CBPs but without CBP-like heating, perhaps from lack of further emergence and/or small-scale reconnection as do occur in the more active Bifrost star of Hansteen et al. (2019) used by Frogner et al. (2020) which also sports Ellerman bombs (endnote 91) and UV bursts (Young et al. 2018).

The public Bifrost star also lacks spicules-II and return fibrils constituting opaque internetwork canopies in $H\alpha$, so missing an important quiet-chromosphere ingredient unlike what the actual Sun would show around such network. This shortcoming may be due to lack of e.g., resolution, small-scale vorticity, small-scale charged-neutral separation (cf. Martínez-Sykora et al. 2017, 2020; Nóbrega-Siverio et al. 2020b, 2020a; Bose et al. 2021b; Khomenko et al. 2021). [Back] [Main call]

77. Photosphere, chromosphere, corona: hydrogen ionization

The Sun is 90% hydrogen. Neutral in the photosphere, ionized in the corona. The chromosphere in between is the domain of partial hydrogen ionization, complexly small-scale and time-dependent. A radiative-equilibrium atmosphere has outward temperature decline without hydrogen ionization and without further interest: much solar atmosphere physics is about ionization, essentially of hydrogen. The large threshold per particle provides a substantial sink of energy in heating and gain of energy in cooling. Caveats:

- the sink and gain can be non-local radiation, even for optically thick features when effectively thin;
- the key threshold is not 13.6 eV as commonly coded but the 10.2 eV $Ly\alpha$ jump because the rest concerns the Balmer continuum from/to elsewhere (Sect. 7);
- not plane-parallel time-independent as in Pandora stars but small-scale and rapid in explosive events, repetitively cycling in ubiquitous heating events as spicules-II;
- not obeying SE as in most modeling but significantly retarded in cooling phases (Sect. 7).

The upshot is that simulations must treat H I ionization with multilevel RT. However, reasonable shortcuts are to assume detailed radiative balancing in $Ly\alpha$ and $T_{\text{rad}} = 5300$ K for the impinging Balmer continuum J_{ν} . [Back] [Main call]

78. No transition region

I skip the so-called “transition region” because none such exists as a separable domain in the solar atmosphere. Plane-parallel stars need such a layer to furnish substantial lines with formation temperatures around 10^5 K as observed in the solar spectrum. The Sun doesn’t have a spherical shell like that. But it is okay to write “TR line” if you mean transition radiation (endnote 84).

The shocks in the Fig 1 movie of Leenaarts et al. (2007) lift the corona (let’s define that as fully ionized hydrogen) above them tremendously up and down, doing so effortlessly with a steep space-time-varying temperature jump as instantaneous

highly-warped envelope. The simulated corona there reaches deeper in the MCs. This simulation describes quiet chromosphere; in active regions the outbursts are yet further from 1D shell description. The dynamics in this simulation are mostly acoustic shocks with more field guiding in the network, less in the internetwork. The simulation does not have spicule-II jets emanating from network which would lift and warp the internetwork transition to the corona yet more. This transition is not a shell but a highly dynamic thin envelope of the chromosphere (endnote 81) locally producing transition radiation (endnote 84). [Back] [Main call]

79. Internetwork fields and basal flux

Internetwork¹²⁹ MCs riding supergranular outflows to cell boundaries as the “persistent flasher” of Brandt et al. (1994) are traditionally identified as disjoint members of newly emerged tiny bipolar ephemeral regions (Harvey and Martin 1973) on their way to sustain quiet network (Schrijver et al. 1997, Sect. 5.1.2 of Schrijver and Zwaan (2000, 2008)). Such quiet network tends to be small-scale bipolar whereas plage in active regions and plage emerging in smaller failed active regions without sunspots tends to be unipolar obeying the large-scale dipole nature of active region emergence. Subsequent shredding into more open plage and active network then adds bipolarity.

More recently another type of internetwork field became attributed to local field production by a granular-scale near-surface turbulent dynamo. Its action was observationally suggested from Hanle depolarization (Trujillo Bueno et al. 2004) and by the detection of abundant primarily horizontal weak fields at granular scales in sensitive full-Stokes spectropolarimetry with Hinode (Lites et al. 2008, 2017), theoretically simulated by Pietarila Graham et al. (2010). The primarily horizontal signature implies that opposite-polarity closing loops occur on granular scales within the photosphere, a lower and denser “magnetic carpet” than the traditional network-scale one made by ephemeral regions and invoked to supply coronal heating (Simon et al. 2001, Priest et al. 2002). No direct chromospheric interest therefore, but subsequent supergranular-flow migration giving frequent encounters causing cancelation or enhancement up to fluxtube collapse led Gošić et al. (2014) to suggest that this superficial dynamo action competes with ephemeral active region emergence in quiet-network replenishment

Since this contribution should operate similarly in any star with convective granulation and supergranulation, even stars without any internal dynamo, it may contribute cycle-independently to building network and hence to cool-star basal flux in addition to acoustic brightening.¹³⁰ In solar quiet-Sun

¹²⁹ Naming: H. Zirin and (ex-)associates used “intranetwork” arguing that one drives interstates on, not off, the highway while not appreciating that intravenous means within veins rather than between them. Zirin’s wife was a linguist and corrected his books – but only the text, not the equations so that he blamed her for the Planck functions in Eqs. 4.29–4.32 of Zirin (1988) inspiring [IART Question 4.8 (pdf 51)]. All four are wrong; his Rayleigh-Jeans limit goes infinite with wavelength whereas Planck put the bosonic -1 in his best-fit distribution to avoid Wien infinity (endnote 9).

¹³⁰ Naming: defining a minimal level of chromospheric emission in solar-type stars was a major activity at Utrecht initiated by C.J. Schrijver by plotting X-ray fluxes from the Einstein satellite and UV fluxes from the IUE satellite against emission in Ca II H & K measured at Mount Wilson (manually on log-log graph paper) and noticing the need to include a ubiquitous chromospheric pedestal (e.g., Mewe et al. 1981, Schrijver et al. 1982, Zwaan 1986, Schrijver 1987b, Rutten et al. 1991) with an overview in Fig. 5 (pdf 16) of the not-me last. Schrijver named it

ultraviolet images (TRACE 1550, 1600, 1700 Å; SDO 1600, 1700 Å; IRIS 1400 Å slitjaws) network (also quiet network) usually shows larger brightness contribution (from MC hole deepening) than internetwork acoustics. When network produced by the surface dynamo outweighs the acoustic contribution by internetwork shocks it may dominate the basal flux observed at these wavelengths (Table 2.7 on p. 68 of Schrijver and Zwaan 2008). Schrijver et al. (1989) found that basal flux in Ca II H & K from solar-type stars equals the solar flux in supergranular cell centers dominated by internetwork shocks, but Schrijver (1992) found additional basal contribution in weak network and plage. With a cool-star survey Ayres (2021) also finds evidence that basal flux measures the presence of network not made by an activity dynamo. [Back] [Main call]

80. Spicules-II

In my (not so humble) opinion these are the main agents causing the fibrillar H α and sheath-radiation He II 304 Å quiet-Sun chromospheres, being the only candidate agent sufficiently ubiquitous even in quiet network. I use the name generically for off-limb and on-disk manifestations.

I noted them as “straws” near the limb in DOT Ca II H movies (Fig. 1 (pdf 2)) of Rutten 2006). They were then detected and measured using Hinode off-limb Ca II H sequences, attributed to Alfvén waves and named “spicules type-II” by de Pontieu et al. (2007) and De Pontieu et al. (2007)¹³¹.

Spicules-I reach less high above the limb, crowd into the “spicule forest” in H α limb images, and were attributed to active-region dynamic fibrils (endnote 73) by Pereira et al. (2012).

Spicules-II are ubiquitously ejected from quiet-Sun network including monopolar network and also in coronal holes. On the disk these ejections were likely described earlier as “fine mottles” (cf. de Jager 1957), as upflows by Title (1966) in his thesis (now on ADS) and as outer-wing H α “jets” by Suematsu et al. (1995) and in later Big Bear reports. More recently they became known as “rapid blue-wing excursion” (RBE) (Roupe van der Voort et al. 2009) and “rapid red-wing excursion” (RRE) (Sekse et al. 2013b), first in the wings of Ca II 8542 Å and then in the outer wings of H α , with heating up to EUV visibility (Henriques et al. 2016).

Spicule-II aftermaths of cooling recombining return flows cause dark H α -core fibrils around network (known as “coarse mottles” in spectroheliogram days and listed as discovery 6 in the abstract (pdf 1) of Leighton et al. 1962) minutes later with their H α opacities probably much enhanced by NLT cool-down retardation as in the post-shock clouds of Leenaarts et al. (2007). Evidence are the darkest-darkest time-delay correlations in Rutten et al. (2019) and the ubiquity of these downflowing H α red excursions in Bose et al. (2021a). More in endnote 81.

“basal flux”. Duncan et al. (1991) summarized the Mount Wilson monitoring; reviews are by Schrijver (1987a, 1995) and in Sect. 2.7 of Schrijver and Zwaan (2000, 2008).

¹³¹ Author spelling: no bibtex a, b distinction here because the first spells Dutch so that bibtex classifies a split personality (but wrongly: Dutch would be B. de Pontieu but De Pontieu and De Pontieu, B. as for De Jager, C. for Kees de Jager – misspelled as de Jager, C. by ADS in 600+ bibitems, as many other Dutch). The proper spellings B. De Pontieu and L.H.M. Roupe van der Voort, respectively, indicate where they originated. Presently ADS offers 4 solar publications by “van der Voort, L.”, 102 for Kostyk, R.I. and 61 for Kostik, R.I. while half the responses for “Rutten, R.” are not mine. What’s in a name? Using my ADS author strings may help. With these I maintain my solar abstract collection.

The spicule-II driver mechanism is not known (Pereira et al. 2012) but because spicules-II exhibit torsion modes near and at the limb (De Pontieu et al. 2012, Rutten 2013) vorticity in granular convection affecting embedded network fluxtubes seems a candidate, perhaps with fly-by reconnection as in Meyer et al. (2012) kicking up Alfvén waves and perhaps with coupling to gravity waves (endnote 67).

Comparing spicules-II with simpler dynamic fibrils in active-region plage seems a promising topic for simulations. The latter (endnote 73) are p -mode-excited magneto-acoustic shocks along more crowded and less slanted fluxtubes as waveguide. They appear less important in active-region chromosphere heating than spicules-II are in quiet-Sun chromosphere heating and return-flow canopy formation. Since the p -mode pattern undulations occur similarly over the whole solar surface, sloshing waves up into all evacuated fluxtubes, other agents must add dominance in spicules-II. I speculate that the suppression of granular convection in denser plage (showing as “abnormal granulation”) gives larger relative importance to undulation feeding of dynamic fibrils whereas spicules-II suffer more small-scale torsion in fiercer and vortex-richer normal granular convection and may also gain from gravity-wave coupling by spreading over uninhibited overshooting granulation in adjacent internetwork. These agents also operate in unipolar network without flux emergence or cancellation which in multiple quiet-Sun SST data sets also show spicules-II, for example the data of my alignment practical.¹³² [Back] [Main call]

81. RBE–RRE–fibril ionization-recombination

RBEs and RREs reach higher degrees of hydrogen ionization than the shocks in the Fig 2 movie of Leenaarts et al. (2007). There are more and they extend further in H α than in Ca II 8542 Å (Fig. 2 (pdf 4) of Roupe van der Voort et al. 2009, lower-left panel of Fig. 1 (pdf 3) of Sekse et al. 2012) because Ca II ionizes before H I¹³³ and is much less abundant. Where their tips reach AIA EUV visibility (Henriques et al. 2016) hydrogen is nearly or fully ionized.

The resulting recombining return fibrils (Rutten et al. 2019) are more numerous and also much longer in H α than in Ca II 8542 Å (Fig. 3 (pdf 4) of Cauzzi et al. 2009); larger H α opacity is also seen in the aftermath of the exemplary return contrast in Fig. 5 (pdf 6) of Rutten and Roupe van der Voort (2017).

The bottom row in Fig. 6 (pdf 7) of Cauzzi et al. (2009) shows correlations between H α core width and Ca II 8542 Å core width and profile-minimum intensity, instantaneously and time-averaged per pixel. These diagrams quantify the scene similarities in the first, third and fourth-panel scenes in their Fig. 3 (pdf 4) and Fig. 4 (pdf 5). They suggest that both core widths reflect temperature, with correlation calibration in Fig. 9 (pdf 9). The Ca II 8542 Å Doppler-following minimum intensity also re-

¹³² In conflict with the claim of Samanta et al. (2019) that all spicules represent strong-field reconnection, based on a single data set in which juxtaposition of bipolar MC pairs and RBE feet looks unconvincing and non-causal to me and which does not show QSEBs as telltale of quiet-network reconnection. The notion also clashes with the attribution of polar plumes rather than spicules to mixed-polarity network interactions by Wang and Sheeley (1995) and Wang et al. (1997). An obvious test is whether network that is more bipolar and emergence-rich launches more RBEs.

¹³³ The Ca II ionization limit from the ground state is at 11.9 eV (paragraph 16 (pdf 46) of venerable Allen 1976); the edge from the metastable $3d$ levels (Grotrian diagram (pdf 16) in venerable Moore and Merrill 1968) covers Ly α so that large J_v in Ly α within heated features kills their Ca II lines.

sponds to feature temperature but the $H\alpha$ minimum intensity does not (scatter diagrams in the next higher row in Fig. 6 (pdf 7)). Both are scattering lines with similar outward $\sqrt{\epsilon} S(\tau)$ decay to the feature surface (endnote 71) but they differ strongly in opacity-defined return-fibril mapping with the $H\alpha$ opacity much enhanced by NLT retardation (Sect. 7).

You can check these findings yourself with the higher-resolution SST quiet-Sun data in my alignment practical. Its last showex command browses SST $H\alpha$ and Ca II 8542 Å image sequences sampling many wavelengths and also adding the three core measures of Cauzzi et al. (2009) for both lines. Blink these while activating scatter diagrams and also hit the button for sequence time-averaging. The well-correlated width-width blink shows how much further the $H\alpha$ spicules-II reach. Time-delay blinking $H\alpha-0.6$ Å against $H\alpha+0.2$ Å confirms Rutten et al. (2019) with yet better data showing striking darkest-darkest correlation between RBEs and subsequent redshifted core fibrils at about 5-min delay, and also that these reach close to the spicule-II firing network. This suggests that in the cooling returns $H\alpha$ gains largest NLT overopacity keeping it $\sqrt{\epsilon}$ dark much beyond the actual lowering temperature. Blinking the core minima and shifts for the two lines shows that in Ca II 8542 Å these return fibrils get visible only close to network where finally Ca II recombines from Ca III. Thus, large spicule-II H ionization is followed by cooling return recombination producing core fibrils that are much more prominent in the $H\alpha$ core. In contrast, in the ALC7 star the “chromosphere” is ha-ha-sampled the same in the two lines (endnote 71).

The few-percent ionization in the shocks in the Fig 2 movie of Leenaarts et al. (2007) with its two-orders of magnitude electron density increase already suffices to reach near-SB proton densities (3rd movie row). Hence large electron densities and SB partitioning must also occur in spicules-II, warranting straight-forward SB extinction comparisons as in Fig. 7 (pdf 7) of Rutten and Rouppe van der Voort (2017) for the hot spicule-II phases while recognizing that these high extinction values persist NLT-wise afterwards in the recombining return fibrils constituting opaque canopies while instantaneous SB values drop Boltzmann-steep with their temperature. Similar SB curves imply the same for the mm wavelengths of ALMA (endnote 21).

Summary: in spicule-II heating the hydrogen-top populations and extinction slide fast up along the SB curves to high values at large hydrogen ionization, but in subsequent cooling they hang minutes near these high values. They would eventually drop back to the SB value for the actual temperature but get refreshed before that at the 1.4 min RBE recurrence rate (Sekse et al. 2013a). The resulting temporary hydrogen-top overpopulations can be large, as the enormous $b_2 = 10^{12}$ values reached in post-shock cooling in the Fig 1 movie of Leenaarts et al. (2007) (Sect. 7), and so furnish fibrillar $\sqrt{\epsilon} H\alpha$ visibility far beyond the SB expectation. The NLT-opaque fibrillar appearance of the quiet $H\alpha$ chromosphere is due to continuous refurbishment by frequent small-scale ionization and retarded recombination: *the chromosphere ain't stacked in layers but is dynamically structured and unstuck in time.*¹³⁴ [Back] [Main call]

82. Quiet-Sun SDO images

I recommend page-blinking the three members of each set in Fig. 17–46 (pdf 35) of LAR-1. I find it uncanny how well the detector images separate localized quiet-chromosphere heating

(ubiquitous grey patches around any network but scarcer in coronal holes) from sparser localized coronal heating (cyan CBP feet in denser bipolar network also in coronal holes). This separation implies that quiet-Sun atmospheric heating is not traditionally “via the chromosphere to the corona” (with larger energy need for the heavier chromosphere) but that it is done by unrelated mechanisms for quiet chromosphere (Alfvénic-wave spicules-II in my opinion) and quiet corona (reconnective CBPs in my opinion). [Back] [Main call]

83. SDO – STX alignment

My SDO pipeline (manual) consists of IDL programs to request and download SDO sequences for any field, location, time, duration, for precise co-alignment with image sequences from another smaller-field higher-resolution telescope (STX = Solar Telescope X). I started it for the DOT in its final year of operation (2010, the first year for SDO) and have refined it with many datasets from the SST.

The requesting and downloading gets SDO data for your specified target field and also for a large disk-center field for internal SDO cross-alignment. This is desirable because the different SDO diagnostics are usually offset from each other over multiple pixels, with daily modulation from earthshine irradiation peaking at local noon around 19 UT. Much larger offsets occur during thermal resettling after SDO eclipses taking place near equinox.

The pipeline finds the internal SDO shifts from the large disk-center fields by cross-correlation in a sequence of best-fitting pairs after image manipulation to make them more alike and tiling them into many subfields for zonal averaging with projection-shift corrections using apparent limb heights determined from full-disk tiling. Examples for 1600–1700 Å cross-alignment are shown in Fig. 70 (pdf 88) - Fig. 72 (pdf 90) of LAR-1. The hardest step is to cross-align the AIA EUVs to HMI for which I use 304 Å images¹³⁵ and magnetograms exploiting their network pattern equality in quiet areas (endnote 84). This elaborate cross-correlation procedure usually gives ten times better SDO cross-alignment than the aia_prep.pro startup.¹³⁶ Sample results are shown in Fig. 75 (pdf 93) of LAR-1.

The SDO sequences for the target field are first cross-aligned with the center-field results and then co-aligned to the other telescope (or vice versa) including correction of differential guiding drifts.¹³⁷ This is easy for groundbased telescopes when the

¹³⁵ Earlier I matched 304 Å to 1600 Å, later to 1700 Å, after matching these to HMI magnetograms, but direct use of large quiet disk-center fields of 304 Å images and magnetograms as anchor pair is better because the magnetograms suffer smaller limbward projection shifts. The tiled matching applies apparent 304 Å height 3600 km derived from full-disk azimuthal tile averaging as in Fig. 71 (pdf 89) of LAR-1.

¹³⁶ SDO image offsets are corrected by SolarSoft aia_prep.pro using “Master Pointing” lookup tables determined from limb fits. These fits were first done once a week but since early 2019 at 3-hour cadence and also retro-actively throughout the SDO database. The 3-hr values are used by aia_prep.pro also for the earlier dates unless no_mpo_update is set. The remaining 1-2 px shifts vary on time scales of minutes and are largely removed by my cross-correlation pipeline. The scales and rotation angles of all AIA diagnostics were determined by R.A. Shine from the 2012 Venus transit using the precise planetary ephemeris. My alignment practical for the 2019 Mercury transit suggests that they remain valid.

¹³⁷ The SDO target sequences are collected per JSOC im_patch cutout either tracking or not tracking the nominal solar differential rotation at the field center evaluated with SolarSoft rot_xy.pro. The pipeline removes sub-pixel rotation modulation left in these cutouts. The SST and

¹³⁴ Billy Pilgrim syndrome. Multi-wavelength chromosphere observation is as Tralfamadorian multi-time viewing; $H\alpha$ fibril canopies show what happened before (Rutten et al. 2019). So it goes.

imaging sequences include granulation (as for SST wide-band MOMFBD registration, *endnote 11*) and then usually reaches 0.1 arcsec precision. For IRIS the longest-wavelength slitjaw sequences may correspond to co-pointed outer-wing Ca II 8542 Å imaging. ALMA is difficult unless there is co-pointed H α imaging spectroscopy (*endnote 88*); otherwise GONG H α may help (*endnote 89*), in the future SOLIS/FDP H α (*endnote 90*).

For small fields this pipeline is fast by not handling full-disk images but only JSOC cutouts. All programs use IDL assoc to avoid memory loads. Inspection is facilitated with browser showex.pro (*footnote 125*).

My [alignment practical](#) instructing use of this pipeline first cross-aligns all SDO diagnostics during the last Mercury transit with Mercury serving as check. It then co-aligns the quiet-Sun SST data of *endnote 60* with SDO. The disk-center coronal hole sampled there also sports a few “SolO campfires” (*endnote 86*). [[Back](#)] [[Main call](#)]

84. Transition radiation, sheath ionization, coronal contact cooling

The transition region in Pandora stars is sampled by He II 304 Å (the Ly α of hydrogen-like He⁺ (*pdf 10*)) which is therefore called a transition-region line. However, the Sun is not a Pandora star and does not possess a transition region, neither plane-parallel nor spherical (*endnote 78*). The line emits transition radiation. Please use TR only for that.

AIA 304 Å images show chromospheric canopies everywhere in quiet areas outside coronal holes, sampled full-disk over the past decade in my [LAR-3 SDO album](#). These transition-temperature canopies extend above and around magnetic network and so their patterns over the disk are defined by the underlying network patterns. I use this pattern correspondence to co-align AIA 304 Å directly to HMI magnetograms in my alignment pipeline (*endnote 83*). The 304 Å canopies also resemble the fibrillar H α canopies, not in fibrillar detail but in location pattern, so that one may co-align reversed-intensity quiet-Sun H α (even from GONG, *endnote 89*) and 304 Å images by pattern correlation, as shown in blinkable [Figs. 11 – 12 \(pdf 29\)](#) discussed in [Appendix B \(pdf 11\)](#) of [LAR-1](#). This pattern similarity extends even to AIA 131 Å images, making the “fire detector” multiplication¹³⁸ of 304 and 131 Å images in the triple blinkers in [Fig. 17 ff \(pdf 35\)](#) a good transition-temperature quiet-chromosphere mapper: the non-cyan grey clouds everywhere in quiet areas except coronal holes.

The 304 Å and 131 Å emission around quiet network firstly represents hot ionization phases, i.e., hot tips of spicules-II and their still hot initial aftermaths. This emission marks local heating to “transition” temperatures. The H α –Ca II 8542 Å core width correlation fit in [Fig. 9 \(pdf 9\)](#) of [Cauzzi et al. \(2009\)](#) extends as high as 60 000 K with many samples in the input next-to-last panel of [Fig. 6 \(pdf 7\)](#) reaching yet larger values.¹³⁹ How-

ever, other groundbased telescopes correlation-track the granulation pattern or some magnetic feature near field center which usually drifts its own way with respect to nominal differential rotation.

¹³⁸ Multiplication emphasizes what they share in common: “warm” (10⁴–10⁵ K) chromospheric gas and brighter CBP feet. The detector algorithm uses iterative quiet-area intensity scaling to set the greyscale clip and CBP threshold as described in the caption of [Fig. 69 \(pdf 87\)](#) in [LAR-1](#).

¹³⁹ Such temperatures may seem excessively high in terms of H α formation in quiet Pandora stars but it can go worse: [Fig. 13 \(pdf 18\)](#) of [Rutten \(2007\)](#) shows matching H α and 171 Å brightness in an active region.

ever, the fire detector images in the triple blinkers do not show wreaths as pearl-studded crowns around magnetic network but fairly smooth patches extending from it and also covering it. They extend further and appear smoother than the corresponding H α patches in [Figs. 11 – 12 \(pdf 29\)](#). Hence tip heating is only part of this ultraviolet chromosphere mapping.

Such TR canopies are largely absent in coronal holes although these do contain spicules-II as exemplified by H α RBEs and RREs in the high-resolution SST showex display of a disk-center coronal hole in my [alignment practical](#). The 2014–2015 (*pdf 4*) active-Sun triptychs in LAR-3 show good correspondence between the many coronal holes in AIA 304 Å and 171 Å, with the latter somewhat wider. Also the very quiet 2019 (*pdf 6*) sampling shows a fair match for the less prominent non-polar holes.

A traditional explanation for quiet-Sun emission in He II 304 Å is He I ionization by EUV irradiation from above, as also invoked for coronal-hole visibility in He I 10830 Å equivalent width (*endnote 96*), but generally the 193 Å images in the [Fig. 17 ff \(pdf 35\)](#) LAR-1 triple blinkers show wider-spread diffuse brightness providing blanket irradiation without network patterning.

Another candidate is 304 Å emission from local helium ionization by kinetic sheath heating in thin skin-like boundary layers around cooler and denser structures by turbulent mixing with surrounding hot coronal gas per Kelvin-Helmholtz instability, as proposed for prominence threads by [Hillier and Arregui \(2019\)](#) in the form of contact coronal cooling. Their article was an eye-opener to me because it suggests another mechanism to explain that the quiet-Sun chromospheric canopies observed in He II 304 Å match those in H α so closely in their patterning across the Sun. With this mechanism the first result from turbulent contact cooling of the corona surrounding the latter.

A RT aspect beyond thin understanding is that if such turbulent sheath heating by the adjacent corona reaches He I ionization and He II 304 Å emission then it spreads radiatively into the cool substrate since 304 Å lies in the bound-free edge beyond the He I ionization threshold at 504 Å [[RTSA Table 8.1 \(pdf 196\)](#)]. Therefore 304 Å photons penetrating into the cool structure cause more ionization, enabling more 304 Å photons to scatter yet further, eating their way in. An exemplary example is the HI Ly α penetration into the upper photosphere from the abrupt chromosphere in the FCHHT-B 1D model in [[SSF \(pdf 113\)](#)] giving a high b_2 peak in the central panel, after [Fig. 10 \(pdf 7\)](#) of [Rutten and Uitenbroek \(2012\)](#). Irradiative ionization likewise affects denser neutral-helium structures sheathwise over the penetration depth.

Both sheath ionization mechanisms may affect cooling recombining return fibrils from spicule-II ejections and explain that the 304 Å canopies extend across network and also that 304 Å shows fewer canopies in coronal holes where both lower EUV irradiation and lower surrounding-corona density lessen sheath ionization.

I then wondered whether the active-network (“plagette”) H α contrail fibril in [Rutten and Rouppe van der Voort \(2017\)](#) may be exemplary for post-spicule-II H α fibrils in quieter network (*endnote 80*) since it inspired their identification in [Rutten et al. \(2019\)](#). The images in [Fig. 1 \(pdf 2\)–3](#) suggest that both ionization mechanisms operate. The first shows fair overall pattern matching of the active patch in 304 Å with 193 Å (similar in 211 Å, 335 Å, 94 Å but different in 171 Å and 131 Å) suggesting irradiative ionization. The pattern is finer-scale in 304 Å

but higher-density structures can pick up more radiative ionization and likewise suffer more turbulent interface heating. In the cutout sequences in Fig. 2 (pdf 3) the fat RBE-like jet in the first column reaches maximal extent in row 4 where it shows heated-tip brightening in 304 Å and 171 Å. In rows 5–8 the RBE jet retracts and the dark H α line-center cooling contrafil fibril develops. The bright streaks in 193 Å and in 171 Å (Fig. 3 (pdf 4)) break up but the 304 Å streak lingers longer, suggesting turbulent sheath ionization. Both dark and bright H α -center features appear mapped by 304 Å brightness which may be expected if they have similar gas density.

In contrast to this plagette quiet-Sun 304 Å canopies show no matching 193 Å patterns in the Fig. 17 ff (pdf 35) LAR-1 triple blinkers so that I suspect that turbulent sheath heating dominates there. This implies that the ubiquitous quiet-Sun canopies in the AIA 304×131 fire detector images represent chromospheric heating through kinetic (not radiative as in *endnote 33*) coronal contact cooling as in Hillier and Arregui (2019).

In H α line center they are finely structured by opacity dependence on history, i.e., duration after the slender spicule-II causing them in their subsequent retarded Ly α settling to the cooling temperature and defining their individual opacity and $\sqrt{\epsilon}$ darkness per fibril. Sheath-radiating 304 Å canopies sense only fibril gas density and so can appear smoother as they indeed do.

Altogether this suggests that H α (and ALMA, *endnote 87*) as well as “transition” EUV lines outline canopies with similar surface patterns by sampling the quiet chromosphere around network in successive manifestations of continually repeated small-scale brief heating perturbations followed by cooling return flows (“dynamic refurbishment”, *endnote 81*).

There is no difference in “height of formation” between H α , ALMA and 304 Å canopies if these are effectively the same, in stark contrast to layered-star stratification. Observations confirm this equality. The spicules-II producing H α canopies show Balmer-line extent as Lockyer’s “chromosphere” to 4000 km above the limb in Table 3A (pdf 94) of Dunn et al. (1968) and my corresponding decay plot while my estimate for the mean height of the 304 Å chromosphere from my SDO pipeline matching (*endnote 83*) is 3600 km (double the Pandora-star value), also evident for the ALMA chromosphere in Fig. 1 (pdf 2) of Yokoyama et al. (2018). [Back] [Main call]

85. CBP foot visibility

CBP feet are bright in AIA 304 Å and its “fire detector” (pdf 87) product with 131 Å but sharper in IRIS 1400 Å slitjaw images because Si IV has similar temperature-defined presence as He II but 10³ lower abundance. This is evident for the complex CBP in the 1400 Å and 304 Å columns of Fig. 2 (pdf 3) of Rutten and Rouppe van der Voort (2017), discussed at the end of Appendix B (pdf 14) of LAR-1.¹⁴⁰ The SDO cutouts for a dozen CBPs in Fig. 48 ff (pdf 66) suggest additional 304 Å brightness around bright CBP feet due to EUV irradiation (*endnote 84*). [Back] [Main call]

86. SoLO campfires

Small bright EUV features in the first Solar Orbiter/EUI image that were press-released named and claimed as new coronal heating agent, triggering Rutten (2020). I found them already reported as smallest SoHO/EIT CBPs by Falconer et al. (1998)

and less sharp but less hullabalooed present throughout the AIA database without getting attention. They are the smallest cyan features in the fire detector images in the ten triple blinkers starting at Fig 17 (pdf 35). Counting the many cyan features in these snapshots suggests that at any moment smaller CBPs and campfires are more numerous than larger CBPs but the latter live much longer (see fifteen cutout sequences starting at Fig. 48 (pdf 66)).

The cyan detector CBP feet are at chromospheric heights and are heated from above as in Fig. 12 (pdf 13) of Frogner et al. (2020) where features 1 and 2 resemble CBP-loop feet and feature 3 resembles a small isolated low-lying campfire, loop-less conform the absence of loop features at campfires in the AIA blinkers, but likewise heated by a particle beam from above and shining harmlessly as an electric St. Elmo’s fire. It marks, not causes, higher-up reconnective heating as a small telltale. While writing LAR-1 the work of Frogner et al. (2020) was an eye-opener to me because it explained how campfires and larger brushfire feet represent features coming from above, as I had tentatively concluded from comparing a dozen SoLO campfires with their SDO counterparts in Fig. 48 ff (pdf 66) there.

It is a mistake to sum observed CBP or campfire brightnesses as contribution to coronal heating since this energy is gone: bright momentary flames contain no information on non-lost heating (*endnote 33*). The actual more steady and diffuse coronal heating patterns in the AIA 193 Å triple images suggest negligible heating from the smallest campfires and most from the largest CBP reconnection events. [Back] [Main call]

87. Quiet chromosphere with ALMA

Outside rare truly quiet internetwork (*endnote 68*) ALMA samples chromospheric canopies that are also but differently sampled by H α and Ly α (Rutten 2017b). The IBIS H α core-width (pdf 8) scene discussed in *endnote 93* represents an analogon of an ALMA active region scene (but mapping rather than measuring temperature). The SST H α core-width scene in the final showex display of my alignment practical samples a quiet disk-center coronal hole and represents a quietest-Sun ALMA analogon.

Claiming that longer ALMA wavelengths sample higher layers from the λ^2 increase in $\alpha_\lambda^{\text{ff}} \sim N_e N_p T^{-3/2} \lambda^2$ [RTSA Eq. 2.79 (pdf 47)] is as plane-parallel wrong as interpreting H α images with the famous VALIIC diagram [SSX (pdf 60)] (Sect. 6). The quiet chromosphere is not layered but dynamically structured with NSE hydrogen-top opacities (*endnote 81*). ALMA brightness does measure temperature for optically thick features but the feature proton densities and hence the $\propto \lambda^2$ feature opacities and hence the $\tau=1$ feature sampling locations were set NLT-wise in the recent past. Some features may be thin at 1 mm and thick at 3 mm, others so thick that the measured temperatures sample adjacent outer feature surfaces, further out at longer wavelength. The H α opacities are also set NLT-wise but H α and Ly α obtain relative feature contrasts from variations in $\sqrt{\epsilon}$ scattering with deep $\tau_{\text{eff}}=1$ signature and from Dopplershifts.

The large NLT opacity enhancements that the hydrogen top ($n = 2$ and higher levels including the ion population) suffers in cooling return fibrils after spicule-II heating jets (*endnote 81*) implies that ALMA in quiet areas likely samples chromospheric canopies as predicted in Rutten (2017b) and pattern-matching those in He II 304 Å (*endnote 84*).

Studying the nature and formation of canopy features requires follow-the-motion along-the-feature tracking with temporal delay comparisons. Frequency-resolving Fourier power,

¹⁴⁰ The ALMA-detected “microflare” of Shimizu et al. (2021) had similar large-CBP morphology and similarly occurred between feet-heated bipolar patches of active network, not as an active-region outburst.

phase difference and coherency analysis should also be along-the-feature.

ALMA already excels in obtaining fast cadence and potentially excels in obtaining angular resolution¹⁴¹ while spectral profile resolution in Balmer and Lyman lines offers larger opacity diversity and Dopplershift encoding; combination of these diagnostics and/or less saturated companions (*footnote 148*) is desirable. [Back] [Main call]

88. ALMA – H α – SDO alignment

Another confirmation that ALMA sees chromospheric canopies in quiet-Sun areas is that there ALMA images can be co-aligned with H α images through cross-correlation. This is easy on the disk with co-pointed H α imaging spectroscopy delivering temperature-mapping H α core width (also shown in the IBIS – SDO blinker of *endnote 93*). The correspondence is not 1:1 because hot RBE and RRE tips, emanating furthest from the spicule-II launching network, are not seen in H α core-width imaging which mostly charts cooling return fibrils. Blurring may improve pattern correlation.

Near the limb ALMA emphasizes hot tips of spicules-II that appear as upright hedges of straws, bright in Ca II H & K (DOT Ca II H movie, Fig. 1 (pdf 2)) of Rutten 2006), dark in the H α red and blue wings (Fig. 5 (pdf 5) of De Pontieu et al. 2012, Fig. 1 (pdf 4) of Rutten 2013) and with bright feet in IRIS 1400 Å slitjaw images (Fig. 1 (pdf 2) of Yokoyama et al. 2018). Hence, near-limb ALMA images may be cross-correlated to underneath summed and reversed H α blue-wing and red wing intensity. Off the limb non-reversed H α core intensity of sufficient resolution may serve for tall spicules-II jutting out from the spicule-I forest which appears opaque up to 3500 km height in the ALMA image and furnishes bound-free scattering blackness (*endnote 20*) in the 171 Å image in Fig. 1 (pdf 2) of Yokoyama et al. (2018).

The first co-pointed ALMA – H α data were with DST/IBIS (Molnar et al. 2019) but IBIS has left the DST. The DST is located at 2.5 hours later longitude than ALMA. The SST on La Palma is at 3.3 hours earlier, the GST at Big Bear 3.3 hours later, the DKIST on Maui 5.9 hours later. Afternoon seeing can be good at La Palma after the Sun has passed the Caldera while the USA sites usually have best seeing soon after sunrise.

An attractive alternative is to move the mothballed and relocatable DOT from La Palma to ALMA. It anyhow has to make room for the planned EST and it packs into a few containers. On the disk two-channel speckle bursts in 3 or 5 H α wavelengths with its tunable Lyot filter would deliver qualitative core width mapping, simultaneous granulation images giving co-registration with SDO/HMI and other SDOs with my alignment pipeline (*endnote 83*). Inside the limb summed and reversed H α wings would do, off-limb non-reversed H α core summation, both with Ca II H to AIA 1700 Å outer-disk co-alignment. Continuous co-pointing may then often enable precise co-alignment of solar ALMA data with all SDO diagnostics. DOT mosaicing around the small ALMA field would supply similar-diagnostic

context imaging. Pointing mosaicing is straightforward with the DOT because it has a parallactic mount (no image rotation) and does not use adaptive optics (speckle restoration suffices at 45 cm aperture). Examples in Fig. 6 (pdf 9) of Rutten (2007) and Fig. 2 (pdf 6) of Rutten (2017b); more in the DOT image album. [Back] [Main call]

89. ALMA – GONG – SDO alignment

In the absence of co-pointed H α spectrometry (*endnote 88*) co-alignment may be tried for quiet on-disk scenes with wider-band H α core images exhibiting cooling return fibrils that remain dark through non-SE overopacity. With greyscale reversal rough pattern agreement with the fibril temperatures mapped by ALMA enables co-alignment, easiest for large quiet fields. This correspondence is not 1:1 also temporally because the cooling return fibrils follow a few minutes after the hottest spicule-II tips (Rutten et al. 2019). Space-time blurring and delayed H α sampling may improve pattern matching.

Such images are almost always available from GONG¹⁴². Since these are full-disk they may contain a suited large quiet closed-field area somewhere for precise co-alignment (with H α intensity reversed) to simultaneous AIA 304 Å images as in the blink for the first SoLO/EUI target in Figs. 11 – 12 (pdf 29) of LAR-1 and discussed in Appendix B (pdf 11) there. The GONG H α part (also greyscale-reversed) covering the small ALMA target field may then serve as ALMA-to-SDO intermediary for wherever ALMA pointed.

I succeeded in this for the quiet-Sun ALMA data of Nindos et al. (2021) with suited GONG images sampled in their Fig. 1 (pdf 4). I found the second-step ALMA-to-GONG matching easier than the first-step GONG-to-304 Å matching, and indeed found good pattern correlation between the ALMA, GONG and AIA chromospheres. This suggests that many ALMA quiet-Sun on-disk sequences can be precisely co-aligned with all SDO diagnostics via GONG.

For active regions the partial match between the IBIS H α core-width scene (pdf 8) and AIA 304 Å (pdf 10) in the IBIS – SDO active region blinker of *endnote 93* suggests that direct ALMA to 304 Å alignment maybe the best to try but it will be severely hampered by small ALMA field size and the AIA 304 Å deterioration (*footnote 50*). [Back] [Main call]

90. ALMA – SOLIS – SDO alignment

Fig. 2 (pdf 6) of Brajša et al. (2021) taught me unexpectedly that NSO not only furnishes full-disk H α monitoring with GONG (*endnote 89*) but has done this also with the Full-Disk Patrol extension of the SOLIS telescope. Not around-the-world around-the-clock but sporadic during 2012 – 2017 with SOLIS first at Kitt Peak and then at Tucson. Ever since SOLIS is being moved to a site on the shore of Big Bear Lake close to the GST – I hope on a tall Hammerschlag tower as in the mockup for future ng-GONG.

SOLIS/FDP takes H α line-core images but also summed-wing images with 0.5 Å bandpass sampling ± 0.3 Å from nominal line center. These inner-wing images emphasize the onset of dark outgoing blueshifted spicules-II and the arrival of incoming redshifted return fibrils and so show the agents producing and constituting quiet-Sun internetwork canopies more directly than the GONG H α -core images of *endnote 89*. I therefore expected

¹⁴¹ Addition of many longer baselines may improve ALMA's sharpness beyond SST/CRISP H α scenes, also beyond yet sharper SST/CHROMIS H β , even beyond DKIST since $D/\lambda = 10 \text{ km}/1 \text{ mm}$ equals $4 \text{ m}/0.4 \mu\text{m}$ but DKIST will likely reach its diffraction limit only beyond $1 \mu\text{m}$ where seeing with $r_0 \sim \lambda^{6/5}$ spoils less but nothing shows the chromosphere. Asymmetric (U, V)-plane filling yielding anisotropic resolution is an option since the solar scenes consist of long thin fibrils spread in all directions so that high resolution only transverse to or along suited ones is already worthwhile, as with the 11-m GISOT design of Hammerschlag et al. (2004) with an elliptic aperture (Fig. 1a (pdf 2)) to minimize prime-focus heat load.

¹⁴² With large quality variations with time and between stations. Fortunately ALMA's longitude suits the usually better ones (Big Bear, Cerro Tololo, Mauna Loa).

that they suit better for two-step ALMA-SDO co-alignment than through GONG. This proved correct.

I first ran tests with co-alignment program `nisp_sdo.pro` trying both GONG and SOLIS/FDP image sequences from the [NSO NISP archive](#) on 2012-08-15 when the Sun was very quiet around disk center and AIA 304 Å still had high S/N. I found that indeed the FDP summed-wing H α scenes resemble AIA 304 Å more closely than simultaneous GONG images: for the quiet area at disk center the Pearson cross-correlation coefficient versus 304 Å increases from 0.3 for GONG H α to 0.7 for SOLIS/FDP summed-wing H α . Hence co-aligning SOLIS H α to AIA 304 Å is much easier and more reliable than for GONG H α .

I then tested the two approaches with the data of [Brajša et al. \(2021\)](#). Their [Fig. 2 \(pdf 6\)](#) shows that the ALMA target was an active region but with some quieter area at bottom-right. As expected, the ALMA appearance there is much closer to reversed SOLIS summed-wing intensity than to reversed GONG intensity. I found that precise co-alignment using only a small subfield was easy with the SOLIS images but impossible with the GONG images, even though the first show larger image distortions and more image motion that require substantial self-alignment and time averaging.

However, a zonal shift-per-tile analysis as in [Fig. 70 \(pdf 88\)](#) of [LAR-1](#) between the simultaneous GONG and SOLIS images shows radially increasing offset between the two up to 2400 km difference at the limb. Most of this is projective height difference because the SOLIS/FDP wing images sample canopy bases while the GONG as well as the 304 Å images emphasize outward extensions reaching much higher. This can be corrected with a `heightdiff` limb offset parameter in `nisp_sdo.pro` but requires precise pixel scale calibration. So far the archived SOLIS/FDP images are only level 1 without flatfielding or calibration. When SOLIS finally goes into renewed operation at Big Bear which promises much better seeing and when the image processing improves to level 2 including precise scale calibration then SOLIS/FDP may become the best monitoring facility to assist as intermediate step in co-aligning ALMA observations precisely to SDO. [[Back](#)] [[Main call](#)]

91. Ellerman bombs and flaring active-region fibrils

EBs are active-region MC reconnection events in the low photosphere. After growing interest in the past decade¹⁴³ and successful simulation by [Hansteen et al. \(2017\)](#) and [Ortiz et al. \(2020\)](#) EBs¹⁴⁴ now represent another H α feature that is largely understood. RR next to spicules-II, fibrils

Here they are of chromospheric interest because the spectral signature of these events is complex and instructive. EBs appear bright only in the H α wings because their H α line cores remain shielded by overlying dark active-region fibrils ([Fig. 3 \(pdf 4\)](#) of [Rutten et al. 2013](#)). They are therefore similarly shielded and

invisible for ALMA ([prediction 9 \(pdf 9\)](#) of [Rutten \(2017b\)](#) confirmed by [da Silva Santos et al. 2020](#)).

EBs are not visible in the Na I D and Mg I b lines ([Ellerman 1917](#), [Rutten et al. 2015](#)) because they are hot enough to fully ionize neutral metals. Similarly EBs appear bright in UV continua from Balmer continuum brightening with neutral-atom bound-free opacity ionized away (as in flare feet showing optical flares). [Vissers et al. \(2019\)](#) have defined and calibrated an EB detector using AIA 1700 Å images which opens the entire SDO database for studying EB occurrence.

In AIA 1600 Å images EBs gain additional brightness from the C IV lines in the passband, similarly to the large Si IV enhancements in [Fig. 4 \(pdf 7\)](#) and [Fig. 8 \(pdf 9\)](#) of [Vissers et al. \(2015\)](#). The latter figure also shows Mn I, Fe II and Ni II absorption blends on high Si IV, C II and Mg II emission peaks. [Figure 2 \(pdf 5\)](#) of [Rutten \(2016\)](#) added a schematic EB into the last panel of [Fig. 1](#) of the simulation of [Leenaarts et al. \(2007\)](#) to show how these can arise from undisturbed EB surroundings, not part of the phenomenon as suggested for IRIS bombs by [Peter et al. \(2014\)](#).

Because EBs are hotter and denser than internetwork and dynamic-fibril shocks in which Ly α already reaches collisional equilibrium their H α extinction obeys SB partitioning, permitting the straightforward SB opacity comparisons in [Fig. 5 \(pdf 9\)](#) of [Rutten \(2016\)](#). In this figure H α reaches similar extinction maxima as the Mg II and Si IV IRIS lines, so that the actual EB H α profile under the canopy is probably similar to Mg II k with a high peak and a small central dip as in [Fig. 4 \(pdf 7\)](#) of [Vissers et al. \(2015\)](#), hence with much larger profile-summed brightness than observed. It is a mistake to count the observed H α EB wing enhancements as contribution to coronal heating since this energy is radiated away ([endnote 33](#)) while the H α core photons are boxed in by overlying NLT-opaque canopies but appear insufficient to brighten these.

Small hot photospheric structures as EBs containing intense Ly α irradiate their cool surroundings causing aureole boosting of the hydrogen top including ionization [[SSX \(pdf 171\)](#)] and making the feature visible even if the actual reconnection site is too small. NSE recombination is slow so that such boosts linger longer, in a wake if the reconnection progresses upward. The Zanstra mechanism for detour photon conversion in planetary nebulae [[SSX \(pdf 144\)](#)] [[IART Sect. 8.3.3.1 \(pdf 137\)](#)] likely also operates in their cool surroundings.

Presently EB interest has moved to non-active quiet-Sun QSEBs (“quiet-Sun Ellerman-like brightening”) marking ubiquitous but hard-to-detect small-scale photospheric reconnection ([Roupe van der Voort et al. 2016](#), [Danilovic 2017](#)) and best seen in SST/CHROMIS H β ([Joshi et al. 2020](#)).

FAFs were called “transient loops” by [Pariat et al. \(2009\)](#). [Vissers et al. \(2015\)](#) used “flaring arch filaments” but I renamed them to “flaring active-region fibril” in [Rutten \(2016\)](#) to avoid confusion with arch filament systems. In active regions with much flux emergence they appear in AIA 1600 Å image sequences with shorter duration and more abrupt changes than comparatively stable and roundish EBs, have elongated morphology, and show fast apparent brightness motion along filamentary strands. Further description including EB and FAF distinction is in [Appendix A \(pdf 9\)](#) of [LAR-1](#). [[Back](#)] [[Main call](#)]

92. Moss

“Spongy” active-region plage showing many short loops and bright footpoints interspersed with darker patches at small scales in 171 Å and other EUV lines (e.g., [Berger et al. 1999b](#), [1999a](#),

¹⁴³ History: I participated in [Watanabe et al. \(2011\)](#), [Rutten et al. \(2013\)](#), [Vissers et al. \(2013\)](#), [Rutten et al. \(2015\)](#), [Vissers et al. \(2015\)](#), [Rutten \(2016\)](#), [Young et al. \(2018\)](#), [Vissers et al. \(2019\)](#) and think that I helped boost interest in [Ellerman \(1917\)](#): after half a century of disregard it shot up in [ADS citations](#) passing 100 in its centennial year, near 200 now. Moral: if your nice discovery goes unnoticed then relax waiting for ADS to revive it.

¹⁴⁴ Naming: my laptop got confiscated by border police spotting the b* word in an EB-modeling email on its screen. It then took them months to reclassify me from terrorist suspect to [harmless Ellerman b*er](#) – better use b=burst as in [Young et al. \(2018\)](#). Note that a solar EB releasing 20 Gt ([Rezaei and Beck 2015](#)) is a bigger blast than the champion man-made “Tsar Bomba” hydrogen b* of only 50 Mt.

de Pontieu et al. 1999, Martens et al. 2000, De Pontieu et al. 2003). Polito et al. (2020) differentiate moss and outflow regions in active-region plage where the latter likely contribute to the slow wind and non-CME FIP generation (Fig. 8.8 (pdf 170) of Reames 2021; *endnote 95*). [[Back](#)] [[Main call](#)]

93. IBIS–SDO active-region blinker

[Download here](#). I made it in 2011 courtesy K.P. Reardon while teaching this course at LMSAL (Palo Alto) and displayed it ever since in my teaching escapades. Most of these images have enhanced grey scales¹⁴⁵ by bytescaling the square root or the square of the measured intensity plus clipping. All have a small area near center magnified four times in the upper-right corner for more detailed blinking.

Here are my inventory and tentative interpretations (better blink yourself! – how in *footnote 51*):

HMI Stokes I–V (p1–p2): Stokes *I* shows only granules, pores and the spot, not the network and plage seen in Stokes *V* (higher resolution would show abnormal granulation in plage). Plage brightens in such continuum sampling only near the limb, from MC transparency in slanted viewing (righthand cartoon in Fig. 73 (pdf 91) of LAR-1). The flare is along connections from the spot to opposite polarity in the sunspot moat (blink p2–p6).

HMI Stokes V – AIA 1700 Å (p2–p3): ultraviolet MC brightening is not from higher-up heating (as commonly thought) but from magnetic hole deepening (lefthand cartoon and caption of Fig. 73 (pdf 91) of LAR-1). Blinking these disk-center images shows co-spatiality but towards the limb 1700 Å bright points shift relatively limbward, 1600 Å yet more, also not due to offset in formation height but to increasing MC transparency (*endnote 69*). A few bright 1700 Å points in internetwork mark isolated MCs (*footnote 79*). Elsewhere the grey fine structure in 1700 Å internetwork areas represents clapotispheric shocks (*endnote 64*).

AIA 1700 Å – Ca II 8542 Å wing I (p3–p4): in the Ca II 8542 Å wing MC brightening in plage and network is hole brightening from less collisional damping and additional downdrafts, but the inset suggests much shielding within plage. Enhanced bright points in the sunspot moat are likely not EBs since they lack corresponding excess 1700 Å brightness (Vissers et al. 2019) and may mark MC downdrafts common in moats (Beck et al. 2007). Internetwork areas show predominant reversed granulation (inset) and also sporadic shock brightening in grains (Sect. 5.5 (pdf 13) of Rutten et al. 2011). Slender dark fibrils extending from plage and network represent the plage counterpart of network RBEs combining blueshift and line broadening in this blue-wing sampling as in Fig. 1 (pdf 3) of Rouppe van der Voort et al. (2009).

Ca II 8542 Å wing I–core I (p4–p5): dramatic difference. The core shows the chromosphere with bright-grained network and plage hearts signifying onset of heating. Magnified blinking shows that many of these dense bright grains are roughly co-spatial with wing MCs, suggesting upward heating, mostly in unipolar plage (p2). Blinking to 171 Å (p11) shows a few areas appearing as EUV moss (*endnote 92*) over bipolar plage (one patch is above the cutout square but HMI does not show all opposite-polarity field). Dark fibrils extend far over internetwork but do not cover all of that, some internetwork still shows up in the qui-

etest areas with shock brightening in grains of which some are also visible in the wing image.

Ca II 8542 Å core I – Hα core I (p5–p6): similar scenes but all fibrils are much fatter and longer in Hα which I attribute to large NSE opacity (*endnote 81*). All internetwork is covered by fibrils in Hα. The bright plage grains often correspond well between the two (inset). Some may be heated tips of dynamic fibrils observed down-the-throat. There are long slender dark active-region filaments above polarity inversion lines (blink either against p2). The spot flare shows its concurrent loop and feet brightening similarly in both line cores.

Hα core I – minimum shift (p6–p7): the second is the shift of the Hα profile minimum per pixel following Cauzzi et al. (2009), with blueshift dark. The hearts of the plage areas have small-scale grainy appearance with sizable patches of large blueshift. The fibrils extending away show lower-amplitude fibril-to-fibril modulation, a signature of their intermittent repetitiveness in extending out and shrinking back (called “breathing” by a colleague). Blinking the inset shows short dark blueshifted heating onsets; the longer grey fibrils are return flows. The latter show similar but finer structure in Ca II 8542 Å core I (blink p5–p7); showex zoom-in shows double-branch scatter diagrams there because Doppler-shifting the narrow Ca II 8542 Å core brightens its intensity for both blue- and redshift. In Hα the umbra shows flashes on their way to running penumbral waves. Only the brightest are visible in Ca II 8542 Å but they are well-known from Ca II H & K as in Figs. 2–4 (pdf 4) of Rouppe van der Voort et al. (2003). The spot flare shows a bright core-shift feature in the loop and also a dark shift companion feature further out, at image edge. Diametrically opposite on the other side of the spot there is a conspicuous bright-dark feature pair that also seems connected.

Hα core width (p8): width of the Hα core per pixel regardless of Dopplershift following Cauzzi et al. (2009) (*endnote 81*). This is the most telltale scene in this blinker with respect to heating. The plage hearts are grainy and mostly hot. The bushes extending away from there are shorter than the fibrils in core intensity (p6) because these are RBE-type heating onsets. Network RBEs reach much further out while heating and accelerating, but their profile signature moves out from the core to the far wing (Fig. 5 (pdf 6) of Rouppe van der Voort et al. 2009). The same likely happens for these active-plage fibrils, as for the active-network fibrils in the data of Rutten and Rouppe van der Voort (2017) analyzed in Rutten et al. (2019). Blinking the inset against minimum shift (p7) confirms that the short dark blueshifted features there are part of these. The active-region filaments appear about as wide as in He II 304 Å, wider than in Hα core I and Ca II 8542 Å core I which are affected by Dopplershifts. The Dopplershift features of the spot flare show heating here, also on the other side of the spot.

He I D₃ – He II 304 Å (p9–p10): the He I D₃ equivalent-width image is naturally noisy but nevertheless intriguing. The two scenes show fair bright-bright correspondence, better further away from the spot and not 1:1 as one might expect from irradiative EUV ionization invoked to explain coronal-hole visibility in optical He I lines or from turbulent sheath ionization (*endnote 84*). Furthermore, this blink shows significant feature shifts, also in the inset, for the bright beginnings of dark fibrils; they occur further out from network in 304 Å whereas the He I D₃-opaquest (bright) parts remain co-located with corresponding Hα features. These offsets suggest outwardly increasing heating as occurs for network RBEs in the bottom panels of fig. 6 (pdf 8) of Sekse et al. (2012), here for fatter fibrils origi-

¹⁴⁵ Real scientists do not fake-color intensity scenes: our eyes are good in appreciating shades of grey. When color coding graphs consider that colleagues may have difficulty distinguishing red and/or green.

nating from plage. This blink also indicates that the 304 Å dark filaments are also present in He I D₃, barely outlined by showing slightly less noise.

He II 304 Å (p10): blinking against H α core I (p6), H α core Doppler (p7), H α core width (p8) and He I D₃ equivalent width (p9) are all interesting. The first (p10–p6) shows coarse similarity between H α and 304 Å: active chromosphere roughly corresponds between these diagnostics, opposite in sign to the reversed-H α –304 Å correlation for quiet closed-field chromosphere (*endnote 84*). The correlation improves with spatial and temporal averaging (options in `showex`). I have used this likeness for direct co-alignment of H α to AIA 304 Å for SST targets with much activity and many active-region filaments and it became an option in my SDO pipeline (*endnote 83*), but usually alignment of quiet-area AIA 304 Å to HMI magnetograms plus SST alignment to HMI per granulation works better. The second (p10–p7) blink shows that the brightest 304 Å patches and correspondingly the brightest He I D₃ opacity patches match best with the plage hearts where H α Doppler is fine-scale black-and-white speckled indicating upward heating (*endnote 94*).

171 Å (p11): obviously mostly corona, no chromosphere. Blinking to HMI Stokes I (p1) shows that all long loops connect spot areas. The mossy patches near image center correspond to bright areas in both He diagnostics (p9 and p10); in H α (p6) these may harbor dynamic fibrils but their identification needs a time sequence. Otherwise, the grainy areas of chromospheric plage heating in H α width (p8) show no coronal counterpart. The separation between chromospheric and coronal heating in quiet closed-field areas is already striking (*endnote 82*); here it extends to an active region. Some thick 304 Å filament parts are also dark in 171 Å, suggesting bound-free scattering as in *endnote 20*. [*Back*] [*Main call*]

94. Around and upward heating

In quiet areas dark fibrillar H α canopies and similar-pattern but bright He II 304 Å canopies are made by spicules-II extending from network (*endnote 80*). The active region in the *IBIS blinker* shows similar but denser, fatter, longer H α fibril canopies (pdf 6) that are relatively dark in 304 Å (pdf 10). It seems likely that such active canopies stem from similar mechanisms as quiet canopies; I call these “around heating”. However, the hearts of plage and network show dense grainy heating in H α core width (pdf 8), especially where mostly unipolar, that I call “upward heating” – meaning at chromospheric heights, not high-reaching as coronal plumes in coronal holes as in Wang et al. (1997). This heating follows fields that do eventually bend back to the surface but connect along long coronal loops to faraway activity.

H α core-width (pdf 8) shows remarkable difference: grainy bright upward heating in the plage hearts versus around heating as extended bushes pointing away from network and plage that seem comparable to spicule-II onsets (*endnote 93*). I attribute this difference to MC clustering and upward field forcing. Active network and plage contain discrete MCs in larger number and at larger density than quiet network. In classic magnetostatic flux-tube cartoons [*SSX* (pdf 44)] the field flares out with height; in classic “Zürich wineglass” models (Fig. 4 (pdf 6) of Bünte et al. 1993) neighboring fluxtubes inhibit flaring wide. Denser near-unipolar collections so have more upward field, as in the inversion map in Fig. 7 (pdf 9) of Jafarzadeh et al. (2017).

I think that the resulting dominance of upward heating over around heating causes larger brightness in 304 Å, outshining the surrounding fibril canopies that then appear dark in byte-scaled

comparison. Where plage and network are more bipolar they have small-scale short-loop connectivity leading to moss appearance (*endnote 92*).

For both around and upward heating the driving mechanisms are not known, as is the case for spicules-II producing canopies around quiet network in closed-field areas (fewer in coronal holes, e.g., Fig. 42 (pdf 60) of LAR-1). However, also for quiet canopies there is observational inclination dichotomy between more horizontal and more vertical. On-disk RBEs and RREs are easiest detected in the H α wings when they reach far out from their launching network, therefore preferentially showing wide-spread around heating, but at the limb spicules-II are easiest noted and isolated amid their projective confusion when they are more upward, as shown in the inclination histograms in Fig. 4 (pdf 5) of Pereira et al. (2012) and seen near the limb e.g., in this *DOT straw movie* and in Fig. 5 (pdf 5) of De Pontieu et al. (2012). Hence distinction between around versus upward morphology and heating seems gradual, suggesting similar driving but difference in appearance and detectability set by variation in dominating field topography defined by MC clustering density and polarity.

The CLASP2–IRIS co-observation of Ishikawa et al. (2021) indicates that fields keep longitudinal strength up to 300 Gauss high in the chromospheric above dense plage, suggesting preponderance of straight-up fields. The precise pattern correlation between field strength and Mg II k core intensity and the good correspondence with AIA He II 304 Å intensity in their Fig. S1 (pdf 44) confirm straight-up heating.

For He I D₃ the sparse and minor on-disk presence in the *IBIS blinker* (pdf 9) versus its bright Balmer-like prominence in the flash spectrum, also away from active regions, suggests sensitive response to upward network and plage heating (*endnote 96*). [*Back*] [*Main call*]

95. FIP effect

About 3 \times relative overabundances compared to photospheric values in the slow solar wind (SSW) and in solar energetic particles (SEP) for elements with low neutral-atom ionization “potential” (FIP) (e.g., Meyer 1985, 1991, Fig. 7 (pdf 11) of von Steiger and Geiss 1989, Fig. 8.5 (pdf 164) of Reames 2021). These include the most abundant electron-donor elements Mg, Fe, Si, Al [*SSF* (pdf 56)] which are predominantly ionized everywhere but amount to only 10^{−4} N_H in the photosphere where H and hence the gas are near-neutral. This “FIP effect” is generally attributed to ion-neutral segregation involving the degree of line-tying to open field and hence attributed to low-atmosphere origins (e.g., von Steiger and Geiss 1989, cf. Laming et al. 2019, Reames 2021). Modeling thus must include neutral-ion separation already at low heights.

The upper panel of Reames’ Fig. 8.5 (pdf 164) indicates pivots near 10 eV for the SSW values, 14 eV for the SEP values. This split suggests that for the SSW the 10.2 eV Ly α jump is the key in hydrogen ionization by controlling the feeding level of the Balmer ionization-recombination loop and so defining NSE retardance of the hydrogen-top (high levels and ion) populations in post-hot cooling gas, as described for shocks and spicules-II in *Sects. 7* and *8*. Presence or absence of frequent hot-cool cycling may be important. The SEP pivot instead suggests hydrogen ionization directly from the ground level, hence in more abrupt and fiercer heating events.

The IRIS study of Polito et al. (2020) points to non-mossy upward active-region heating (*endnote 94*) in slow-wind generation. The match in the *IBIS–SDO blinker* of “brightest” plage-

heart patches in He I D₃ opacity with grainiest H α core Doppler-shift patches in plage (p7 versus p9 of the [blinker](#)) marking upward heating suggests to test the He I lines ([endnote 96](#)) as potential proxies for locating upward-heating FIP-offset source areas, possibly thanks to similar retardance boosting. [[Back](#)] [[Main call](#)]

96. Optical He I lines

The formation of optical He I lines remains an outstanding enigma. The main ones are He I 10830 Å, weaker He I D₃ at 5876 Å, and He I 6678 Å “occasionally making its appearance” ([Lockyer 1868](#)). He I 10830 Å reaches largest extinction because its lower level is metastable and collects population. Its observed depth is claimed as coronal activity mapper in the optical (e.g., [Fig. 1 \(pdf 3\)](#) of [Penn et al. 1998](#)) – but blinking He I D₃ against AIA EUV in the [IBIS blinker](#) shows better He I matching with chromospheric 304 Å than with coronal 171 Å. The line serves as coronal hole mapper in the McIntosh Archive (e.g., [Webb et al. 2017](#)), perhaps better than coronal activity mapping since the AIA fire detectors ([endnote 82](#)) show less heated quiet chromosphere in holes, hence less He II and He I-top population.

Lockyer proposed element “helios” for He I D₃ which became helium and remains the only extra-terrestrially discovered element since coronium ([\[SSX \(pdf 8\)\]](#)) and nebulium ([\[SSX \(pdf 142\)\] ff](#)) went away. I am not aware of a sound explanation why his He I D₃ is so extraordinary strong off-limb, equal to H α in [his engraved Fig 42 \(pdf 95\)](#) and ranking between H γ and H β in brightness and off-limb extent in [pages 94–95 of Table 3A \(pdf 94\)](#) of [Dunn et al. \(1968\)](#) and in my corresponding [summary plot](#) and [decay plot](#), much brighter and higher than its Na I D neighbors whereas it is nearly invisible on the disk and hence not even mentioned on [page 258 \(pdf 292\)](#) of the line table of [Moore et al. \(1966\)](#) from the Utrecht Atlas of [Minnaert et al. \(1940\)](#) in which the Na I D lines are the darkest in the optical and the Balmer lines are prominent wide dips ([Fig. 10 \(pdf 18\)](#) of [Rutten 2019](#)). Similarly, He I 10830 Å is absent in the ALC7 spectrum [\[SSX \(pdf 94\)\]](#). How can the Balmer lines in the top of the hydrogen atom and the He I lines in the top of the helium atom differ so enormously between transverse and top-down viewing?¹⁴⁶

Off-limb (no continuum) large emissivity can go with small extinction through large εB and/or large ηS^d contributions in [Eq. 4](#). Because He I D₃ shows Balmer-like extent above the limb while the Balmer extent is dominated by quiet-Sun spicules-II and He II 304 Å shows quiet-chromosphere canopies pattern-matching the spicule-II-made reversed-H α ones outside coronal holes ([endnote 84](#)) I speculate that in quiet-Sun around heating ([endnote 94](#)) the He I top shares in the spicule-II emissivity phase giving large εB off-limb brightness, but less in the subsequent recombination phase giving the He I top sufficient NSE extinction to show opaque canopies on the disk with $\sqrt{\varepsilon}$ darkness in H α and with temperature-defined brightness for ALMA. Small top-down extinction in resolved on-disk features can go with large off-limb emissivity from summing many features along the tangential line of sight. The ubiquity of quiet-Sun He II 304 Å canopies over the surface attributed to turbulent sheath ionization in [endnote 84](#)

suggests indeed that very many features are sampled along the line of sight to the limb. The He I top containing the optical lines follows suit in overpopulation.

At more activity the 304 Å–193 Å match for the active plagette in [Fig. 1 \(pdf 2\)](#) of [Rutten and Rouppe van der Voort \(2017\)](#) is attributed to irradiative ionization in [endnote 84](#). The same may hold for the correspondence between He I D₃ absorption and He II 304 Å brightness for active plage in the IBIS–SDO blinker ([endnote 93](#)). [[Back](#)] [[Main call](#)]

97. Ly α dream

Let me dream further re imaging spectroscopy in Ly α ([footnote 98](#); paradise = 5×5 arcmin field, 0.1 arcsec resolution, 20 wavelengths all at 1 s cadence)¹⁴⁷ and compare that with what we know (awake) from SST/CRISP in H α ¹⁴⁸. Co-observing with the Chinese ASO-S/LST (Ly α) and CHASE (H α) space missions may come closest in the near future.

Ly α and H α are both H I α and even share the $n = 2$ level but differ tremendously. Any feature visible in H α has much higher opacity in Ly α that will only show its outer surface. Within hot and dense features as internetwork shocks, dynamic fibrils, spicules-II, EBs and EB-like lower-atmosphere reconnection sites Ly α has fast collision-up rates [\[SSX \(pdf 166\)\]](#) while remaining boxed-in even though being champion resonance scatterer (many random steps but of small length [\[SSX \(pdf 90\)\]](#)). The high radiative 1–2 up and down rates then nearly cancel to net radiative rate zero [\[SSX \(pdf 165\)\]](#), the $n = 2$ level gains near-Boltzmann population, Ly α has $S'_v \approx B_v(T)$ and H α has SB line extinction.

H α does not show such features in its core when they are underneath the opaque H α fibril canopies spreading from network and then samples them only in its outer wings, bright for EBs but Doppler-shifted thermally-broadened dark for spicule-II RBEs and RREs. H α also skips internetwork shocks by its opacity chasm in the upper photosphere ([endnote 60](#), [\[SSX \(pdf 91\)\]](#)).

Ly α does not have such gap so that shifting my narrow dream passband from core to wing means sampling the whole non-coronal atmosphere down to the low (dark) photosphere (first plot of [\[SSX \(pdf 90\)\]](#)).

In addition, Ly α is the worst PRD line in the spectrum (second plot of [\[SSX \(pdf 90\)\]](#)) but this is actually a boon because it gives each part of the line its own source function and response, as in the [\[SSF \(pdf 111\)\]](#) cartoon, and hence specific surface-sampling signature in the dream-resolved emergent profile. At each wavelength the emergent intensity does not sample the LTE source function within hot and dense features but the outer monofrequent $\sqrt{\varepsilon_v}$ scattering decline towards the feature surface. As in [endnote 36](#) the emergent intensity is defined around $\tau_{\text{eff}} = 1$, polarization and Doppler signature around $\tau = 1$. Outer-wing passbands that form in the upper photosphere should be well modelable with MURaM and Bifrost ([endnote 55](#)). [[Back](#)] [[Main call](#)]

98. Ly α features

The Ly α image in [Fig. 2 \(pdf 6\)](#) of [Rutten \(2017b\)](#) is from the VAULT-II flight ([Korendyke et al. 2001](#), [Vourlidas et al. 2010](#), [Patsourakos et al. 2007](#)) and is one of 17 images near disk center. A second sequence of four limb images was assembled by [Koza](#)

¹⁴⁶ History: the 400+ -page book by [Athay and Thomas \(1961\)](#) (wrong order at ADS) addressed this question without clear answer. It was grandly titled “Physics of the solar chromosphere” earning a scathing review from De Jager ([\[SSX \(pdf 15\)\] ff](#)) for not mentioning magnetism nor dynamism. De Jager added that Thomas’ “photoelectric control” producing $S > B$ was the main item of interest but even that was misleading ([endnote 40](#)).

¹⁴⁷ Yet rosier dreaming: add the same in [He I 584 Å \(pdf 11\)](#).

¹⁴⁸ SST/CHROMIS H β at 4861 Å ([pdf 9](#)) may be yet better because it images features sharper ($\sim D/\lambda$) and with less saturation (smaller transition probability, [paragraph 29 \(pdf 80\)](#) of [Allen 1976](#)). Adding less saturated higher Lyman lines enabling intercomparison is also desirable.

et al. (2009) into a [limb movie](#) and a [centerward movie](#). They show dense bright grains in plage and active region of which a few change already during the 51-s movies. [Koza et al. \(2009\)](#) suggested that the latter are Ly α counterparts to H α dynamic fibrils ([endnote 73](#)).

The dense more stable grains seem tips of longer-lived upward heating jets that may also produce the numerous bright grains in non-mossy hearts of network and plage in the [IBIS H \$\alpha\$ core-width scene \(pdf 8\)](#) and contribute the upward chromosphere heating of [endnote 94](#).

Away from the bright-grain plage areas in the Ly α panel of [Fig. 2 \(pdf 6\)](#) the emission blobs are fuzzier and appear remarkably as the short bright bushes extending towards internetwork in the [IBIS display \(pdf 8\)](#), suggesting that they sample similar spicule-II-like roundabout heating onsets.

The dense NSE H α fibril canopies in the lefthand panel of [Fig. 2 \(pdf 6\)](#) of [Rutten \(2017b\)](#) and in the [IBIS H \$\alpha\$ image \(pdf 6\)](#) appear dark not from sampling temperature but from H α 's self-made $\sqrt{\epsilon}$ scattering decline ([\[SSX \(pdf 91\)\]](#), [endnote 71](#)) with large NSE overopacity for cooling recombining hydrogen. These canopies must be yet more opaque in Ly α with $S^I \approx b_2 B(T)$ superthermal internal source function boosting but similarly sampling the monochromatic $\sqrt{\epsilon}$ Ly α declines towards the canopy surface, as suggested by dark quieter areas in [Fig. 2 \(pdf 6\)](#) of [Rutten \(2017b\)](#) where they are not out-radiated by brighter features in profile-summed brightness. The same applies to filaments. [[Back](#)] [[Main call](#)]

99. Rydberg HI candidate for ALMA

There may exist chromospheric features with sufficient Rydberg-ladder ([endnote 72](#)) NLT recombination emissivity for visibility in the HI 30- α line at 231.901 GHz in ALMA band 6 ([Sect. 6 \(pdf 13\)](#) of [Rutten 2017a](#)). Detection would furnish sensitive chromosphere magnetometry.

[Carlsson and Rutten \(1992\)](#) predicted Rydberg lines up to lower level $n = 18$ for the MACKKL star assuming SE. The formation spans between $\tau = 1$ at line center and in the continuum at the bottom of the third panel of [Fig. 1 \(pdf 2\)](#) shift upward with n but remain below the MACKKL temperature minimum. Reasonable reproduction of observed profiles is shown in [Fig. 3 \(pdf 3\)](#) but for higher n - α lines the predicted line strengths exceed corresponding observations in [Fig. 6 \(pdf 5\)](#) of [Clark et al. \(2000a\)](#). Reasonable reproduction with Pandora-star SE line synthesis may be expected for the lower n lines, as for the Mg I 12-micron lines of [endnote 45](#), because the upper photosphere is the domain where Pandora stars come closest to represent a proper mean of actual reality ([endnote 55](#)).

Both the modeling and the higher- n observations (including the limb detection of 21- α by [Clark et al. 2000b](#)) suggested absence of Rydberg lines beyond $n \approx 25$. However, at mm wavelengths the extinction increase (with HI free-free following [Fig. 1 \(pdf 4\)](#) of [Rutten 2017b](#)) causes formation at chromospheric heights where dynamic NSE opacity boosting of the hydrogen top applies, not only for H α and the ALMA continua but also for the high- n Rydberg lines in the ALMA range. Hence, dynamic long-lasting NLT overextinction of the HI top may make 30- α yet higher-formed, at sufficiently low density to bring it out of the reach of collisional ionization lowering, and also stronger. It may be visible. It may be strongest off-limb since also the Balmer lines extend there as far and bright as non-NLT Ca II H & K while weaker on the disk. Strength prediction may be done with NSE Rydberg synthesis from numerical NSE simulations that produce spicules-II as copiously as observed.

Detection of this line enables exciting measurement of profile-resolving Zeeman splitting because it scales $\sim \lambda^2$ while competing Dopplerwidth scales $\sim \lambda$ [[RTSA Eq. 3.66 \(pdf 79\)](#)]¹⁴⁹. Their ratio produces significant intensity-profile signature already at 12 μm for 300–500 Gauss in [Fig. 9 \(pdf 12\)](#) of [Rutten and Carlsson \(1994\)](#); at hundredfold wavelength one Gauss chromospheric sensitivity is in sight. [[Back](#)] [[Main call](#)]

100. Filament blobs

Filaments and prominences may be seen as “*merely local aggregations of a gaseous medium which entirely envelopes the sun*” ([Lockyer 1868](#)) but yet they present the weirdest and toughest features to understand in the rich solar H α zoo. How can cool chromospheric gas show up endlessly in the hot corona in these exceedingly long, slender, high-reaching features exuberantly rich in fine structure and dynamics? Why well visible only in H and He diagnostics? A nightmare for plane-parallel colleagues. Who ordered these?

The [SST/SOUP H \$\alpha\$ movie](#) of [endnote 73](#) shows an active-region filament where small bright bullet-like blobs run intermittently along its length (first panel of [Fig. 1 \(pdf 2\)](#) in the analysis by [Lin et al. 2012](#)). Since then I have noted many such fast disturbances running through filaments in AIA 304 \AA movies, suggesting frequent ionization-recombination cycling. I suspect that they are not disturbances of a mean state but that they actually make and remake filaments continuously with subsequent cooling gas in down-raining condensations causing the extraordinary He I D₃-like off-limb visibility of prominences in H α and He II 304 \AA and that this cannot be modeled assuming static SE.

For H α NLT retardation may cause large cooling-gas overemissivity off-limb and large overextinction on the disk; let me repeat ([Sect. 7](#)) that modest hydrogen ionization in simple internetwork shocks already produces post-shock hydrogen-top retardation reaching 10^{12} H α overopacity (last panel of [Fig 1 movie](#) of [Leenaarts et al. 2007](#)), truly in the “extraordinary” ballpark.

For He II 304 \AA off-limb brightness a likely candidate is sheath heating around rain-down blobs in prominence threads by turbulent Kelvin-Helmholtz coronal cooling as modeled by [Hillier and Arregui \(2019\)](#) ([endnote 84](#)). For He II 304 \AA darkness on disk, as for the active-region filaments in the [blinker 304 \$\text{\AA}\$ image \(pdf 10\)](#), bound-free HI scattering is likely ([endnote 20](#)).

That filaments may reform in place as happened after the exemplary failed Rosetta eruption of [Mason et al. \(2021\)](#) also suggests dynamic refurbishment. [[Back](#)] [[Main call](#)]

¹⁴⁹ Erratum under [[RTSA Eq. 3.66 \(pdf 79\)](#)]: $\text{FWHM} = 2 \sqrt{\ln(2)} \Delta \lambda_{\text{D}} \approx 1.665 \Delta \lambda_{\text{D}}$

References

- Al, N., Bendlin, C., Hirzberger, J., Kneer, F., & Trujillo Bueno, J. 2004 "Dynamics of an enhanced network region observed in H α " 2004A&A...418.1131A ADS
- Allen, C. W. 1976 "Astrophysical Quantities" 1976asqu.book.....A ADS
- Allende Prieto, C. & García López, R. J. 1998 "A catalogue of accurate wavelengths in the optical spectrum of the Sun" 1998A&AS...131.431A ADS
- Anders, E. & Grevesse, N. 1989 "Abundances of the elements: Meteoritic and solar" 1989GeCoA...53..197A ADS
- Ando, H. & Osaki, Y. 1975 "Nonadiabatic nonradial oscillations: an application to the five-minute oscillation of the sun." 1975PASJ...27..581A ADS
- Antolin, P. & Rouppe van der Voort, L. 2012 "Observing the Fine Structure of Loops through High-resolution Spectroscopic Observations of Coronal Rain with the CRISP Instrument at the Swedish Solar Telescope" 2012ApJ...745..152A ADS
- Antolin, P., Vissers, G., Pereira, T. M. D., Rouppe van der Voort, L., & Scullion, E. 2015 "The Multithermal and Multi-stranded Nature of Coronal Rain" 2015ApJ...806...81A ADS
- Asplund, M., Grevesse, N., Sauval, A. J., & Scott, P. 2009 "The Chemical Composition of the Sun" 2009ARA&A...47..481A ADS
- Athay, R. G., Low, B. C., & White, O. R. 2008 "The Solar Interior-Atmospheric System" 2008ASPC...383..315A ADS
- Athay, R. G. & Skumanich, A. 1967 "Broadening of H and K Emission Cores and the Wilson-Bappu Effect." 1967AJ....72..784A ADS
- Athay, R. G. & Thomas, R. N. 1961 "Physics of the solar chromosphere" 1961psc.book.....A ADS
- Auer, L. H. & Mihalas, D. 1969a "Non-Lte Model Atmospheres. I. Radiative Equilibrium Models with - Alpha" 1969ApJ...156..157A ADS
- Auer, L. H. & Mihalas, D. 1969b "Non-Lte Model Atmospheres. II. Effects of Balmer α " 1969ApJ...156..681A ADS
- Avrett, E., Tian, H., Landi, E., Curdt, W., & Wülser, J. P. 2015 "Modeling the Chromosphere of a Sunspot and the Quiet Sun" 2015ApJ...811...87A ADS
- Avrett, E. H. 1965 "Solutions of the Two-Level Line Transfer Problem with Complete Redistribution" 1965SAOSR.174..101A ADS
- Avrett, E. H. 1985 "Recent thermal models of the chromosphere." 1985cdm...proc...67A ADS
- Avrett, E. H. 1990 "Models of the Solar Outer Photosphere" 1990IAUS...138...3A ADS
- Avrett, E. H., Kurucz, R. L., & Loeser, R. 1984 "New Models of the Solar Temperature Minimum Region and Low Chromosphere" 1984BAAS...16..450A ADS
- Avrett, E. H. & Loeser, R. 1992 "The PANDORA Atmosphere Program (Invited Review)" 1992ASPC...26..489A ADS
- Avrett, E. H. & Loeser, R. 2008 "Models of the Solar Chromosphere and Transition Region from SUMER and HRTS Observations: Formation of the Extreme-Ultraviolet Spectrum of Hydrogen, Carbon, and Oxygen" 2008ApJS...175..229A ADS (ALC7)
- Ayres, T. R. 1979 "Chromospheric scaling laws, width-luminosity correlations, and the Wilson-Bappu effect." 1979ApJ...228..509A ADS
- Ayres, T. R. 1989 "How deep can one see into the Sun?" 1989SoPh...124...15A ADS
- Ayres, T. R. 2021 "In the Trenches of the Solar-Stellar Connection. III. The HST/COS Ecliptic-poles Stellar Survey (EclipsS)" 2021ApJ...910...71A ADS
- Bahcall, J. 1999 "Ulrich's Explanation for the Solar Five Minute Oscillations" 1999ApJ...525C1199B ADS
- Barklem, P. S., Piskunov, N., & O'Mara, B. J. 2000 "VizieR Online Data Catalog: Broadening of metallic lines by H collisions (Barklem+ 2000)" 2000yCat..41420467B ADS
- Baschek, B., Holweger, H., & Traving, G. 1966 "Ein ALGOL-Programm für die quantitative Analyse von Sternspektrern" 1966AAHam...8...26B ADS
- Bashkin, S. & Stoner, J. O. 1975 "Atomic energy levels and Grotrian Diagrams - Vol.1: Hydrogen I - Phosphorus XV; Vol.2: Sulfur I - Titanium XXII" 1975aalg.book.....B ADS
- Bashkin, S. & Stoner, J. O. 1978 "Atomic energy levels and Grotrian Diagrams. Addenda: Hydrogen I - Phosphorus XV" 1978aalg.book.....B ADS
- Bashkin, S. & Stoner, J. O. 1981 "Atomic energy levels and Grotrian Diagrams. Vol.3: Vanadium I - Chromium XXIV" 1981aalg.book.....B ADS
- Bashkin, S. & Stoner, J. O. 1982 "Atomic energy levels and Grotrian Diagrams. Vol.4: Manganese I-XXV" 1982aalg.book.....B ADS
- Beck, C., Bellot Rubio, L. R., Schlichenmaier, R., & Sütterlin, P. 2007 "Magnetic properties of G-band bright points in a sunspot moi" 2007A&A...472..607B ADS
- Beckers, J. M. 1964 "A Study of the Fine Structures in the Solar Chromosphere" 1964PhDT.....83B ADS
- Beckers, J. M. 1968 "Solar Spicules (Invited Review Paper)" 1968SoPh...3..367B ADS
- Beckers, J. M., Bridges, C. A., & Gilliam, L. B. 1976 "High resolution spectral atlas of the solar irradiance from 380 to 700 nanometers" 1976hrsa.book.....B ADS
- Beckers, J. M. & Milkey, R. W. 1975 "The Line Response Function of Stellar Atmospheres and the Effective Depth of Line Formation" 1975SoPh...43..289B ADS
- Bel, N. & Leroy, B. 1977 "Analytical Study of Magnetoacoustic Gravity Waves" 1977A&A...55..239B ADS
- Bell, R. A., Eriksson, K., Gustafsson, B., & Nordlund, A. 1976 "A grid of model atmospheres for metal-deficient giant stars. II." 1976A&AS...23...37B ADS
- Belluzzi, L., Trujillo Bueno, J., & Landi Degl'Innocenti, E. 2007 "The Magnetic Sensitivity of the Ba II D1 and D2 Lines of the Fraunhofer Spectrum" 2007ApJ...666..588B ADS
- Berger, T. E., de Pontieu, B., Fletcher, L., et al. 1999a "What is Moss?" 1999SoPh...190..409B ADS
- Berger, T. E., De Pontieu, B., Schrijver, C. J., & Title, A. M. 1999b "High-resolution Imaging of the Solar Chromosphere/Corona Transition Region" 1999ApJ...519L..97B ADS
- Berger, T. E., Rouppe van der Voort, L. H. M., Löfdahl, M. G., et al. 2004 "Solar magnetic elements at 0.1 arcsec resolution. General appearance and magnetic structure" 2004A&A...428..613B ADS
- Blamont, J. E. & Roddier, F. 1961 "Precise Observation of the Profile of the Fraunhofer Strontium Resonance Line. Evidence for the Gravitational Red Shift on the Sun" 1961PhRvL...7..437B ADS
- Böhm-Vitense, E. 1989 "Introduction to stellar astrophysics. Vol. 2. Stellar atmospheres." 1989isa2.book.....B ADS
- Bonnet, R. M. 1996 "C. de Jager, Europe, Space, and the Sun" 1996SoPh...169..233B ADS
- Bose, S., Henriques, V. M. J., Joshi, J., & Rouppe van der Voort, L. 2019 "Characterization and formation of on-disk spicules in the Ca II K and Mg II k spectral lines" 2019A&A...631L...5B ADS
- Bose, S., Joshi, J., Henriques, V. M. J., & Rouppe van der Voort, L. 2021a "Spicules and downflows in the solar chromosphere" 2021A&A...647A..147B ADS
- Bose, S., Rouppe van der Voort, L., Joshi, J., et al. 2021b "Evidence of the multi-thermal nature of spicular downflows. Impact on solar atmospheric heating" 2021A&A...654A..51B ADS
- Bostanci, Z. F. & Al Erdogan, N. 2010 "Cloud modeling of a quiet solar region in Halpha." 2010MmSAI...81..769B ADS
- Brajša, R., Skokić, I., Sudar, D., et al. 2021 "ALMA small-scale features in the quiet Sun and active regions" 2021A&A...651A...6B ADS
- Brandt, P. N., Rutten, R. J., Shine, R. A., & Trujillo Bueno, J. 1994 "On photospheric flows and chromospheric corks" 1994ASIC.433..251B ADS
- Brault, J. & Noyes, R. 1983 "Solar emission lines near 12 microns" 1983ApJ...269L..61B ADS
- Bruls, J. H. M. J. 1992 "Formation of diagnostic lines in the solar spectrum" 1992Bruls..PhDthesis
- Bruls, J. H. M. J., Rutten, R. J., & Shchukina, N. G. 1992 "The formation of helioseismology lines. I. NLTE effects in alkali spectra." 1992A&A...265..237B ADS
- Büntje, M., Solanki, S. K., & Steiner, O. 1993 "Centre-to-limb variation of the Stokes V asymmetry in solar magnetic flux tubes" 1993A&A...268..736B ADS
- Burgess, A. 1964 "Delectronic Recombination and the Temperature of the Solar Corona." 1964ApJ...139..776B ADS
- Canfield, R. C. 1971a "Deviations from Local Thermodynamic Equilibrium in Weak Complex Spectra" 1971A&A...10...54C ADS
- Canfield, R. C. 1971b "Formation of Solar Rare-Earth Lines inside and outside H and K" 1971A&A...10...64C ADS
- Canfield, R. C. & Cram, L. E. 1977 "Analysis of the solar magnesium I spectrum. II. Sensitivity of lambda 2852 to partial redistribution effects." 1977ApJ...216..654C ADS
- Cannon, C. J. 1973 "Frequency-Quadrature Perturbations in Radiative-Transfer Theory" 1973ApJ...185..621C ADS
- Carlsson, M. 1986 "A computer program for solving multi-level non-LTE radiative transfer problems in moving or static atmospheres." 1986UppOR...33.....C ADS
- Carlsson, M., De Pontieu, B., & Hansteen, V. H. 2019 "New View of the Solar Chromosphere" 2019ARA&A...57..189C ADS
- Carlsson, M., Hansteen, V. H., Gudiksen, B. V., Leenaarts, J., & De Pontieu, B. 2016 "A publicly available simulation of an enhanced network region of the Sun" 2016A&A...585A...4C ADS
- Carlsson, M. & Rutten, R. J. 1992 "Solar hydrogen lines in the infrared" 1992A&A...259L..53C ADS
- Carlsson, M., Rutten, R. J., Bruls, J. H. M. J., & Shchukina, N. G. 1994 "The non-LTE formation of Li I lines in cool stars" 1994A&A...288..860C ADS
- Carlsson, M., Rutten, R. J., & Shchukina, N. G. 1992 "The formation of the MG I emission features near 12 microns" 1992A&A...253..567C ADS

- Carlsson, M. & Stein, R. F. 1994 “Radiation shock dynamics in the solar chromosphere - results of numerical simulations” 1994chdy.conf...47C ADS
- Carlsson, M. & Stein, R. F. 1995 “Does a Nonmagnetic Solar Chromosphere Exist?” 1995ApJ...440L..29C ADS
- Carlsson, M. & Stein, R. F. 1997 “Formation of Solar Calcium H and K Bright Grains” 1997ApJ...481..500C ADS
- Carlsson, M. & Stein, R. F. 2002 “Dynamic Hydrogen Ionization” 2002ApJ...572..626C ADS
- Carlsson, M., Stein, R. F., Nordlund, Å., & Scharmer, G. B. 2004 “Observational Manifestations of Solar Magnetocvection: Center-to-Limb Variation” 2004ApJ...610L.137C ADS
- Carlyle, J., Williams, D. R., van Driel-Gesztelyi, L., et al. 2014 “Investigating the Dynamics and Density Evolution of Returning Plasma Blobs from the 2011 June 7 Eruption” 2014ApJ...782...87C ADS
- Castor, J. I. 2007 “Radiation Hydrodynamics” 2007rahy.book.....C ADS
- Cauzzi, G. & Reardon, K. 2012 “The IBIS Mosaic” 2012IAUSS...6E.511C ADS
- Cauzzi, G., Reardon, K., Rutten, R. J., Tritschler, A., & Uitenbroek, H. 2009 “The solar chromosphere at high resolution with IBIS. IV. Dual-line evidence of heating in chromospheric network” 2009A&A...503..577C ADS
- Cayrel, R. & Steinberg, M. (Eds.) 1976 “Physique des Mouvements dans les Atmospheres Stellaires” 1976pmas.conf.....C ADS
- Chae, J. 2014 “Spectral Inversion of the H α Line for a Plasma Feature in the Upper Chromosphere of the Quiet Sun” 2014ApJ...780..109C ADS
- Chalonge, D. & Kourganoff, V. 1946 “Recherches sur le spectre continu du Soleil. I: L'ion négatif hydrogène dans la photosphère solaire” 1946AnAp...9...69C ADS
- Chandrasekhar, S. & Breen, F. H. 1946 “On the Continuous Absorption Coefficient of the Negative Hydrogen Ion. III.” 1946ApJ...104..430C ADS
- Chang, E. S. & Noyes, R. W. 1983 “Identification of the solar emission lines near 12 microns” 1983ApJ...275L..11C ADS
- Cheung, M. C. M., Boerner, P., Schrijver, C. J., et al. 2015 “Thermal Diagnostics with the Atmospheric Imaging Assembly on board the Solar Dynamics Observatory: A Validated Method for Differential Emission Measure Inversions” 2015ApJ...807..143C ADS
- Christensen-Dalsgaard, J. 2021 “Solar structure and evolution” 2021LRSP...18...2C ADS
- Cimino, M., Cacciani, A., & Soprani, N. 1968 “An Instrument to measure Solar Magnetic Fields by an Atomic-Beam Method” 1968SoPh...3..618C ADS
- Clark, T. A., Naylor, D. A., & Davis, G. R. 2000a “Detection and limb brightening of the H β $n=20-19$ Rydberg line in the submillimetre spectrum of the Sun” 2000A&A...357..757C ADS
- Clark, T. A., Naylor, D. A., & Davis, G. R. 2000b “Detection of the H I $n=22-21$ Rydberg line in emission at the solar submillimetre limb” 2000A&A...361L..60C ADS
- Cook, J. W., Cheng, C. C., Jacobs, V. L., & Antiochos, S. K. 1989 “Effect of Coronal Elemental Abundances on the Radiative Loss Function” 1989ApJ...338.1176C ADS
- Cram, L. E. & Damé, L. 1983 “High spatial and temporal resolution observations of the solar CA II H line” 1983ApJ...272..355C ADS
- Cram, L. E., Rutten, R. J., & Lites, B. W. 1980 “On the formation of Fe II lines in stellar spectra. I - Solar spatial intensity variation of λ 3969.4” 1980ApJ...241..374C ADS
- Curdt, W., Brekke, P., Feldman, U., et al. 2001 “The SUMER spectral atlas of solar-disk features” 2001A&A...375..591C ADS
- da Silva Santos, J. M., de la Cruz Rodríguez, J., White, S. M., et al. 2020 “ALMA observations of transient heating in a solar active region” 2020A&A...643A..41D ADS
- Danilovic, S. 2017 “Simulating Ellerman bomb-like events” 2017A&A...601A.122D ADS
- de Boer, T., Busse, R., Kappes, A., Klasen, M., & Zeinstra, S. 2021 “Neutrino constraints to scotogenic dark matter interacting in the Sun” 2021arXiv210505613D ADS
- de Jager, C. 1952 “The hydrogen spectrum of the sun” 1952RAOU...1.....D ADS
- de Jager, C. 1957 “The interpretation of hydrogen spectroheliograms” 1957BAN...13..133D ADS
- de Jager, C. 1963 “The temperature minimum in the upper solar photosphere” 1963BAN...17..209D ADS
- De Jager, C. (Ed.) 1965 “The solar spectrum” 1965ASSL...1.....D ADS
- De Jager, C. (Ed.) 1967 “The structure of the quiet photosphere and the low chromosphere” 1967sqpl.conf.....D ADS
- de Pontieu, B., Berger, T. E., Schrijver, C. J., & Title, A. M. 1999 “Dynamics of Transition Region ‘Moss’ at high time resolution” 1999SoPh...190..419D ADS
- De Pontieu, B., Carlsson, M., Rouppe van der Voort, L. H. M., et al. 2012 “Ubiquitous torsional motions in type-II spicules” 2012ApJ...752L..12D ADS
- De Pontieu, B., Hansteen, V. H., Rouppe van der Voort, L., van Noort, M., & Carlsson, M. 2007 “High-Resolution Observations and Modeling of Dynamic Fibrils” 2007ApJ...655..624D ADS
- de Pontieu, B., McIntosh, S., Hansteen, V. H., et al. 2007 “A Tale of Two Spicules: The Impact of Spicules on the Magnetic Chromosphere” 2007PASJ...59S.655D ADS
- De Pontieu, B., McIntosh, S. W., Carlsson, M., et al. 2007 “Chromospheric Alfvénic Waves Strong Enough to Power the Solar Wind” 2007Sci...318.1574D ADS
- De Pontieu, B., Tarbell, T., & Erdélyi, R. 2003 “Correlations on Arcsecond Scales between Chromospheric and Transition Region Emission in Active Regions” 2003ApJ...590..502D ADS
- De Wijn, A. G., De Pontieu, B., & Rutten, R. J. 2007 “Fourier Analysis of Active-Region Plage” 2007ApJ...654.1128D ADS
- del Toro Iniesta, J. C. 2007 “Introduction to Spectropolarimetry” 2007insp.book.....D ADS
- Del Zanna, G. & Mason, H. E. 2018 “Solar UV and X-ray spectral diagnostics” 2018LRSP...15....5D ADS
- Delbouille, L., Roland, G., & Neven, L. 1973 “Atlas photométrique du spectre solaire de $[\lambda]$ 3000 à $[\lambda]$ 10000” 1973apds.book.....D ADS
- Dere, K. P. 2007 “Ionization rate coefficients for the elements hydrogen through zinc” 2007A&A...466..771D ADS
- Deubner, F.-L. 1972 “Some Properties of Velocity Fields in the Solar Photosphere. IV: Long Periods, Five Minute Oscillations, and the Supergranulation at Lower Layers” 1972SoPh...22..263D ADS
- Deubner, F. L. 1975 “Observations of low wavenumber nonradial eigenmodes of the sun.” 1975A&A...44..371D ADS
- Deubner, F. L. & McIntyre, J. 1976 “Observations of low wavenumber non radial eigenmodes of the sun” 1976pmas.conf...259D ADS
- Doyle, J. G., Jevremović, D., Short, C. I., et al. 2001 “Solar Mn I 5432/5395 Å line formation explained” 2001A&A...369L..13D ADS
- Duncan, D. K., Vaughan, A. H., Wilson, O. C., et al. 1991 “CA II H and K Measurements Made at Mount Wilson Observatory, 1966–1983” 1991ApJS...76..383D ADS
- Dunn, R. B., Evans, J. W., Jefferies, J. T., et al. 1968 “The Chromospheric Spectrum at the 1962 Eclipse” 1968ApJS...15..275D ADS
- Eberhard, G. & Schwarzschild, K. 1913 “On the reversal of the calcium lines H and K in stellar spectra.” 1913ApJ...38..292E ADS
- Eddington, A. S. 1929 “The formation of absorption lines” 1929MNRAS...89..620E ADS
- Eklund, H., Wedemeyer, S., Snow, B., et al. 2021 “Characterization of shock wave signatures at millimetre wavelengths from Bifrost simulations” 2021RSPTA.37900185E ADS
- Ellerman, F. 1917 “Solar Hydrogen ‘bombs’” 1917ApJ...46..298E ADS
- Falconer, D. A., Moore, R. L., Porter, J. G., & Hathaway, D. H. 1998 “Network Coronal Bright Points: Coronal Heating Concentrations Found in the Solar Magnetic Network” 1998ApJ...501..386F ADS
- Feautrier, P. 1964 “Sur la résolution numérique de l'équation de transfert.” 1964CR...258.3189F ADS
- Fletcher, A. C., Dimant, Y. S., Oppenheim, M. M., & Fontenla, J. M. 2018 “Effects of Ion Magnetization on the Farley-Buneman Instability in the Solar Chromosphere” 2018ApJ...857..129F ADS
- Fokker, A. D. & Rutten, R. J. 1967 “Coronal scattering of radiation from an anisotropically radiating solar radio source.” 1967BAN...19..254F ADS
- Fontenla, J. M. 2005 “Chromospheric plasma and the Farley-Buneman instability in solar magnetic regions” 2005A&A...442.1099F ADS
- Fontenla, J. M., Avrett, E. H., & Loesser, R. 1993 “Energy Balance in the Solar Transition Region. III. Helium Emission in Hydrostatic, Constant-Abundance Models with Diffusion” 1993ApJ...406..319F ADS (FAL)
- Fontenla, J. M., Balasubramaniam, K. S., & Harder, J. 2007 “Semiempirical Models of the Solar Atmosphere. II. The Quiet-Sun Low Chromosphere at Moderate Resolution” 2007ApJ...667.1243F ADS
- Fontenla, J. M., Curdt, W., Haberiter, M., Harder, J., & Tian, H. 2009 “Semiempirical Models of the Solar Atmosphere. III. Set of Non-LTE Models for Far-Ultraviolet/Extreme-Ultraviolet Irradiance Computation” 2009ApJ...707..482F ADS
- Fontenla, J. M., Peterson, W. K., & Harder, J. 2008 “Chromospheric heating by the Farley-Buneman instability” 2008A&A...480..839F ADS
- Fontenla, J. M., Stancil, P. C., & Landi, E. 2015 “Solar Spectral Irradiance, Solar Activity, and the Near-Ultra-Violet” 2015ApJ...809..157F ADS
- Fossum, A. & Carlsson, M. 2005a “High-frequency acoustic waves are not sufficient to heat the solar chromosphere” 2005Natur.435..919F ADS
- Fossum, A. & Carlsson, M. 2005b “Response Functions of the Ultraviolet Filters of TRACE and the Detectability of High-Frequency Acoustic Waves” 2005ApJ...625..556F ADS
- Frogner, L., Gudiksen, B. V., & Bakke, H. 2020 “Accelerated particle beams in a 3D simulation of the quiet Sun” 2020A&A...643A..27F ADS
- Froment, C., Antolin, P., Henriques, V. M. J., Kohutova, P., & Rouppe van der Voort, L. H. M. 2020 “Multi-scale observations of thermal non-equilibrium cycles in coronal loops” 2020A&A...633A..11F ADS
- Gary, D. E. & Hurford, G. J. 2004 “Radio Spectral Diagnostics” 2004ASSL...314...71G ADS

- Gingerich, O. & de Jager, C. 1968 “The Bilderberg Model of the Photosphere and Low Chromosphere” 1968SoPh...3...5G ADS
- Gingerich, O., Noyes, R. W., Kalkofen, W., & Cuny, Y. 1971 “The Harvard-Smithsonian reference atmosphere” 1971SoPh...18...347G ADS
- Giovannelli, R. G. 1967 “Excitation of hydrogen and CaII under chromospheric conditions” 1967AuJPh...20...81G ADS
- Giovannelli, R. G. & Jones, H. P. 1982 “The Three-Dimensional Structure of Atmospheric Magnetic Fields in Two Active Regions” 1982SoPh...79...267G ADS
- Gogoberidze, G., Voitenko, Y., Poedts, S., & Goossens, M. 2009 “Farley-Buneman Instability in the Solar Chromosphere” 2009ApJ...706L...12G ADS
- Goldberg, L. 1964 “The Origin of the Emission Reversals in the Fraunhofer h- and K-Lines” 1964ApJ...140...384G ADS
- Goldberg, L. & Noyes, R. W. 1964 “Origin of Emission Cores in Lines of Ionized Calcium and Magnesium.” 1964AJ...69R.542G ADS
- Golding, T. P., Leenaarts, J., & Carlsson, M. 2017 “Formation of the helium extreme-UV resonance lines” 2017A&A...597A.102G ADS
- Goldman, A., Blatherwick, R. D., Murcray, F. H., et al. 1980 *New atlas of IR solar spectra* 1980STIN...8031298G ADS
- Goldreich, P. 1999 “Discovery of Solar Atmospheric Motions” 1999ApJ...525C.962G ADS
- Gomez, M. T., Severino, G., & Rutten, R. J. 1991 “Photospheric dynamics and the NLTE formation of the solar K I 769.9 NM line” 1991A&A...244...501G ADS
- Gošić, M., Bellot Rubio, L. R., Orozco Suárez, D., Katsukawa, Y., & del Toro Iniesta, J. C. 2014 “The Solar Internetwork. I. Contribution to the Network Magnetic Flux” 2014ApJ...797...49G ADS
- Gray, D. F. 1977 “A test of the micro-macroturbulence model on the solar flux spectrum.” 1977ApJ...218...530G ADS
- Gray, D. F. 1992 “The Observation and Analysis of Stellar Photospheres.” 1992oasp.book....G ADS
- Gray, D. F. 2005 “The Observation and Analysis of Stellar Photospheres” 2005oasp.book....G ADS
- Greve, A. & Zwaan, C. 1980 “Methods for the analysis of stellar spectra veiled by lines (III).” 1980A&A...90...239G ADS
- Grevesse, N., Noels, A., & Sauval, A. J. 1996 “Standard Abundances” 1996ASPC...99...117G ADS
- Grevesse, N. & Sauval, A. J. 1998 “Standard Solar Composition” 1998SSRv...85...161G ADS
- Grottrian, W. 1928 “Graphische Darstellung der Spektren von Atomen und Ionen mit ein, zwei und drei Valenzelektronen” Grottrian1928diagrams URL
- Grottrian, W. 1931 “Ergebnisse der Potsdamer Expedition zur Beobachtung der Sonnenfinsternis am 9. Mai 1929 in Takengon (Nordsumatra). 6. Mitteilung. Über die Intensitätsverteilung des kontinuierlichen Spektrums der inneren Korona. Mit 8 Abbildungen. (Eingegangen am 27. Juni 1931)” 1931ZA...3...199G ADS
- Gudiksen, B. V., Carlsson, M., Hansteen, V. H., et al. 2011 “The stellar atmosphere simulation code Bifrost. Code description and validation” 2011A&A...531A.154G ADS
- Gurtovenko, E., Ratnikova, V., & de Jager, C. 1974 “On the Average Optical Depth of Formation of Weak Fraunhofer Lines” 1974SoPh...37...43G ADS
- Hammerschlag, R. H., von der Lühse, O. F., Bettonvil, F. C., Jägers, A. P., & Snik, F. 2004 “GISOT: a giant solar telescope” 2004SPIE.5489...491H ADS
- Hansteen, V., Ortiz, A., Archontis, V., et al. 2019 “Ellerman bombs and UV bursts: transient events in chromospheric current sheets” 2019A&A...626A...33H ADS
- Hansteen, V. H., Archontis, V., Pereira, T. M. D., et al. 2017 “Bombs and Flares at the Surface and Lower Atmosphere of the Sun” 2017ApJ...839...22H ADS
- Hansteen, V. H., De Pontieu, B., Rouppe van der Voort, L., van Noort, M., & Carlsson, M. 2006 “Dynamic Fibrils Are Driven by Magnetoacoustic Shocks” 2006ApJ...647L...73H ADS
- Harvey, K. L. & Martin, S. F. 1973 “Ephemeral Active Regions” 1973SoPh...32...389H ADS
- Heeck, J. 2013 “How Stable is the Photon?” 2013PhRvL.111b1801H ADS
- Hegglund, L., De Pontieu, B., & Hansteen, V. H. 2007 “Numerical Simulations of Shock Wave-driven Chromospheric Jets” 2007ApJ...666.1277H ADS
- Heinzel, P., Gunár, S., & Anzer, U. 2015 “Fast approximate radiative transfer method for visualizing the fine structure of prominences in the hydrogen H α line” 2015A&A...579A...16H ADS
- Heinzel, P., Mein, N., & Mein, P. 1999 “Cloud model with variable source function for solar H α structures. II. Dynamical models” 1999A&A...346...322H ADS
- Henriques, V. M. J., Kuridze, D., Mathioudakis, M., & Keenan, F. P. 2016 “Quiet-Sun H α Transients and Corresponding Small-scale Transition Region and Coronal Heating” 2016ApJ...820...124H ADS
- Hillier, A. & Aregui, I. 2019 “Coronal Cooling as a Result of Mixing by the Nonlinear Kelvin-Helmholtz Instability” 2019ApJ...885...101H ADS
- Hines, C. O. 1960 “Internal atmospheric gravity waves at ionospheric heights” 1960CaJPh...38.1441H ADS
- Holweger, H. 1967 “Ein empirisches Modell der Sonnenatmosphäre mit lokalem thermodynamischem Gleichgewicht” 1967ZA...65...365H ADS
- Holweger, H. & Müller, E. A. 1974 “The Photospheric Barium Spectrum: Solar Abundance and Collision Broadening of Ba II Lines by Hydrogen” 1974SoPh...39...19H ADS (HOLMUL)
- House, L. L. 1964 “Ionization Equilibrium of the Elements from H to Fe.” 1964ApJS...8...307H ADS
- Houtgast, J. 1942 “The variations in the profiles of strong Fraunhofer lines along a radius of the solar disc” 1942PhDT.....12H ADS
- Hubeny, I. 1987a “Probabilistic Interpretation of Radiative Transfer - Part Two - Rybicki Equation” 1987A&A...185...336H ADS
- Hubeny, I. 1987b “Probabilistic interpretation of radiative transfer: I - The square root of epsilon law. II - Rybicki equation” 1987A&A...185...332H ADS
- Hubeny, I. & Mihalas, D. 2014 “Theory of Stellar Atmospheres” 2014tsa..book....H ADS
- Hummer, D. G. 1962 “Non-coherent scattering: I. The redistribution function with Doppler broadening” 1962MNRAS.125...21H ADS
- Ishikawa, R., Bueno, J. T., del Pino Alemán, T., et al. 2021 “Mapping solar magnetic fields from the photosphere to the base of the corona” 2021SciA...7.8406I ADS
- Jafarzadeh, S., Rutten, R. J., Solanki, S. K., et al. 2017 “Slender Ca II H Fibrils Mapping Magnetic Fields in the Low Solar Chromosphere” 2017ApJS...229...11J ADS
- Jafarzadeh, S., Wedemeyer, S., Fleck, B., et al. 2021 “An overall view of temperature oscillations in the solar chromosphere with ALMA” 2021RSP TA.37900174J ADS
- Jefferies, J. T. 1968 “Spectral line formation” 1968sf..book....J ADS
- Jefferies, J. T. & Thomas, R. N. 1959 “Source Function in a Non-Equilibrium Atmosphere. III. The Influence of a Chromosphere.” 1959ApJ...129...401J ADS
- Jejčić, S. & Heinzel, P. 2009 “Electron Densities in Quiescent Prominences Derived from Eclipse Observations” 2009SoPh...254...89J ADS
- Jordan, C. 1969 “The ionization equilibrium of elements between carbon and nickel” 1969MNRAS.142...501J ADS
- Jordan, S. D. 1996 “Obituary: Richard Nelson Thomas, 1921-1996” 1996BAAS...28.1465J ADS
- Joshi, J., Rouppe van der Voort, L. H. M., & de la Cruz Rodríguez, J. 2020 “Signatures of ubiquitous magnetic reconnection in the lower solar atmosphere” 2020A&A...641L...5J ADS
- Kato, Y., Steiner, O., Steffen, M., & Suematsu, Y. 2011 “Excitation of Slow Modes in Network Magnetic Elements Through Magnetic Pumping” 2011ApJ...730L...24K ADS
- Keller, C. U. 1994 “Speckle techniques for spectroscopic observations” 1994ASIC...433...43K ADS
- Keller, C. U. & von der Lühse, O. 1992 “Solar speckle polarimetry” 1992A&A...261...321K ADS
- Khomenko, E., Collados, M., Vitas, N., & González-Morales, P. A. 2021 “Influence of ambipolar and Hall effects on vorticity in three-dimensional simulations of magneto-convection” 2021RSP TA.37900176K ADS
- Korendyke, C. M., Vourlidas, A., Cook, J. W., et al. 2001 “High-resolution Imaging of the Upper Solar Chromosphere: First Light Performance of the Very-high-Resolution Advanced Ultraviolet Telescope” 2001SoPh...200...63K ADS
- Kostik, R., Khomenko, E., & Shchukina, N. 2009 “Solar granulation from photosphere to low chromosphere observed in Ba II 4554 Å line” 2009A&A...506.1405K ADS
- Kostik, R. I. & Orlova, T. V. 1975 “On the Possible Mechanism of Formation of Emission Rim in Hydrogen Filaments” 1975SoPh...45...119K ADS
- Kostik, R. I., Shchukina, N. G., & Rutten, R. J. 1996 “The solar iron abundance: not the last word.” 1996A&A...305...325K ADS
- Kourganoff, V. 1952 “Basic methods in transfer problems; radiative equilibrium and neutron diffusion” 1952bmtp.book....K ADS
- Koza, J., Rutten, R. J., & Vourlidas, A. 2009 “Dynamic Ly α jets” 2009A&A...499...917K ADS
- Krijger, J. M., Rutten, R. J., Lites, B. W., et al. 2001 “Dynamics of the solar chromosphere. III. Ultraviolet brightness oscillations from TRACE” 2001A&A...379.1052K ADS
- Kurucz, R. L. 2009 “Including All the Lines” 2009AIPC.1171...43K ADS
- Labs, D. & Neckel, H. 1972 “Remarks on the Convergence of Photospheric Model Conceptions and the Solar Quasi Continuum” 1972SoPh...22...64L ADS
- Lambert, J., Paletou, F., Josselin, E., & Glorian, J.-M. 2016 “Numerical radiative transfer with state-of-the-art iterative methods made easy” 2016EJPh...37a5603L ADS
- Laming, J. M., Vourlidas, A., Korendyke, C., et al. 2019 “Element Abundances: A New Diagnostic for the Solar Wind” 2019ApJ...879...124L ADS

- Lamy, P. L., Nguyen-Trong, T., Adjabschirzadeh, A., & Koutchmy, S. 1979 “Astronomical applications of infrared television imaging.” 1979A&A...77..257L ADS
- Landi Degl’Innocenti, E. & Landolfi, M. 2004 “Polarization in Spectral Lines” 2004ASSL...307.....L ADS
- Leenaarts, J. 2020 “Radiation hydrodynamics in simulations of the solar atmosphere” 2020LRSP...17....3L ADS
- Leenaarts, J. & Carlsson, M. 2009 “MULTI3D: A Domain-Decomposed 3D Radiative Transfer Code” 2009ASPC...415...87L ADS
- Leenaarts, J., Carlsson, M., Hansteen, V., & Rutten, R. J. 2007 “Nonequilibrium hydrogen ionization in 2D simulations of the solar atmosphere” 2007A&A...473..625L ADS
- Leenaarts, J., Carlsson, M., & Rouppe van der Voort, L. 2012a “The Formation of the H α Line in the Solar Chromosphere” 2012ApJ...749..136L ADS
- Leenaarts, J., Carlsson, M., & Rouppe van der Voort, L. 2015 “On Fibrils and Field Lines: the Nature of H α Fibrils in the Solar Chromosphere” 2015ApJ...802..136L ADS
- Leenaarts, J., Pereira, T., & Uitenbroek, H. 2012b “Fast approximation of angle-dependent partial redistribution in moving atmospheres” 2012A&A...543A.109L ADS
- Leenaarts, J., Rutten, R. J., Carlsson, M., & Uitenbroek, H. 2006a “A comparison of solar proxy-magnetometry diagnostics” 2006A&A...452L..15L ADS
- Leenaarts, J., Rutten, R. J., Reardon, K., Carlsson, M., & Hansteen, V. 2010 “The Quiet Solar Atmosphere Observed and Simulated in Na I D1” 2010ApJ...709.1362L ADS
- Leenaarts, J., Rutten, R. J., Sütterlin, P., Carlsson, M., & Uitenbroek, H. 2006b “DOT tomography of the solar atmosphere. VI. Magnetic elements as bright points in the blue wing of H α ” 2006A&A...449.1209L ADS
- Leibacher, J. W. & Stein, R. F. 1971 “A New Description of the Solar Five-Minute Oscillation” 1971ApL...7..191L ADS
- Leighton, R. B., Noyes, R. W., & Simon, G. W. 1962 “Velocity Fields in the Solar Atmosphere. I. Preliminary Report.” 1962ApJ...135..474L ADS
- Lenke, M. & Holweger, H. 1987 “A non-LTE study of the solar emission lines near 12 microns” 1987A&A...173..375L ADS
- Lewis, G. N. 1926 “The Conservation of Photons” 1926Natur...118..874L ADS
- Lighthill, M. J. 1967 “Predictions on the Velocity Field Coming from Acoustic Noise and a Generalized Turbulence in a Layer Overlying a Convectively Unstable Atmospheric Region” 1967IAUS...28..429L ADS
- Lin, Y., Engvold, O., & Rouppe van der Voort, L. H. M. 2012 “Small-scale, Dynamic Bright Blobs in Solar Filaments and Active Regions” 2012ApJ...747..129L ADS
- Linsky, J. L. & Avrett, E. H. 1970 “The Solar H and K Lines” 1970PASP...82..169L ADS
- 1985 “Chromospheric Diagnostics and Modelling” 1985cdm...proc....L ADS
- Lites, B. W. 1972 “Observation and Analysis of the Solar Neutral Iron Spectrum.” 1972PhDT.....7L ADS
- Lites, B. W., Kubo, M., Socas-Navarro, H., et al. 2008 “The Horizontal Magnetic Flux of the Quiet-Sun Network as Observed with the Hinode Spectropolarimeter” 2008ApJ...672.1237L ADS
- Lites, B. W., Rempel, M., Borrero, J. M., & Danilovic, S. 2017 “Are Inter-network Magnetic Fields in the Solar Photosphere Horizontal or Vertical?” 2017ApJ...835...14L ADS
- Lites, B. W., Rutten, R. J., & Kalkofen, W. 1993 “Dynamics of the Solar Chromosphere. I. Long-Period Network Oscillations” 1993ApJ...414..345L ADS
- Liu, S. Y. & Skumanich, A. 1974 “An empirical interpretation for the time evolution of the Ca ii K line” 1974SoPh...38..109L ADS
- Livingston, W., Wallace, L., White, O. R., & Giampapa, M. S. 2007 “Sun-as-a-Star Spectrum Variations 1974-2006” 2007ApJ...657.1137L ADS
- Lockyer, J. N. 1868 “Spectroscopic Observation of the Sun, No. II.” 1868RSPS...17..131L ADS
- Lundblad, R. 1923 “On the Radiation and Temperature of the External Photospheric Layers” 1923ApJ...58..113L ADS
- Madjarska, M. S. 2019 “Coronal bright points” 2019LRSP...16....2M ADS
- Madjarska, M. S., Chae, J., Moreno-Insertis, F., et al. 2021 “The chromospheric component of coronal bright points. Coronal and chromospheric responses to magnetic-flux emergence” 2021A&A...646A.107M ADS
- Madsen, C. A., Dimant, Y. S., Oppenheim, M. M., & Fontenla, J. M. 2014 “The Multi-species Farley-Buneman Instability in the Solar Chromosphere” 2014ApJ...783..128M ADS
- Magain, P. 1986 “Contribution functions and the depths of formation of spectral lines” 1986A&A...163..135M ADS
- Malanushenko, O., Jones, H. P., & Livingston, W. 2004 “Imaging the Chromosphere using Photospheric Hn 539.4 nm” 2004IAUS...223..645M ADS
- Maltby, P., Avrett, E. H., Carlsson, M., et al. 1986 “A New Sunspot Umbral Model and Its Variation with the Solar Cycle” 1986ApJ...306..284M ADS (MACKKL)
- Martens, P. C. H., Kankelborg, C. C., & Berger, T. E. 2000 “On the Nature of the ‘Moss’ Observed by TRACE” 2000ApJ...537..471M ADS
- Martínez-Sykora, J., De Pontieu, B., Carlsson, M., et al. 2017 “Two-dimensional Radiative Magnetohydrodynamic Simulations of Partial Ionization in the Chromosphere. II. Dynamics and Energetics of the Low Solar Atmosphere” 2017ApJ...847...36M ADS
- Martínez-Sykora, J., Leenaarts, J., De Pontieu, B., et al. 2020 “Ion-neutral Interactions and Nonequilibrium Ionization in the Solar Chromosphere” 2020ApJ...889...95M ADS
- Mason, E. I., Antiochos, S. K., & Vourlidas, A. 2021 “An Observational Study of a ‘Rosetta Stone’ Solar Eruption” 2021ApJ...914L...8M ADS
- Mein, N., Mein, P., Heinzel, P., et al. 1996 “Cloud model with variable source function for solar H α structures.” 1996A&A...309..275M ADS
- Mein, P. 1966 “Champ macroscopique des vitesses dans l’atmosphère solaire d’après les mesures de déplacements des raies de Fraunhofer” 1966AnAp...29..153M ADS
- Mein, P. 1971 “Inhomogeneities in the Solar Atmosphere from the Ca II Infra-Red Lines” 1971SoPh...20....3M ADS
- Merrill, P. W. 1956 “Lines of the chemical elements in astronomical spectra” 1956lcea.book....M ADS
- Mewe, R., Schrijver, C. J., & Zwaan, C. 1981 “Coronal Activity in F-Type G-Type and K-Type Stars” 1981SSRv...30..191M ADS
- Meyer, J. P. 1985 “Solar-stellar outer atmospheres and energetic particles, and galactic cosmic rays” 1985ApJS...57..173M ADS
- Meyer, J.-P. 1991 “Diagnostic methods for coronal abundances” 1991AdSpR...11a.269M ADS
- Meyer, K. A., Mackay, D. H., & van Ballegoijen, A. A. 2012 “Solar Magnetic Carpet II: Coronal Interactions of Small-Scale Magnetic Fields” 2012SoPh...278..149M ADS
- Michalitsanos, A. G. 1973 “The Five Minute Period Oscillation in Magnetically Active Regions” 1973SoPh...30...47M ADS
- Mihalas, D. 1970 “Stellar atmospheres” 1970stat.book....M ADS
- Mihalas, D. 1978 “Stellar atmospheres, 2nd edition” 1978stat.book....M ADS
- Milne, E. A. 1921 “Radiative equilibrium in the outer layers of a star” 1921MNRAS...81..361M ADS
- Minnaert, M. 1930 “On the continuous spectrum of the corona and its polarisation. With 3 figures. (Received July 30, 1930)” 1930ZA.....1..209M ADS
- Minnaert, M., Houtgast, J., & Mulders, G. F. W. 1940 “Photometric atlas of the solar spectrum” 1940pass.book....M ADS
- Mitchell, S. A. & Mulders, G. F. W. 1938 “Energy Distribution in the Continuous Spectrum of the Corona (Abstract)” 1938PASP...50..225M ADS
- Molnar, M. E., Reardon, K. P., Chai, Y., et al. 2019 “Solar Chromospheric Temperature Diagnostics: A Joint ALMA-H α Analysis” 2019ApJ...881...99M ADS
- Molowny-Horas, R., Heinzel, P., Mein, P., & Mein, N. 1999 “A non-LTE inversion procedure for chromospheric cloud-like features” 1999A&A...345..618M ADS
- Moore, C. E. 1959 “A multiplet table of astrophysical interest. Part I” 1959mtai.book....M ADS
- Moore, C. E. & Merrill, P. W. 1968 “Partial Grotrian Diagrams of Astrophysical Interest” 1968pgda.book....M ADS
- Moore, C. E., Minnaert, M. G. J., & Houtgast, J. 1966 “The solar spectrum 2935 Å to 8770 Å” 1966sst...book....M ADS
- Muñoz-Jaramillo, A., Sheeley, N. R., Zhang, J., & DeLuca, E. E. 2012 “Calibrating 100 Years of Polar Faculae Measurements: Implications for the Evolution of the Heliospheric Magnetic Field” 2012ApJ...753..146M ADS
- Mulders, G. F. W. 1936 “On the energy distribution in the Continuous Spectrum of the Sun. (Communication from the Heliophysical Institute of the Physical Laboratory at Utrecht.) Mit 4 Abbildungen.” 1936ZA.....11..132M ADS
- Murcray, F. J., Goldman, A., Murcray, F. H., et al. 1981 “Observation of new emission lines in the infrared solar spectrum near 12.33, 12.22, and 7.38 microns” 1981ApJ...247L..97M ADS
- Neckel, H. 1999 “Announcement” 1999SoPh...184..421N ADS
- Neckel, H. 2003 “On the sun’s absolute disk-center and mean disk intensities, its limb darkening, and its ‘limb temperature’ ($\lambda\lambda 330$ to 1099 nm)” 2003SoPh...212..239N ADS
- Neckel, H. 2005 “Analytical Reference Functions $F(\lambda)$ for the Sun’s Limb Darkening and Its Absolute Continuum Intensities ($\lambda\lambda 300$ to 1100 nm)” 2005SoPh...229...13N ADS
- Neckel, H. & Labs, D. 1984 “The solar radiation between 3300 and 12500 Å” 1984SoPh...90..205N ADS
- Ng, K. C. 1974 “Hypernetted chain solutions for the classical one-component plasma up to $\Gamma=7000$ ” 1974JChPh...61.2680N ADS
- Nindos, A., Patsourakos, S., Alissandrakis, C. E., & Bastian, T. S. 2021 “ALMA observations of the variability of the quiet Sun at millimeter wavelengths” 2021A&A...652A..92N ADS
- Nóbrega-Siverio, D., Martínez-Sykora, J., Moreno-Insertis, F., & Carlsson, M. 2020a “Ambipolar diffusion in the Bifrost code” 2020A&A...638A..79N ADS

- Nóbrega-Siverio, D., Moreno-Insertis, F., Martínez-Sykora, J., Carlsson, M., & Szydlarski, M. 2020b “Nonequilibrium ionization and ambipolar diffusion in solar magnetic flux emergence processes” 2020A&A...633A..66N ADS
- Nordlund, A. 1984a “Modelling of Small-Scale Dynamical Processes: Convection and Wave Generation (Keynote)” 1984ssdp.conf..181N ADS
- Nordlund, A. 1984b “A Re-evaluation of the Granular Δ Irms” 1984ssdp.conf..174N ADS
- Nordlund, Å. 1985a “The 3-D structure of the magnetic field, and its interaction with granulation.” 1985MPARp.212..101N ADS
- Nordlund, Å. 1985b “The dynamics of granulation, and its interaction with the radiation field.” 1985MPARp.212....1N ADS
- Nordlund, Å., Stein, R. F., & Asplund, M. 2009 “Solar Surface Convection” 2009LRSP...6....2N ADS
- Novotny, E. 1973 “Introduction to stellar atmospheres and interiors” 1973itsa.book.....N ADS
- Noyes, R. W. 1965 “Dielectronic Recombination and the Solar H and K Lines” 1965SAOSR.174..405N ADS
- Noyes, R. W. 1967 “Observational Studies of Velocity Fields in the Solar Photosphere and Chromosphere” 1967IAUS...28..293N ADS
- Noyes, R. W. & Leighton, R. B. 1963 “Velocity Fields in the Solar Atmosphere. II. The Oscillatory Field.” 1963ApJ...138..631N ADS
- Olson, G. L., Auer, L. H., & Buchler, J. R. 1986 “A rapidly convergent iterative solution of the non-LTE radiation transfer problem.” 1986JQSR...35..431O ADS
- Ortiz, A., Hansteen, V. H., Nóbrega-Siverio, D., & Rouppe van der Voort, L. 2020 “Ellerman bombs and UV bursts: reconnection at different atmospheric layers” 2020A&A...633A..58O ADS
- Pais, A. 1982 “Subtle is the Lord. The science and the life of Albert Einstein” 1982sils.book.....P ADS
- Pais, A. 1986 “Inward bound. Of matter and forces in the physical world” 1986ibmf.book.....P ADS
- Paletou, F. 2018 “On Milne-Barbier-Unsöld relationships” 2018OAS...27...76P ADS
- Pankhurst, M., Stevenson, C., & Coldwell, B. 2021 “Meteorites that produce K-feldspar-rich ejecta blankets correspond to mass extinctions” 2021JGS...055.....P URL
- Pannekoek, A. 1930 “The theoretical contours of absorption lines” 1930MNRAS...91..139P ADS
- Pariat, E., Masson, S., & Aulanier, G. 2009 “Current Buildup in Emerging Serpentine Flux Tubes” 2009ApJ...701.1911P ADS
- Parker, E. N. 1972 “Topological Dissipation and the Small-Scale Fields in Turbulent Gases” 1972ApJ...174..499P ADS
- Patsourakos, S., Gouttebroze, P., & Vourlidis, A. 2007 “The Quiet Sun Network at Subarcsecond Resolution: VAULT Observations and Radiative Transfer Modeling of Cool Loops” 2007ApJ...664.1214P ADS
- Pecker, J.-C. 1951 “Contribution à la théorie du type spectral: IV. La formation des raies dans les spectres stellaires” 1951AnAp...14..115P ADS
- Penn, M., Altrock, R. C., Henry, T., & Guhathakurta, M. 1998 “Synoptic Coronal Temperature; Magnetic Field and He II 1083 NM Observations” 1998ASPC...140..325P ADS
- Pereira, T. M. D. 2019 “The dynamic chromosphere: Pushing the boundaries of observations and models” 2019AdSpR...63.1434P ADS
- Pereira, T. M. D., De Pontieu, B., & Carlsson, M. 2012 “Quantifying Spicules” 2012ApJ...759...18P ADS
- Pereira, T. M. D., De Pontieu, B., Carlsson, M., et al. 2014 “An Interface Region Imaging Spectrograph First View on Solar Spicules” 2014ApJ...792L..15P ADS
- Pereira, T. M. D. & Uitenbroek, H. 2015 “RH 1.5D: a massively parallel code for multi-level radiative transfer with partial frequency redistribution and Zeeman polarisation” 2015A&A...574A...3P ADS
- Peter, H., Tian, H., Curdt, W., et al. 2014 “Hot explosions in the cool atmosphere of the Sun” 2014Sci...346C.315P ADS
- Pierce, A. K. 1968 “The Chromospheric Spectrum Outside of Eclipse, lambda lambda 3040 to 9266 Å” 1968ApJS...17....1P ADS
- Pierce, A. K. & Breckenridge, J. B. 1974 “The Kitt Peak table of photographic solar spectrum wavelengths” 1974kptp.book.....P ADS
- Pietarila Graham, J., Cameron, R., & Schüssler, M. 2010 “Turbulent Small-Scale Dynamo Action in Solar Surface Simulations” 2010ApJ...714.1606P ADS
- Planck, M. 1900a “Ueber eine Verbesserung der Wien’schen Spektralgleichung, Verhand. Deutschen Physik. Gesellschaft 2, 204” planck1900a
- Planck, M. 1900b “Zur Theorie des Gesetzes der Energieverteilung im Normalspektrum, Verhand. Deutschen Physik. Gesellschaft 2, 237” planck1900b
- Polito, V., De Pontieu, B., Testa, P., Brooks, D. H., & Hansteen, V. 2020 “IRIS Observations of the Low-atmosphere Counterparts of Active Region Outflows” 2020ApJ...903...68P ADS
- Pottasch, S. R. 1964 “On the Interpretation of the Solar Ultraviolet Emission Line Spectrum” 1964SSRv....3..816P ADS
- Pottasch, S. R. 2011 “The history of the creation of Astronomy & Astrophysics” 2011EAS...49...23P ADS
- Priest, E. R., Heyvaerts, J. F., & Title, A. M. 2002 “A Flux-Tube Tectonics Model for Solar Coronal Heating Driven by the Magnetic Carpet” 2002ApJ...576..533P ADS
- Reames, D. V. 2021 “Solar Energetic Particles. A Modern Primer on Understanding Sources, Acceleration and Propagation” 2021LNP...978.....R ADS
- Reardon, K. & Cauzzi, G. 2012a “New insight on the coupling of the solar atmosphere from imaging spectroscopy” 2012decs.confE..20R ADS
- Reardon, K. P. & Cauzzi, G. 2012b “The IBIS Mosaic - A Broad View Of The Solar Atmosphere” 2012AAS...22020111R ADS
- Rezaei, R. & Beck, C. 2015 “Multiwavelength spectropolarimetric observations of an Ellerman bomb” 2015A&A...582A.104R ADS
- Rosner, R., Tucker, W. H., & Vaiana, G. S. 1978 “Dynamics of the quiescent solar corona.” 1978ApJ...220..643R ADS
- Rouppe van der Voort, L. & de la Cruz Rodríguez, J. 2013 “Short Dynamic Fibrils in Sunspot Chromospheres” 2013ApJ...776...56R ADS
- Rouppe van der Voort, L., Leenaarts, J., de Pontieu, B., Carlsson, M., & Vissers, G. 2009 “On-disk Counterparts of Type II Spicules in the Ca II 854.2 nm and H α Lines” 2009ApJ...705..272R ADS
- Rouppe van der Voort, L. H. M., De Pontieu, B., Hansteen, V. H., Carlsson, M., & van Noort, M. 2007 “Magnetoacoustic Shocks as a Driver of Quiet-Sun Mottles” 2007ApJ...660L.169R ADS
- Rouppe van der Voort, L. H. M., Rutten, R. J., Sütterlin, P., Sloover, P. J., & Krijger, J. M. 2003 “La Palma observations of umbral flashes” 2003A&A...403..277R ADS
- Rouppe van der Voort, L. H. M., Rutten, R. J., & Vissers, G. J. M. 2016 “Reconnection brightenings in the quiet solar photosphere” 2016A&A...592A.100R ADS
- Russell, A. J. B. 2018 “Commentary: Discovery of the Sun’s million-degree hot corona” 2018FrASS...5....9R ADS
- Rutten, R. G. M., Schrijver, C. J., Lemmens, A. F. P., & Zwaan, C. 1991 “Magnetic structure in cool stars. XVII. Minimum radiative losses from the outer atmosphere.” 1991A&A...252..203R ADS
- Rutten, R. J. 1977 “Extreme limb observations of Ba II λ 4554 and Mg I λ 4571” 1977SoPh...51....3R ADS
- Rutten, R. J. 1978 “Empirical NLTE analyses of solar spectral lines. II - The formation of the Ba II λ 4554 resonance line” 1978SoPh...56..237R ADS
- Rutten, R. J. 1985 “Review of Richard N. Thomas: Stellar Atmospheric Structural Patterns” 1985SSRv...41..394T ADS
- Rutten, R. J. 1988 “The NLTE formation of iron lines in the solar photosphere” 1988ASSL..138..185R ADS
- Rutten, R. J. 1990 “Summary Lecture” 1990IAUS...138..501R ADS
- Rutten, R. J. 1995 “Chromospheric Oscillations” 1995ESASP.376a.151R ADS
- Rutten, R. J. 1999 “(Inter-)Network Structure and Dynamics” 1999ASPC...184..181R ADS
- Rutten, R. J. 2002 “Solar Atmosphere Models” 2002JAD...8....8R ADS
- Rutten, R. J. 2003 “Radiative Transfer in Stellar Atmospheres” 2003rtsa.book.....R ADS (RTSA)
- Rutten, R. J. 2006 “On the Nature of the Solar Chromosphere” 2006ASPC...354..276R ADS
- Rutten, R. J. 2007 “Observing the Solar Chromosphere” 2007ASPC...368...27R ADS
- Rutten, R. J. 2011 “The solar activity sensitivity of Mn I lines” 2011bandung URL
- Rutten, R. J. 2013 “Twists to Solar Spicules” 2013ASPC...470...49R ADS
- Rutten, R. J. 2016 “H α features with hot onsets. I. Ellerman bombs” 2016A&A...590A.124R ADS
- Rutten, R. J. 2017a “Solar ALMA predictions: tutorial” 2017IAUS...327....1R ADS
- Rutten, R. J. 2017b “Solar H-alpha features with hot onsets. III. Long fibrils in Lyman-alpha and with ALMA” 2017A&A...598A..89R ADS
- Rutten, R. J. 2018 “A year at Sunspot. Reminiscences of 1977-1978 at the Sacramento Peak Observatory” 2018arXiv180408709R ADS
- Rutten, R. J. 2019 “Non-Equilibrium Spectrum Formation Affecting Solar Irradiance” 2019SoPh...294..165R ADS
- Rutten, R. J. 2020 “Small-scale solar surface magnetism” 2020smvc.book...29R ADS
- Rutten, R. J. 2020 “Solo campfires in SDO images” 2020arXiv200900376R ADS (LAR-1)
- Rutten, R. J. 2021 “De zon op Keesdagen / The Sun on Kees days” 2021LingAstRep...3R URL (LAR-3)
- Rutten, R. J. & Carlsson, M. 1994 “The Formation of Infrared Rydberg Lines” 1994IAUS...154..309R ADS
- Rutten, R. J., Engvold, O., & Nieuwenhuizen, A. C. T. 2022 “Cornelis de Jager: In Memoriam” 2022SoPh...297...15R ADS

- Rutten, R. J. & Kostik, R. I. 1982 “Empirical NLTE analyses of solar spectral lines. III - Iron lines versus LTE models of the photosphere” 1982A&A...115..104R ADS
- Rutten, R. J. & Krijger, J. M. 2003 “Dynamics of the solar chromosphere IV. Evidence for atmospheric gravity waves from TRACE” 2003A&A...407..735R ADS
- Rutten, R. J., Leenaarts, J., Rouppe van der Voort, L. H. M., et al. 2011 “Quiet-Sun imaging asymmetries in Na I D₁ compared with other strong Fraunhofer lines” 2011A&A...531A..17R ADS
- Rutten, R. J. & Milkey, R. W. 1979 “Partial redistribution in the solar photospheric Ba II spectrum” 1979ApJ...231..277R ADS
- Rutten, R. J. & Rouppe van der Voort, L. H. M. 2017 “Solar H α features with hot onsets. II. A contraal fibril” 2017A&A...597A..138R ADS
- Rutten, R. J., Rouppe van der Voort, L. H. M., & De Pontieu, B. 2019 “Solar H α features with hot onsets. IV. Network fibrils” 2019A&A...632A..96R ADS
- Rutten, R. J., Rouppe van der Voort, L. H. M., & Vissers, G. J. M. 2015 “Ellerman Bombs at High Resolution. IV. Visibility in Na I and Mg I” 2015ApJ...808..133R ADS
- Rutten, R. J. & Schrijver, C. J. (Eds.) 1994 “Solar Surface Magnetism” 1994ASIC..433.....R ADS
- Rutten, R. J. & Stencel, R. E. 1980 “Solar limb emission lines near CA II H & K and their spatial intensity variations” 1980A&AS...39..415R ADS
- Rutten, R. J. & Uitenbroek, H. 1991a “Ca II H $2v$ and K $2v$ Cell Grains” 1991SoPh...134...15R ADS
- Rutten, R. J. & Uitenbroek, H. 1991b “K $2v$ Cell Grains and Chromospheric Heating” 1991mcch.conf...48R ADS
- Rutten, R. J. & Uitenbroek, H. 2012 “Chromospheric backradiation in ultraviolet continua and H α ” 2012A&A...540A..86R ADS
- Rutten, R. J. & van Amerongen, H. J. 1975 “A very simple digital microdensitometer-comparator” 1975ASSL...54..261R ADS
- Rutten, R. J. & van der Zalm, E. B. J. 1984a “Clean lines in the solar flux spectrum” 1984A&AS...55..171R ADS
- Rutten, R. J. & van der Zalm, E. B. J. 1984b “Revision of solar equivalent widths, Fe I oscillator strengths and the solar iron abundance.” 1984A&AS...55..143R ADS
- Rutten, R. J., van Veelen, B., & Sütterlin, P. 2008 “DOT Tomography of the Solar Atmosphere VII. Chromospheric Response to Acoustic Events” 2008SoPh...251..533R ADS
- Rutten, R. J., Vissers, G. J. M., Rouppe van der Voort, L. H. M., Sütterlin, P., & Vitas, N. 2013 “Ellerman bombs: fallacies, fads, usage” 2013JPhCS.440a2007R ADS
- Rutten, R. J. & Zwaan, C. 1983 “Empirical NLTE analyses of solar spectral lines. IV - The Fe I curve of growth” 1983A&A...117...21R ADS
- Rybicki, G. B. & Hummer, D. G. 1992 “An accelerated lambda iteration method for multilevel radiative transfer. II. Overlapping transitions with full continuum.” 1992A&A...262..209R ADS
- Rybicki, G. B. & Lightman, A. P. 1986 “Radiative Processes in Astrophysics” 1986rpa...book.....R ADS
- Samain, D. 1979 “Solar continuum data on absolute intensities, center to limb variations and Laplace inversion between 1400 and 2100 Å.” 1979A&A...74..225S ADS
- Samanta, T., Tian, H., Yurchyshyn, V., et al. 2019 “Generation of solar spicules and subsequent atmospheric heating” 2019Sci...366..890S ADS
- Scharmer, G. B. 1976 “The Wilson-Bappu effect as a result of supersonic turbulence.” 1976A&A...53..341S ADS
- Scharmer, G. B. & Carlsson, M. 1985 “A new approach to multi-level non-LTE radiative transfer problems.” 1985JCoPh...59...56S ADS
- Scharmer, G. B., Löfdahl, M. G., Slieden, G., & de la Cruz Rodríguez, J. 2019 “Is the sky the limit?. Performance of the revamped Swedish 1-m Solar Telescope and its blue- and red-beam reimaging systems” 2019A&A...626A..55S ADS
- Scheffler, H. & Elsaesser, H. 1974 “Physik der Sterne und der Sonne” 1974psus.book.....S ADS
- Schoenfeld, W. G., Chang, E. S., Geller, M., et al. 1995 “High excitation Rydberg levels of Fe I from the ATMOS solar spectrum at 2.5 and 7 μ m.” 1995A&A...301..593S ADS
- Schoolman, S. A. 1972 “Formation of the Solar H α Profile” 1972SoPh...22..344S ADS
- Schrijver, C. J. “Heating of Stellar Chromospheres and Coronae: Evidence for Non-Magnetic Heating (Invited review)” in J. L. Linsky and R. E. Stencel (Eds.), Cool Stars, Stellar Systems and the Sun Vol. 291 135–145 1987LNP...291..135S ADS
- Schrijver, C. J. 1987b “Magnetic structure in cool stars. XI. Relations between radiative fluxes measuring stellar activity, and evidence for two components in stellar chromospheres.” 1987A&A...172..111S ADS
- Schrijver, C. J. 1992 “The basal and strong-field components of the solar atmosphere” 1992A&A...258..507S ADS
- Schrijver, C. J. 1995 “Basal heating in the atmospheres of cool stars” 1995A&ARv...6..181S ADS
- Schrijver, C. J., Dobson, A. K., & Radick, R. R. 1989 “The Magnetic, Basal, and Radiative Equilibrium Components in Mount Wilson CA II H+K Fluxes” 1989ApJ...341.1035S ADS
- Schrijver, C. J., Mewe, R., & Zwaan, C. 1982 “Coronal activity in F-, G-, and K-type stars; relations between parameters characterizing stellar structures and X-ray emission” 1982AdSpR...2i.243S ADS
- Schrijver, C. J., Title, A. M., van Ballegoijen, A. A., Hagenaar, H. J., & Shine, R. A. 1997 “Sustaining the Quiet Photospheric Network: The Balance of Flux Emergence, Fragmentation, Merging, and Cancellation” 1997ApJ...487..424S ADS
- Schrijver, C. J. & Zwaan, C. 2000 “Solar and Stellar Magnetic Activity” 2000ssma.book.....S ADS
- Schrijver, C. J. & Zwaan, C. 2008 “Solar and Stellar Magnetic Activity” 2008ssma.book.....S ADS
- Schrijver, K., Bagenal, F., Bastian, T., et al. 2019 “Principles Of Helio-physics: a textbook on the universal processes behind planetary habitability” 2019arXiv191014022S ADS
- Schuster, A. 1905 “Radiation Through a Foggy Atmosphere” 1905ApJ...21....1S ADS
- Sekse, D. H., Rouppe van der Voort, L., & De Pontieu, B. 2012 “Statistical Properties of the Disk Counterparts of Type II Spicules from Simultaneous Observations of Rapid Blueshifted Excursions in Ca II 8542 and H α ” 2012ApJ...752..108S ADS
- Sekse, D. H., Rouppe van der Voort, L., & De Pontieu, B. 2013a “On the Temporal Evolution of the Disk Counterpart of Type II Spicules in the Quiet Sun” 2013ApJ...764..164S ADS
- Sekse, D. H., Rouppe van der Voort, L., De Pontieu, B., & Scullion, E. 2013b “Interplay of Three Kinds of Motion in the Disk Counterpart of Type II Spicules: Upflow, Transversal, and Torsional Motions” 2013ApJ...769..44S ADS
- Shchukina, N. & Trujillo Bueno, J. 2001 “The Iron Line Formation Problem in Three-dimensional Hydrodynamic Models of Solar-like Photospheres” 2001ApJ...550..970S ADS
- Shchukina, N. G., Olshevsky, V. L., & Khomenko, E. V. 2009 “The solar BaII 4554 Å line as a Doppler diagnostic: NLTE analysis in 3D hydrodynamical model” 2009A&A...506.1393S ADS
- Sheeley, N. R., J. 2008 “A Century of Polar Faculae Variations” 2008ApJ...680.1553S ADS
- Sheminova, V. A., Rutten, R. J., & Rouppe van der Voort, L. H. M. 2005 “The wings of Ca II H and K as solar fluxtube diagnostics” 2005A&A...437.1069S ADS
- Shimizu, T., Shimojo, M., & Abe, M. 2021 “Simultaneous ALMA-Hinode-IRIS Observations on Footpoint Signatures of a Soft X-Ray Loop-like Microflare” 2021ApJ...922..113S ADS
- Shine, R. A., Milkey, R. W., & Mihalas, D. 1975 “Resonance Line Transfer with Partial Redistribution. V. The Solar CA II Lines” 1975ApJ...199..724S ADS
- Simões, P. J. A., Reid, H. A. S., Milligan, R. O., & Fletcher, L. 2019 “The Spectral Content of SDO/AIA 1600 and 1700 Å Filters from Flare and Plage Observations” 2019ApJ...870..114S ADS
- Simon, G. W. & Leighton, R. B. 1964 “Velocity Fields in the Solar Atmosphere. III. Large-Scale Motions, the Chromospheric Network, and Magnetic Fields.” 1964ApJ...140.1120S ADS
- Simon, G. W., Title, A. M., & Weiss, N. O. 2001 “Sustaining the Sun’s Magnetic Network with Emerging Bipoles” 2001ApJ...561..427S ADS
- Skogsrud, H., Rouppe van der Voort, L., & De Pontieu, B. 2016 “On the Active Region Bright Grains Observed in the Transition Region Imaging Channels of IRIS” 2016ApJ...817..124S ADS
- Smitha, H. N., Holzreuter, R., van Noort, M., & Solanki, S. K. 2020 “The influence of NLTE effects in Fe I lines on an inverted atmosphere. I. 6301 Å and 6302 Å lines formed in 1D NLTE” 2020A&A...633A.157S ADS
- Smitha, H. N., Holzreuter, R., van Noort, M., & Solanki, S. K. 2021 “The influence of NLTE effects in Fe I lines on an inverted atmosphere. II. 6301 Å and 6302 Å lines formed in 3D NLTE” 2021A&A...647A..46S ADS
- Snik, F., Bos, S. P., Brackenhoff, S. A., et al. 2020 “Detection of polarization neutral points in observations of the combined corona and sky during the 21 August 2017 total solar eclipse” 2020ApOpt...59F..71S ADS
- Straus, T., Fleck, B., Jefferies, S. M., et al. 2008 “The Energy Flux of Internal Gravity Waves in the Lower Solar Atmosphere” 2008ApJ...681L.125S ADS
- Suematsu, Y., Wang, H., & Zirin, H. 1995 “High-Resolution Observation of Disk Spicules. I. Evolution and Kinematics of Spicules in the Enhanced Network” 1995ApJ...450..411S ADS
- Sukhorukov, A. V. & Leenaarts, J. 2017 “Partial redistribution in 3D non-LTE radiative transfer in solar-atmosphere models” 2017A&A...597A..46S ADS
- Sütterlin, P., Rutten, R. J., & Skomorovsky, V. I. 2001 “Ba II 4554 Å speckle imaging as solar Doppler diagnostic” 2001A&A...378..251S ADS
- Thomas, R. N. 1957 “The Source Function in a Non-Equilibrium Atmosphere. I. The Resonance Lines.” 1957ApJ...125..260T ADS

- Thomas, R. N. 1960 “The Source Function in a Non-Equilibrium Atmosphere. IV. Evaluation and Applications of the Net Radiative Bracket.” 1960ApJ...131..429T ADS
- Thomas, R. N. 1983 “Stellar atmospheric structural patterns” 1983NASSP.471.....T ADS
- Title, A. M. 1966 “Selected Spectroheliograms” Title1966a
- Title, A. M. 1966 “A Study of Velocity Fields in the Hydrogen-Alpha Chromosphere by Means of Time-Lapse Doppler Movies.” 1966PhDT.....1T ADS
- Trujillo Bueno, J., Shchukina, N., & Asensio Ramos, A. 2004 “A substantial amount of hidden magnetic energy in the quiet Sun” 2004Natur.430..326T ADS
- Turck-Chièze, S., Carton, P. H., Barrière, J. C., et al. 2012 “Solar Global Oscillations of Low-Degree modes (GOLD): The Status of the Multi-channel Resonance Spectrometer GOLF-NG” 2012ASPC..462..240T ADS
- Tziotziou, K. 2007 “Chromospheric Cloud-Model Inversion Techniques” 2007ASPC..368..217T ADS
- Uitenbroek, H. 1989 “Operator perturbation method for multi-level line transfer with partial redistribution” 1989A&A...213..360U ADS
- Uitenbroek, H. 2000 “The CO Fundamental Vibration-Rotation Lines in the Solar Spectrum. I. Imaging Spectroscopy and Multidimensional LTE Modeling” 2000ApJ...531..571U ADS
- Uitenbroek, H. 2001 “Multilevel Radiative Transfer with Partial Frequency Redistribution” 2001ApJ...557..389U ADS
- Uitenbroek, H. & Bruls, J. H. M. J. 1992 “The formation of helioseismology lines. III. Partial redistribution effects in weak solar resonance lines.” 1992A&A...265..268U ADS
- Uitenbroek, H. & Criscuolo, S. 2011 “Why One-dimensional Models Fail in the Diagnosis of Average Spectra from Inhomogeneous Stellar Atmospheres” 2011ApJ...736..69U ADS
- Uitenbroek, H., Tritschler, A., & Rimmele, T. 2007 “The Discrepancy in G-Band Contrast: Where is the Quiet Sun?” 2007ApJ...668..586U ADS
- Ulmschneider, P. & Kalkofen, W. “Heating of the solar chromosphere” in B. N. Dwivedi and F. b. E. N. Parker (Eds.), Dynamic Sun 181–195 2003dysu.book..181U ADS
- Ulrich, R. K. 1970 “The Five-Minute Oscillations on the Solar Surface” 1970ApJ...162..993U ADS
- Unruh, Y. C., Solanki, S. K., & Fligge, M. 1999 “The spectral dependence of facular contrast and solar irradiance variations” 1999A&A...345..635U ADS
- Unsöld, A. 1955 “Physik der Sternatmosphären” 1955QB461.U55..... ADS
- van de Hulst, H. C. “The Chromosphere and the Corona” in G. P. Kuiper (Ed.), The Sun 207 1953sun..book..207V ADS
- van Noort, M., Rouppe van der Voort, L., & Löfdahl, M. G. 2005 “Solar Image Restoration by Use Of Multi-frame Blind De-convolution With Multiple Objects And Phase Diversity” 2005SoPh..228..191V ADS
- Vernazza, J. E., Avrett, E. H., & Loeser, R. 1976 “Structure of the solar chromosphere. II. The underlying photosphere and temperature-minimum region.” 1976ApJS...30.....1V ADS (VALII)
- Vernazza, J. E., Avrett, E. H., & Loeser, R. 1981 “Structure of the solar chromosphere. III. Models of the EUV brightness components of the quiet sun.” 1981ApJS...45..635V ADS (VALIII)
- Vissers, G. J. M., Rouppe van der Voort, L. H. M., & Rutten, R. J. 2013 “Ellerman Bombs at High Resolution. II. Triggering, Visibility, and Effect on Upper Atmosphere” 2013ApJ...774...32V ADS
- Vissers, G. J. M., Rouppe van der Voort, L. H. M., & Rutten, R. J. 2019 “Automating Ellerman bomb detection in ultraviolet continua” 2019A&A...626A...4V ADS
- Vissers, G. J. M., Rouppe van der Voort, L. H. M., Rutten, R. J., Carlsson, M., & De Pontieu, B. 2015 “Ellerman Bombs at High Resolution. III. Simultaneous Observations with IRIS and SST” 2015ApJ...812...11V ADS
- Vitas, N., Viticchiè, B., Rutten, R. J., & Vögler, A. 2009 “Explanation of the activity sensitivity of Mn I 5394.7 Å” 2009A&A...499..301V ADS
- Vitense, E. 1951 “Der Aufbau der Sternatmosphären. IV. Teil. Kontinuierliche Absorption und Streuung als Funktion von Druck und Temperatur. Mit 16 Textabbildungen” 1951ZA....28...81V ADS
- Vögler, A., Shelyag, S., Schüssler, M., et al. 2005 “Simulations of magneto-convection in the solar photosphere. Equations, methods, and results of the MURaM code” 2005A&A...429..335V ADS
- von Steiger, R. & Geiss, J. 1989 “Supply of fractionated gases to the corona” 1989A&A...225..222V ADS
- Vourlidas, A., Sánchez Andrade-Nuño, B., Landi, E., et al. 2010 “The Structure and Dynamics of the Upper Chromosphere and Lower Transition Region as Revealed by the Subarcsecond VAULT Observations” 2010SoPh..261...53V ADS
- Wang, Y. M. & Sheeley, N. R., J. 1995 “Coronal Plumes and Their Relationship to Network Activity” 1995ApJ...452..457W ADS
- Wang, Y. M., Sheeley, N. R., Dere, K. P., et al. 1997 “Association of Extreme-Ultraviolet Imaging Telescope (EIT) Polar Plumes with Mixed-Polarity Magnetic Network” 1997ApJ...484L..75W ADS
- Watanabe, H., Vissers, G., Kitai, R., Rouppe van der Voort, L., & Rutten, R. J. 2011 “Ellerman Bombs at High Resolution. I. Morphological Evidence for Photospheric Reconnection” 2011ApJ...736...71W ADS
- Webb, D. F., Gibson, S. E., Hewins, I. M., et al. 2017 “Preserving a Unique Archive for Long-Term Solar Variability Studies” 2017SpWea...15.1442W ADS
- Wedemeyer-Böhm, S. & Rouppe van der Voort, L. 2009 “On the continuum intensity distribution of the solar photosphere” 2009A&A...503..225W ADS
- Whitaker, W. A. 1963 “Heating of the Solar Corona by Gravity Waves.” 1963ApJ...137..914W ADS
- White, O. R. & Cha, M. Y. 1973 “Analysis of the 5 min Oscillatory Photospheric Motion. I: A Problem in Waveform Classification” 1973SoPh...31...23W ADS
- Wiersma, J., Rutten, R. J., & Lanz, T. 2003 “NLTE in a Hot Hydrogen Star: Auer & Mihalas Revisited” 2003ASPC..288..130W ADS
- Wijbenga, J. W. & Zwaan, C. 1972 “Empirical NLTE Analyses of Solar Spectral Lines. I: A Method and Some Applications to Earlier Analyses” 1972SoPh...23..265W ADS
- Wildt, R. 1939 “Electron Affinity in Astrophysics.” 1939ApJ...89..295W ADS
- Wilson, O. C. & Vainu Bappu, M. K. 1957 “H and K Emission in Late-Type Stars: Dependence of Line Width on Luminosity and Related Topics.” 1957ApJ...125..661W ADS
- Withbroe, G. L. 1978 “The thermal phase of a large solar flare.” 1978ApJ...225..641W ADS
- Wolff, C. L. 1972 “The Five-Minute Oscillations as Nonradial Pulsations of the Entire Sun” 1972ApJ...177L..87W ADS
- Wolff, C. L. 1973 “What is the Horizontal Scale of the 5-min Oscillations?” 1973SoPh...32...31W ADS
- Yadav, N., Cameron, R. H., & Solanki, S. K. 2021 “Slow magneto-acoustic waves in simulations of a solar plage region carry enough energy to heat the chromosphere” 2021A&A...652A..43Y ADS
- Yokoyama, T., Shimojo, M., Okamoto, T. J., & Iijima, H. 2018 “ALMA Observations of the Solar Chromosphere on the Polar Limb” 2018ApJ...863...96Y ADS
- Young, P. R., Tian, H., Peter, H., et al. 2018 “Solar Ultraviolet Bursts” 2018SSRv...214..120Y ADS
- Zirin, H. 1988 “Astrophysics of the sun” 1988assu.book.....Z ADS
- Zirin, H. & Popp, B. 1989 “Observations of the 12 Micron MG i Lines in Various Solar Features” 1989ApJ...340..571Z ADS
- Zwaan, C. “Relations Between Magnetic Activity and Stellar Properties” in M. Zeilik and D. M. Gibson (Eds.), Cool Stars, Stellar Systems and the Sun Vol. 254 19 1986LNP...254...19Z ADS

Version history

- March 3, 2021 – initial pre-school [arXiv post](#), 16 pages.
- April 29, 2021 – [arXiv v2](#) honoring [C. de Jager's 100th birthday](#): more content, faster serving, 27 pages.
- May 7, 2021 – notes → endnotes.
- May 31, 2021 – endnotes on yellow pages, [arXiv v3](#), 34 pages.
- July 20, 2021 – more informative reference format.
- July 29, 2021 – reached deep-thought page limit.
- August 2, 2021 – [arXiv v4](#), 42 pages.
- August 25, 2021 – [arXiv v5](#), 42 pages.
- December 13, 2021 – [arXiv v6](#), 50 pages.
- April 7, 2022 – 100 endnotes, 150 footnotes: time to stop.
- April 12, 2022 – [arXiv v7](#), 56 pages.

Status

I intend to keep this text somewhat alive with updates (see [footnote 57](#) for notifications) and welcome corrections and suggestions for improvements. [My website](#) serves the [current version](#) with a [summary here](#). ADS serves the [latest arXived version](#). ArXiv serves [all posted versions](#) including their latex sources¹⁵⁰.

¹⁵⁰ The arXiv sources include my latex tricks which you are welcome to. I get them via ArXiv's [Other formats](#) by hitting [Download source](#) and uncompress in my Downloads directory with `tar xvf 2103.02369`. My latex input files contain explanatory comments (to myself) with Stack-exchange referrals. My bibtex automation (just one command generates all references) is [described here](#). I have no manual for it but the [download scripts](#) and the [bibtex bst style](#) are also self-commenting.